The endocytic adaptor stonin 1 regulates cell signalling and focal adhesion dynamics

Inaugural-Dissertation

to obtain the academic degree
Doctor rerum naturalium (Dr. rer. nat.)

submitted to the Department of Biology, Chemistry and Pharmacy
of Freie Universität Berlin

by

MARIETTA BERGMANN

from Löbau, Germany

2017

PERIOD OF DOCTORAL STUDIES:	February 2013 to December 2016
INSTITUTE:	Leibniz Institute for Molecular Pharmacology

1. REFEREE:	PROF. DR. VOLKER HAUCKE
2. REFEREE:	PD DR. TANJA MARITZEN

DATE OF DISPUTATION:	18.07.2017

Hereby I declare that I have completed the doctoral thesis *The endocytic adaptor stonin 1 regulates cell signalling and focal adhesion dynamics* on my own and with no other aid and sources than noted.

Berlin, May 2nd, 2017

If it wasn't this ... It'd be something else.

Elisabethtown

Contents

List of Figures

List of Tables

Summary

Endocytosis determines the number and localisation of cell surface receptors thereby regulating recognition of environmental cues and cell signalling cascades. General endocytic adaptors like the adaptor protein 2 (AP2) recognise most cell surface receptors destined for internalisation via clathrin-mediated endocytosis. In contrast, cargo recognition by specific endocytic adaptors convey specificity for distinct cargos to allow fine tuning of processes ranging from neurotransmission to cellular motility. The stonin (Stn) protein family comprises two homologues representing such specialised endocytic adaptors. Stn2 has been described in detail to regulate neurotransmission by facilitating the uptake of the synaptic vesicle protein synaptotagmin 1. In contrast, Stn1 modulates cell motility by controlling the surface levels of neuron glial 2 (NG2). However, the molecular details and physiological importance of Stn1 function remained unresolved. In the present study, we demonstrate that Stn1 acts as a tumour suppressor and describe two distinct Stn1 functions which might contribute to tumour development.

First, we establish that Stn1 as a specialised endocytic adaptor for the oncogene NG2 regulates cellular signalling which might have implications during cancer development. Using biochemical approaches, we show that Stn1 interacts with the cytosolic domain of NG2 via its μ-homology domain and that Stn1 links NG2 with the endocytic machinery. Since endocytic adaptors regulate the surface levels of their cargos, absence of the adaptors often leads to accumulation of the cargo on the cell surface. In fact, immunohistological stainings performed on mouse brains demonstrated that in absence of Stn1 NG2 levels are increased in the olfactory bulb of young animals. NG2 is a well-known oncogene that stimulates cell signalling as well as cell adhesion and directional cell migration. Therefore, elevated NG2 levels in Stn1-depleted cells suggest an increased functionality of the cell surface receptor. Accordingly, we show that the elevated NG2 levels of Stn1-depleted cells correlate with enhanced signalling via the platelet-derived growth factor β - a signalling cascade that is regulated via NG2 to modulate tumour neovascularisation. The results therefore suggest that Stn1, by

limiting the surface levels of its cargo NG2, acts as tumour suppressor. In fact, analysis of the molecular signature of human glioblastoma via public databases revealed that an increased Stn1 expression correlates with a prolonged survival of the patients. Vice versa, induction of glioblastoma in Stn1-depleted mice amplified the tumour growth.

Besides cell signalling also cell movements via focal adhesions plays a central role for tumour growth. Using cell biological approaches we demonstrate that Stn1 facilitates focal adhesion dynamics by accelerating focal adhesion disassembly. Consequently, this effect potentially contributes to an increased protrusion and trailing end stability in absence of Stn1 thereby promoting directional migration. In addition, we provide evidence that Stn1 controls focal adhesion maturation via the actin cytoskeleton. The specific interaction with the actin-depolymerisation factor Destrin indicates a collaborative action of both proteins within that context.

Taken together our results establish Stn1 as an important regulator of NG2-dependent signalling and cell migration. Since both processes play central roles during tumour development, this work deepens the current understanding of this serious disease.

Zusammenfassung

Endozytose bestimmt die Anzahl und Lokalisation von Oberflächenrezeptoren und reguliert damit die Erkennung von Signalen des nahen Umfeldes sowie deren Signalgebung. Allgemeine endozytische Erkennungsmotive erkennen die meisten Zelloberflächenrezeptoren, wohingegen spezielle endozytische Adaptoren Spezifität für bestimmte Frachten vermitteln und somit Prozesse wie Neurotransmission und Zellbewegung genau abstimmen können. Die Stonin (Stn) Proteinfamilie umfasst zwei Homologe, die solch spezialisierte endozytische Adaptoren darstellen. Für Stn2 wurde bereits detailliert beschrieben, auf welche Weise es Neurotransmission durch die Aufnahme des synaptischen Proteins Synaptotagmin 1 beschleunigt. Stn1 hingegen steuert die Zellbewegung, indem es die Oberflächenlevel des Neuronen-Glia Antigen 2 (NG2) kontrolliert. Allerdings sind die molekularen Details und die physiologische Bedeutung dieser Stn1-Funktion im Unklaren geblieben. In der vorliegenden Studie zeigen wir, dass Stn1 als Tumorsuppressor fungiert und beschreiben zwei distinkte Stn1-Funktionen, die dazu beitragen.

Als Erstes begründen wir den Fakt, dass Stn1 der endozytische Adaptor für das Onkogen NG2 ist und darüber die Signalgebung in der Zelle beeinflusst, was potentiell Bedeutung für die Ausbildung von Tumoren haben könnte. Hierfür zeigen wir mit Hilfe von biochemischen Methoden, dass die μ-homologe Domäne von Stn1 mit der zytosolischen Domäne von NG2 interagiert und seine Fracht NG2 mit dem allgemeinen endozytischen Adaptor AP2 verknüpft. Da endozytische Adaptoren die Oberflächenlevel ihrer Fracht regulieren, resultiert ein Fehlen dieser Adaptoren oftmals in einer Akkumulation der Fracht an der Zelloberfläche. Tatsächlich zeigen wir in immunhistologischen Färbungen von Mausgehirnen, dass ohne die Anwesenheit von Stn1 die Proteinlevel seiner Fracht NG2 im Riechkolben von Jungtieren erhöht sind. NG2 ist ein allgemein bekanntes Onkogen, das die Signalgebung von Zellen ebenso stimuliert wie die Zelladhäsion und damit verbundene Zellmigration. Erhöhte NG2-Proteinlevel in Zellen, in denen Stn1 dezimiert wurde, weisen somit auf eine verstärkte Funktionalität des Oberflächenrezeptors hin. Entsprechend weisen wir in Stn1-depletierten Zellen, die erhöhte

NG2-Proteinlevel aufweisen, eine verstärkte Signalgebung des Rezeptors für Blutplättchen-extrahierte Wachstumsfaktoren des Typs β nach. Dies ist eine Signalkaskade, die von NG2 maßgeblich beeinflusst wird, um die Neovaskularisierung - unter anderem von Tumoren - zu stimulieren. Diese Ergebnisse deuten darauf hin, dass Stn1, indem es die Oberflächen-level seiner Fracht NG2 limitiert, eine Tumor-supprimierende Wirkung aufweisen könnte. Tatsächlich korreliert eine erhöhte Stn1-Expression mit einer längeren Überlebenswahrscheinlichkeit von Gliomapatienten. Im Gegensatz dazu weisen induzierte Glioblastomen in Stn1-depletierten Mäusen ein verstärktes Wachstum auf.

Neben der Signalgebung spielt die Zellfortbewegung via fokaler Adhäsionen eine zentrale Rolle beim Tumorwachstum. Mit Hilfe von zellbiologischen Experimenten weisen wir nach, dass Stn1 die Dynamiken der fokalen Adhäsionen beschleunigt, indem es deren Disassemblierung fördert. Dementsprechend trägt dieser Effekt potentiell zu einer erhöhten Stabilität der Zellfront sowie des Zellschwanzes in Stn1-depletierten Zellen bei und unterstützt damit deren direktionale Fortbewegung. Zusätzlich deuten erste Ergebnisse darauf hin, dass Stn1 die Reifung von fokalen Adhäsionen über das Aktinzytoskelett kontrolliert. Die Interaktion mit dem Aktin-depolymerisierenden Faktor Destrin deutet auf eine Zusammenarbeit beider Proteine in diesem Kontext hin.

Zusammenfassend etablieren unsere Ergebnisse Stn1 als einen wichtigen Regulator der Zellfortbewegung und NG2-abhängigen Signalgebung. Da beide Prozesse bei der Entwicklung von Tumoren eine zentrale Rolle spielen, vertieft diese Studie das derzeitige Verständnis dieser schwerwiegenden Krankheit.

1. Introduction

1.1. Clathrin-mediated endocytosis (CME)

The uptake of nutrients, particles and growth factors is essential for the survival of cells. In a process called endocytosis, macromolecules and particles are engulfed by the plasma membrane, invaginated and pinched-off thereby generating transport vesicles. One of the best characterised receptor-mediated processes is clathrin-mediated endocytosis (figure 1.1) in which membrane invaginations are enclosed by clathrin molecules. Clathrin is a three-legged (greek: 'triskelia') structure composed of three heavy and three light chains that assemble into pentameric and hexameric segments of a soccer ball-like cage around the budding vesicle (Kirchhausen et al., 2014). Clathrin itself, however, is incapable to interact with the membrane or the cargo. Instead it makes use of accessory proteins that bind the cargo on the plasma membrane and bridge the interaction towards clathrin. The main adaptor protein found in purified clathrin-coated vesicles is the assembly polypeptide 2 (AP2). AP2 is a heterotetrameric complex composed of four subunits each fulfilling a specific function during clathrin-mediated endocytosis (Kirchhausen et al., 2014). The AP2 core consists of the medium-sized μ- and the small σ-subunit, both mediating cargo recognition (section 1.1.1). μ- and σ-subunits are enclosed by the trunks of two large subunits called α- and β-adaptin. While the trunk of α-adaptin targets the AP2 complex to the plasma membrane by recognising phosphoinositol (4,5)-bisphosphate ($PI(4,5)P_2$), β-adaptin interacts with the coat protein clathrin. In addition, the ear-domains of both, α- and β-adaptin, interact with accessory proteins thereby serving as interaction hubs for the endocytic machinery (Wieffer et al., 2009). Clathrin-mediated endocytosis can be subdivided into 5 stages: nucleation, cargo selection, coat assembly, scission and uncoating (McMahon and Boucrot, 2011). Each step is accompanied by a conversion of phosphoinositides (PIs) which define membrane identity and regulate protein recruitment(Schink et al., 2016). At nucleation, $PI(4,5)P_2$ is recognised by bin-amphiphysin-rvs (BAR) domain proteins like the Fes/CIP4 homolgy only (FCHo) pro-

teins 1/2. BAR-domain proteins are characterised by an α-helical coiled-coiled region that recognises phospholipids thereby inducing or stabilising membrane curvature (Daumke et al., 2014). FCHo proteins only mildly bend the membrane inducing a shallow curvature. In addition PI(4,5)P_2 recruits AP2, thereby opening the multimeric complex for cargo recognition and potentiating clathrin assembly (Kelly et al., 2014). Clathrin coat assembly is accompanied by transformation of PI(4,5)P_2 towards PI(3,4)P_2 at the neck of the growing pit allowing the BAR-domain protein sorting nexin (SNX) 9/18 to interact and constrict the pit into an Ω-shape. This allows binding of the strongly bent BAR-proteins amphiphysin and endophilin which recruit the GTPase dynamin via Src homology 3 (SH3) domains. GTP hydrolysis leads to pinching off (Antonny et al., 2016) and binding of auxilin recruits the heat shock cognate 70 (Hsc70) catalysing coat release in an ATP-dependent manner (Eisenberg and Greene, 2007). At the same time the PI content of the vesicle will be modulated towards PI(3)P rendering the vesicle with an endosome identity which allows recycling and sorting events.

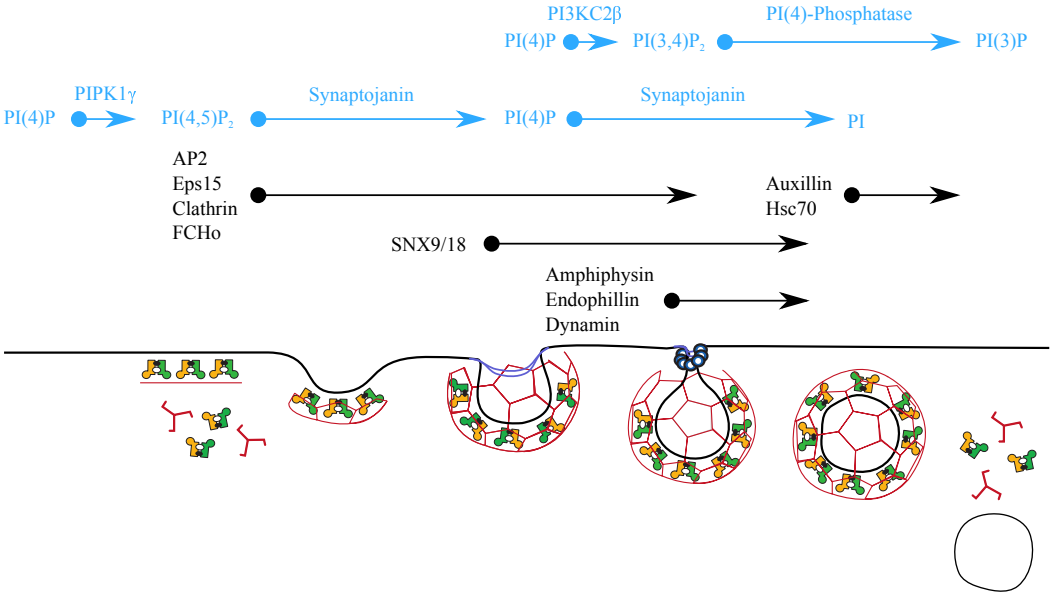

Figure 1.1.: Clathrin-mediated endocytosis. PI(4,5)P_2 generation by PIPK1γ clusters AP2 (yellow/green trunks), clathrin (red triskelia) and FCHo proteins during nucleation. Clathrin coat assembly is accompanied by PIP conversion allowing recuitment of BAR domain proteins with a stronger curvature (SNX9/18, amphiphysin, endophillin, purple) to constrict the neck and recruit the GTPase dynamin (spheres) for pinching off. Hsc70 gets recruited to the vesicle by auxilin and induces uncoating. Parallel PIP conversion changes the vesicle membrane to an endosomal identity. Phosphoinositide conversion and corresponding enzymes are depicted in blue. Modified from Conner and Schmid (2003), license number: 4075990510604. (*FCHo - Fes/CIP4 homolgy only, Hsc - heat shock cognate, PI(P) - phosphoinositide (phosphate), SNX9/18 - sorting nexin 9/18*).

1.1.1. Cargo recognition in CME

AP2 is one of the most important regulators of the internalisation via CME (Wieffer et al., 2009). As the main endocytic adaptor, AP2 recognises cargo proteins via its μ- and σ-subunit which interact with the classical interaction motifs (Traub and Bonifacino, 2013): the 'tyrosine-based motif' YXXΦ (X can be every amino acid, Φ stands for an amino acid with bulky hydrophobic side chains) as in case of the transferrin receptor and the 'dileucine motif' [DE]XXXL[LI] (brackets mean that either amino acid can be used) which is located in the cytosolic domain of the epidermal growth factor receptor for example. Besides specific motifs, also posttranslational modifications like phosphorylation or ubiquitination provide interactions sites for endocytic adaptors (Traub and Bonifacino, 2013). For instance, the epidermal growth factor receptor pathway substrate 15 (Eps15) as well as epsins interact with ubiquitinated receptors to facilitate their internalisation. The use of specialised endocytic adaptors, however, enables the cell to efficiently facilitate receptor internalisation thereby controlling activity of cell surface receptors more closely.

For instance, the heterodimeric cell surface receptors called integrins can be internalised via clathrin-mediated endocytosis in two different ways to regulate cell motility and migration. Recently, a subset of integrin α-subunits has been shown to contain the conserved tyrosine-based motif that binds to μ-subunits of AP2 (Franceschi et al., 2016). Alternatively, integrin complexes can be sorted into endocytic pits via the β-subunits, in which case the β-subunits are recognised by either disabled 2 (Dab2, Chao and Kunz 2009), autosomal recessive hypercholesteremia (ARH, Ezratty et al. 2009) or numb 1 (Nishimura and Kaibuchi, 2007). Numb and Dab phosphotyrosine binding (PTB) domains interact with NPxY motifs within the intracellular domain of β1 integrins (Calderwood et al., 2003). As a consequence, depletion of either, Dab2 or numb, increases surface levels of β1-integrins due to a reduced internalisation rate which affects total path length of migrating cells. Further fine tuning of β-integrin surface availability is achieved by differential localisation of the endocytic adaptors based on β-integrin activation status demonstrating the need for their specialisation. While Dab2 preferentially localises to unbound β-integrin at the dorsal surface to maintain an internal pool of inactivated adhesion receptors for recycling towards the leading edge (Teckchandani et al., 2009), numb 1 recruits the endocytic machinery to β1-integrins at the ventral surface in a phosphorylation-dependent manner (Nishimura and Kaibuchi, 2007)).

Also stonins represent such a specialised group of endocytic adaptors.

1.1.2. The stonin family

Originally, the stoned locus has been identified in a screen with temperature-sensitive *Drosophila melanogaster* (Grigliatti et al., 1973). At higher temperatures, mutants have had severe neurological defects and were paralysed inspiring researchers for the name 'stoned'. In *Drosophila melanogaster* the stoned gene is a dicistronic locus that translates into two proteins named stoned A and stoned B (Andrews et al., 1996). Stoned A and B are both expressed within the brain of flies (Andrews et al., 1996; Phillips et al., 2000) where stoned A expression and function depends on stoned B (Estes et al., 2003). Stoned B associates with synaptic vesicles and interacts via its μ-homology domain with C2B domains of synaptotagmins (Syt) which are calcium sensors localising on synaptic vesicles and mediating synaptic vesicle docking and fusion (Gustavsson and Han, 2009). Consequently, stoned depletion affects Syt endocytosis and sorting, resulting in defects in stimulated excitatory junctional potentials (Stimson et al., 2001), clearly demonstrating a pivotal role for stoned in synaptic vesicle retrieval and recycling (Stimson et al., 2001). In fact, genetic ablation of stoned is lethal for *Drosophila melanogaster* (Phillips et al., 2000).

Later on, the regulatory role for synaptic vesicle retrieval has been solely ascribed to stoned B (Estes et al., 2003) of which two orthologues exist in mammals, stonin 1 and 2 (Martina et al., 2001). Like stoned B, stonin (Stn) 2 fulfils an important role in synaptic vesicle retrieval. It functions as endocytic adaptor for synaptotagmin 1 and 2 (Diril et al., 2006; Martina et al., 2001) and facilitates Syt1/2 uptake via clathrin-mediated endocytosis (Diril et al., 2006). In mice, Stn2 is required for proper sorting of Syt1 to balance retrieval rate and release probability of synapses (Kononenko et al., 2013).

While Stn2 is pronouncedly expressed in the hippocampus of the brain (Walther et al., 2004), its close homologue Stn1 is mainly found in lung tissue and female reproductive organs (Feutlinske, 2014) indicating a function distinct from Stn2. Stn1 co-localises with members of the endocytic machinery including clathrin, AP2, dynamin and intersectin but most strikingly with numb (Feutlinske, 2014). Like numb, Stn1 localises directly behind focal adhesions (FAs) at the protrusive front and at the trailing end of migrating cells indicating an important role of Stn1 in cell motility. In fact, depletion of Stn1 increases directional migration of mouse embryonic fibroblasts pointing towards a role for focal adhesion dynamics. Based on the assumption that specific cargos would accumulate at the cell surface if their endocytic adaptor is missing, Feutlinske (2014) has identified potential cargos of Stn1. Amongst these,

the neuron glial antigen 2 (NG2) - an important regulator of cell adhesion, signalling and migration (see section 1.2.4) - has been found to be strikingly enriched at the plasma membrane of Stn1 KO cells. Further analysis has revealed that Stn1 facilitates the uptake of NG2 to balance the migratory behaviour between random and persistent migration.

All stonins have the same basic structural design: they consist of an unfolded N-terminus of variable length, a central stonin homology domain (SHD) specific for stonin members and a C-terminal μ-homology domain (μHD) which is homologous to the μ-subunit of AP2 (figure 1.2). Comparing protein sequences of mouse Stn1 and 2 shows that homology exists mainly between the SHDs and the μHDs (Diril, 2005). The N-terminal regions are only thus far comparable as they contain serine- and proline-rich sequences and interaction motifs for the endocytic machinery. WxxF motifs interact with the β-barrel of the AP2 α-ear linking the endocytic adaptors together (Mishra et al., 2004; Walther et al., 2004). Further complex formation and reinforcement with the endocytic machinery is supported by NPF motifs that interact with Eps15-homology (EH) domains of intersectin 1 and Eps15 (Martina et al., 2001).

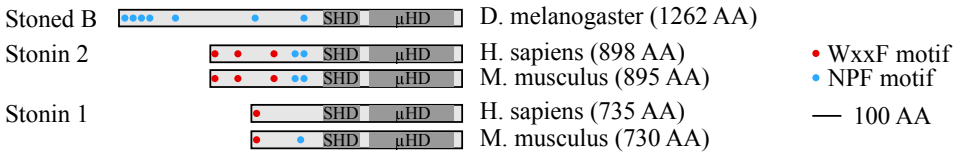

Figure 1.2.: Domain structure of stonins. Stonins comprise an unstructured aminoterminus, a central SHD and a carboxyterminal μHD. Localisation of interaction motifs is indicated by colour-coded dots. Legend and AA scale are indicated on the right side. Modified from Maritzen et al. (2010). (*AA - amino acids, μHD - μ-homology domain, SHD - stonin homology domain*)

1.2. Migration

CME is substantial for cell signalling processes by controlling cell surface receptor availability. Particularly focal adhesions depend on the precise spatio-temporal distribution of adhesion receptors at the cell surface allowing cell polarisation and directed cell migration (Maritzen et al., 2015). For example, numb and Dab2 act as specific endocytic adaptors for ligand-bound and unbound β1 integrins to regulate their subcellular localisation thereby controlling migration of cells (section 1.1.1). Hence, altered endocytosis affects focal adhesion dynamics and migration.

To achieve displacement, cells need to balance attachment and detachment. As such, cell

migration is characterised by four main steps also known as 'cell motility cycle': Polarised protrusion extensions (1) are stabilised by focal adhesions on the substratum (2) to allow acto-myosin contraction for displacement (3). Finally, disassembly of of focal adhesions releases the trailing end (4, Reig et al. 2014).

1.2.1. The Actin cytoskeleton of mesenchymally migrating cells

Mesenchymal cells migrating in two dimensions typically exhibit a fan-like shape (figure 1.3). Cellular shape is defined by the cell cytoskeleton consisting of microtubules, intermediate filaments and the Actin cytoskeleton. However, only the Actin cytoskeleton provides the predominant contractile element to regulate mechanical tension and traction force needed for translocation (Huber et al., 2015; Pollard and Cooper, 2009).

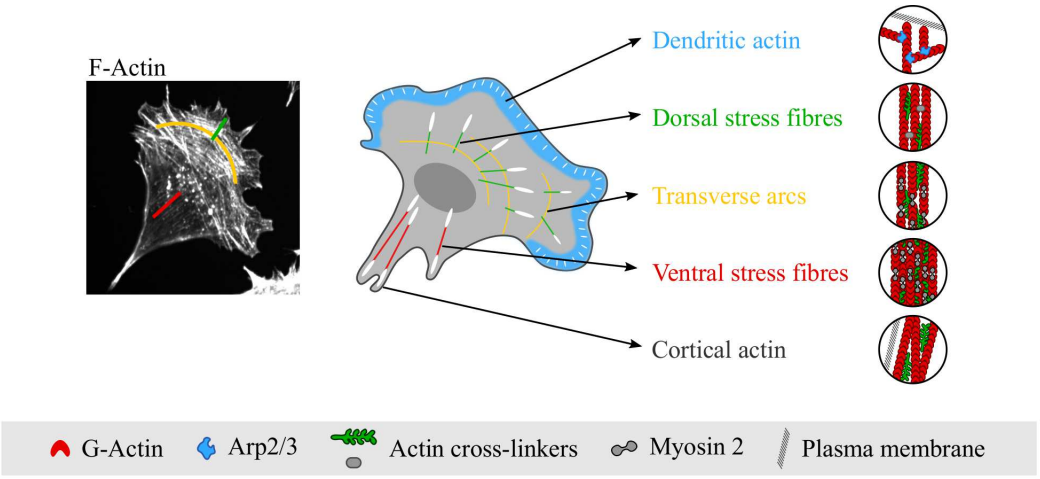

Figure 1.3.: Actin stress fibre subtypes of migrating mesenchymal cells. F-Actin network in mouse embryonic fibroblasts (left side) and a colour-coded schematic representation of the Actin cytoskeleton (middle). The structural organisation of the Actin cytoskeleton is highlighted on the right side.

The Actin cytoskeleton consists of a variety of Actin filaments assembled as two helix-like entwined Actin monomer chains. Globular Actin (G-Actin) exists in an ATP-bound and ADP-bound state which controls self-assembly. ATP-bound G-Actin can spontaneously assemble into trimers in a thermodynamically unfavourable reaction. Once trimers are formed rapid elongation with simultaneous ATP hydrolysis generates filamentous (F-Actin) of up to 10 µm length (Huber et al., 2015). Actin filaments possess a pointed and barbed end defined by a lower and a higher concentration of ATP-bound G-Actin, respectively. Since

F-Actin polymerisation is favoured at the barbed end, the average Actin filament moves forward. Additionally, G-Actin assembly as well as F-Actin disassembly are controlled by Actin regulatory proteins. Profilin mainly interacts with ATP-bound G-Actin thereby stimulating Actin nucleation and assembly (Carlier and Shekhar, 2017). At the plasma membrane nucleation is facilitated by Actin nucleation factors like formins which stimulate linear elongation of Actin filaments or the Arp2/3 complex generating branched Actin networks with a 70° angle. Spatio-temporal control of the Actin nucleation factors is achieved through small GTPases of the Rho family (Hodge and Ridley, 2016). Small GTPases cycle between an active GTP-bound, membrane-associated state and an inactive GDP-bound cytosolic pool (Fritz and Pertz, 2016). Their activity is regulated by interactions with guanine nucleotide exchange factors (GEFs) and GTPase activating proteins (GAPs) that facilitate GDP to GTP exchange and GTP hydrolysis, respectively. Once activated, a membrane anchor is unleashed from guanine nucleotide dissociation inhibitors (GDIs) allowing free diffusion within membrane compartments and interaction with effector proteins. The best studied members involved in migration are Cdc42, Rac1 and RhoA which control protrusion formation and acto-myosin contraction (Fritz and Pertz, 2016).

Cell locomotion is initiated by protrusion formation at the leading edge of the cell in response to guidance cues embedded in the extracellular matrix (ECM). Cdc42 and Rac1 act complementary downstream of cell signalling receptors and stimulate association of the nucleation promoting factors N-WASP and WAVE association with the Arp2/3 complex (Clainche and Carlier, 2008). Subsequent activation of the Arp2/3 complex initiates extensive Actin branching and formation of the characteristic dendritic Actin network in the lamellipodium (figure 1.3). RhoA opposes the action of Cdc42 and Rac1 by increasing the bundling of Actin filaments and stimulating contractility along Actin stress fibres. Enhanced engagement with the plasma membrane through β1 integrins increases RhoA activity leading to stimulation of Rho kinase (ROCK) (Danen et al., 2002, 2005). Subsequent phosphorylation of myosin-light chain phosphatase inhibits dephosphorylation of myosin 2 and increases its contractile activity. In parallel, ROCK acts on LIM kinase (LIMK) thereby leading to stabilisation of Actin filaments by regulating the activity of the Actin depolymerising factors Destrin/Cofilin (Arber et al., 1998; Yang et al., 1998).

Destrin and Cofilin have been demonstrated to bind to F-Actin leading to depolymerisation of Actin filaments (Vartiainen et al., 2002). Since both proteins share over 70% amino

acid sequence homology (Vartiainen et al., 2002) they are believed to function in similar ways and often referred to as Cofilins (Kanellos and Frame, 2016). On the structural level, Cofilin binding to Actin filaments increases the torsion along the filament which increases the filament flexibility and ultimately severs the Actin filament (Bravo-Cordero et al., 2013). Cofilin activity is tightly controlled by three main mechanisms. First, phosphorylation at Serine 3 by LIMK inhibits F-Actin binding and subsequent severing (Arber et al., 1998; Yang et al., 1998). Second, binding to PI(4,5)P_2 sequesters the actin depolymerising factors at the plasma membrane and inhibits their Actin depolymerisation activity (Gorbatyuk et al., 2006; Yonezawa et al., 1990). And third, the interaction of Cofilin with Cortactin blocks Cofilin activation in invadopodia. F-Actin filaments that have been separated by Destrin/Cofilin can get either capped for filament stabilisation and re-usage or depolymerised to allow regrowth of the protrusion (Carlier and Shekhar, 2017).

The generated Actin stress fibres differ in their molecular composition and form specific subtypes (figure 1.3, Vallenius 2013). Dorsal stress fibres (DSFs) are formed by formins which localise to focal complexes to stimulate linear elongation of Actin filaments towards the cell center (Gateva et al., 2014; Skau et al., 2015). DSFs depend on α-Actinin incorporation to crosslink the generated parallel Actin filaments (Kovac et al., 2013). While associating with focal contacts on one side, DSFs often attach to transverse arcs (TAs) on the other. TAs do not associate with focal contacts on either side (Hotulainen and Lappalainen, 2006). They assemble through antiparallel annealing of short Actin fragments generated in the lamellipodium. Annealing is achieved by Myosin 2 incorporation which make TAs contractile structures which flow towards the cell nucleus as the cell moves forward. Similar to TAs, ventral stress fibres (VSFs) form, however, VSFs maintain focal adhesion association (Tojkander et al., 2015). These have been shown to form through annealing of distal DSFs attached to the TAs in the process of Actin retrograde flow. Hence, also VSFs are enriched in Myosin 2 and contribute to acto-myosin contractility of the cell.

Through interaction with focal contacts Actin fibres allow cell displacement. DSFs and TAs convey tension to leading edge focal adhesions supporting focal adhesions growth and traction force transmission. VSFs control front-rear polarity by maintaining focal adhesions within the retracting tail to direct cell locomotion.

1.2.2. The focal adhesion lifecycle

Focal adhesions (FAs) are cell - ECM contact sites that transmit the force generated from the Actin cytoskeleton to the ECM via cell surface receptors. They are highly complex and intrinsically dynamic to allow fast responses to extracellular cues. This is also illustrated by the fact that over 2400 proteins have been identified to localise to focal adhesions (Horton et al., 2015). However, the core of these structures consists only of about 60 proteins. Central element of focal adhesions are integrins. Integrins are complexes of α and β subunits generating 24 heterodimeric adhesion receptor combinations that cluster into higher order structures during focal adhesion growth (Margadant et al., 2011). Each subunit consists of a large ectodomain binding to ECM components, a transmembrane stretch and a short cytosolic tail. Integrin dimers exist in three different conformations defining their activation status: resting receptors convert from a bent 'closed' into an extended-closed and further into a ligand-bound, extended-open conformation that correspond to a low affinity, an activated and an activated ligand-bound state (Eng et al., 2011). Of note, integrin activation and subsequent signalling can occur in two directions. As traditional signalling receptors, integrins bind to their corresponding ligand, like fibronectin or collagen, to regulate cell polarity through the Actin cytoskeleton (outside-in signalling, Shattil et al. 2010). By interaction with integrin-activating proteins like kindlin or talin, integrins control cell adhesion strength and ECM remodelling (inside-out signalling).

In the course of cell migration, focal adhesions undergo extensive maturation which crucially depends at all stages on the Actin cytoskeleton (figure 1.4). Small punctate structures (∼1 μm) forming within the protrusive front are called nascent adhesions (NA, Sun et al. 2014). Formation of NAs requires Actin polymerisation and is proportional to the rate of protrusion expansion (Choi et al., 2008). Bachir et al. (2014) have demonstrated that within nascent adhesions, β1 integrin activation is initially stabilised and promoted by kindlin. The integrin engagement acts as a molecular clutch to mechanically link the Actin cytoskeleton to the ECM (Mitchison and Kirschner, 1988). Tension above a certain threshold is transmitted to the mechanosensitive protein talin which further activates integrins but also increases the integrin - Actin bonding through direct binding and vinculin recruitment (Elosegui-Artola et al., 2016; Swaminathan and Waterman, 2016). Nascent adhesions not receiving tension will disassemble. In addition to kindlin and talin, focal adhesion kinase (FAK) is recruited by integrin engagement at early time points. Subsequent FAK autophosphorylation at position

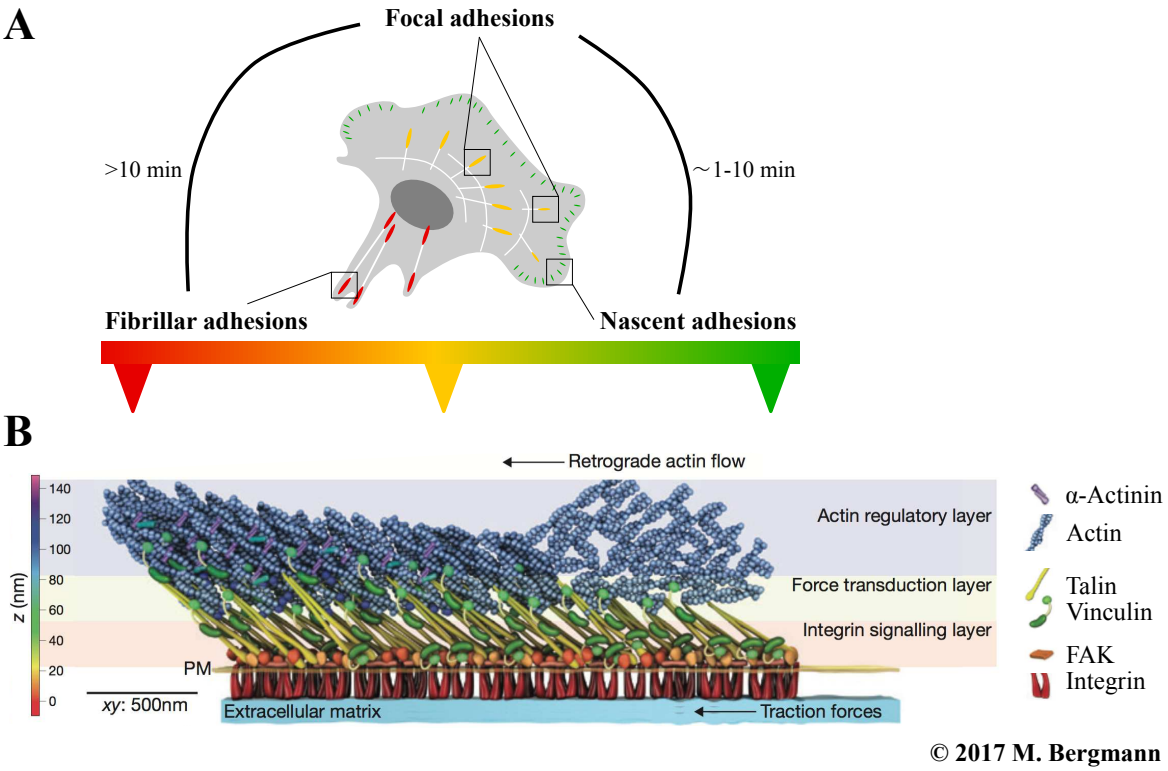

Figure 1.4.: Structure of focal adhesions. **A)** During migration cells develop three main types of focal adhesions. Small nascent adhesions (green) residing within the lamellipodium mature into focal adhesions (yellow) that are associated with the Actin cytoskeleton (white). Ongoing maturation results in formation of fibrillar adhesions (red) that determine trailing end stability by being strongly connected to the Actin network. Maturation times are indicated (Scales and Parsons, 2011). **B)** Focal adhesions of all stages consist of three layers in z-direction: the integrin signalling, the force transduction and the Actin regulatory layer. With increasing maturation (right to left, note arrows above), the density within the focal adhesion rises due to recruitment of further focal adhesion components. Additionally, the dendritic Actin network gets bundled and crosslinked to allow traction force transmission. All steps are within a continuum preventing discrete separation between focal adhesion types. Characteristic components are indicated on the right side. Modified from Case and Waterman (2015), license number: 4075981422979. (*FAK - focal adhesion kinase, PM - plasma membrane*)

Y397 results in FAK activation which is required to form a dense band of NAs but is dispensable for NA stabilisation. p(Y397)FAK induces a dense NA - Actin network by recruiting Arp2/3. This in turn lowers FAK activity and leads to NA stabilisation and focal adhesion growth (Swaminathan et al., 2016). Mature focal adhesions are bigger in size (~10 μm, Sun et al. 2014) and show an increased density of integrins (Ballestrem et al., 2001). Maturation depends on cell signalling proteins and increasing structural support both reinforcing recruitment of further focal adhesion proteins (Polacheck et al., 2012). FAK recruitment is a

hallmark of focal adhesion maturation by post-translationally modifying downstream targets which affects their FA residential time (Horton et al., 2015). Additionally, maturation needs a stress fibre template allowing feed-forward reinforcement of focal adhesions (Choi et al., 2008). α-Actinin binding establishes first connections with the Actin cytoskeleton thereby allowing focal adhesion maturation (Bachir et al., 2014). However efficient force transmission is only achieved after Actin filament rearrangement into parallel fibres (Hotulainen and Lappalainen, 2006). Subsequent myosin 2 incorporation generates the necessary contractility which activates and recruits stretch-sensitive focal adhesion proteins resulting in focal adhesion growth (Vicente-Manzanares et al., 2009). Since enhanced contractility increases ECM stiffness (inside-out signalling), focal adhesion growth is further stimulated (outside-in signalling). This activation loop stimulates formation of fibrillar adhesions (>10 μm) which are strongly associated with Actin fibres that have a high degree of crosslinking with myosin 2 as well as α-Actinin.

To balance adhesion and detachment, focal adhesions undergo constant component exchange (Horton et al., 2015) and disassembly (Nagano et al., 2011). Microtubules have been shown to contact focal adhesions to initiate their disassembly (Stehbens and Wittmann, 2012). It has been suggested that microtubules are recruited to FAs by (+)-end microtubule interacting proteins (Stehbens et al., 2014) where they potentially activate p(Y397)FAK-bound dynamin (Ezratty et al., 2005) to induce clathrin-mediated endocytosis (Chao et al., 2010; Ezratty et al., 2009). This mechanism contributes to FA turnover at the distal region of the lamellipodium as well as at the trailing end. Additionally, focal adhesion stability at the trailing end is regulated by the calcium-dependent cysteine protease calpain (Franco and Huttenlocher, 2005). Calcium influx, for instance through the stretch-sensitive TRPM7 ion channel (Su et al., 2006), activates the protease near FAs and subsequent cleavage of FA components like talin, paxillin or FAK triggers structural weakening of focal contacts (Franco and Huttenlocher, 2005).

1.2.3. Steering directional cell migration

Mesenchymal cells migrating on a two-dimensional surface can switch between directional and random movements (Petrie et al., 2009). Random motility behaviour describes an indiscriminate migration mode often occurring when no chemoattractant is present. Directional

migration is characterised as continuous cell body translocation into one direction. This migration mode is predominantly found when cells follow a chemotactic gradient. Visually both migration modes can be differentiated by the protrusion appearance: Randomly migrating cells probe the substratum into multiple directions while directional migrating cells reinforce the most stable protrusion giving the cells an elongated shape (Arrieumerlou and Meyer, 2005). While growth factor signalling guides the orientation of the leading edge, protrusion stability is predominantly influenced by the ECM topography and cell adhesion (Andrew and Insall, 2007).

Chemotactic gradients of growth factors lead to polarisation of cells and subsequent directional migration (Petrie et al., 2009). Most growth factors like the epidermal (EGF) or platelet derived growth factor (PDGF) bind cell surface receptor tyrosine kinases. Upon ligand binding at the ectodomain the receptors dimerise and activate their cytosolic receptor tyrosine kinase for *trans* autophosphorylation at multiple sites. This enhances on the one hand the internal kinase activity and generates on the other hand src homology 2 (SH2) or PTB domain binding sites for interaction partners like Grb2 (Lemmon and Schlessinger, 2010) which stimulates the classical PI3K/Akt and mitogen-activated protein kinase (MAPK) signalling pathway amongst others (Berg et al., 2007). Concomitantly, the receptor dimers are internalised via endocytosis, sorted into recycling endosomes or multi-vesicular bodies resulting in trafficking to the plasma membrane or lysosomal degradation, respectively (Goh and Sorkin, 2013).

PDGF is a well-studied, potent chemoattractant for fibroblasts (Seppa et al., 1982). It exists as a dimer of four different polypeptide chains, and to date 5 different ligands have been identified (PDGF-AA, AB, BB, CC and DD, Fredriksson et al. 2004). Though PDGF was originally identified to be secreted by activated platelets, its expression has been demonstrated in all tissues and most cell types including cells of the neovasculature, immune cells and muscle cells (Noskovicova et al., 2014). The three PDGF receptor subtypes ($\alpha\alpha$, $\alpha\beta$ and $\beta\beta$) have a characteristic specificity for the different ligands. Amongst these only PDGF-BB can activate all receptors (Fretto et al. (1993) inducing the canonical pathway (see above). In addition, the active PDGF receptor binds the cytosolic tyrosine kinase Src via SH2 domains which subsequently phosphorylates FAK (Seong et al., 2011) and links the FA as well as the PDGFR signalling pathway together. Active FAK promotes the association between the Rac

GEF βPix and the RhoGTPase, thereby enhancing Rac localisation to focal adhesions at the cell front (Goicoechea et al., 2014). Hence, FAK plays a key role for PDGF-stimulated cell migration (Sieg et al., 2000). In addition, Src creates paxillin docking sites for the p130Cas-Crk complex which recruits Rac via its GEF DOCK180 to leading edge focal adhesions. Downstream of growth factor signalling, Cdc42 is activated by the GEF Vav2 which is recruited and activated by active Src. Additionally, Cdc42 phosphorylation through Src potentiates its action (Tu et al., 2003). However RhoGTPase activation requires PDGF receptor endocytosis and traffic through the early endosomal compartment (Huang et al., 2011). Following PDGFR internalisation, Cdc42 as well as Rac1 are recruited to the leading edge in a RhoB dependent mechanism which stimulates cell motility.

Furthermore, stimulation with growth factors like EGF (Orth et al., 2006), PDGF (Eriksson et al., 1992) or the hepatocyte growth factor (Dowrick et al., 1993) induces the characteristic formation of circular dorsal ruffles (CDRs). Amongst the growth factors identified, PDGF is one of the best studied growth factors inducing the phenomenon, however, from the 5 ligands only activation of PDGFRβ via PDGF-BB binding induces CDRs (Eriksson et al., 1992; Hammacher et al., 1989). These are Actin filaments emerging as 'Actin-rings' at a central region of the dorsal plasma membrane within few minutes after stimulation in a Rac-dependent way (Hoon et al., 2012; Itoh and Hasegawa, 2012). Actin polymerisation via Arp2/3 is accompanied by BAR-domain proteins shaping membrane curvature. CDR constriction leads to lamellipodium formation and cell migration along the chemotactic gradient (Krueger et al., 2003; Sero et al., 2011). Although their function is still under debate, CDRs have been demonstrated to stimulate fast internalisation of growth factor receptors, particularly the EGF receptor (Orth et al., 2006). This might potentiate receptor signalling and subsequent cell motility (see above, Hoon et al. 2012). In addtion, PDGF stimulation facilitates rapid recycling of α5β1 but not αVβ1 integrin through the fast recycling route via Rab4 (Roberts et al., 2001). In fact Gu et al. (2011) demonstrated that integrins are rapidly internalised from the ventral surface through fast relocalisation to CDRs and internalisation via macropinocytosis. This allows fast breakdown of focal adhesions upon a stimulus to redirect cell polarity towards the chemoattractant.

In the organism, cell signalling molecules like growth factors are typically released from the ECM. The extracellular matrix is composed as a meshwork of proteins and polysaccharides

which is unique for every tissue and surrounds cells thereby acting as substratum (Frantz et al., 2010; Theocharis et al., 2016). Through focal adhesions, cells probe the ECM for compositional as well as biomechanical information. Specific cell surface receptors like the α1β1 integrin sensing collagens or α7β1 integrin binding laminin (Margadant et al., 2011) translate the ECM composition for the cell and support cell polarisation. The RhoGTPase Cdc42 plays crucial roles for cell polarisation (Etienne-Manneville, 2004). Integrin ligand recognition induces cell polarisation via active Cdc42 recruiting Par3/6 and its associated protein kinase Cζ to reorientate the microtubule orientation centre and Golgi network towards the leading front of the cells (Etienne-Manneville and Hall, 2001). Thus integrin-rich adhesions translate the ECM composition into a guidance cue. Simultaneously focal adhesions act as molecular clutches that remodel the ECM architecture in a positive feed-backward loop (section 1.2.2) which generates a mechanical cue for following cells (Gaggioli et al., 2007).

Migration persistence also depends on focal adhesion stability which is determined by integrin surface levels regulating cell polarisation via Cdc42 and Rac1 activity (section 1.2.1). Besides CME (section 1.1.1) integrin surface expression is also regulated via the small GTPase ADP-ribosylation factor 6 (Arf6, Morgan et al. 2013). Differential phosphorylation of the proteoglycan syndecan 4 by Src controls Arf6 activity to regulate the surface levels of the integrin subtypes αVβ3 and α5β1 thereby controlling persistence of migration. Following endocytosis, cooperative action of different trafficking routes provides fast recovery of the integrin pool at the leading edge (De Franceschi et al., 2015). Integrins are either rapidly recycled via Rab4 compartments or via the long loop through the Rab11 positive recycling endosomal compartment towards the leading edge. In addition, transport of inactive β1 integrin through the trans-Golgi network to the leading edge complements the Rab4 endocytic route to steer persistent cell migration (Shafaq-Zadah et al., 2016). Kif1-dependent rearward trafficking of β1 integrins stabilises trailing end focal adhesions to establish the migratory direction (Theisen et al., 2012).

1.2.4. Neuron glial antigen 2 (NG2) - A cargo of Stn1

Besides integrins also other cell surface receptors like proteoglycans contribute to ECM recognition and cell adhesion (Theocharis et al., 2016) thereby playing important roles in health and disease including embryonic development and cancer progression (Cattaruzza and Per-

ris, 2005). Proteoglycans are characterised as a core protein modified with at least one glucosaminoglycan (GAG) chain of variable length and composition. Transmembrane proteoglycans encompass syndecans, glypicans, betaglycan, phosphacan and the neuron glial 2 (NG2). By performing surface biotinylation experiments with WT and Stn1 KO cells we identified NG2 internalisation to be dependent on Stn1 expression (Feutlinske, 2014).
NG2, also known as melanoma-associated chrondroitin sulfate proteoglycan 4 (CSPG4), is differentially expressed during development (Niehaus et al., 1999) and healing processes following injuries (Jones et al., 2002). Originally NG2 was identified to be expressed by oligodendrocyte precursor cells which cease its expression upon differentiation into mature oligodendrocytes (Stallcup and Beasley, 1987) thereby limiting proliferation of the cell type (Dawson et al., 2003; Kucharova and Stallcup, 2010). Similarly NG2 is present at early stages of cartilage development being expressed by immature chrondrocytes (Midwood and Salter, 1998; Nishiyama et al., 1991). Its presence on pericytes, a cell type covering predominantly capillaries, supports endothel connectivity (Ozerdem et al., 2002; Ozerdem and Stallcup, 2004). Also here development into higher-degree vessels which is accompanied by differentiation of pericytes into vascular smooth muscle cells or myofibroblasts diminishes the expression of the proteoglycan (Barron et al., 2016; Hung et al., 2013). The role of NG2 in pathological situations can often be traced back to its progenitor role in NG2-positive cells. For instance, upon lesion precursor oligodendrocytes upregulate NG2 expression levels to stimulate cell proliferation thereby supporting wound healing by remyelination (Jones et al., 2002; Kucharova et al., 2011).

Through interactions with growth factors, cell surface receptors and extracellular matrix (ECM) components, proteoglycans participate in the organisation of the ECM and support signal transduction towards the inside of the cell and vice versa (Theocharis et al., 2016). NG2 is a 300 kDa type 1 transmembrane protein whose structure was first described by Nishiyama et al. (1991). Most of the protein is exposed to the extracellular space and only 76 amino acids represent the cytosolic domain (figure 1.5). The extracellular part can be subdivided into 3 domains: the N-terminal domain whose globular structure is stabilised by disulfide bridges, the central part containing the collagen binding domain with a chrondroitin sulfate chain, and the globular domain which is post-translationally modified with N-linked sugars and can get proteolytically cleaved by metalloproteases (Stallcup and Huang, 2008). The globular amino-terminal laminin G domains of the proteoglycan NG2 are thought to

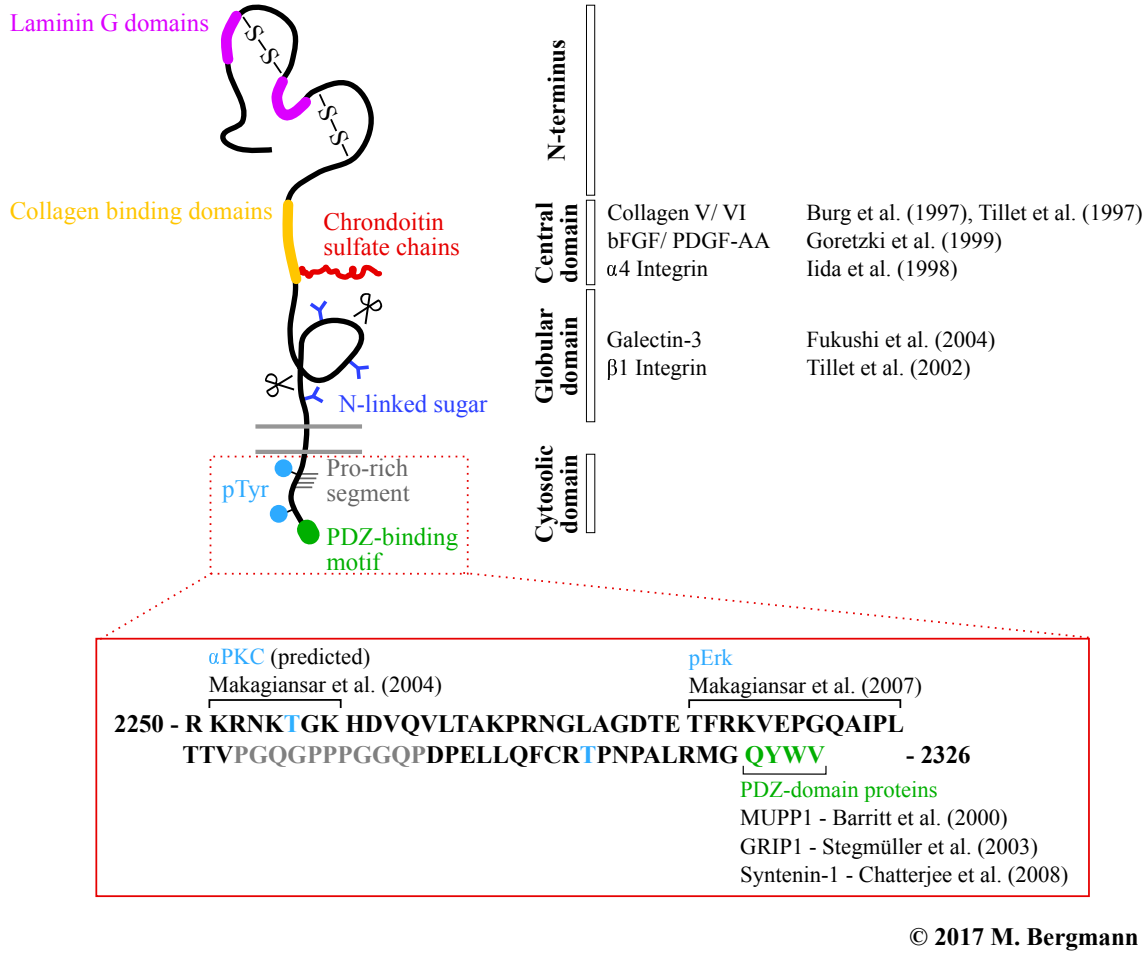

Figure 1.5.: NG2 domain structure and interaction sites. The extracellular part of NG2 constitutes over 90% of the proteoglycan and is subdivided into the N-terminus, the central and the globular domain. The transmembrane segment separates the ectodomain from the short cytosolic stretch (lower box, sequence from rat). The type 1 transmembrane protein captures ligands for cell signalling and binds extracellular matrix components as well as integrins to facilitate cell adhesion. Localisation of the protein is regulated by intracellular phosphorylation events mediated by αPKC and pErk and by recruitment of PDZ-domain proteins like MUPP1, GRIP1 or syntenin 1. Structural features and modifications are indicated on the left side. Mapped interaction sites and according references for the ectodomain are stated on the right side while those of the cytosolic domain are noted within the lower box. Within the primary sequence of rat NG2, the phosphorylation sites, the proline-rich segment as well as the PDZ-binding domain are marked in the same colour code as within the scheme. Scheme is based on Stallcup and Huang (2008), license number: P052317-03. (*pErk - phosphorylated extracellular signal-regulated kinase 1, PDZ - PSD95/ Dlg1/ ZO1, PKC - protein kinase C, GRIP1 - glutamate receptor-interacting protein 1, MUPP1 - multi-PDZ domain protein 1*)

mediate the interaction with the extracellular matrix protein laminin 1 (Burg et al., 1996; Tillet et al., 1997) however no function has been reported so far (Tillet et al., 2002). NG2 also interacts with collagen V and VI via the central domain of NG2 (Burg et al., 1997)

to reinforce cell adherence as well as spreading (Stallcup and Huang, 2008) and chemotaxis towards Collagen VI. NG2 also potentiates engagement with the extracellular matrix via integrin receptors. By binding to the α4 subunit of α4β1 integrin complexes with the central domain (Iida et al., 1998, 1995) and also by interacting with α3β1 integrin heterodimers with the globular domain (Tillet et al., 2002) NG2 supports cell attachment. Integrin activation by NG2 can be further increased by galectin-3 association which stimulates endothelial cell migration and angiogenesis (Fukushi et al., 2004). In addition, NG2 can act as a co-receptor for cell signalling receptors by capturing ligands like the platelet-derived growth factor AA (PDGF-AA) or the basic fibroblast growth factor (bFGF, Goretzki et al. (1999) to facilitate growth factor signalling. Block of its co-receptor function for PDGFRα or the FGF receptor types 1 and 3 results in decreased proliferation and chemotaxis (Cattaruzza et al., 2013; Grako et al., 1999; Grako and Stallcup, 1995).

While the extracellular domain exerts major functionality with regard to co-receptor function (Cattaruzza et al., 2013), the intracellular domain bears key regulatory elements for cell polarisation and cell adhesion (Binamé, 2014). The intracellular domain contains two phosphorylation sites that regulate migration and proliferation of cells. Phosphorylation on T2256 by PKCα stimulates cell motility by shifting the subcellular localisation of NG2 to the leading edge (Makagiansar et al., 2004). Subsequent phosphorylation at T2314 by the activated extracellular signal-regulated kinase (pErk) stimulates cell proliferation (Makagiansar et al., 2007). The balance between both is believed to depend on the differential interaction of NG2 with α3β1 integrins (Stallcup and Huang, 2008). Upon T2256 phosphorylation NG2 co-localises with the adhesion receptor at the protrusive front stimulating clustering of focal adhesion components. Phosphorylation on T2314 enhances the localisation of the NG2 - integrin complex to microprojections on the apical surface of cells. There, α3β1 integrins signal predominantly through cell signalling molecules that are involved in proliferation. Additionally, interactions with the PDZ-domain containing proteins multi-PDZ domain protein 1 (MUPP1, Barritt et al. 2000) and Syntenin 1 (Chatterjee et al., 2008) support clustering of NG2 with cell signalling components thereby stimulating cell motility (Binamé, 2014). NG2 also forms a complex together with the glutamate receptor-interacting protein 1 (GRIP), another PDZ-domain containing protein, and AMPA receptors in glial cells potentially to assist the formation of synapses between glial cells and neurons (Stegmüller et al., 2003).

Additional interactions with the PDZ-domain containing proteins glutamate receptor-inter-

acting protein 1 (GRIP1, Stegmüller et al. 2003), multi-PDZ domain protein 1 (MUPP1, Barritt et al. 2000) and Syntenin 1 (Chatterjee et al., 2008) support clustering of NG2 with receptors, cell signalling and stimulate cell motility, respectively (Binamé, 2014). However, most substantially NG2 assists intracellular signalling via the RhoGTPases Cdc42 (Eisenmann et al., 1999), Rac1 (Majumdar et al., 2003) and RhoA (Binamé et al., 2013; Pankova et al., 2012). NG2 clustering activates Cdc42 which recruites p130Cas that might associate with the Rac1 GEF DOCK180 to direct α4β1 integrin-mediated spreading. Increased surface levels of NG2 stimulates RhoA activity thereby promoting cell polarity and directional migration of oligodendrocyte precursor cells and invasive behaviour of cancer cells. Balance of the RhoGTPase activity of RhoA and Rac1 is mediated by T2256 phosphorylation of NG2 which stimulates recruitment of the PAR polarity complex via the Rac1 GEF Tiam1 (Binamé et al., 2013).

Taken together, NG2 is a surface-bound proteoglycan supporting the readout of the ECM topology into cellular guidance cues and promoting cell polarity and cell motility by intracellular signalling. It is therefore not surprising that NG2 has been shown to promote tumour growth (section 1.3.4).

1.3. Tumour development and progression

In 2014 every fourth German died due to cancer. As a result, cancer is behind cardiovascular diseases the second most frequent cause of death in Germany (Robert-Koch-Institut, 2016). 2013 about 480.000 new cases were recorded and an increasing tendency is expected over the next years urging for successful therapies. A combination of surgery, radio- and chemotherapy heals about 60% of patients, however, 40% cannot be cured still.

1.3.1. Key aspects of tumour progression

Once cells suffer from genetic modifications that support tumour growth the following main stages of tumour progression can be observed (figure 1.6). The initial proliferation of the pre-malignant cells is accompanied by secretion of chemoattractants like PDGF to recruit surrounding cells. Amongst these are typically fibroblasts, residential macrophages and cells of the perivasculature which will support stiffening of the surrounding extracellular matrix to enable tumour cell invasion and connectivity to the vasculature to overcome hypoxia and nutrient starvation. Escaping malignant cells often use the blood circulation to occupy new

areas of the organism. With increasing progression through these stages chances of a cure decrease steadily.

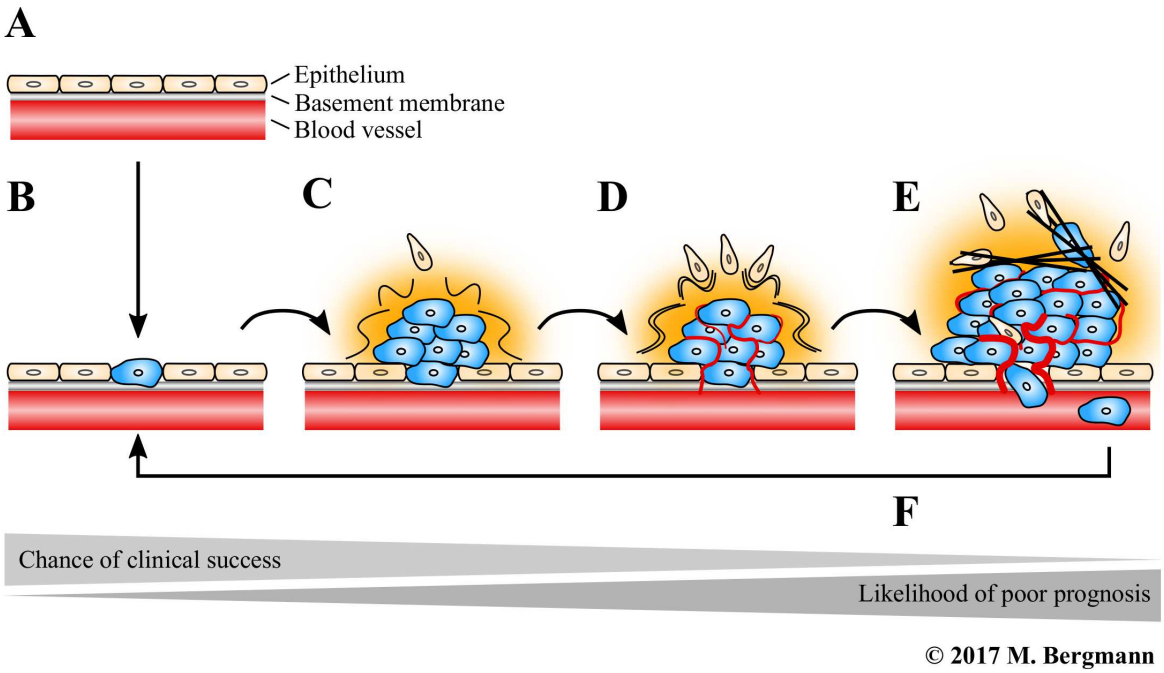

Figure 1.6.: Stages of tumour development. **A)** Healthy tissue. **B)** Oncogenic event within epithelium or adhesion of malignant cells. **C)** Manifestation of pre-malignant tumour due to increased proliferation. Secretion of chemoattractants recruits stromal cells like pericytes and macrophages. **D)** Tumour vascularisation to supply growing tissue with nutrients. Stromal cells support stiffening of the surrounding ECM. **E)** Stromal cells guide the malignant cells through ECM fibres and assist tumour invasion. **F)** Cancer cells invade blood vessels to settle at new regions of the body.

Cancer development and severity has been suggested to depend on eight hallmarks that are progressively attained by genetically altered cells (Hanahan and Weinberg, 2011). Resistance against autologous (1) and immunological apoptotic signals (2) and the evasion of growth suppressors (3) prevents shrinkage of the cancerous colony. Together with a maintained proliferative signalling (4) a constant increase in total cells can be ensured. Tumour growth is accompanied by an increasing demand for nutrients and oxygen which is satisfied with reprogramming to an anaerobic metabolism (5) and increased neovascularisation (6). Alternatively, to escape from a limited or adverse growth area, malignant cells will promote cell invasion and metastasis of surrounding tissues (7). Finally, the emergence of cancer stem cells that secure the immortality of clonal colonies (8) ensures the necessary flexibility to react to environmental signals and resist chemotherapies. Though the initiation of a tumour mainly depends on the malignant potential of the tumour cells themselves, there is increasing evi-

dence that tumour cells manipulate cells of their environment (stromal cells) to assist tumour growth by supporting neovascularisation and tumour escape (Quail and Joyce, 2013).

1.3.2. Tumour vascularisation

Neovascularisation of tumour tissue ensures a sufficient supply of nutrients and oxygen for the growing tumour tissue thereby enabling large-scale tumour growth. Angiogenesis progresses through multiple steps that are tightly controlled (Herbert and Stainier, 2011). Endothelial cells outline the vasculature and prevent vessel leakiness by being tightly connected amongst each other in a resting state. When endothelial cells receive an angiogenic cue, they secrete proteases to degrade the basement membrane and gain an invasive behaviour to initiate vessel sprouting. Amongst the activated endothelial cells, leading cells (also called tip cells) guide the sprout by probing the surrounding for guidance cues. Follower endothelial cells (also named stalk cells) ensure the connectivity with the original vessel. When the 'convoy' reaches neighbouring vessels, fusion of the two structures generates lumen continuity to allow the blood flow.

The major driver of angiogenesis is the vascular endothelial growth factor (VEGF) which is expressed upon hypoxia of the tissue (Krock et al., 2011). Secreted from the surrounding tissue the ligand binds to its receptor which belongs to the receptor tyrosine kinases to stimulate growth factor signalling via the PI3K and MAPK pathways (see above). The receptor is typically expressed by endothelial cells and aids the discrimination between tip and stalk cells. The leading cells sensing VEGF gain a highly motile and invasive behaviour (Gerhardt et al., 2003). Additionally, VEGF signalling induces expression of the Notch ligand Delta-like 4 (Dll4 Lobov et al. 2007). Subsequent Notch signalling downregulates VEGFR expression to prevent tip cell behaviour in stalk cells (DelToro et al., 2010; Hellström et al., 2007; Williams et al., 2006).

To support integrity of the newly formed vessel, endothelial tip cells secrete PDGF-BB to attract pericytes which express the PDGFRβ (Trost et al., 2016). Pericytes are closely associated with the outer surface of the endothelial tube (Sims, 1986) and communicate with the endothelium to regulate the blood flow and vessel connectivity (Bergers and Song, 2005). Importantly, the PDGF-BB retention by the ECM seems crucial for the spatial regulation of PDGF-BB signalling to ensure tight association and functional communication between the two neighbouring cell types (Abramsson et al., 2003; Lindblom et al., 2003). Besides

stimulating the attraction of pericytes, PDGF-BB also promotes their proliferation to increase vessel coverage. In response to PDGF-BB, pericytes upregulate the gene expression of the transforming growth factor β (TGFβ) via the MAPK pathway (Nishishita and Lin, 2004) which stimulates pericyte attachment on the endothelium (Winkler et al., 2011). In addition, PDGF-BB signalling induces expression of the Tie2 ligand angiopoietin 1 via the PI3K/Akt signalling pathway (Nishishita and Lin, 2004) to support junction formation between endothelial cells resulting in stabilisation of the nascent vessel (Winkler et al., 2011).
Fast tumour growth and the increasing demand for oxygen increases VEGF secretion by malignant cells to stimulate angiogenesis (Krock et al., 2011). However, the VEGF-stimulated proliferation of the endothelium needs to be limited to establish functional blood vessels (Hellström et al., 2001). Secretion of PDGF attracts stromal cells including macrophages and pericytes, both contributing substantially to tumour development (Cao, 2013). In fact, pericyte recruitment leads to a hypervascularisation enabling large-scale tumour growth (Guo et al., 2003; Nissen et al., 2007; Xue et al., 2012) based on the mechanism described above. In addition to perivascular cells, residential as well as bone marrow derived monocytes are attracted by PDGF-BB and the colony-stimulating factor 1 (CSF-1). Upon arrival at the cancerous tissue monocytes differentiate into reactive macrophages to promote tumour angiogenesis (Noy and Pollard, 2014). Through the expression of Tie2, macrophages interact with angiopoietin 2 secreted by the endothel to stimulate release of additional angiogeneic factors (Mazzieri et al., 2011).

1.3.3. Tumour escape and metastasis

Another important aspect of tumour growth is the escape of malignant cells from the primary tumour tissue (metastasis). Extraction of metastases during autopsy and subsequent sequencing of the whole genome of each allowed Gundem et al. (2015) to follow cancer spreading through the human body. Metastasis occurred not only from the primary tumour but also from its subclones. From each of these mutagenesis can occur which might cause a high potential of multi-drug resistences in chemotherapy. Nevertheless, the individual heterogenity of cancer colonies is relatively little when compared to interindividual tumours (Kumar et al., 2016).
Macrophages as well as cancer-associated fibroblasts (CAFs) have been demonstrated to crucially regulate tumour escape and metastasis (Quail and Joyce, 2013). Fibroblasts are

normally quiescent but become activated following an injury. Reactive fibroblasts can be identified by α smooth muscle actin expression and their contractility that is necessary for wound closure (Kalluri, 2016). CAFs are reactive fibroblasts that have been recruited by the tumour tissue by PDGF-BB secretion (Forsberg et al., 1993; Franco et al., 2010). Similar to injury-situations, tumour secreted PDGF-BB stimulates fibroblast migration and proliferation as well as ECM secretion (Mueller and Fusenig, 2004). Due to their extensive deposition of ECM around the tumour tissue as well as their increased contractility, CAFs generate stiff collagen fibres that function as 'highways' for malignant cells (Frantz et al., 2010; Kalluri, 2016). Reactive macrophages complement the generated collagen fibres by secreting EGF into the generated collagen fibres to guide tumour cells to a site of intravasation (Noy and Pollard, 2014).

1.3.4. NG2-dependent contributions to tumour development

The proteoglycan NG2 has been demonstrated to stimulate tumour growth in many ways (Stallcup et al., 2016). Firstly, NG2 phosphorylation at T2314 by pErk stimulates cell proliferation (Makagiansar et al., 2007). In fact, the NG2-expressing cell population in brain is known to be the most proliferating cell population in the adult brain (Dawson et al., 2003). Hence, during development NG2 expression is tightly controlled to balance cell growth (Niehaus et al., 1999). In pathological situations such as during tumour development, however, the cells upregulate NG2 expression and elude the growth restriction (Wang et al., 2011). Furthermore, NG2 modulates RhoGTPase activity to control cell polarity and migration (Binamé, 2014). In fact, Pankova et al. (2012) have demonstrated that elevated NG2 levels correlate with a higher RhoA activity which stimulates increased invasiveness of cancer cells.

Nevertheless, a thorough analysis by Huang et al. (2010) demonstrated that NG2 expression in the tumour stroma has a far more severe consequence for the organism. NG2 is a well-established marker for the mural cell type pericytes (Ozerdem and Stallcup, 2004) which are recruited by PDGF-BB secretion to support neovascularisation (section 1.3.2). Pericyte-specific ablation of NG2 inhibited pericyte coverage of the endothelium resulting in decreased vessel integrity and reduced tumour growth (You et al., 2013). This is thought to depend on the pericyte - endothelium interaction mediated via NG2 - Galectin which promotes integrin

activation in the endothelium leading to increased tight-junction formation between endothelial cells (Fukushi et al., 2004; You et al., 2013). Deletion of NG2 in macrophages has an even more benefitial consequence (Yotsumoto et al., 2015). Like pericytes, macrophages are attracted by the tumour and promote angiogenesis of the tissue (section 1.3.2). In absence of NG2, macrophage recruitment is inhibited and consequently tumour progression is slowed due to reduced neovascularisation.

1.3.5. The role of clathrin-mediated endocytosis in tumour development

By regulating the surface availability of receptor proteins, CME controls many cellular functions including cell growth (McMahon and Boucrot, 2011). Consequently, clathrin-mediated endocytosis is often affected in malignant cells (McMahon and Boucrot, 2011; Mosesson et al., 2008). Classically, CME is known to regulate cell signalling by directing activated receptors like the ligand-bound EGF receptor into the endosomal-lysosomal pathway thereby leading to degradation of the receptor and termination of the signal. Thus, by downregulating the expression of endocytic proteins, malignant cells circumvent early termination of e.g. growth signals. Additionally, CME promotes internalisation of activated receptors to endosomes which are a central element of the endosomal-recycling pathway and function as internal signalling platforms. As a consequence, CME can also lead to amplification of cell signalling. Hence, by lowering expression levels of endocytic proteins, malignant cells may also circumvent signals that limit tumour growth.

For instance, the endocytic adaptor numb secures cells from malignancy by regulating the protein levels of the tumour supressor p53 (Colaluca et al., 2008). Numb forms a complex with p53 thereby blocking the E3 ubiquitin ligase Hdm2 from p53 ubiquitination which would result in p53 degradation. Consequently, the expression levels of the endocytic adaptor numb are often downregulated in malignant tissue (McMahon and Boucrot, 2011) leading to failures in p53-controlled functions. Like numb, Dab2 is downregulated in different cancer types suggesting a function as tumour suppressor (Tao et al., 2016). Though its precise function in cancer progression is still enigmatic, Dab2 has been demonstrated to be involved in controlling the MAPK pathway as well as focal adhesion dynamics and migration.

In contrast to numb and Dab2, epsin has been shown to be upregulated in cancer tissues to regulate neovascularisation via VEGF and Notch signalling (Tessneer et al., 2013). The epsin family facilitates the uptake of ubiquitinated surface-bound receptors like the EGFR

or VEGFR. VEGF signalling enhances the invasive, tip cell behaviour of endothelial cells (section 1.3.2). Epsin interacts with the ubiquitinated VEGF receptor to stimulate receptor internalisation and lysosomal degradation to downregulate receptor signalling. During angiogenesis this is of particular importance, to allow discrimination of stalk cells which maintain connectivity with the parental vasculature. In fact, epsin-deficiency promotes excessive VEGF signalling resulting in reduced tumour size due to insufficient blood flow through the newly formed leaky vessels (Pasula et al., 2012). In addition, epsin is required for Notch transcytosis and signalling (Chen et al., 2009; Tian et al., 2004) which is also indispensable for stalk cell identity (section 1.3.2).

1.4. Aims of the study

Clathrin-mediated endocytosis is of particular importance to regulate surface levels of receptor proteins which control diverse signalling cascades and cellular processes in health and disease. Nevertheless, many aspects of CME are still poorly understood. Since often cargo-specific endocytic adaptors support efficient uptake of cell surface receptors, their careful investigation will broaden our understanding of CME and the cellular processes CME is regulating. The stonins represents such cargo-specific endocytic adaptors. But although the stonin protein family was first identified over four decades ago (Grigliatti et al., 1973), we still lack detailed knowledge about one of its members - stonin 1. A previous study performed in our lab described Stn1 as a member of the endocytic machinery localising to focal adhesions (Feutlinske, 2014). In addition, Feutlinske (2014) identified the cell surface proteoglycan NG2 as a cargo of Stn1 and showed that Stn1-mediated internalisation of NG2 is required to prevent its accumulation at the plasma membrane and subsequent alterations in cellular motility. The molecular basis for the NG2 - Stn1 interaction, additional consequences of the impaired endocytic regulation of NG2 in absence of Stn1 as well as potential NG2-independent functions of Stn1 remained unexplored.

Consequently, the first part of the study aimed to dissect the molecular details of how Stn1 links its cargo NG2 with the endocytic machinery using biochemical experiments. To validate that the interaction between Stn1 and NG2 is also needed *in vivo* to regulate NG2 levels, we performed immunohistology in lung and brain of WT and Stn1 knockout mice. Since NG2 is a well known oncogene (section 1.3.4), we investigated the functional relevance of Stn1 *in vivo* with a particular focus on tumour development. To understand the impact

of Stn1-dependent internalisation of NG2 in tumour development, NG2-dependent processes including cell signalling, cell adhesion and directional migration (section 1.2.4) were carefully examined in cell biological experiments.

Since cell adhesion and migration are intimately linked to focal adhesion dynamics, the final aim was to deepen our understanding of how Stn1 might influence focal adhesion dynamics using cell biological approaches.

2. Material and methods

2.1. General material

Chemicals & common disposables

Reagents and common disposables were purchased from Carl Roth GmbH & Co. KG, Sigma Aldrich and Sarstedt & Co. if not noted otherwise. Specifications can be found in supplementary material B.

Buffers and Media

Buffers and solutions were prepared with ultra pure-filtered water from a Millipore system (Millipore/Merck). The pH was adjusted using HCl or NaOH.

Table 2.1.: Buffers and media used for molecular biology.

Buffer	Composition
LB medium	5 g/l Trypan 5 g/l NaCl 10 g/l Yeast extract
2×YT	16 g/l Trypan 5 g/l NaCl 10 g/l Yeast extract
Antibiotics (stock solutions)	50 mg/ml Ampicillin, sterile filtered (500×) 10 mg/ml Kanamycin, sterile filtered (200×)
10×TBE	20 mM EDTA 890 mM Tris 890 mM Boric acid
1×TE buffer	10 mM Tris pH 8.0 2 mM EDTA
6×DNA loading dye	0.03% (w/v) Bromphenol blue 0.03% (w/v) Xylene cyanol FF 60% (v/v) Glycerol

	60 mM EDTA
OrangeG loading dye	Spatula tip of OrangeG 70% (v/v) Glycerol
10×Annealing buffer	10 mM Tris/ HCl pH 7.4 100 mM NaCl
Tail lysis buffer	100 mM Tris pH 8.5 5 mM EDTA 200 mM NaCl 0.2% (w/v) SDS

Table 2.2.: Buffers used for immunohistochemistry.

Buffer	Composition
Anaesthetic	1×PBS 1.2% (v/v) Ketamin 0.16% (v/v) Rompun
0.4 M PB	0.4 M NaH_2PO_4 (Buffer A) 0.4 M Na_2HPO_4 (Buffer B) to yield final 0.4 M PB buffer add buffer A to buffer B until pH 7.4 is reached ($\sim$ 85% (v/v) Buffer B; $\sim$ 15% (v/v) Buffer A)
0.125 M PB (freshly mixed)	diluted from 0.4 M PB
PBT	0.125 M PB 0.3% (v/v) TritonX-100
Ringer solution	0.85% (w/v) NaCl 0.025% (w/v) KCl 0.02% (w/v) $NaHCO_3$ adjust to pH 6.9 add 0.1% (w/v) Heparin freshly filter and warm to 40°C
4% PFA	4% (w/v) PFA 0.125 M PB adjust pH 7.4 once solution is cooled down
Cryoprotection solution	0.125 M PB 20% (v/v) Glycerol 2% (v/v) DMSO
Antibody solution	PBT 15 µl 1M azide per ml
Gelatine solution	50 mM Tris pH 7.6

	dissolve 0.2% gelatine at 60°C freshly
Cresyl violet solution	0.1% (w/v) Cresyl violet acetate dissolved in water overnight in the dark at 60°C add 0.25% (v/v) Glacial acetic acid filtered through a fluted filter
Embedding medium	50% (v/v) 1×PBS 50% (v/v) Optimum cutting temperature (OCT) formulation of water-soluble glycols and resins

Table 2.3.: Buffers and media used for cell biology.

Buffer	Composition
10×PBS pH 7.4	1.37 M NaCl 43 mM Na_2HPO_4 14 mM NaH_2PO_4 27 mM KCl
PBS/$MgCl_2$	1×PBS 10 mM $MgCl_2$
EB	25 mM HEPES pH 7.6 10 mM K_2HPO_4/ KH_2PO_4 pH 7.6 2 mM $MgCl_2$ 120 mM KCl
0.1×TE buffer	1 mM Tris 0.1 mM EDTA pH adjusted to 8.0; sterile filtered (0.2 µm)
2×HBS	50 mM HEPES 280 mM NaCl 10 mM KCl 1.5 mM Na_2PO_4 12 mM Dextrose pH adjusted to 7.0 - 7.1; sterile filtered (0.2 µm)
2 M $CaCl_2$	sterile filtered (0.2 µm)
4% PFA/sucrose	1×PBS 4% (w/v) Paraformaldehyde (PFA) 4% (w/v) Sucrose
Cell culture medium ($DMEM_{full}$)	DMEM, 4.5 g/l Glucose 10% (v/v) Fetal/ bovine calf serum 100 U/l Penicillin 0.1 mg/ ml Streptomycin

NPC medium	DMEM/F12 10 ng/ml human EGF 10 ng/ml bFGF 1×B-27 supplement 100 U/l Penicillin 0.1 mg/ml Streptomycin
HBSS/HEPES	HBSS 10 mM HEPES pH 7.4
2×Freezing solution	20% (v/v) DMSO 80% (v/v) Fetal/ bovine calf serum
Goat serum dilution buffer (GSDB)	1×PBS 10% (v/v) Goat serum (0.3% (v/v) TritonX-100 for permeabilisation)
DAPI-containing mounting solution (1µg/ml)	5 mg/ml DAPI is diluted 1:500 in 50% glycerol yielding 10 µg/ml stock solution 10 µg/µl stock solution is further diluted 1:10 in Immunomount
Live cell imaging buffer	HBSS (+Ca^{2+}, +Mg^{2+}) 10 mM HEPES pH 7.4 5% (v/v) Fetal/ bovine calf serum
FCS buffer	10 mM EDTA 5% (w/v) BSA 1×PBS filtered through 0.45 µm

Table 2.4.: Buffers and media used for biochemistry.

Buffer	Composition
Lysis buffer	20 mM HEPES pH 7.4 100 mM KCl 2 mM $MgCl_2$ 1% (v/v) TritonX-100 1 mM PMSF 0.3% (v/v) Protease inhibitor cocktail
Homogenisation buffer	1× Lysis buffer without TritonX-100
Lysis buffer with Igepal	50 mM Tris pH 8.0 150 mM NaCl 1% (v/v) Igepal (nonident-P40) 1 mM PMSF

	0.3% (v/v) Protease inhibitor cocktail
2×Bradford reagent	200 ml 85% H_3PO_4
	100 ml Ethanol
	140 g/l Coomassie G250
5×SDS sample buffer (SB)	250 mM Tris pH 6.8
	10% (w/v) SDS
	0.5% (w/v) Bromphenol blue
	50% (v/v) Glycerol
	5% (v/v) β-Mercaptoethanol added directly before use
10×TBS	200 mM Tris pH 7.6
	1.4 M NaCl
4×SDS separating gel buffer	1.5 M Tris pH 8.8
	0.4% (w/v) SDS
4×SDS stacking gel buffer	0.5 M Tris pH 6.8
	0.4% (w/v) SDS
10×SDS running buffer	246 mM Tris
	1.92 M Glycine
	10% (w/v) SDS
Semi-dry blotting buffer	1x SDS running buffer
	10% (v/v) Methanol
Wet blotting buffer	25 mM Tris
	192 mM Glycine
	20% (v/v) Methanol
Antibody dilution solution	1×TBS
	2% (w/v) Bovine serum albumin
	0.03% (w/v) NaN_3
	sterile filtered (0.2 μm)
Antibody blocking solution	1×TBS
	3% (w/v) Skim milk powder
Ponceau staining solution	0.3% (w/v) Ponceau-S
	1% (v/v) Acetic acid
Ponceau destain solution	1% (v/v) Acetic acid
Coomassie staining solution	1 g/l Coomassie G250
	10% Acetic acid
	25% Methanol
	filtered through a fluted filter
Coomassie destain solution	10% Acetic acid
	25% Methanol

Instruments and technical devices

Table 2.5.: Instruments and technical devices.

Instrument	Specification
General equipment	
Ultrapure water system	Sartorius, Arium advance
Fridges and -20°C freezer	Liebherr
-80°C freezer	New Brunswick, C585 Innova
	New Brunswick, U725 Innova
Ice machine	Manitowoc
Scale	VWR/Sartorius, max. 6100 g, d=0.1 g
	VWR/Sartorius, max. 150 g, d=0.01 g
	Sartorius, max. 120 g, d=0.01 mg
pH meter	Mettler Toledo, FiveEasy
Stirrer	VWR, VMS-C7
Spectrophotometer	Eppendorf, BioPhotometer Plus/ Thermal Printer DPU-414
Heating block	Stuart, Block heater SBH130D/3
Vortex mixer	Scientific industries, Vortex-Genie 2
Water bath	GFL, 1002
Pump	Vacubrand, VNC2
Bacteria shaker	New Brunswick, Incubator Shaker Series, Innova44
Shaker	VWR, Rocking platform
	VWR, Orbital shaker Standard 1000
	Grant-bio, PHMT PSC-24
Rotating wheel	Labinco BV, Model L-28
Sonifier	Bandelin electronic, UW-70/ Sonoplus HD-2070
Pipet boy	Brand, Accu-jet pro
	Thermo Scientific, pipette filler S1
Power supply	Biometra, Standard power pack P25-T
Microwave	Exquisit, 700 W
Pipettes	Gilson, Pipetman
	Brand, Transferpipette S
SDS-PAGE and Blotting equipment	BioRad Biometra
Cell culture instruments	
Incubator	Jouan IG150
	New Brunswick, Galaxy 170S
Laminar flow hood	BDK
Water bath	GFL, 1086

Pump	Integra, Vacusafe
Cell culture microscope	Olympus CKX41, Olympus U-RFL-T
Liquid nitrogen tank	VWR, S170-10, Cryo controller BSS-6000
Electroporator	Lonza, Amaxa Nucleofactor IIb, programme A-023
Centrifuges	VWR, Microstar 17
	VWR, Microstar 17R
	VWR, Ministar silverline
	Thermo Scientific, Heraeus Multifuge X1R
	Thermo Scientific, Micro-Ultracentrifuge MTX-150, Rotor S110-AT
	Thermo Scientific, Sorvall Evolution RC, Rotor SS34
	Thermo Scientific, Sorvall RC 5C, Rotor SLA3000
Immunohistochemistry equipment	
Peristaltic pump	World Precision Instruments, Peri-Star Pro, small tubing
Microtome	Thermo Scientific, Sliding Microtome HM430
	Knife angle: 10°
	Temperature: -40°C
Cryostat	Leica, Research Cryostat CM3050 S
Tissue sample slide dryer	Medite, Stretching table OTS 40 series
Cloning material	
Thermoshaker	Grant-Bio, PHMT PSC-24
UV table	Herolab, UVT-28 LV
Horizontal gel system	Peqlab, Perfect Blue
Thermocycler	Peqlab, peqSTAR
Acquisition instruments	
Plate reader	BMG Labtech, SpectroStar Nano, Mars v3.20
	Tecan, Safire, X-Fluor4
NanoDrop	Peqlab, ND1000, v3.5.2
Gel imaging systems	BIO-RAD, ChemiDoc MP system, ImageLab v5.2
	LI-COR, Odyssey Fc, ImageStudioLite v4.0.21
	Syngene, G:Box gel documenting system
FACS	BD, LSR Fortessa, FACS Diva Software v8.0.1
Epifluorescence Microscope	Nikon, Eclipse Ti
	Filter sets: F36-526, F36-504, F46-009, F46-000
	Lamp: Prior Scientific, Lumen 200
	Objective: Nicon, 10x, 40x
	Camera: Andor, Neo sCMOS Camera
	Software: ImageJ-based Micromanager v1.4.14

Microscope for Nissl stainings	Zeiss, Axiovert 200M Objective: 2.5× Camera: Axiocam MRm Software: Axiovision
Laser Scanning Microscope	Zeiss, LSM 780/ 710 Software: ZEN2010 B SP1
Spinning Disc Confocal Microscope	Zeiss, Axiovert 200M Spinning Disc: Perkin Elmer, Ultraview ERS Objective: 63× Camera: Hamamatsu, EE-CCD-Camera Software: Perkin Elmer, Volocity v6.2.1
Magnetic resonance imaging	Bruker, Biospec 94/20 (9.4T field strength) Software: Bruker, Paravision v5 Working System: Red Hat RHEL4

Software and internet resources

Table 2.6.: Software and internet resources.

Programmes	Source	Application
ImageJ, v1.51h	https://imagej.nih.gov/ij/	Image quantification and depiction of exemplary images
Fiji	https://fiji.sc	Package containing most useful plug-ins for ImageJ-based analysis
Inkscape, v0.91	www.inkscape.org/	Arrangement of figures
ApE, v2.0.50	http://biologylabs.utah.edu/jorgensen/wayned/ape/	Development of cloning strategies, analysis of sequencing results
GraphPad PRISM, v5.04	GraphPad	Statistics
	http://graphpad.com/quickcalcs/grubbs1/	Outlier detection
Origin Pro v8.5	Origin Lab	Curve fittings
Microsoft Office 2010, v14.0.7128.5000	Microsoft	Presentations, quantifications
REMBRANDT	http://www.betastasis.com/glioma/rembrandt/kaplan-meier_survival_curve/	Glioma expression profiles
Scansite 3 Beta	http://scansite3.mit.edu/	Search for PDZ domains

Plasmids

Mammalian expression plasmids: pcDNA3.1(+) was purchased from Thermo Fisher Scientific and is a plasmid for transient strong overexpression by a CMV promotor. Ampicillin resistence was used for bacterial growth. pcDNA-HA was generated from pcDNA3.1(+) by insertion of the hemagglutinin (HA, amino acid sequence: YPYDVPDYA) tag at Not1 and Sml1 restriction sites after the CMV promotor.

Backbone pEGFP-C1 was bought from Clonetech and used to generate N-terminally enhanced green fluorescent protein (eGFP) tagged fusion proteins. Resistence against kanamycin was used for bacterial growth. The fluorophore can be excited at 488 nm and emits at 509 nm.

Table 2.7.: Plasmids for mammalian overexpression.

Construct	Species	Backbone	Tag	Origin
FL NG2	rat	pcDNA3.1(+)	-	W. Stallcup
FL Stn1-HA	ms	pcDNA-HA	HA (C)	F. Feutlinske
1-404 Stn1-HA	ms	pcDNA-HA	HA (C)	-
405-730 Stn1-HA	ms	pcDNA-HA	HA (C)	-
AxxA Stn1-HA	ms	pcDNA-HA	HA (C)	-
eGFP	-	pEGFP-N2	eGFP (C)	-
Pax-GFP	ch	pEGFP-C1	GFP (N)	G. Gunderson

C - C-terminal tag, N - N-terminal tag, FL - full length, ms - mouse, ch - chicken

Table 2.8.: Plasmids for bacterial overexpression.

Construct	Insert	Backbone	Tag	Generator
GST	-	pGEX4T1	GST	-
GST-NG2 CD1	rat-NG2 AA2256-2326	pGEX4T1	GST (C)	-
GST-NG2 CD2	rat-NG2 AA2270-2326	pGEX4T1	GST (C)	-
GST-NG2 CD3	rat-NG2 AA2305-2326	pGEX4T1	GST (C)	-
GST-NG2 CD4	rat-NG2 AA2305-2322	pGEX4T1	GST (C)	-
GST-AP2 α-ear	ms α-ear AP2	pGEX4T1	GST	A.Pechstein
GST-AP1 γ-ear	ms γ-ear AP1	pGEX4T1	GST	M. Schmidt

C - C-terminal tag, CD - cytosolic domain, ms - mouse

DNA and protein standards for gel electrophoresis

Table 2.9.: Standards for gel electrophoresis.

Ladder	Company/ ordering number	Marker bands
DNA ladder		
Generuler 1 kBp DNA ladder	Thermo Fisher Scientific, #SM311	10,000/ 8000/ 6000/ 5000/ 4000/ 3500/ 3000/ 2500/ 2000/ 1500/ 1000/ 750/ 500/ 250 Bp
100 Bp DNA ladder	Serva, #003931601	1500/ 1000/ 900/ 800/ 700/ 600/ 500/ 400/ 300/ 200/ 100 Bp
Protein marker		
Pre-stained protein ladder	New England Biolabs, #7708	175/ 80/ 58/ 46/ 30/ 25/ 17/ 7 kDa
Triple colour protein standard III	Serva, #003925701	245/ 180/ 135/ 100/ 75/ 63/ 48/ 35/ 25/ 20/ 17/ 11/ 5 kDa

Antibodies

Primary antibodies were adjusted to 50% (v/v) glycerol for longterm storage at -20°C and utilised according to table 2.10. Antibodies were diluted in GSDB (table 2.3) for immunofluorescence and in antibody solution (table 2.4) for western blotting. Diluents for Immunohistochemistry (section 2.3.5) and flow cytometry (section 2.4.10) are indicated at the according sections.

Secondary antibodies were diluted according to the manufacturers instructions and adjusted to a final 50% (v/v) glycerol concentration to prevent freeze-thawing. To prepare fluorescent, secondary antibody dilutions, antibodies were pre-cleared from aggregates for 5 min at 17,000×g and diluted as noted in table 2.11 with the diluents used for the primary antibody incubation. Often secondary antibody solutions for immunofluorescence were supplemented with Phalloidin-568 to stain for fibrillar actin (F-Actin). Phalloidin-568 was diluted in methanol according to the manufacturers instructions - no glycerol was added. HRP-coupled secondary antibody solutions for western blotting were prepared in antibody blocking solution.

Table 2.10.: Primary antibodies.

Antigen	Host	Company/ catalog nr.	Dil. IF	Dil. WB
β-Actin	ms	Sigma Aldrich/ a5441	-	1:1000
α-Actinin	ms	Sigma Aldrich/ A5044	1:200	-
CHC	ms	Homebrew/ TD1	-	1:500
CNPase	ms	Sigma Aldrich/ C5922	-	1:500
Destrin	rb	Sigma Aldrich/ D8815	1:500	-
FAK	ms	BD Transduction/ 610087	-	1:250
Gadkin γBAR	rb	Homebrew/ #13	-	1:500
GAPDH	ms	Sigma Aldrich/ G8795	-	1:1000
GFAP	ms	Sigma Aldrich/ G3893	1:1000	1:1000
HA	ms	Babco/ 14861601	-	1:1000
Hsc70	ms	Thermo Scientific/ MA3006	-	1:5000
Integrin β1 (active)	rat	BD Bioscience/ 550531	1:250	-
Integrin α5	rb	Santa Cruz/ sc10729	1:50	-
Integrin αV	rat	BD Bioscience/ 550024	1:50	-
N-Cadherin	ms	BD Transduction/ 610920	-	1:5000
Nestin	ms	eBioscience/ 14-5843-82	-	1:500
NG2 (Chem)	rb	Chemicon/ AB5320	-	1:200
NG2	gp	Gift from Stallcup lab	1:50	-
NG2 (MilliMAB)	ms	Millipore/ MAB5384	1:100	1:250
NG2 553	rb	Gift from Stallcup lab	-	1:500
p(Y397)FAK	rb	Abcam/ ab39967	1:50	1:200
Pax	ms	BD Transduction/ 610051	1:2000	-
PDGFRβ	rb	Santa Cruz/ sc432	-	1:500
p(Y1021)PDGFRβ	rb	Santa Cruz/ sc12909-R	1:250	-
PECAM1 (CD31)	rat	BD Bioscience/ 550274	1:10	-
Septin2	rb	Sigma Aldrich/ HPA018481	1:100	-
αSMA	ms	Sigma Aldrich/ A2547	1:200	-
Stn1	rb	Homebrew/ #86.1	1:10	1:200
Vinc	ms	Sigma Aldrich/ V9264	1:100	-
Vinc	rb	Abcam/ ab73412	1:200	-

ms - mouse; gp - guinea pig; rb - rabbit

Table 2.11.: Secondary antibodies and probes.

Species	Origin	Conjugate	Company	Ordering number	Dilution
ms	Goat	Alexa Fluor 488	Invitrogen	A11029	1:400
		Alexa Fluor 647	Invitrogen	A21235	1:200
gp	Goat	Alexa Fluor 568	Invitrogen	A11075	1:200
		Alexa Fluor 647	Invitrogen	A21244	1:200
rb	Goat	Alexa Fluor 488	Invitrogen	A11008	1:200
		Alexa Fluor 647	Invitrogen	A21244	1:200
rt	Goat	Alexa Fluor 647	Invitrogen	A21247	1:200
rt	Donkey	Alexa Fluor 647	Invitrogen	/	1:200
Phall		Alexa Fluor 568	Invitrogen	A12380	1:50
ms	Goat	HRP	Jackson/Dianova	115-035-003	1:10,000
rb	Goat	HRP	Jackson/Dianova	111-035-003	1:10,000

ms - mouse; gp - guinea pig; rb - rabbit; rt - rat; Phall - Phalloidin

2.2. Molecular biology

2.2.1. Cloning

Cloning strategies were designed with the open source programme ApE. DNA oligonucleotides used as primers in polymerase chain reactions (PCR) were designed to contain 4-6 random nucleotides (nt) before the restriction site followed by at least 16 nt of the target gene and to end with G or C to increase annealing efficiency. Melting temperatures of DNA oligonucleotides were noted from the overlapping sequence of the target gene and the primer using ApE and ranged from 57°C - max. 70°C depending on the GC content.

To generate constructs with very short target gene sequences, DNA oligonulceotides were ordered containing the complete target sequence (table 2.12, NG2 CD3 and NG2 CD4) surrounded by digested restriction sites.

All DNA oligonucleotides (table 2.12) were ordered from BioTeZ, dissolved as 100 µM stocks in sterile water and long-term stored at -20°C. Working concentrations for PCR were diluted to 10 µM in sterile water.

Enzymes and according buffers for cloning procedures were purchased from Thermo Fisher Scientific if not stated differently. Application details and ordering numbers were specified at the according sections.

Table 2.12.: Primers.

Primer	Sequence	RS	Usage
TM_242	ataagaGAATTCggtaagcatgatgtccaggtgttg	EcoR1	NG2 CD1
TM_244	gccgacCTCGAGtcacacccagactggccattc	Xho1	
TM_243	ataagaGAATTCggcctagctggtgacacagag	EcoR1	NG2 CD2
TM_244	gccgacCTCGAGtcacacccagactggccattc	Xho1	
TM_245	AATTCgaactattacagttttgccggacacccaatcctgc cctcaggaatggccagtactgggtgtgaC	EcoR1	NG2 CD3
TM_246	TCGAGtcacacccagtactggccattcctgagggcagga ttgggtgtccggcaaaactgtaatagttcG	Xho1	
TM_255	AATTCgaactattacagttttgccggacacccaatcctg ccctcaggaatggctgaC	EcoR1	NG2 CD4
TM_256	TCGAGtcagccattcctgagggcaggattgggtgtccg gcaaaactgtaatagttcG	Xho1	
MB_011	gcatGAATTCatgtattctacaaacccgggcagcgcgg tcaccgctgatgatgaccctg	EcoR1	AvxA Stn1-HA
MB_009	cgatGAATTCcttgagttacacagccaccagttttatct	EcoR1	
FF_01	atgcGAATTCatgtattctacaaacccgg	EcoR1	1-404
MB_007	cgatGAATTCcgcttttgttcttgggc	EcoR1	Stn1-HA
MB_008	gcatGAATTCatgtacgaggaacaagaaatttgcctg	EcoR1	405-730
MB_009	cgatGAATTCcttgagttacacagccaccagttttatct	EcoR1	Stn1-HA

Restriction sites (RS) are written in capital letters within the primer sequence. Exchanged nucleotides to insert mutations are marked in blue.

2.2.2. Polymerase chain reaction (PCR)

The polymerase chain reaction (PCR) is a method to amplify DNA to high magnitudes. Thermal cycling allows melting of template DNA, primer annealing and amplification of the target DNA fragment in few repetitive cycles. Double-stranded DNA is melted at ∼95°C resulting in single-stranded DNA which is accessible for primers. With cooling down to 55-70°C, primer annealing onto single stranded DNA is achieved. Polymerase reaction occurs at 72°C which is the optimal temperature for the polymerase.

The high-fidelity (HF) phusion polymerase (#F530, 2 U/µl) has a very low error rate and was used to generate PCR products finally incorporated into plasmids. The PCR reaction mix was prepared according to table 2.13 and PCR performed as noted (table 2.14). Colony-PCRs and genotyping PCRs were performed with the rather error-prone Dream Taq DNA polymerase (Bio&Sell, 5 U/µl).

Table 2.13.: PCR reaction mix using HF phusion polymerase.

Component	Specifications	Volume used [µl] for one reaction
Sterile ultrapure water		31.5
5x HF buffer	#F530	5
5 mM dNTPs	Bio&Sell	2.5
Primer forward/reverse	Table 2.12, 10 µM	2.5
HF phusion polymerase	#F530, 2 U/µl	0.5
DNA template	Table 2.7	1.0

Table 2.14.: PCR programme using HF phusion polymerase.

	Step	Temperature [°C]	Time
1)	Initial melting	98	30 s
2)	Melting	98	7 s
3)	Annealing	57-70	20 s
4)	Polymerisation	72	15 s/kBp
5)	Final elongation	72	10 min
6)	Storage	8	forever

Steps 2-4 were repeated for 20 cycles.

2.2.3. Agarose gel electrophoresis and DNA purification

DNA was analysed and purified with agarose gel electrophoresis using an electric field to separate DNA fragments according to their size within a three-dimenional agarose gel. Depending on the DNA length, 0.7% - 2% (w/v) agarose was dissolved in 1×TBE by heating in a microwave. The solution was supplemented with ethidiumbromide at a final concentration of 100 ng/ml to allow visualisation of DNA with UV light. DNA solutions were adjusted to 1×DNA loading dye, loaded on the agarose gel and run at 110-180 V. Documentation was done using the G:Box gel documenting system (Syngene). DNA generated for cloning purposes was excised from the gel while keeping UV light exposure times and intensities as low as possible to prevent mutations.

DNA was extracted from agarose gels using the NucleoSpin Gel and PCR Clean-up kit from Machery-Nagel (#740609) according to the manufacturer instructions.

2.2.4. DNA digestion

For integration of PCR-amplified DNA into vector backbones, both need to be linearised by enzymatic digestion with DNAses. Enzymes were carefully chosen to only have one restriction site within insert and backbone using ApE. Digestions were performed in a final volume of 50 µl, containing 1×FastDigest buffer, 1 µl of each FastDigest enzyme (EcoR1 #FD0274/ Xho1 #FD0694) and either 1 µg DNA or the complete PCR product. Reactions were incubated for 45 min at 37°C. After 15 min incubation time, 1 µl calf intestinal alkaline phosphatase (CIP, New England Biolabs, #M0290, 10 U/µl) was added to the reaction mixture. CIP dephosphorylates the 5' end of DNA double strands consequently preventing re-circularisation of the vector backbone and therefore false positive clones.

2.2.5. DNA ligation and transformation of chemically competent E.coli

DNA ligation: Purified and digested DNA was loaded at equal volumes on an agarose gel to calculate the molar ratio of vector and insert used for DNA ligation. For ligation 3:1 molar ratios of insert:vector backbone were preferred. Ligation reactions were performed in a final volume of 20 µl, adjusted to 1×rapid ligation buffer (#K1422) and supplemented with 1 µl T4 DNA ligase (#K1422, 5 U/µl). The reaction tube was incubated overnight at 4°C.

Bacterial transformation: Plasmid DNA was transformed into chemically competent bacteria strains (table 2.15) with a heat shock. 25 µl Calcium-competent *E.coli* were thawed on ice and incubated with 10 µl ligation mixture or 100 ng purified DNA for 30 min on ice. Heat shock was performed for 80 s in a water bath adjusted to 42°C. Suspensions were chilled for 2 min on ice before 500 µl LB medium without antibiotics were added. Bacteria were grown for 1 h at 37°C before being plated on pre-warmed LB agar plates with corresponding antibiotic to select for positive clones.

2.2.6. Colony PCR and sequencing

Colonies were transferred with a pipette tip into 96 wells containing 100 µl LB medium supplemented with antibiotics and grown for 4 h at 37°C. Colony PCR was performed based on genotyping PCRs (table 2.17 and table 2.18) using 1 µl of bacteria suspension instead of genomic DNA. Positive clones were transferred to 6 ml of antibiotic-containing LB medium and grown overnight at 37°C. DNA of bacterial suspension were purified using the NucleoSpin

Table 2.15.: Bacteria strains.

E. coli strain	Origin	Specifications
TOP10	Thermo Fisher Scientific	used for long-term storage and amplification of plasmid DNA
BL21-CodonPlus	Stratagene	lack the proteases Lon and OmpT and contain additional copies of rare tRNAs that would limit protein expression used for production of GST-fused proteins

Plasmid kit from Machery-Nagel (#740588) and sent for Sanger sequencing (Sanger et al., 1977) provided by the company BioTez. Results were analysed with ApE. If sequences were positive and correct, purified DNA was used for retransformation (section 2.2.5) followed by bacterial cryopreservation (section 2.2.8).

2.2.7. Cloning using long DNA oligonucleotides

20 µl of each DNA oligonucleotide (100 µM stock solution) were adjusted to 1×annealing buffer and incubated at 70°C for 10 min. Tubes were placed in a 1 l beaker filled with 400 ml water at 70°C and slowly cooled down to RT within 3 h. 5 µl annealed oligonucleotide solution were adjusted to 1×rapid ligation buffer (#K1422) and 1 µl of T4 polynucleotide kinase (PNK, #EK0031, 10 U/µl) was added. Oligonucleotides were phosphorylated within 30 min at 37°C and PNK was inactivated for 20 min at 65°C. 60 ng of digested (section 2.2.4) vector and 5 µl of a 1:75 dilution of annealed and phosphorylated DNA oligonucleotides were adjusted to 1×rapid ligation buffer (#K1422) and supplemented with 1 µl T4 DNA ligase (#K1422, 5 U/µl). Ligation of vector and DNA oligonucleotides was achieved with overnight incubation at 4°C.

2.2.8. Preparation of glycerol stocks and regain of bacteria cultures

Transformed bacteria cultures were preserved at -80°C as 1:1 mixture of sterile 50% glycerol and cell suspension. To regain bacterial suspension cultures from glycerol stocks, a pin-sized part of the frozen glycerol stock was transferred to an Erlenmeyer flask containing 100-200 ml LB medium supplemented with antibiotics. Bacteria were cultivated overnight ($\sim$ 15 h) at 37°C. Alternatively, 100 ng purified DNA could also be transformed into TOP10 bacteria

(section 2.2.5) and directly transferred into the Erlenmeyer flask for overnight propagation.

2.2.9. Isolation of plasmid DNA from Bacteria (MIDI)

Plasmid DNA was purified using the NucleoBond Xtra Midi kit from Machery-Nagel (#740410) according to the manufacturer's instructions. The DNA amount was determined by spectrometric measurement with a NanoDrop. Purity from proteins was defined by the 260/280 ratio (∼1.8 for DNA) whereas RNA was excluded by the 260/230 ratio (∼2.0 for DNA). Purified DNA was stored at -20°C.

2.3. Practical work with mice

All experiments performed with animals respected the ethical regulations of the Landesamt für Gesundheit und Soziales (LaGeSo) and were conducted with their permission. Conditional AP2 as well as Stn1 knockout animals were generated as described previously (Feutlinske et al., 2015; Kononenko et al., 2013). Heterozygous animals were interbred yielding heterozygous, knock out (KO) and wild type (WT) mice at mendelian ratios.

2.3.1. Purification of genomic DNA and genotyping

Tail biopsies of new born animals were incubated for 0.5-2 h at 55°C with 300 µl tail lysis buffer supplemented with 3 µg of proteinase K (New England Biolabs). Remaining tissue fragments and hair was pelleted at 17,000×g for 5 min at room temperature. The supernatant was transferred to a new tube and DNA was precipitated with 300 µl isopropanol and spun down at 17,000×g for 5 min at room temperature. The DNA pellet was washed with 800 µl of 70% ethanol and dried for 1 h at 55°C. Purified genomic DNA was dissolved in 50 µl sterile ultrapure water for 10 min at 60°C.
The DNA was used as template in PCR mixtures (table 2.17) and PCR was carried out as indicated in table 2.18 revealing the genotype (table 2.16).

2.3.2. Preparation of cortical astrocytes

Extracted brains of p2 to p3 animals were transferred into ice-cold HBSS and the meninges were removed. Cortices were cut into small pieces and transferred into a 15 ml Falcon. The HBSS was exchanged with 5 ml Trypsin/EDTA and the tissue pieces were incubated in a

Table 2.16.: Primers for genotyping.

Primer	Detection	Product	Primer sequence
TM52_st1_del_F	Stn1 WT allele	301 bp	CTGGACCAGGAACCTTCAGA
TM95_st1_rev			CGAGCAAGCACTCATCTCTC
TM96_st1koneo_f	Stn1 KO allele	401 bp	GAGTGTAGAGTGTGGCGCTC
TM95_st1_rev			CGAGCAAGCACTCATCTCTC
TM185_AP2_Ex3F	AP2 LoxP	441 bp	CTCATATACGAGCTGCTGGATG
TM191_AP2_Ex4R	AP2 WT	265 bp	CCAAGGGACCTACAGGACTTC
TM63_cre1	CAG Cre	400 bp	CCGGGCTGCCACGACCAA
TM64_cre2			GGCGCGGCAACACCATTTTT

KO - knock out, WT - wild type

Table 2.17.: PCR reaction mix for genotyping.

Component	Company	Volume used [µl] for one reaction
Sterile ultrapure water	-	11.15
10x Buffer B	Bio&Sell	2.0
25 mM $MgCl_2$	Bio&Sell	2.0
OrangeG loading dye	-	2.0
Primer mix (table 2.16, 10 µM)		0.75
5 mM dNTPs	Bio&Sell	0.6
Taq DNA polymerase (5U/µl)	Bio&Sell	0.5
Genomic DNA	-	1.0

Table 2.18.: PCR programme for genotyping.

	Step	Temperature [°C]	Time
1)	Initial melting	95	5 min
2)	Melting	95	30 s
3)	Annealing	55 - 57	30 s
4)	Polymerisation	72	1 min/kBp
5)	Final elongation	72	5 min
6)	Storage	4	forever

Steps 2-4 were repeated for 30 cycles.

water bath for 15 min at 37°C while being mixed softly every 5 min. Trypsin was removed and the cortex pieces were washed 2× with 5 ml $DMEM_{full}$. Then, cells were triturated in 3 ml $DMEM_{full}$ with a 21×g needle to generate a homogenous suspension. The suspension was filled up to 10 ml and cells were pelleted with 200×g for 8 min at room temperature. Excess $DMEM_{full}$ was removed, cells were resuspended and plated at cell densities ranging from 0.5 - 3.0×10^6 cells per 10 cm plate. The next day the medium was exchanged to remove cell debris. After 1-2 weeks cells were split to coverslips for immunocytochemistry.
To generate AP2-deficient glial cells, glial cultures derived from AP2 Lox/Lox×CAG cre/Esr1 mice were treated with tamoxifen at a final concentration of 0.1 µM to delete exon 2 and 3 of AP2m1 which encodes the murine AP2 µ-subunit. The tamoxifen-containing medium was exchanged every 3-4 days. After 3 weeks of tamoxifen treatment, AP2 protein levels reached a minimum of ∼ 5-10% in AP2 Lox/Lox CAG cre glial cell cultures (determined by Dr. Tania Lopez-Hernandez) and the cells were used for the experiment. These glial cells represented AP2 knockout (AP2 Lox/Lox CAG cre = Flox cre) conditions and were compared to the wildtype (AP2 Lox/Lox = Flox(-)).

2.3.3. Generation and maintenance of neuronal precursor cells (NPCs)

Timed matings between adult heterozygous mice were initiated and 14.5 days later the females were killed by cervical dislocation. The abdomen was opened and the uterus placed into a 50 ml falcon with sterile HBSS/HEPES. Embryos were separated, pressed out of the uterus and cleaned from maternal blood by transferring the embryo 2× into fresh plastic dishes with ice-cold HBSS/HEPES. The embryonal brain was extracted and meninges, olfactory bulb and cerebellum were removed. The cortex was divided into left and right hemisphere and about 1/3 of the outer cortex was dissted away. The remaining pieces of cortex were centrifuged (400×g, 5 min, RT) and incubated in 2 ml Trypsin/EDTA for 20 min in a water bath adjusted to 37°C. The cortices were triturated with a flamed Pasteur pipette until the suspension was homogeneous. The enzymatic reaction was stopped with 3 washing steps with 10 ml NPC medium (centrifugation 400×g, 5 min, RT). Cells from one embryo were seeded on two Poly-D-Lysin-coated 12 wells. Coating was achieved by covering the 12 wells with Poly-D-Lysin at a dilution of 50 µg/ml in water for 5 min at RT. The solution was aspirated, wells were washed 1× with 1 ml sterile water and dried for 2 h at RT.
When the cells had reached confluency, the medium was aspirated and the cells were incubated

in 500 µl Accutase for 2-3 min at 37°C. Afterwards, the cells were collected in 5 ml NPC medium, centrifuged (400×g, 5 min, RT) and the solution was replaced with fresh NPC medium to remove excess Accutase. Cells from one embryo were transferred to a single 6 cm dish to allow fast confluency of cells and early formation of spheres. Subsequently, cells were split every 2-3 days: NPCs were centrifuged (400×g, 5 min, RT), resuspended in 1 ml NPC medium until a homogeneous cell suspension was observed and 200,000 - 300,000 cells were seeded into 75 cm^2 tissue culture flasks.
Cryopreservation of NPCs was achieved by collecting spheres of a confluent flask. Spheres were washed with NPC medium and partially triturated. The resulting miniaturised spheres were aliquoted into labelled cryotubes yielding a 1:1 mixture of 2×NPC freezing medium (10% (v/v) DMSO in NPC medium) and cell suspension. Suspensions were slowly frozen in a sealed styropor box at -80°C overnight before long-term storage in liquid nitrogen.

2.3.4. Tumour studies

Tumour growth of WT and Stn1 KO NPCs in WT-C57BL/6 mice: Experiments to monitor tumour growth in WT and Stn1 KO animals *in vivo* were carried out in collaboration with Prof. Dr. Rainer Glass (Munich) who performed NPC transformation, injection into animals as well as animal perfusion and brain fixation. In brief, lentivirus was generated by transfecting HEK293T cells with the lentiviral genome together with packaging (pMDL.G, pRSV-Rev) and envelope (pMD2.G) plasmids. Cell supernatant with virus particles was used for transformation of WT and Stn1 KO NPCs (section 2.3.3) with a PDGF-BB/IRES/GFP construct in a pCEG backbone. 1 µl with 20,000 transformed NPCs was injected into the brain (1.5 mm lateral and 1 mm anterior to the bregma, 3-4 mm below the meninges) of WT-C57BL/6 mice under anaesthesia. The wound was sutured and 41 days post-injection, animals were anaesthetised for perfusion with 0.9% (w/v) NaCl solution followed by fixation with freshly prepared 4% PFA. Extracted brains were post-fixed with 4% PFA overnight and cryopreserved for at least 2 days in 30% sucrose solution. Complete brains in cryomolds were covered in OCT for shipment on dry ice. OCT was removed by keeping brains in cryopreservation medium overnight. Brains were cut sagittally (40 µm thick slices) and 6 series were cryopreserved at -80°C.

Cresyl Violet/ Nissl Staining: The Nissl staining is based on an aniline dye that colours

RNA and DNA blue. As a result nuclei and rough endoplasmic reticulum can be visualised. Brain sections were thawed, sorted in sequential order and mounted in gelatine solution on SuperfrostPlus microscopy slides, covered a second time with gelatine solution once dried and then thoroughly dried overnight at 42°C. Sections were rinsed by dipping the glass slide rack 3-5× in water. Slices were stained for 20 min in 0.1% cresyl violet solution and washed 3× for 2 min in water. Sections were destained - 2 min each - in 80%, 90%, 100% ethanol followed by 2 min xylene and 1 min xylene. Slices were mounted in entellan.

Tumour growth of glioma cells (GL261) in WT and Stn1 KO mice: Experiments to observe *in vivo* tumour growth using magnetic resonance imaging (MRI) were performed by Dr. Min-Chi Ku from the group of Dr. Sonia Waiczies and Prof. Dr. Thoralf Niendorf. In brief, 1 µl with 20,000 murine GL261 glioma cells was injected with a Hamilton syringe into the brain (1 mm anterior to the bregma, 1.5 mm lateral from the midline, 4 mm below the meninges) of WT and Stn1 KO mice under anaesthesia. The wound was sealed with bone wax and tumour growth was observed 14 days post-injection by MRI while animals were kept in narcosis with 0.5% - 1.5% isofluorane. The imaging protocol consisted of a 3D rapid acquisition with relaxation enhancement (RARE) sequence allowing an isotropic resolution of 125 μm^3 for ^1H (TR/TE = 1500/47 ms). Regions with tumour were selected and the total volume calculated with ImageJ v1.47p by summarising voxel volumes. For further analysis, all brains were processed for immunohistochemistry under supervision of Dr. Tanja Maritzen (section 2.3.5).

2.3.5. Perfusion and immunohistochemistry

Brain perfusion and staining: Mice were anaesthetised by intraperitoneal injection of anaesthetic (table 2.2) with a dosage of 100 µl per gram. For perfusion, the thorax was opened, the perfusion needle placed into the left ventricle and the right atrium was cut to allow blood leakage. Animals were perfused slowly at 2.66 ml/min rate with 20 ml Ringer solution followed by 40 ml of 4% PFA solution. The brain was dissected and post-fixed in 5 ml 4% PFA solution at 4°C overnight. The next day PFA solution was exchanged with cryoprotection solution. Within one week brains were cut sagittally (40 µm thick slices) and 6 series were cryopreserved at -80°C.

For immunohistochemistry slices of interest were transferred into 0.125 M PB. Slices of dif-

ferent genotypes were marked and stained in the same bowl to ensure comparability. All following steps were performed on an orbital shaker in embryo dishes (internal diameter 30 mm). Slices were washed 3× for 20 min with 0.125 M PB and permeabilised 6× for 20 min with PBT before being blocked for 1 h in 30% normal goat serum in PBT. Brain slices were incubated for 2 days at 4°C with 250 µl primary antibody (diluted in antibody solution (table 2.2) according to table 2.10) in parafilm-sealed embryo dishes. Slices were washed 9× for 20 min with PBT and incubated with 250 µl secondary antibody (table 2.11) for 2 h at RT in the dark. Slices were washed 3× for 15 min with 0.125 M PB and stretched onto Superfrost-Plus microscopy slides at 41°C in gelatine. Dried slices were mounted in DAPI-containing mounting medium.

Lung perfusion and staining: Lung perfusion was performed based on Arlt et al. (2012). Mice were weighed and intraperitoneally anaesthetised with 100 µl per gram anaesthetic (table 2.2). Peritoneum as well as thorax were opened and the vena cava caudalis was cut underneath the liver. 10-15 ml iPBS were slowly injected into the right ventricle of the heart until the heart stopped beating using a 20 ml syringe equipped with a new 26×g needle. The trachea was exposed and the lower parts of each lung lobe were punctured. 3 ml embedding medium were injected into the trachea until lungs were completely inflated using a 5 ml syringe equipped with a 21×g needle. The trachea was disconnected from the lung using vascular clamps (Bulldog serrefines 35 mm) to prevent embedding medium to leak out. The lung was carefully removed and the lung lobes were dissected. Each lobe was placed into an OCT filled embedding mold and pressed to the ground. Molds were filled up with OCT and incubated for 20 min at 4°C. Embedded lung lobes were slowly frozen in a mixture of dry ice and isopentane before being wrapped in aluminium foil for long term storage at -80°C. To cut 12 µm thick slices, cryostat temperature for object (-8°C) and blade (-11°C) were equilibrated for at least 30 minutes. Stretched slices were transferred to SuperfrostPlus microscopy slides and stored at -80°C.

Immunohistochemistry of lung tissue was performed in a humidified chamber and all washing steps were carried out by dipping slides 3× into a beaker filled with 250 ml PBS. Excessive OCT was removed and tissue surrounded with a PAP pen to create a hydrophobic barrier. Slices were fixed for 10 min at RT in 4% PFA/sucrose. Following washing, slices were permeabilised and blocked for 1 h at RT with GSDB. Slides were incubated with 250 µl primary

antibody (table 2.10) diluted in GDSB overnight at 4°C. Slides were washed and incubated with 250 µl secondary antibody (table 2.11) dilution for 1 h in the dark at RT. Slides were washed and remaining PBS was carefully aspirated before slices were mounted in DAPI-containing mounting medium.

2.4. Cell biology

2.4.1. Mammalian cell lines

Mouse embryonic fibroblasts (MEFs): MEFs from WT and Stn1 KO mice were generated by Dr. Fabian Feutlinske (Feutlinske, 2014). In brief, head and inner organs of E13.5 animals of random sex were removed and the remaining tissue was minced as well as incubated in Trypsin/EDTA. Following trituration, cells were collected and seeded on 10 cm dishes. Cells were immortalised with SV40 large T-antigen on day 10 of *in vitro* culture. Two independent MEF cell lines were generated (pair #1 and #2) to exclude cell line specific phenotypes.

Human embryonic kidney cells (HEK293Ts): HEK293T cells were purchased from ATCC. The original cell line HEK293 was generated by Graham et al. (1977) and expresses adenovirus 5 DNA. The cell line was transformed with SV40 large T antigen - giving them the name HEK293T - to increase retrovirus harvest (DuBridge et al., 1987; Pear et al., 1993). HEK293T cells were used for biochemical interaction analysis because of their strong protein expression and high transfection efficiency with calcium phosphate and jetPRIME (section 2.4.3).

2.4.2. Cell culture

Cells were cultured in $DMEM_{full}$ in a humidified incubator with 5% CO_2 at 37°C. For passaging, cells were briefly washed with 1×PBS and detached with 0.05% Trypsin/EDTA for 5 min at 37°C. The enzymatic reaction of Trypsin was stopped with an equal volume of $DMEM_{full}$ and cells were seeded to new cell culture dishes and plates. MEFs were split every 2 to 4 days with dilutions ranging from 1:5 to 1:30. MEFs were not used after passage 30, due to morphological changes and altered proliferative behaviour with high passage number. HEK293T cells were passaged every 2 to 3 days at dilutions ranging from 1:2 to 1:5.

Cryopreservation of MEF and HEK293T cells was achieved by detaching cells from a con-

fluent dish using Trypsin/EDTA solution as described before. Cells were resuspended in $DMEM_{full}$ and aliquoted into labelled cryotubes. Adding 2×Freezing medium yielded a 1:1 mixture of Freezing medium and cell suspension. Suspensions were slowly frozen in a sealed styropor box at -80°C overnight before long-term storage in liquid nitrogen.
Cell biological experiments were performed on 12 mm or 18 mm glass coverslips. Unless stated differently, coating of coverslips and cell culture plates was performed for 1 h at 37°C with concentrations listed in table 2.19.

Table 2.19.: Coating.

Reagent	working concentration	CS size/ Cell culture dish	volume used	final conc. on surface
Collagen 1	1.0 µg/µl in water	96 well	50 µl	1.6 µg/cm^2
Collagen 6	1.0 µg/µl in water	96 well	50 µl	1.6 µg/cm^2
Laminin 1	1.0 µg/µl in water	96 well	50 µl	1.6 µg/cm^2
Fibronectin	0.1 µg/µl in water	18 mm CS	50 µl	2.5 µg/cm^2
	0.01 µg/µl in water	6 cm dish	5 ml	2.3 µg/cm^2
	1.0 µg/µl in water	96 well	50 µl	1.6 µg/cm^2
Matrigel	1:50 dilution in Opti-MEM	18 mm CS	50 µl	-
		24 mm CS	200 µl	-
		96 well	50 µl	-

CS - coverslip

2.4.3. Transfections for overexpression and knockdown

Throughout the study, transfection techniques were adjusted to the type of experiment and cell type. Sufficient overexpression in MEF cells could not be achieved using transfection reagents like Lipofectamine 2000. Instead electroporation was used if low numbers of transfected cells were sufficient as for life cell imaging experiments. Strong overexpression in a limited amount of cells was achieved with Lipofectamine 3000. For a more homogenous expression within a huge cell population viral overexpression was used.

Overexpression with electroporation: Electroporation uses a current to induce pores into the plasma membrane of cells which allow DNA to be taken up.
MEFs were trypsinised as usual and counted with a Neubauer haemocytometer. 1×10^6 cells were aliquoted and centrifuged (300×g, 5 min, RT). 5 µg DNA at a maximum of 5 µl was

added to the pellet. The pellet was resuspended in 100 µl EB and directly transferred to a cuvette. Electroporation was performed with programme A-023 of the Nucleofector IIb which was specifically designed for MEFs. Directly afterwards 500 µl $DMEM_{full}$ was added and 75 - 150 µl cell suspension were plated on matrigel-coated 24 mm coverslips (table 2.19).

Overexpression with Lipofectamine 3000: Lipofectamine 3000 is a lipid-nanoparticle based transfection reagent yielding high transfection efficiencies for hard-to-transfect cell lines like MEFs.
150,000 MEFs per 6 well were seeded to yield 70% confluency the next day. 3.75 µl Lipofectamine 3000 were diluted in 125 µl Opti-MEM and transferred to an Opti-MEM solution of an equal volume containing 5 µg DNA and 10 µl P3000 reagent. The mixture was incubated for 5 min and added in a dropwise manner to the cells. Experiments were carried out 2 days after transfection.

Overexpression with calcium phosphate transfection: The method was developed and described by Graham and van der Eb (1973). It generates neutral DNA-Calcium phosphate precipitates that can be taken up by cells via endocytosis.
HEK293T cells were split 1:3 from 100% confluent plates to yield 60-70% confluency the next day. 0.1×TE buffer, DNA and $CaCl_2$ were mixed according to table 2.20 and incubated for 5 min at RT. The DNA solution was added to 2×HBS in a dropwise manner while vortexing to ensure optimal precipitate formation. After 20 min incubation time, DNA-precipitates were added dropwise to HEK293T cells.

Table 2.20.: Calciumphosphate transfection.

Buffer	15 cm cell culture dish for interaction analysis
0.1 x TE	1100 µl
total DNA amount	20 µg
2M $CaCl_2$	150 µl
2x HBS	1250 µl

Overexpression with jetPRIME: jetPRIME reagent is a cationic polymer used to yield high transfection efficiencies in HEK293T cells for interaction analysis. The positively charged reagent binds DNA and forms complexes that can be taken up by endocytosis.

The transfection was carried out as indicated by the manufacturer and the experiment was performed after 24 hours.

Knockdown with RNAiMax: Cells can regulate protein expression not only by post-translational modification and degradation but also by modifying the translation of mRNAs using short RNA molecules. Initially a single-stranded RNA, complementary to the mRNA sequence of the target protein, is incorporated into the RNA-induced silencing complex (RISC) complex and called miRNA from thereon. A perfect match of miRNA and mRNA leads to the degradation of the mRNA via the RISC complex while in case of non perfect complementarity miRNA translation is blocked. This mechanism is used by scientists to knockdown expression of target proteins by transfecting synthetic, small interfering RNAs (siRNAs) into cells. Knockdowns of proteins were carried out by using the liposome-based reagent RNAiMax which yields optimal knockdown efficiencies in fibroblasts.
Since treatment of cells with RNAiMax is affecting cell proliferation and survival, control cells were seeded with 90,000 cells per 6 well while MEFs receiving siRNA were seeded at a density of 150,000 cells per 6 well. The next day 1.4 µl siRNA (table 2.19) was diluted in 200 µl Opti-MEM and mixed with 7.5 µl RNAiMax. The solution was incubated for 20 min at RT and added in a dropwise manner to the cells in medium without antibiotics. After 24 h a second round of knockdown was performed in the same way. Cells were split for experiments onto uncoated coverslips on day 3.

Table 2.21.: siRNAs.

Targeted gene	species	Company	siRNA sequence (5' → 3')
NG2	mouse	MWG	GGUCAAUCCUGUCAACGAU
scrambled	rat	MWG	GCUGAUACGCUAUACUGAUTT

siRNAs were diluted in 1×MWG buffer to yield a final concentration of 100 µM. All steps with siRNA, including knockdown procedures, were performed with RNAse-free tips and tubes.

2.4.4. Fluorescence recovery after photobleaching (FRAP)

Electroporated MEFs (section 2.4.3) on coverslips were transferred to live cell imaging buffer. Several distinct focal adhesions per cell were selected for photobleaching. 3 pre-bleach images were acquired, bleach cycles performed (15×15 µm, 500 ms) and recovery was monitored for 60 s at 1 s per frame on the spinning-disc confocal microscope (table 2.5). Images were

exported as TIFFs from Volocity software for further analysis with ImageJ. Fluorescence intensities were corrected for bleaching as well as background, normalised to the pre-bleach intensity and averaged per cell. Data from each experiment was fitted with a single exponential curve with Origin software to obtain half-time recovery ($t_{1/2}$) and mobile fraction. Fitted data was included for further analysis if $R^2 > 0.95$.

2.4.5. Migration assays

Experiments and analysis of cell motility and migration behaviour were carried out and documented by Dr. Fabian Feutlinske (Feutlinske, 2014). In brief, randomly migrating MEF cells were recorded in 15 min intervals with a wide-field microscope (10× objective) overnight. Cells were tracked manually using ImageJ and tracks were further processed with a migration tool developed by Ibidi. Directionality was calculated as the ratio of displacement to total path length based on Petrie et al. (2009).
The same time-lapse movies were used to investigate trailing end stability and protrusion dynamics. The maximum trailing end length of randomly chosen cells was measured using ImageJ. Corresponding lifetimes were calculated based on number of frames per individual cell displaying a trailing end. Protrusion dynamics were visualised using the ImageJ plug-in 'MultiKymograph' along the lines indicated.

2.4.6. Immunocytochemistry

Standard procedure: Cells grown on coverslips were washed with PBS/$MgCl_2$ and fixed with 4% PFA for 10 min at RT. Since the fixation technique influences the availability of the antibody epitope, other fixation procedures were used for some stainings. Tubulin staining was optimal with methanol fixation at -20°C for 7 min. Background of Vinculin staining (ms, Sigma) was reduced when cells were fixed for 2 min at RT followed by 8 min on ice.
After 2 washing steps with PBS, coverslips were blocked with GSDB for 15 min at RT. Primary antibodies were diluted in GDSB (table 2.10) and coverslips were incubated for 1 h in a humidity chamber. Following 3 washing steps with PBS coverslips were incubated with secondary antibody dilution (table 2.11) for 1 h at RT in a dark humidity chamber. Coverslips were mounted in Dapi-containing mounting medium after 3 washing steps with PBS.
For surface immunostainings GSDB without TritonX-100 was applied.

pPDGFRβ: To stain for pPDGFRβ cells were fixed and washed according to the standard protocol. MEFs were permeabilised with 0.3% TritonX-100 for 5 min at RT and blocked with 5% BSA in PBS for 1 h. Primary antibodies (table 2.10) were incubated overnight at 4°C in a humidified chamber. Stainings were continued according to the standard staining protocol.

2.4.7. Nocodazole washout assay

40,000 MEFs per 12 well were seeded on uncoated coverslips 2 days before the experiment. The next day cells at 60% confluency were starved by briefly washing wells with 1 ml PBS and its exchange with 1 ml DMEM without additives. Nocodazole was diluted to a final concentration of 10 µM in warm serum-free medium and 50 µl per coverslip were spotted on parafilm in a humidified chamber. The nocodazole diluent DMSO was used at equal volumes for control samples. After 24 h of starvation MEFs were incubated with nocodazole dilutions for 4 h in the cell culture incubator by placing the coverslip upside down onto nocodazole drops. For washout of the compound, coverslips were transferred into 1 ml warm serum-free medium and incubated in the cell culture incubator for the indicated time intervals. Fixation and staining was performed according to the standard protocol (section 2.4.6).

2.4.8. Cell adhesion assay

Adhesion experiments were performed based on Xu et al. (1998). 96 wells were coated (table 2.19) and washed 2× with 100 µl PBS. Wells were blocked with 100 µl of 2% BSA for 2 h at RT and rinsed 3× with 100 µl PBS. MEFs at 90% confluency were washed with PBS and detached using Trypsin/EDTA. Cells were washed 1× with serum-free medium with 20 µg Trypsin inhibitor and resuspended to a final concentration of 5×10^5 cells/ml. 50,000 cells/well were seeded and incubated for the indicated time points at 37°C. Non-adherent cells were washed off by gently rinsing 3× with PBS. Adherent cells were fixed for 30 min at room temperature with 10% freshly diluted formalin before being stained with 1% Toluidine Blue solution (filtered through 0.45 µm). Plates were washed extensively with water and air dried. Toluidine Blue was diluted in 100 µl of 2% SDS solution and measured with plate readers at OD620.

2.4.9. Spreading assay on fibronectin and detection pFAK activation

Spreading: MEFs were split to 6 cm dishes. The next day cells at 80% confluency were washed briefly with PBS and detached in 100 mM EDTA/PBS. Cells were collected in $DMEM_{full}$ and pelleted for 5 min at RT with 300×g. Cells were resuspended in $DMEM_{full}$ and seeded as 40,000 cells/18 mm fibronectin-coated coverslips (table 2.19) for the indicated time points. Coverslips were processed according to section 2.4.6.

FAK phosphorylation upon spreading on fibronectin: pFAK levels during spreading on fibronectin were investigated based on Cheng et al. (2014). 3×10^6 cells were seeded on 15 cm dishes and starved at 80% confluency with DMEM without serum the next day. Cells did not receive serum from that point on - instead DMEM without serum was used for washing steps of cells. 10 cm dishes were coated with fibronectin (table 2.19) at 4°C overnight. The next day cells were detached with 2.5 ml of 100 mM EDTA/PBS for 10 min at 37°C and collected in equal volumes of DMEM. Cells were pelleted (600×g, 5 min, RT) and resuspended in 15 ml DMEM to remove excess EDTA. Then, cells were centrifuged (300×g, 5 min, RT) and resuspended in 1 ml DMEM. The suspension was adjusted to final 8 ml medium and counted. 1.5 Mio cells in 8 ml medium were seeded to FN-coated 10 cm dishes and incubated at 37°C for the indicated time points. Lysates of adherent cells were generated according to the standard protocol (section 2.5.1) with lysis buffer supplemented with phosphatase inhibitor 2 and 3 (Sigma, 1:50).

2.4.10. Flow cytometry and FACS analysis

MEFs were briefly washed with PBS, then detached with 1.5 ml/10 cm dish of 100 mM EDTA/PBS and collected with equal volumes of $DMEM_{full}$. Cells were centrifuged (300×g, 5 min, 4°C) and resuspended in FCS buffer. All steps from here on were carried out in FCS buffer. Cells were always centrifuged at 300×g for 5 min at 4°C. The suspension were subdivided into 200,000 cells per staining and blocked with FCS buffer for 15 min on ice. FCS buffer was exchanged with 100 µl primary antibody solution (diluted in FCS buffer according to table 2.10) and incubated for 1 h on ice. Cells were washed 3× with 500 µl FCS buffer and incubated in the dark for 1 h at 4°C in secondary antibody solution (diluted in FCS buffer according to table 2.11). MEFs were washed 3× with 500 µl FCS buffer and resuspended in at least 200 µl of FCS buffer for fluorescence-activated cell sorting (FACS) analysis with LSR

Fortessa. Based on forward-sideward scatter plots, cell debris was excluded and only healthy cells were selected for fluorescence intensity quantifications.

2.5. Biochemistry

2.5.1. Preparation of lysates

Organ lysates for western blotting: Organs were weighed and and transferred into a douncer containing lysis buffer (volume in µl corresponds to 5× organ weight in mg). The tissue was homogenized by applying 20 potter strokes at 1000 rpm. The homogenate was kept on ice for 30 min while vortexing every 5 min to allow further cell lysis. Debris was removed by centrifugation for 10 min at 17,000×g at 4°C followed by another centrifugation for 5 min at 17,000×g at 4°C. Clear supernatant was used to determine the protein amount by the Bradford assay (section 2.5.2). Samples were adjusted to 1×SB and boiled for 5 min at 95°C for western blotting.

Cell lysates for western blotting: Cells were washed with iPBS, scraped from cell culture dishes and centrifuged (300×g, 4°C, 5 min). Cell pellets were resuspended in lysis buffer and incubated for 10 min on ice while mixing from time to time. Debris was spun down for 10 min, 17,000×g at 4°C. The protein content of the supernatant was determined by Bradford assay (section 2.5.2), samples were adjusted to 1×SB and boiled for 5 min at 95°C.

2.5.2. Protein determination (Bradford assay)

To determine the protein concentration of lysates and purified proteins, samples were subjected to the Bradford assay - a very sensitive colorimetric method (Bradford, 1976). The Bradford reagent contains Coomassie Brilliant Blue G250 which binds cationic and hydrophobic amino acids shifting the absorption maximum from 465 nm to 595 nm. Following photometric measurement the protein concentration is calculated using the law of Lambert-Beer. Reliable values lie between 0.1 AU and 0.5 AU, therefore, samples were often diluted 1:200 to 1:1000 in 500 µl ultrapure water. Samples were supplemented with 500 µl of 2× Bradford reagent and subsequently incubated for 5 min at RT before measurement with a spectrophotometer. The protein concentration was obtained from a standard curve prepared with bovine

serum albumin.

2.5.3. Affinity purification and co-immunoprecipitation

Interaction analyses were performed using pull-down assays and co-immunoprecipitations. In a pull-down approach resin-bound baits are incubated with the lysate containing the potential prey to allow protein interaction. The immobilised bait can be centrifuged for co-purification of potential partners. Here, glutathione S-transferase (GST) was used to tag bait proteins. The 25 kDa protein strongly binds to glutathione-coupled beads and thus can be used to immobilise the bait protein on the beads. In co-immunoprecipitations, antibodies specific for the 'bait' protein are immobilised on a column. High affinity binding to the antigen - the bait protein - within a lysate allows its purification in complex with potential interaction partners.

Preparation of lung and cell lysate: Lung tissue was weighed and and transferred into a douncer containing lysis buffer (volume in µl corresponds to 5× organ weight in mg). The tissue was homogenised with 13 potter strokes at 900 rpm and the homogenate was centrifuged for 10 min with 900×g at 4°C to remove cell debris. The volume of the supernatant was determined and adjusted to 1× lysis buffer using 5× lysis buffer and incubated for 10 min on ice. The lysate was centrifuged for 15 min with 43,500×g at 4°C and the supernatant was ultracentrifuged for 15 min with 265,000×g at 4°C. The protein content of supernatant was determined by Bradford assay (section 2.5.2).
Cells from cell culture dishes were washed with iPBS and scraped into lysis buffer. The suspension was incubated for 10 min on ice while vortexing from time to time. The suspension was pre-cleared at 17,000×g at 4°C for 5 min and the supernatant was ultracentrifuged at 180,000×g for 15 min at 4°C. The protein amount of the lysate was determined by Bradford assay (section 2.5.2).

Protein purification and GST pull-down: A pin-size part of glycerol stocks was grown overnight at 37°C in 10 ml antibiotic-containing LB medium while shaking at 180 rpm. The bacteria suspension was transferred to a 2 l erlenmeyer flask containing 500 ml antibiotic-containing 2×YT medium and grown overnight at 37°C while shaking at 180 rpm. At OD 0.6, the suspension was adjusted to 0.5 mM IPTG to induce protein expression by BL21 bacteria cells. Protein was expressed for 4 h at 30°C (GST-AP2 constructs) or for 16 h at 16°C

(GST-NG2 constructs). Bacterial cultures were collected at 6000 rpm for 15 min at 4°C and resuspended in 50 ml ice-cold PBS. Suspensions were either frozen in 25 ml aliquots or used directly for protein purification.

For protein purification, bacteria suspensions were supplemented with a spatula tip of lysozyme as well as 5 µl Benzonase and incubated for 10 min on ice to allow hydrolysis of glycosidic bonds of the bacterial cell wall. Suspensions were sonified (1.30 min, 50% power, 5 cylces) and supplemented to a final concentration of 1% TritonX-100 to break cell walls. After 10 min incubation on a rotating wheel at 4°C, debris was pelleted with 17,000 rpm for 20 min at 4°C. In the meantime 250 µl GST-bind resin was washed 1× with 30 ml iPBS (centrifuge at 3000 rpm, 4°C, 1 min, deceleration 6). Cleared bacterial supernatant was incubated with beads for 2 h while rotating in the cold room. The beads were washed 3× with 10 ml iPBS (centrifuge at 3000 rpm, 4°C, 1 min, deceleration 6) and the protein amount was determined by Bradford assay (section 2.5.2).

Protein amounts used in GST-pulldown reactions are listed in table 2.22. Solutions were incubated for 2 h on a rotating wheel in the cold room. Afterwards beads were washed 3× for 10 min with lysis buffer followed by 2×5 min with homogenising buffer. Samples were eluted by boiling pure beads with 20-30 µl 1×SB for 5 min at 95°C.

Table 2.22.: Used protein amounts for GST-pulldowns.

Interaction analysis	Cell/ organ lysate [µg]	lysate concentration [µg/µl]	purified GST-protein [µg]
AP2 - Stn1	500	2.5	25
NG2 - FL Stn1	3500	4.0	100
NG2 - µHD Stn1	800 - 1000	3.0 - 4.0	100
Destrin - FL Stn1	3500	4.0	100

Immunoprecipitation (IP): 50 µl protein A/G agarose slurry per sample were aliquoted with a cut 200 µl tip and washed 1× with 500 µl iPBS before centrifuging at 1200×g, 2 min, 4°C. The agarose was resuspended in 500 µl ice-cold TBS with 0.1% TritonX-100 and incubated with 20 µg antibody for 1 h on a rotating wheel at 4°C. Agarose beads were washed 2× with 500 µl lysis buffer (1200×g, 2 min, 4°C) and incubated with 1 mg HEK293T cell lysate at a protein concentration of 2.9 µg/µl for 4 h on a rotating wheel at 4°C. Agarose beads were briefly washed 3× with 1 ml lysis buffer followed by 1× with 1 ml homogenising buffer. Liquid

was completely removed with a Hamilton syringe and samples were eluated in 40 µl 1×SB by boiling for 5 min at 95°C.

2.5.4. Membrane fractionation

MEFs were split the day before the experiment to 10 cm dishes. The next day cells at 80% confluency were starved in HBSS for 3 h after being washed 3× with 5 ml PBS. Then, indicated samples were stimulated for 30 min with 10% serum. Afterwards cells were briefly washed 2× with 2.5 ml iPBS and lysed in 200 µl cold lysis buffer. Intact cells were broken by shock-freezing in liquid nitrogen followed by thawing in a water bath at room temperature 3×. The suspension was homogenised by sucking the lysate 20× into a 1 ml syringe equipped with a 26×g needle. Nuclei and large debris were pelleted for 3 min at 4°C with 1000×g. The supernatant was collected and an aliquot was placed aside as input material. The remaining supernatant was centrifuged at 265,000×g at 4°C for 30 min and the resulting supernatant (cytosolic fraction) was separated from the pellet (membrane fraction). The protein amount of the total lysate (input) as well as of the cytosolic fraction was determined by Bradford assay (section 2.5.2) and samples for SDS-PAGE were prepared. The pellet was washed once with 200 µl of lysis buffer and resuspended in an equal volume of 1×SB.

2.5.5. SDS polyacrylamide gelelectrophoresis (SDS-PAGE)

Sodium dodecyl sulfate polyacrylamide gel electrophoresis (SDS-PAGE) can be used to separate proteins of different molecular weights. The method uses an electric field to force charged proteins to run through a polymer network. As such the migration speed can be influenced by the shape, size and charge of the protein but also by the pore size of the polymer. To linearise proteins, the anionic detergent SDS together with β-Mercaptoethanol are used to denature proteins. In addition, SDS will bind to the proteins according to their length thereby masking their own charge. To separate proteins according to the molecular weight, a discontinuous SDS-PAGE was used (Laemmli, 1970) which is composed of a stacking and a separating gel. Proteins in the stacking gel encounter a low pH at the isoelectric point of glycine. Due to the electric field, proteins get concentrated between fast running chloride ions and zwitterionic glycin with a low mobility yielding sharp bands according to protein charge. When entering the separating gel with a higher pH the protein mobility is increased and proteins can get separated according to their molecular weight.

Polyacrylamide gels were prepared according to table 2.23. By adding ammonium persulfate (APS), which provides free radicals, the polymerisation of acrylamide is induced which is further catalysed by N,N,N',N'-Tetramethylethylenediamine (TEMED). Long acrylamide chains are crosslinked by N-,N'-Methylenebisacrylamide.
Samples for SDS-PAGE were adjusted to 1×SB and boiled for 5 min at 95°C to ensure complete denaturation of proteins. Tubes were briefly spun to collect the sample which was then loaded on gels using Hamilton syringes. Samples that were not immediately loaded were long-time stored at -20°C.

Table 2.23.: Composition of SDS-polyacrylamide gels.

	Separating gel				Stacking gel
	12%	10%	8%	6%	3%
Ultrapure water	2.5 ml	3.0 ml	3.5 ml	4.0 ml	1.25 ml
Acrylamide/ Bisacrylamide	3.0 ml	2.5 ml	2.0 ml	1.5 ml	0.625 ml
4x Buffer	1.875 ml	1.875 ml	1.875 ml	1.875 ml	0.33 ml
APS	75 µl	75 µl	75 µl	75 µl	37.5 µl
TEMED	7.5 µl	7.5 µl	7.5 µl	7.5 µl	3.75 µl

2.5.6. Coomassie stain of SDS polyacrylamide gels

SDS polyacrylamide gels were placed into coomassie staining solution for 1 h at RT. Staining solution was collected and the gel was washed several times in coomassie destaining solution. Used destaining solution was collected and recycled by filtering through activated carbon powder. Coomassie-stained gels were documented using gel imaging systems.

2.5.7. Immunoblotting

Immunoblotting (also called Western blotting) is a highly sensitive method to visualise proteins separated by SDS-PAGE (section 2.5.5). Here, an electric field is used to transfer proteins from the polyacrylamide gel onto a membrane on which further immuno-labelling can occur. Beside SDS, which masks protein charges proportionally to protein length, methanol is needed to fix proteins onto nitrocellulose membranes. Proteins were either transferred with a semi-dry blotting system (Biometra) for 3 h at 1 mA/cm^2 at RT or with a wet-blotting apparatus (Biorad) for 90 min with 110 V at 4°C if higher transfer efficiency was needed.

Nitrocellulose membranes were reversibly stained for 5 min at RT with ponceau staining solution to assess protein loading and transfer efficiency. Blots were blocked for unspecific antibody binding for 1 h at RT with antibody blocking solution. Membranes were washed 2× with 1×TBS and incubated with primary antibody solution (table 2.10) overnight at 4°C or for 2 h at RT. Antibody solutions were collected for re-use and membranes were washed 3×5 min in 1×TBS. Subsequently, membranes were incubated with secondary antibodies conjugated to horse radish peroxidase (HRP, table 2.11) for 1 h at RT. To reduce background signals from unspecifically bound secondary antibody, membranes were washed 3×5 min with 1×TBS. The signal was evoked by applying enhanced chemiluminescence reagent which serves as a substrate for HRP which catalyses the conversion of luminol to 3-Aminophthalate and light. The chemiluminescence was either detected with X-Ray films or gel imaging systems.

2.6. Image acquisition and analysis

2.6.1. Microscopy of fixed samples and image analysis

Microscopes are optical instruments to visualise structures that cannot be separated by eye. Some subcellular structures can be stained with non-fluorescent dyes like cresyl violet actetate before documentation by conventional transmitted light microscopy in which the specimen is illuminated with light and magnified by objective and ocular.

Cellular structures can also be stained with fluorescent substances like 4',6-Diamidine-2'-phenylindole (DAPI) or with antibodies and probes coupled to fluorochromes. Fluorescence is a physical phenomenon in which electrons of fluorochromes are excited to higher energy levels by absorbing energy of light of a specific wave length. Falling back to the ground state emits light of reduced energy due to relaxation movements.

Epifluorescence microscopy is a type of wide-field microscopy in which the specimen is illuminated in a in multiple planes around the focal plane, hence, collecting fluorescence intensities from whole cells. Using an epi-illuminating system allows to excite and detect from one side of the sample preventing excitation beams to enter the detector which reduces background signals.

Confocal microscopy is a variation of wide-field microscopies in which a pin-hole (also called aperture) prevents emitted light from planes that are out of focus to enter the detector. As a consequence background is reduced and higher resolution achieved. In laser-scanning

confocal microscopy the excitation volume is scanned over the field of view point by point. In spinning-disc confocal microscopy, a rotating pinhole array allows detection of multiple sample points at once thereby increasing acquisition speed.

Organ slices: Images of fluorophore-labelled organ slices were documented on laser scanning microscopes due to the thickness in z-direction. For quantification of brain slices, z-stacks were acquired with a 40× objective with 1 µm intervals. Stacks with 18-20 images were projected onto one image and the intensity per region of interest (ROI) was determined. Immunohistological stainings to observe tissue architecture were documented with a low magnification (lung: 10× objective).
Nissl stainings to quantify tumour growth were imaged with a 2.5× objective with transmitted light microscopy on a Zeiss Axiovert 200M. Tumour regions were identified in comparison to the healthy brain region and width and length were measured perpendicularly. Tumour volume per 40 µm slice was calculated in ImageJ and summed up for each animal.

Analysis of cell area and cell shapes: Image acquisition to evaluate cell shapes at steady state and during spreading was performed with a 63× objective on the spinning disc confocal microscope. Images were exported as TIFFs from Volocity software and converted to batch stacks using the 'Images Converter 3.3' (Feutlinske, 2014) in ImageJ. Fluorescence from F-actin, dyed with Phalloidin, was thresholded to select whole cells. Cell area and shape parameters per cell were generated using the particle analyser plug-in of ImageJ. Calculations applied to determine cell body solidity and circularity are explained in figure 2.1. Number of round cells, determined for spreading assays, was counted manually.

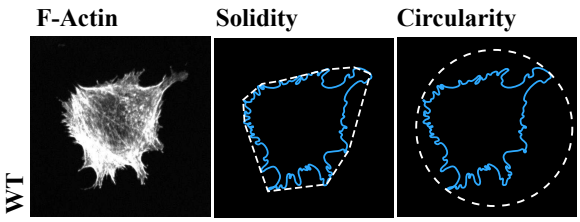

Figure 2.1.: Quantification of shape parameters. Exemplary cells from spreading experiments depicting quantification procedures for cell shape parameters. Cell body solidity is described as the ratio between cell area (blue) and the area of the convex hull (white). Cell body circularity is defined by the ratio of cell area (blue) and the area of the surrounding circle (white).

Quantification of intensities: Epifluorescent as well as confocal images were used for quantification of immunofluorescent stainings. Images from the confocal microscope were exported as TIFFs from Volocity software. TIFFs were converted to batch stacks using the 'Images Converter 3.3' (Feutlinske, 2014) in ImageJ and cells were selected manually. Due to the progression in image-based quantifications, two methods were used within the thesis. Either mean fluorescent intensities were determined using the 'Intensity Quantifier 1.1' (developed by Dr. Fabian Feutlinske as a macro for ImageJ) in which case fluorescence intensities were normalised to the cell area. Or mean fluorescence intensities were measured using the measurement tool in ImageJ and mean fluorescence per cell was calculated. To quantify the extent of colocalisation between two channels, Pearson's Correlation Coefficients were determined using the according ImageJ plug-in 'Coloc2' with 'Costes Threshold regression'. To investigate the localisation of cytosolic proteins from cell edge towards the nucleus, line profiles averaging the mean fluorescent intensity of 20 pixel depth were generated (figure 2.2). For each of the 10-13 cells per condition two line scans were acquired. Averaging of cells was achieved by defining the cell periphery with phalloidin staining and the nucleus by DAPI dye allowing normalisation of distances between cells.

Quantification of cell structures: Epifluorescent images to quantify number of focal adhesions in nocodazole washout assays were converted to batch stacks using the 'Images Converter 3.3' (Feutlinske, 2014) as macro in ImageJ. Cells were selected manually and focal adhesions per cell were calculated using the 'Batch Particle Analyzer 3.3' (developed as macro for Image J by Dr. Fabian Feutlinske). Data was accessed and summarised via an Microsoft Excel macro called 'Modul9-Mathias' a self-made modification of the original macro developed by Dr. Peter Koch.
The amount of circular dorsal ruffles (CDRs), numbers of actin stress fibres as well as destrin clusters was counted manually. 2-5 dorsal stress fibre (DSF) lengths per cell were measured using the measurement tool from ImageJ and averaged per cell.

2.6.2. Detection of chemiluminescence and western blot quantification

To quantify chemiluminescence detected from western blots, two methods were used within the thesis. X-Ray films were analysed using the gel analysis tool from ImageJ in which lane profile plots are generated. After excluding background manually the peak areas were calcu-

lated and normalised to the loading control. Chemiluminescence of western blots recorded with the Biorad gel documenting system were quantified using the ImageLab software provided by the same company. In brief, protein bands were selected manually, band intensity 3D plots generated and the volume of each plot calculated. Pulldowns were normalised to GST controls while phosphorylation levels of proteins were normalised to the total protein amount.

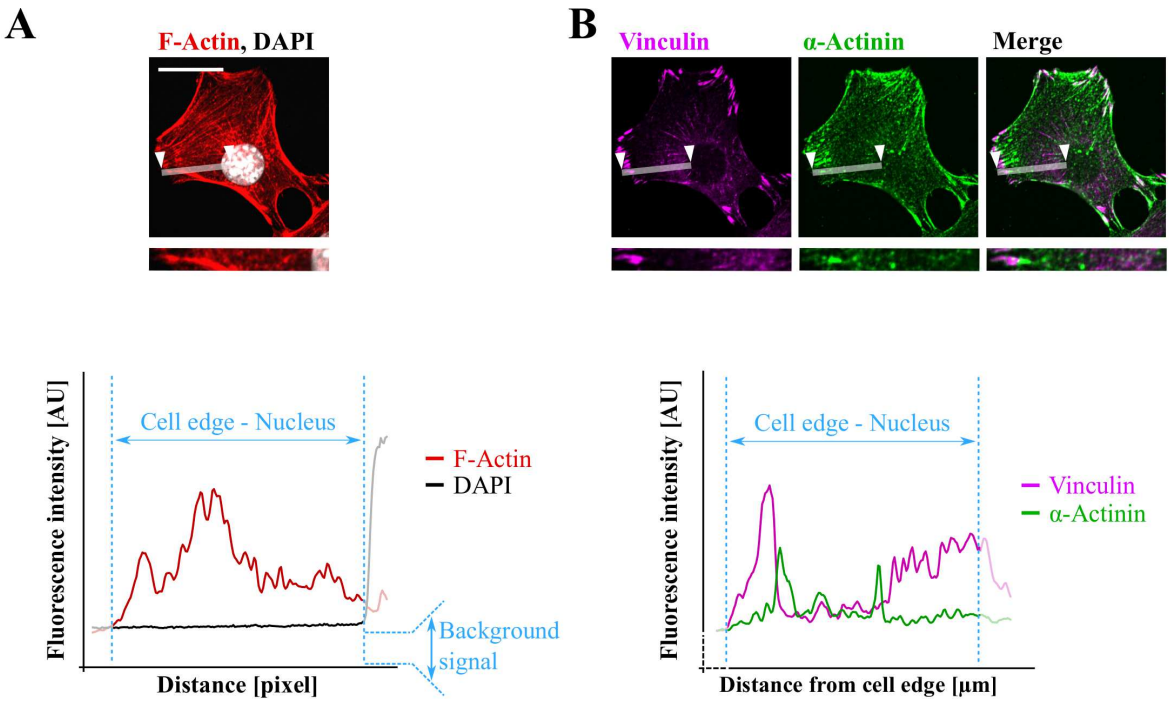

Figure 2.2.: Generation of line profiles. Averaged line scans of fluorescence intensities were generated in two steps. **A)** To define the distance from the cell edge, MEFs were stained for F-Actin and DNA using fluorescent-labelled phalloidin and DAPI dye, respectively. Along a 20 pixel deep line (white arrows, region is zoomed in below) averaged fluorescence intensities of phalloidin and DAPI were acquired (graph below). After background subtraction, the peripheral border of the cell and the localisation of the nucleus were determined to define the distance from the cell edge and to normalise fluorescence intensities of cells (see graph in B). **B)** In the following step, averaged fluorescence intensities of immunostainings (here vinculin and α-Actinin) were acquired along the same 20 pixel deep line (white arrows, regions are zoomed below). Line profiles generated in the second step were normalised using the distance from the cell edge as reference point. Scale bar: 25 µm.

2.7. Statistical analysis

For statistical analysis experiments were performed at least 3×. No statistical approaches were used to pre-determine sample sizes. To achieve reliable statistical data from microscopy-based quantifications 20-30 images were acquired yielding - depending on the magnification used - 20-100 cells per experiment. Quantifications were performed as described in section 2.6 and generated values were illustrated as 'mean ± standard error of mean (s.e.m.)'. Outliers were determined using the Grubbs' test offered by GraphPad. Number of experiments or animals were indicated as 'n'.

To determine whether a statistical difference between two conditions existed, the Student's t-test (or t-test) was used. Gaussian distribution was not determined between experiments due to low experimental numbers, however, normal distribution within experiments was checked regularly. Statistical analyses was performed using the two-sample, paired t-test. However, in case of figure 3.7A and figure 3.9D alternatives of the t-test were applied. Within the Gaussian distribution the two-tailed t-test describes the deviation from a reference value in both directions. To ensure comparability, all samples of one experiment were processed on the same day; animal experiments were only conducted between litter mates. As such 'repeated measures' or 'paired' samples can be assumed. However, different genotypes can also be seen as independent groups allowing statistical analysis with an unpaired t-test. In contrast o the two-tailed t-test, the one-tailed t-test considers only one direction and disregards the other completely.

In case of more than 2 groups tested for statistical significance, 1-Way ANOVA was used followed by either a Tukey or Dunnett post-test. While the Tukey post-test compares all possible means with one another, the Dunnett post-test compares all samples to a control. Both tests are equally accepted.

Statistical significances were calculated using GraphPad and indicated as follows: *** $p < 0.001$; ** $p < 0.01$; * $p < 0.05$.

3. Results

3.1. Stn1 is the endocytic adaptor for neuron glial antigen 2 (NG2)

A plethora of endocytic cargo proteins are selected by general endocytic adaptors like AP2, which captures cargos by recognition motifs like the tyrosine-based motif or the dileucine motif (Traub and Bonifacino, 2013). But some processes, like neurotransmission, need to be tightly regulated in a spatio-temporal manner, hence, specific endocytic adaptors are needed. These adaptors are characterised by binding on the one hand to other endocytic proteins and on the other hand to specific cargo proteins thereby linking both together. The stonins (Stn) are such cargo-specific endocytic adaptors comprising two homologues in mammals, namely Stn1 and Stn2 (Maritzen et al., 2010). Stn2 has been shown to regulate synaptic vesicle retrieval by facilitating the internalisation of Syt1 (Martina et al., 2001). Recently, Stn1 was reported to regulate migration via the neuron glial antigen 2 (NG2, Feutlinske 2014). However, the molecular mechanism remained enigmatic.

3.1.1. Stn1 interaction with AP2 regulates Stn1 protein levels and stabilises Stn1-positive subcellular structures

Stn2 had been demonstrated to interact with the AP2 α-ear via WxxF motifs located in the N-terminal part of Stn2 (Walther et al., 2004). Also Stn1 comprises a WxxF motif in the aminoterminus suggesting a putative site of Stn1 and AP2 interaction. We hypothesised that Stn1 would interact in a similar way with AP2. To test this, we performed GST pull-down experiments using full-length HA-Stn1 overexpressing HEK293T extracts. The GST-α-ear of AP2 strongly precipitated full-length HA-Stn1 while a GST control did not (figure 3.1A). AP1, a heterotetrameric adaptor complex regulating clathrin-mediated transport between the Golgi apparatus and the late endo-lysosomal compartment, also recognises a hydropho-

bic motif similar to the WxxF motif via its γ-ear (Ritter et al., 2004). A weak interaction of HA-Stn1 with the γ-ear of AP1 was detected (figure 3.1A high exposure). However, Stn1 does not localise to the Golgi apparatus in immunostainings (Feutlinske, 2014) indicating no physiological relevance of the interaction.

To validate whether Stn1 interacts with AP2 via the WxxF motif, we mutated the hydrophobic residues of the WxxF motif to AxxA (figure 3.1C) which was shown to abrogate the interaction between Stn2 and AP2 (Walther et al., 2004). Although the interaction with AP2 was diminished, a substantial portion of Stn1 AxxA still interacted with the GST-α-ear of AP2 (figure 3.1B) indicating another site of interaction. In fact, the C-terminus of Stn1 also comprises a non-classical WxxF motif (figure 3.1C, from own observation). This additional motif might support the interaction with the AP2 α-ear.

Interestingly, the protein levels of the Stn1 AxxA mutant in HEK293T cells was also dramatically reduced in comparison to Stn1 WT (figure 3.1B input). Thus, we wondered whether the interaction with AP2 stabilises Stn1 protein levels. To test this we isolated glial cells from AP2 Lox/Lox×CAG cre/Esr1 mice to generate WT (Flox (-)) and AP2-depleted (Flox cre) *in vitro* cell cultures. Treatment with tamoxifen dramatically ceased AP2 expression in Flox cre glial cells after 3 weeks of *in vitro* culture (figure 3.1D). Similar to the expression of the Stn1 AxxA mutant which abrogated AP2 binding, depletion of AP2 resulted in a decrease of endogenous Stn1 levels (figure 3.1D). Quantification of immunoblots for endogenous Stn1 revealed that Stn1 protein levels were diminished by about 40% (figure 3.1E). Next we performed immunostainings to investigate the subcellular localisation of endogenous Stn1 in AP2 Lox/Lox×CAG cre/Esr1 glial cells. There were two distinct pools of Stn1 in AP2 Lox/Lox×CAG cre/Esr1 astrocytes: Stn1 puncta were found at the periphery and nearer to the cell nucleus (figure 3.1F). Although distal Stn1 positive structures were also observed in tamoxifen induced AP2 depleted astrocytes, the central pool seemed remarkably reduced.

In summary, Stn1 was found to be an endocytic adaptor that interacts with the AP2 α-ear in part via a WxxF motif resulting in stabilisation of Stn1 puncta in cells.

3.1.2. The neuron glial antigen 2 (NG2) is a cargo of Stn1

Stn2 facilitates the clathrin-mediated uptake of synaptotagmin 1, 2 and 9 (Diril et al., 2006), calcium sensors that regulate synaptic vesicle fusion (Pang and Südhof, 2010). By mutational analysis Jung et al. (2007) showed that a KYE motif (ms-Stn2: AA 780-782) within the μ-

homology domain of Stn2 mediates its interaction with the C2A and C2B domains of Syt1. Although comprising the KYE motif (ms-Stn1: AA 638-640) within its μ-homology domain, Stn1 does not co-localise with synaptotagmins (Diril et al., 2006) indicating that it does not serve as adaptor for Syt1.

In absence of their specific endocytic adaptor, cargo proteins often accumulate at the plasma membrane. Therefore, Feutlinske (2014) performed surface biotinylations from SILAC-treated WT and Stn1-KO cells and analysed the surface proteome with mass-spectrometry in order to identify potential cargo proteins of Stn1. With this approach Feutlinske (2014) found the

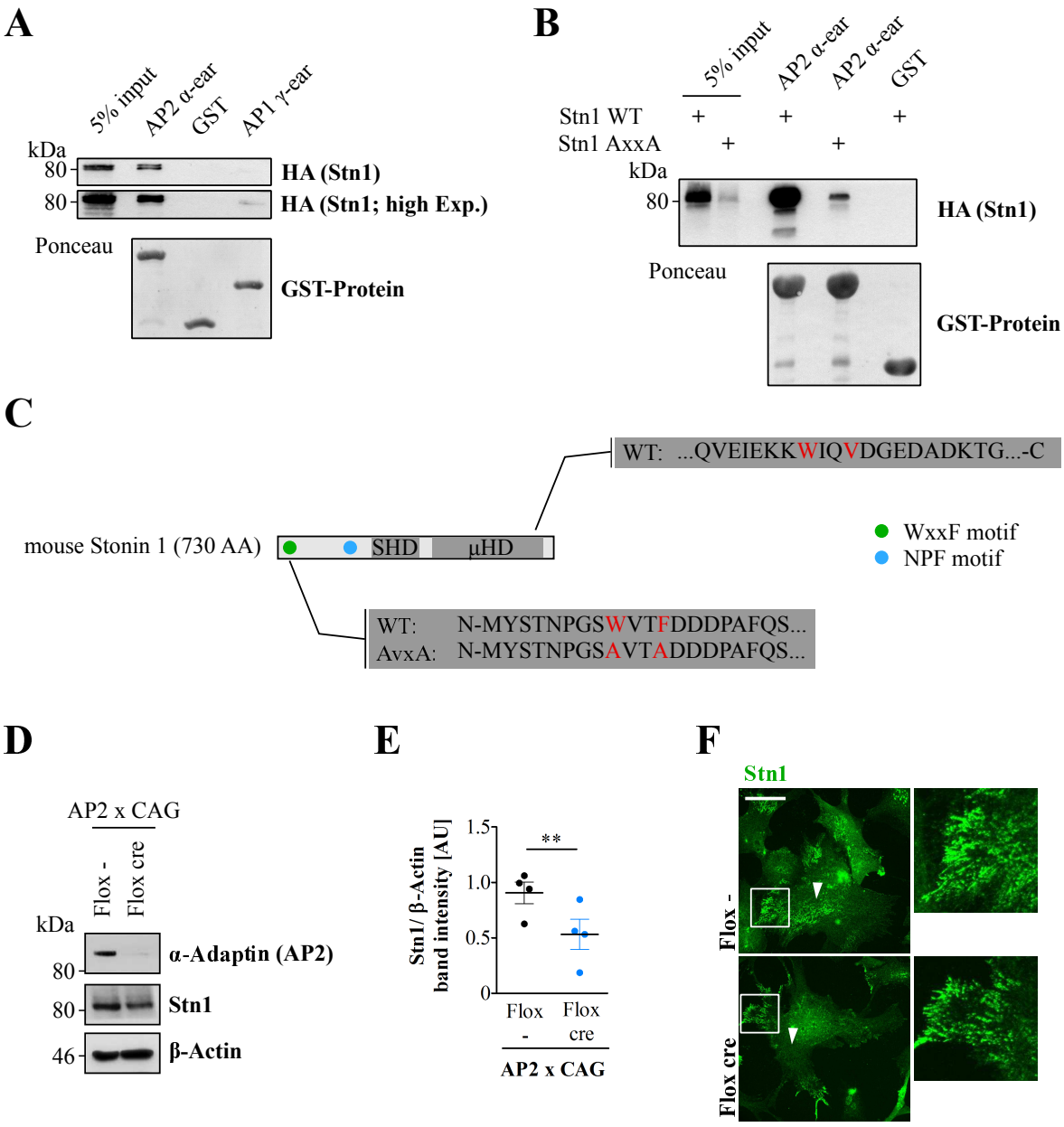

Figure 3.1.: AP2 interacts with Stn1. **A)** Full-length HA-Stn1 interacted with AP2 α-ear in GST pull-down experiments (n=3). Lysates of HEK293T cells that overexpressed full-length HA-Stn1 were used for GST-pulldown experiments with AP2 α-ear and AP1 γ-ear. **B)** Mutating the AP2 interaction motif WxxF of Stn1 in AxxA reduced Stn1 protein levels and its interaction strength towards AP2 α-ear in GST pull-down experiments (n=2). Wild-type (WT) and AxxA mutant HA-Stn1 were overexpressed in HEK293T cells and lysates were subjected to GST-pulldown experiments using AP2 α-ear. **C)** Scheme showing the N-terminal AP2 interaction motif which was mutated for B) to abrogate AP2 binding towards Stn1. Binding towards AP2 might be also mediated by an additional non-classical WxxF motif at the C-terminus. **D,E)** Depletion of AP2 in astrocytes reduced Stn1 protein levels (n=4, paired, two-tailed t-test). Glial cell cultures generated from AP2 lox/lox×CAG cre mice were treated with 0.1 µM tamoxifen to deplete AP2. After 3 weeks, lysates of glial cell cultures were analysed by immunoblotting. **F)** Epifluorescent images of astrocytes showed two pools of Stn1 - one at peripheral sites (zoom), one near the cell nucleus (arrows). Depletion of AP2 caused loss of internal Stn1 puncta. Glial cultures which were generated as described for D) and E) were stained for endogenous Stn1. Scale bar: 50 µm. (*µHD - µ-homology domain, SHD - stonin homology domain*)
Experiments D and E were performed and analysed by Tania Lopez-Hernandez.

---

neuron glial antigen 2 (NG2) to be strikingly enriched at the surface of Stn1 KO cells. We wanted to unravel the molecular mechanism underlying the presumed interaction between Stn1 and NG2.

NG2 is an extremely large protein with a molecular weight of about 330 kDa. Therefore, only the cytosolic domain of NG2 was used in GST pull-down assays to investigate whether Stn1 interacts with NG2. Since the basic stretch of the cytosolic domain (AA 2250-2255) of NG2 lowered the protein stability and yield during the protein purification process, a stretch containing most of the cytosolic domain of NG2 (AA 2256-2326) was generated (CD1, see also figure 3.4C). In GST pulldown assays using lung extracts, NG2 CD1 (AA 2256-2326) interacted with endogenous Stn1 (figure 3.2). No interaction was documented between NG2 and gadkin confirming binding specificity between the endocytic adaptor Stn1 and its cargo. GST which was used as binding control did not interact unspecifically with Stn1.

To understand how Stn1 interacts with NG2 we generated truncations of Stn1 comprising the N-terminal unstructured part together with the stonin homology domain (AA 1-404) and the carboxyterminus with the µ-homology domain (AA 405-730). In combination with full-length NG2, each of the Stn1 constructs was transfected into HEK293T cells and the cell extracts were used for immunoprecipitation of full-length NG2 using NG2-specific antibodies (figure 3.3). While no interaction was detected between full-length NG2 and Stn1 (AA 1-404),

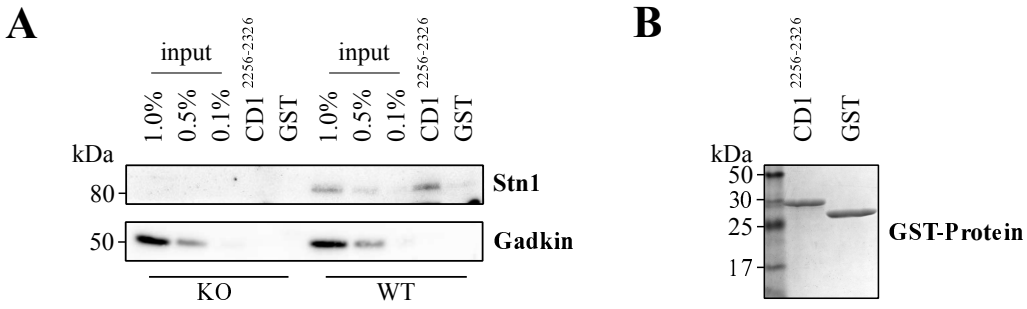

Figure 3.2.: The cytosolic domain of NG2 interacts with Stn1. A) Full-length Stn1 was precipitated from lung tissue by the cytosolic domain of NG2 (AA 2256-2326) in GST pull-down experiments while gadkin, used as negative control, was not (n=5). Stn1 KO samples demonstrated the antibody specificity for endogenous Stn1 during immunoblotting. **B)** Coomassie staining of purified GST-proteins demonstrated purity and equal loading. (*CD - cytosolic domain*)

---

a strong interaction of full-length NG2 with Stn1 (AA 405-730) was observed. Therefore, we can conclude that Stn1 interacts with the endocytic machinery via the aminoterminus (section 3.1.1), while cargo-binding occurs via the μ-homology domain. Though, endogenous Stn1 interacted with the cytosolic domain of NG2 in GST pull-down experiments (figure 3.4), immunoprecipitation of full-length NG2 did not co-precipitate full-length Stn1. This might indicate inefficient binding to NG2 due to autoregulatory mechanisms. In fact, Stn1 had been already shown to be phosphorylated at multiple sites (Feutlinske, 2014) which might form the basis for an autoinhibitory conformation that hinders NG2 binding.

To investigate how NG2 interacts with the μ-homolgy domain of Stn1, we performed GST-pulldown assays using truncated versions of the cytosolic domain of the proteoglycan (figure 3.4C). CD1 (AA 2256-2326), which was already used for figure 3.2, only lacked a basic stretch proximal to the transmembrane domain to increase the protein stability. CD2 (AA 2270-2326) and CD3 (AA 2305-2326) were shortened at the aminoterminus which excludes PKCα and pErk binding sites. CD4 (AA 2305-2320) lacked the PDZ-domain interaction motif in addition. The GST-bound NG2 fragments were incubated with extracts from HA-Stn1 (AA 405-730) overexpressing HEK293T cells and samples were subjected to immunoblotting (figure 3.4A). All NG2 fragments precipitated the Stn1 μ-homology domain from HEK293T extracts while a GST control did not. Of note, absence of the PDZ-domain interaction motif in CD4 significantly decreased the interaction between the cytosolic domain of NG2 and the cargo binding domain of Stn1 (figure 3.4B). This indicated that the interaction between Stn1

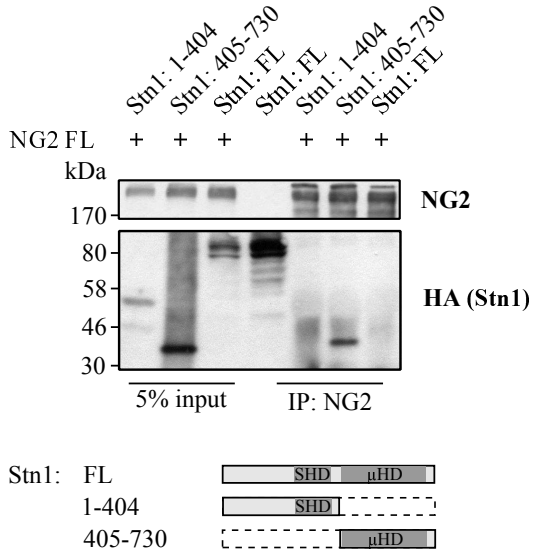

Figure 3.3.: The Stn1 µ-homology domain interacts with NG2. Full-length (FL) NG2 co-immunoprecipitated Stn1 AA 405-730 comprising the µ-homology domain (n=4). No interaction was observed for full-length Stn1 or a fragment containing the aminoterminal part and the stonin homology domain (AA 1-404). NG2-specific antibodies were used for co-immunoprecipitation experiments from HEK293T cell lysates which co-overexpressed full-length NG2 and different Stn1 constructs. Truncations with structural features are documented below. (*µHD - µ-homology domain, SHD - stonin homology domain*)
Immunoprecipitation was performed with a rabbit polyclonal NG2 antibody 'K1' from the Trotter lab raised against mouse NG2 (12 µg/sample).

---

and NG2 is mediated via the PDZ-domain interaction motif. The PDZ-domain interaction motif had been shown to bind PDZ-domain containing proteins like syntenin 1 (Chatterjee et al., 2008) which determines the subcellular distribution of NG2 and regulates cell migration. Sequence analysis of Stn1, however, did not reveal any PDZ domain that might interact with NG2 or any other known PDZ-domain interacting protein (Scansite 3 beta). It is therefore unlikely that Stn1 directly interacts with NG2, yet the linking protein remains to be identified in further studies.

3.1.3. Stn1 controls NG2 protein levels in mouse tissue

We wanted to identify a tissue were NG2 and Stn1 are expressed which would points towards an important function of both proteins within the tissue. Beside astrocytes, oligodendrocytes and microglia, NG2-positive glial cells - or polydendrocytes - are often referred to the fourth cell population present in the adult brain giving raise to so called adult oligodendrocyte

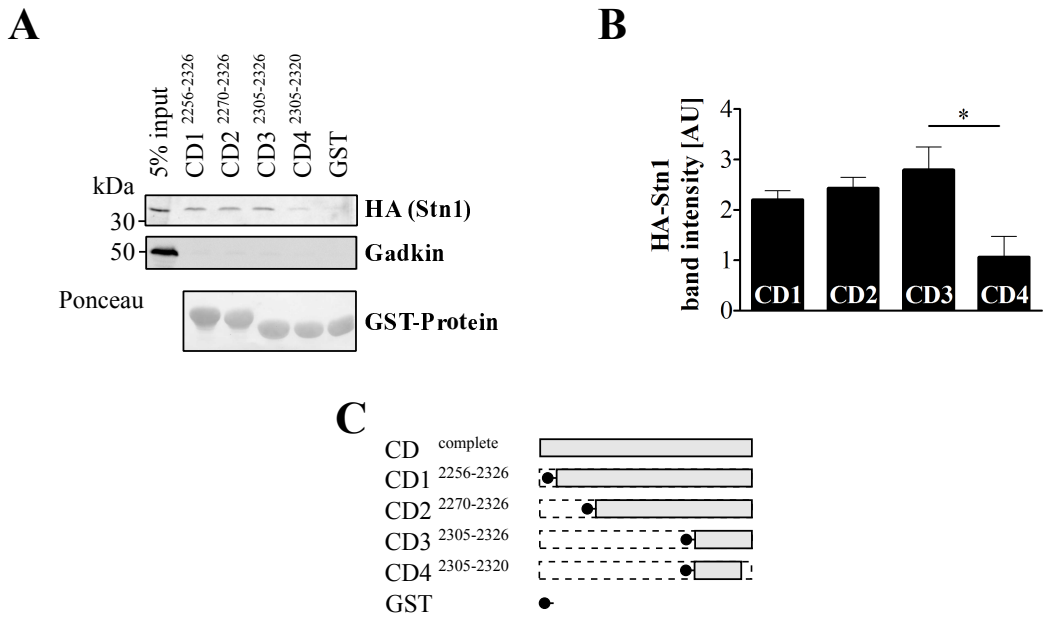

Figure 3.4.: NG2 PDZ-domain interaction motif impairs Stn1 μ-homology domain interaction. A) HA-tagged μ-homology domain of Stn1 (AA 405-730) was pulled by truncations of the NG2 cytosolic domain (CD1-CD4) in GST pull-down assays. GST pull-downs were performed with lysates of HA-Stn1 (AA 405-730) overexpressing HEK293T cells. **B)** Quantification of HA-Stn1 band intensities from A showed a significant reduction of Stn1 interaction with the the cytosolic domain of NG2 lacking the PDZ-binding motif (CD4, n=3, 1-Way Anova, Dunnett post test). **C)** Schematic representation of NG2 fragments used. (*CD - cytosolic domain*)
The experiment was carried out by Philipp Trnka under my supervision.

precursor cells (Levine et al., 2001). NG2 expression coincides with the life time of polydendrocytes that arise from neuronal stem cells and differentiate into mature myelinating oligodendrocytes (Nishiyama et al., 2009). Consistently, Niehaus et al. (1999) demonstrated that NG2 expression peaks in mice between postnatal day 8-12 when myelination starts. Thus, NG2 as a marker for oligodendrocyte progenitors is known to be predominantly expressed in the brain of young animals. However, Stn1 was found to be pronouncedly expressed in lung (Feutlinske, 2014). Therefore, both organs were examined for Stn1 and NG2 expression by western blot analysis (figure 3.5A). Stn1 was detected in both, lung and brain tissue however its presence in brain was remarkably lower compared to lung (note loading amount). Also NG2 was present in both organs with a stronger expression in lung tissue.

The strong expression of Stn1 and NG2 in lung pointed towards an important role in lung function. Besides being a marker for polydendrocytes, NG2 is frequently used to identify

pericytes (Trost et al., 2016). Pericytes are closely associated with arterioles and capillaries (Murfee et al., 2005) directly contacting the endothel to regulate vessel permeability, the blood flow and immune response. Previous studies showed that about 10-20% of all lung cells are pericytes (Hung et al., 2013; Sims, 1986) making it one of the organs with the highest pericyte coverage of the endothel (Armulik et al., 2011). Pericytes can differentiate into multiple cell types including vascular smooth muscle cells (vSMC, Díaz-Flores et al. (2009) and myofibroblasts. Both of these cell types are characterised by α smooth muscle actin (αSMA) expression, but while vSMCs ensheath venules and high-calibre vasculature (Trost et al., 2016), myofibroblasts play substantial roles during fibrosis (Barron et al., 2016).

Feutlinske (2014) demonstrated that Stn1 - like NG2 - is expressed by pericytes. In addition, expression of NG2 by pericytes plays important roles in maintaining endothel connectivity and vessel integrity during angiogenesis. Therefore, we wanted to know whether deletion of Stn1 changed the architecture of the pulmonary vasculature. To identify vasculature, endothelial cells of lung tissue slices were immunostained for the platelet endothelial cell adhesion molecule 1 (PECAM1). Endothelial cells formed a network encompassing pulmonary alveoli, bronchioles were PECAM1 negative (figure 3.5B). αSMA was mainly found on ring-like structures that were also PECAM1 positive indicating large-diameter blood vessels. αSMA was also identified around bronchioles indicating blood vessels sparsely wrapped around these structures. We could not detect αSMA within the capillary network around alveoli indicating a healthy lung without fibrosis and well preserved tissue architecture throughout the staining process. Furthermore, no difference between WT and Stn1 KO animals with respect to PECAM1 or αSMA distribution or intensity was detected. NG2, as marker for pericytes and vSMC, was frequently found around blood vessels and the capillary network around alveoli (figure 3.5C). The NG2 antibody also recognised bronchioles, however, Paez-Cortez et al. (2013) showed, using NG2-tdTomato animals, that NG2 should be absent from these structures. Hence, the antibody likely bound unspecifically to bronchioles. Overall the NG2 staining in WT and Stn1 KO lung displayed a normal distribution of NG2 positive cells as reported by others (Rock et al., 2011).

In absence of the endocytic adaptor Stn1, total protein levels of NG2 increased in extracts of MEFs (Feutlinske, 2014). We wondered whether absence of Stn1 actually alters NG2 expression in lung tissue. In line with the unaltered lung vasculature, however, quantifications of NG2 protein levels did not reveal any difference when Stn1 was deleted (figure 3.5D,E).

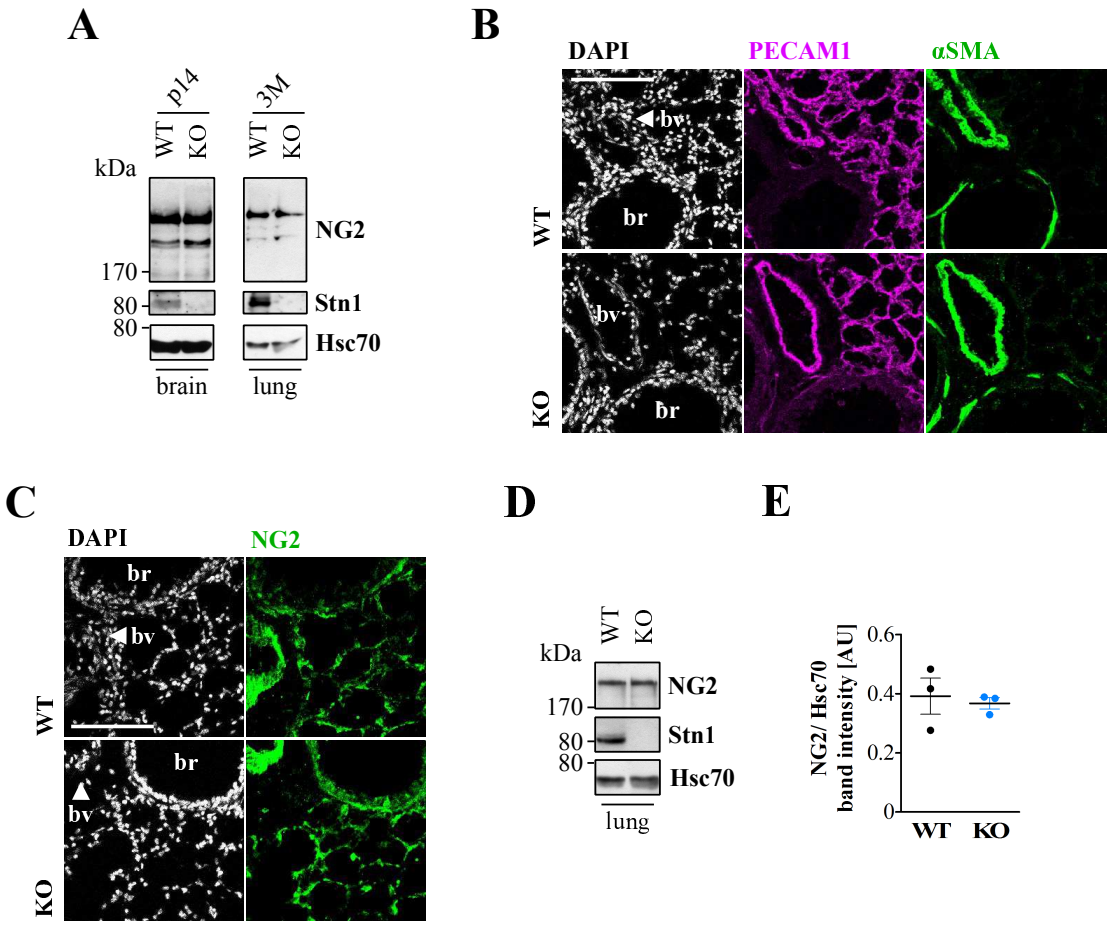

Figure 3.5.: Strong expression of Stn1 and NG2 in lung tissue. **A)** Stn1 was weakly expressed in brain and very pronounced in lung tissue (note loading amount). Same was true for NG2 in both tissues. Extracts of lung and brain of WT and Stn1 KO mice were immunoblotted against endogenous Stn1 and NG2. To prevent overexposure, tissue lysates were loaded at unequal amounts: brain 125 µg, lung 50 µg per sample. **B)** Stn1-depletion did not alter lung architecture. Lung architecture was examined using PECAM1 as marker for endothelial cells and αSMA to identify vSMC and myofibroblasts with confocal microscopy. Lung cryosections were immunolabelled using antibodies against endogenous αSMA and PECAM1. Scale bar: 100 µm. **C)** Confocal images of lung immunostainings using an NG2 specific antibody showed the typical distribution of NG2 within lung tissue. Lung cryosections were immunolabelled using an antibody against endogenous NG2. Scale bar: 100 µm. **D,E)** No change of endogenous NG2 expression levels in adult mouse lung when Stn1 was depleted. Analysis of immunoblots of WT and Stn1 KO extracts from lung tissue. NG2 band intensity was normalised to Hsc70. (*br - bronchiole, bv - blood vessel, αSMA - smooth muscle actin, PECAM1 - platelet endothelial cell adhesion molecule 1*)

In conclusion, Stn1 absence did neither influence NG2 protein levels in lung tissue nor its distribution within the organ. In addition, the contribution of NG2-positive pericytes to the vSMC or myofibroblast population seemed unaltered upon Stn1 deletion.

Despite the striking expression of Stn1 and NG2 in lung tissue, lung architecture and composition was unaltered between WT and Stn1 KO animals arguing maybe for a lung-specific compensation mechanism. Both proteins, however, are also present in p14 brain (figure 3.5A). Previous studies demonstrated that NG2 is expressed throughout the brain including olfactory bulb (OB, Komitova et al. 2009), neocortex (Karram et al., 2008) and cerebellum (Kucharova and Stallcup, 2010). Within these regions NG2 functions mainly in oligodendrocyte precursors allowing fast renewal of mature oligodendrocytes (Dawson et al., 2003). In glial cultures, Stn1 and NG2 nicely co-localised at the cell boundaries (figure 3.6A) indicating that both proteins might play a role in the same cell type within the brain. Due to lack of an antibody suitable for IHC we could not determine the localisation of Stn1 within the brain by IHC. To at least compare Stn1 protein levels across different brain regions, we separated the OB, the neocortex and the cerebellum of p14 animals to analyse Stn1 expression within these brain regions (figure 3.6B). In all three regions Stn1 expression was detected. The strongest Stn1 expression in brain was detected in the olfactory bulb. Importantly, lysates of Stn1 KO animals did not show immunoreactivity confirming antibody specificity in Western blot analysis.

Since deletion of Stn1 was associated with increasing NG2 levels in MEFs (Feutlinske, 2014) we wondered whether absence of Stn1 alters NG2 protein levels in different brain regions. NG2 expression peaks shortly before developmental myelination starts (Niehaus et al., 1999) but remains detectable in adult brains. Therefore, we subjected sagittal brain slices of p14 and 2-3 months old animals to immunohistochemical analysis. At p14 NG2 expression was found in all brain regions mentioned before ranging from olfactory bulb to the molecular layer of the cerebellum. However, only within the granular layer of the olfactory bulb of Stn1 KO animals aged p14, NG2 expression was significantly increased (figure 3.7A). Layering and cell morphology were unaltered in Stn1 KO OB.
During maturation of polydendrocytes into oligodendrocytes NG2 levels decrease until only 8% self-renewing polydendrocytes remain within the adult brain (Dawson et al., 2003). Accordingly, very few NG2 positive cells were detected in adult WT and Stn1 KO brains. In

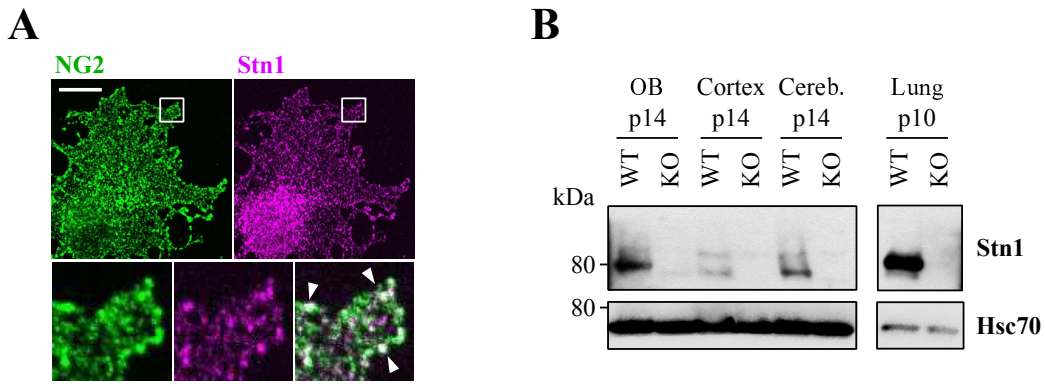

Figure 3.6.: Stn1 is expressed in different brain regions of p14 mice, presumably within glial cells. **A)** Confocal images demonstrating Stn1 co-localisation with NG2 in glial cell cultures (see arrows). Glial cell cultures were immunolabelled for endogenous Stn1 and NG2. Scale bar: 10 µm. **B)** Stn1 was mostly expressed in OBs of p14 animals but also present in the neocortex and the cerebellum (n=2). Tissue lysates of brain and lung of WT and Stn1 KO mice were analysed by immunoblotting. To prevent overexposure, tissue lysates were loaded at unequal amounts: brain 125 µg, lung 50 µg per sample. (*Cereb. - cerebellum, OB - olfactory bulb*)

---

the olfactory bulb and frontal cortex, NG2 was most strongly expressed showing a tendency towards higher levels in Stn1 KO (figure 3.7B,C).

In summary, Stn1 and NG2 are both expressed in lung and brain tissue. Yet, in lung Stn1 absence did not influence NG2 protein levels. It might be that the high protein amount of both, NG2 and Stn1, covered the slight changes caused by Stn1 deletion. Accordingly, in the brain of young animals, where low expression levels of both proteins were detected, Stn1 deletion significantly raised NG2 protein levels.

3.2. Stn1 functions as a tumour supressor

NG2 is an oncogene that supports tumour growth in multiple ways (Stallcup and Huang, 2008; Stallcup et al., 2016). On the one hand, NG2 phosphorylation balances cell proliferation and motility (Makagiansar et al., 2007). Thus, in a pathogenic situation dysregulation of NG2 in the tumour tissue might support tumour growth and metastasis. On the other hand, Huang et al. (2010) showed that NG2 being expressed by stromal cells of the host tissue support tumour progression. Using WT and NG2 KO animals they induced tumours either expressing NG2 or not. Independently of NG2 expression, both tumour types were significantly smaller

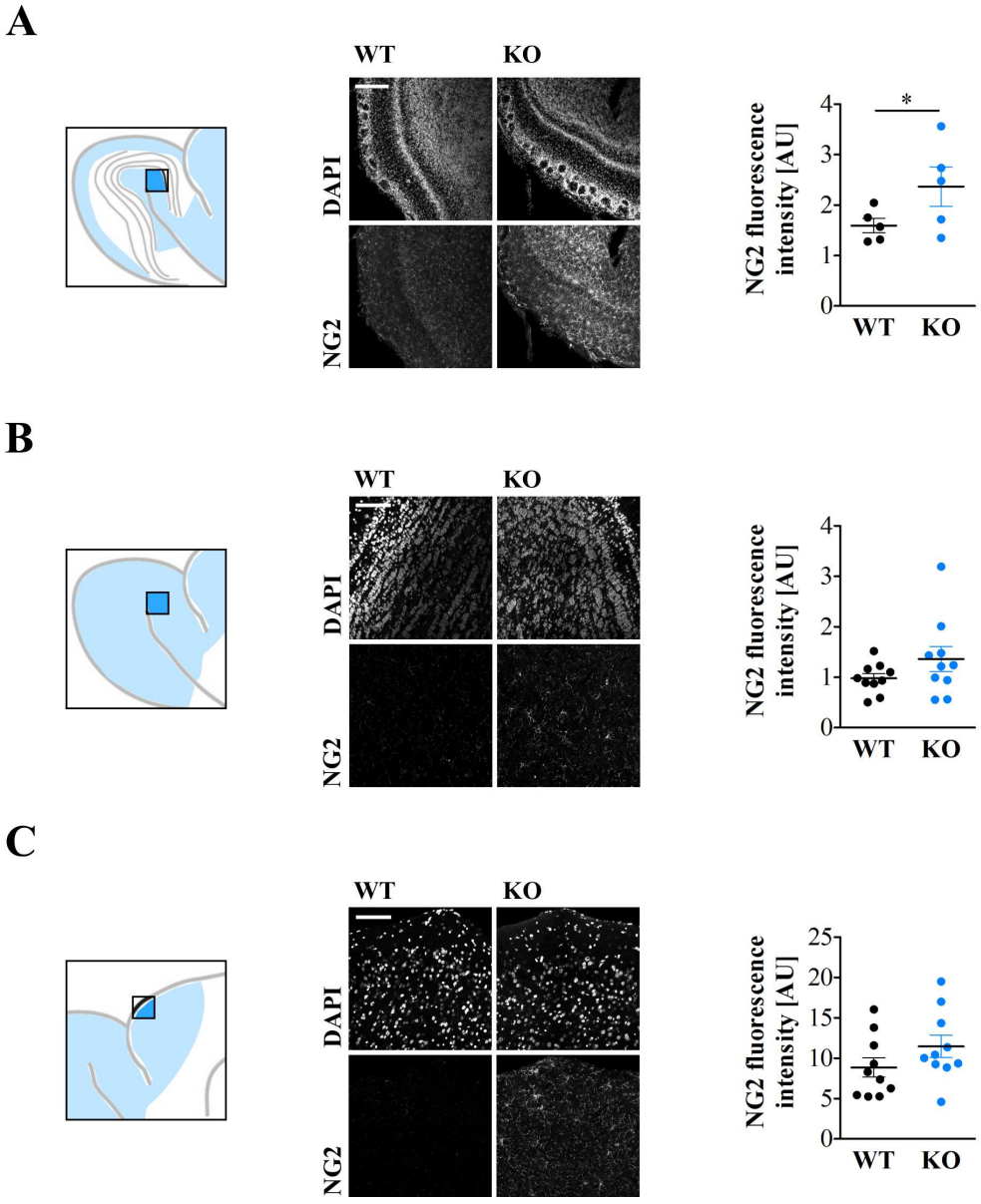

Figure 3.7.: NG2 expression is increased in olfactory bulbs of p14 Stn1 KO brains. Endogenous NG2 immunostainings of brain sections were performed using brains from p14 and 2-3 months old animals. NG2 fluorescence intensities were quantified from confocal stacks in regions (right side) depicted in schemes (left side). Areas in blue indicate the overall expression within these regions. **A)** NG2 expression was significantly increased in the granule cell layer of olfactory bulbs of p14 Stn1 KO animals (n=5, unpaired, one-tailed t-test). Scale bar: 250 μm. **B)** NG2 expression was not significantly altered in the granule cell layer of olfactory bulbs of adult animals. Scale bar: 100 μm. **C)** No significant change in NG2 expression was observed in the frontal cortex of adult animals. Scale bar: 100 μm.

when transplanted in NG2 KO animals indicating that NG2 promotes tumour progression primarily via its expression in the host tissue.

3.2.1. Stn1 diminishes tumour growth.

Stn1 is the endocytic adaptor of NG2 regulating its surface availability and cellular localisation. It was thus tempting to speculate that - in contrast to the oncogene NG2 - Stn1 would act as a tumour suppressor. We used the public database REMBRANDT to investigate survival of glioma patients dependent on Stn1 expression (figure 3.8A). In fact, elevated expression levels of Stn1 correlated with a significantly higher probability of patient survival. To unravel the role of Stn1 in tumour growth we decided to induce cancer in mice with two different approaches. The first one was designed in collaboration with Prof. Dr. Rainer Glass to elucidate whether altered Stn1 expression of transformed cells affects tumour growth. For this, we isolated neuronal precursor cells (NPC) from the subventricular zone - one of the sites of persistent adult neurogenesis - from embryonic WT and Stn1 KO animals. Transformation of NPCs with platelet-derived growth factor BB (PDGF-BB) GFP in cell culture shifts their fate into the oligodendrocyte linage (Appolloni et al., 2009) and gives rise to glioblastomas when transplanted into animals. We used this model to induce glioblastomas from PDGF-BB-GFP transformed WT and Stn1 KO NPCs in WT-C57BL/6 mice.
Radial glial cells residing within the SVZ are stem cell-like cells that differentiate mainly into neurons and astrocytes but also to a minor extend into oligodendrocytes (Bonfanti et al., 2013). As a result isolated NPCs are a mixed neurosphere culture characterised by expression of the neural stem cell marker nestin, the neuronal marker β3-Tubulin and the astrocyte marker glial fibrillary acidic protein (GFAP, Park et al. 2012). Oligodendrocyte linage markers like 2',3'- cyclic- nucleotide 3'- phosphodiesterase (CNPase) are absent from neurosphere cultures. Immunoblotting of NPC lysate confirmed the molecular identity of the extracted cell line (figure 3.8B). Brain tissue of p28 animals was used for comparison of marker abundance. Within the total brain lysate nestin expression was below the detection limit clearly demonstrating how limited stem cell niches are represented within the organ. In contrast, extracted NPCs were positive for nestin. β3-Tubulin as well as CNPase and GFAP were present at equal amounts in WT and Stn1 KO brains. Since NPCs maintain their capability to differentiate into neurons but do not develop into oligodendrocytes, extracted cell cultures expressed β3-Tubulin but not CNPase. To our surprise only Stn1 KO NPCs expressed

GFAP. Further characterisation of additional NPCs isolated from WT and Stn1 KO mice might reveal whether this was due to inter cell line variability or a real phenotype caused by Stn1 ablation. Within the SVZ, NG2 cells are sparse in comparison to the surrounding parenchym (at p30 about 0.15% compared to 3% respectively) and do not represent any of the mentioned cell types found in the SVZ (Komitova et al., 2009). Due to the concentration of SVZ cell types we could detect NG2 at higher levels as compared to total brain tissue. The lower molecular weight of NG2 in NPC cultures suggest that NG2 is proteolytically processed

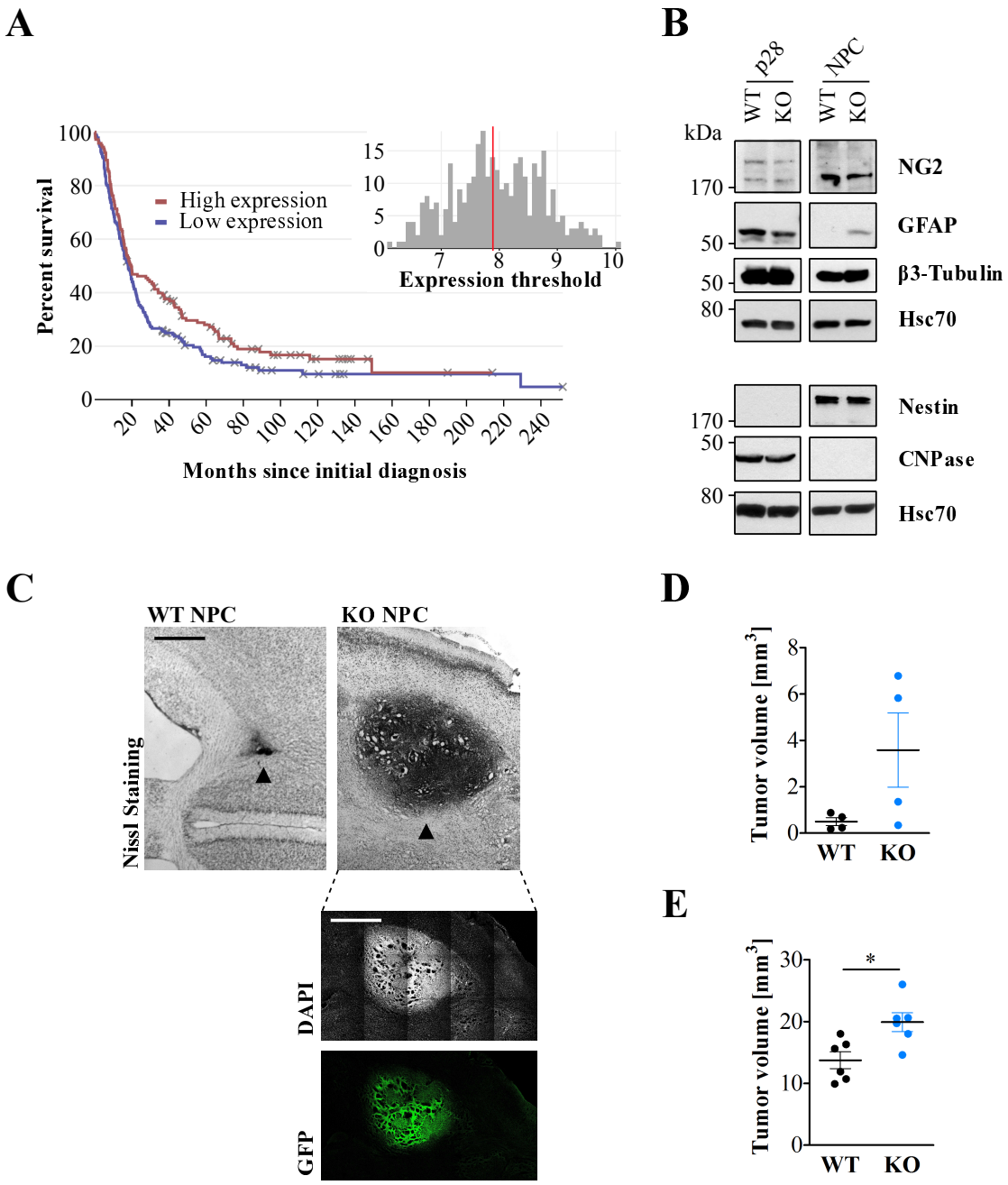

Figure 3.8.: Stn1 deletion increases tumour growth. A) Glioma patients with a higher Stn1 expression survived significantly longer than patients with low Stn1 levels. Data was generated using the platform REMBRANDT (based on Affimetrix microarray technology, all tumours included, median threshold for protein expression, p = 0.001, n=329/523). **B)** Characterisation of neuronal precursor cells (NPCs), isolated from WT and Stn1 KO subventricular zones, for astrocyte (GFAP), oligodendrocyte (CNPase), polydendrocytes (NG2), neuronal (β3-tubulin) and stem cell markers (Nestin). **C,D)** Identification of brain tumours by Nissl staining. Tumour cells were generated by viral overexpression of PDGF-BB-GFP in WT and Stn1 KO NPCs. 42 days after injection into WT-C57BL/6, the mice were sacrificed and the tumour volume was determined (see D) using transmitted-light microscopy. PDGF-BB-GFP overexpression was confirmed by immunohistochemistry of brain sections and confocal imaging (C, lower panel). Scale bars: 1 mm. **E)** MRI-determined tumour volume 14 days after implantation in WT and Stn1 KO animals. Brain tumours were induced by injection of glioblastoma GL261 cells into WT and Stn1 KO animals (n=6, paired, two-tailed t-test). (*CNPase - 2',3'- cyclic- nucleotide 3'- phosphodiesterase, GFAP - glial fibrillary acidic protein*)
Analysis for A was performed by Tania Maritzen. Tumour studies were performed in collaboration with Rainer Glass (C,D) and Min Chi Ku (E).

---

within these cultures. In fact, Asher et al. (2005) demonstrated that the ectodomain of NG2 can get cleaved by metalloproteases resulting in detection of a 250 kDa fragment of NG2 in immunoblots. It might therefore be that the enzyme shedding NG2 has a higher activity in NPCs or that the SVZ-derived cell cultures have a slower turnover of NG2.

The characterised NPCs were transformed with PDGF-BB-GFP to render them cancerogenic. 41 days post-injection into WT-C57BL/6 mice the tumour growth was assessed using Cresyviolet stainings of brain slices (figure 3.8C). Comparison to healthy brain hemispheres allowed identification of pathological brain regions in 4/8 WT and 4/7 Stn1 KO animals. Control staining against GFP confirmed the expansion of transformed PDGF-BB-GFP NPCs within the host tissue (figure 3.8C lower pannel). While tumours developed from WT NPCs remained small (0.5 +/- 0.2 mm^3) Stn1 KO NPCs expanded to a higher degree (3.6 +/- 1.6 mm^3, figure 3.8D). Hence, while the ability of transformed WT and Stn1 NPCs to induced tumours was the same, the tumour growth seemed affected by Stn1 absence. However, since only few animals developed a tumour, the approach using transformed NPCs for brain tumour development needs to be repeated to draw robust conclusions.

The second approach was designed in collaboration with Dr. Min Chi Ku to find out to what degree Stn1 absence in the host tissue influences tumour growth. Glioblastoma GL261 cells were intracranially injected into WT and Stn1 KO animals and tumour growth was assessed

after 14 days using magnetic resonance imaging (MRI). Tumour volume induced in Stn1 KO animals was significantly bigger (19.9 +/- 1.5 mm^3) than in WT (14.5 +/- 1.3 mm^3) animals (figure 3.8E).
Summarising, in accordance with data gained from public data bases both approaches confirmed enhanced tumour growth in absence of Stn1.

3.2.2. Absence of Stn1 sensitises cells towards growth factors

How can Stn1 influence tumour progression? Nutrient and oxygen supply by blood vessels is essential for tumour growth. Besides endothelial cells also pericytes and vSMCs are substantial for vascularisation of the tumour tissue. During angiogenesis pericytes are of particular importance. By expressing the PDGFRβ, pericytes are recruited by PDGF-BB secretion from endothelial tip cells and subsequently stimulate endothelial connectivity to ensure vessel integrity (Barron et al., 2016). NG2, that is highly expressed in pericytes, has been shown to play essential roles for the neovascularisation during tumour growth (Ozerdem and Stallcup, 2004). In fact, pericyte-specific deletion of NG2 diminishes pericyte coverage of the endothel which results in increased vessel leakage and reduced tumour growth (You et al., 2013).
Feutlinske et al. (2015) showed that NG2 and PDGFRβ localise to the same subcellular clusters representing signalling hubs. We speculated that close proximity of NG2 to the PDGFRβ would stimulate PDGF-BB induced signalling. Thus, elevated levels of NG2 due to Stn1 absence might result in a higher PDGFRβ sensitivity towards PDGF-BB.
To exclude the possibility of different receptor levels between the genotypes we first checked whether total levels of PDGFRβ were changed in Stn1 KO MEFs compared to WT cells. Total PDGFRβ levels were unaltered in immunoblots (figure 3.9A) confirming quantifications of total receptor levels based on immunofluorescent images performed before (Feutlinske et al., 2015). Upon ligand binding PDGF receptors dimerise allowing their cytosolic receptor tyrosine kinase domain to auto-phosphorylate in *trans* at multiple sites regulating on the one hand the internal kinase activity and generating on the other hand SH2 domain binding sites for interaction partners (Heldin et al., 1998). Following stimulation with PDGF-BB we observed a strong induction of PDGFRβ phosphorylation at Y1021 (figure 3.9B), a site important for downstream PLCγ as well as PKCα activation (Hellberg et al., 2009; Persson et al., 2004) and ubiquitin-mediated receptor degradation (Chamberlain et al., 2010; Karlsson et al., 2006). Strikingly, Stn1 KO MEFs reacted with an even stronger phosphorylation of

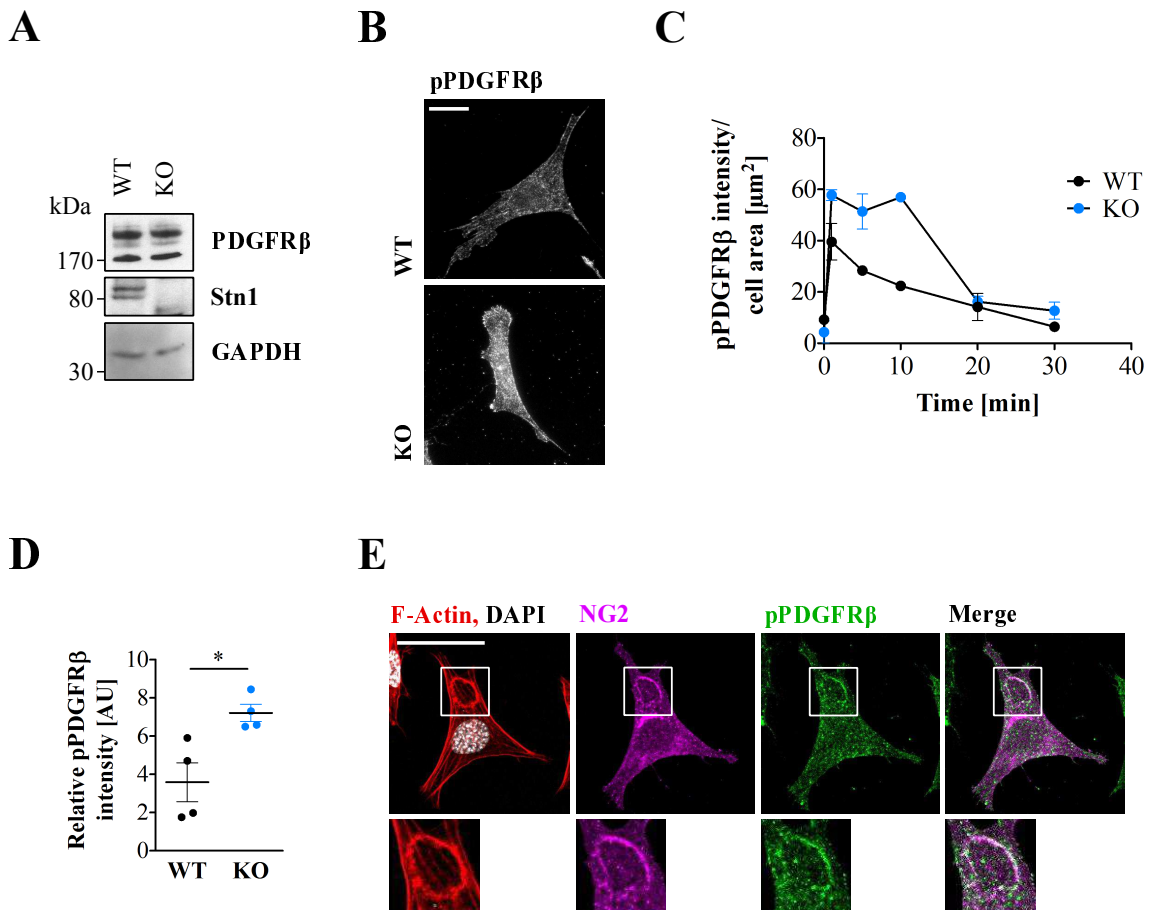

Figure 3.9.: Stn1 inhibits signalling via PDGFRβ. A) Immunoblot analysis of MEF extracts revealed no difference between WT and Stn1 KO cells in total protein levels of PDGFRβ. **B)** Epifluorescent images demonstrating the stronger PDGFRβ autophosphorylation (Y1021) of Stn1 KO MEFs when compared to WT cells following PDGF-BB stimulation. MEFs were starved overnight in DMEM without additives, stimulated with 50 ng/ml PDGF-BB for 3 min and immunolabelled for endogenous p(Y1021)PDGFRβ. Scale bar: 25 µm. **C)** pPDGFRβ levels in Stn1 KO MEFs reached stronger intensities 1 min after stimulation and persisted longer compared to WT MEFs. MEFs were starved overnight (time: 0 min) in DMEM without additives, stimulated with 50 ng/ml PDGF-BB for the indicated time points and immunolabelled using a p(Y1021)PDGFRβ antibody. PDGFRβ phosphorylation (Y1021) level was quantified for the indicated time points (n=2) based on epifluorescent images. **D)** Stn1 KO MEFs displayed a significantly stronger PDGFRβ autophosphorylation (Y1021) upon stimulation with 50 ng/ml PDGF-BB for 10 min (n=4, unpaired, two-tailed t-test). Samples were treated as described for C) and values were normalised to starved controls. **E)** Confocal images demonstrating NG2 localisation towards CDRs following PDGF-BB stimulation. NG2 overexpressing WT MEFs were stimulated for 5 min with 50 ng/ml PDGF-BB and localisation was visualised by immunolabelling of NG2, pPDGFRβ as well as phalloidin to detect F-Actin. Scale bar: 25 µm. (*GAPDH - glyceraldehyde-3-phosphate dehydrogenase, (p)PDGFRβ- (phospho) platelet-derived growth factor receptor β*)

the receptor. Quantitative analysis revealed that already 1 min after PDGF-BB stimulation WT MEFs displayed a strong PDGFRβ auto-phosphorylation (figure 3.9C). pPDGFRβ levels of Stn1 KO MEFs, however, reached even higher values already after 1 min of stimulation. pPDGFRβ levels of WT MEFs continuously declined to baseline levels within 30 min after stimulation. Although also pPDGFRβ levels of Stn1 KO MEFs decreased to baseline within 30 min, the receptor phosphorylation, reached after 1 min of stimulation, persisted for up to 10 min. Quantification of pPDGFRβ levels showed a significant increase in Stn1 KO MEFs 10 min after stimulation (figure 3.9D).

Stimulating MEFs with PDGF triggers a signalling cascade leading to circular dorsal ruffle (CDR) formation, a form of macropinocytosis. Shortly after stimulation F-actin filaments form a circular ring that dorsally protrudes (Itoh and Hasegawa, 2012). Finally the ring constricts and sequesters the growth factor receptor into tubular membrane-enclosed structures in the cytosol from which vesicles are pinched off (Orth et al., 2006). Besides the epidermal and the hepatocyte growth factor, PDGF is the best studied ligand for this process. We wondered whether sequestration of PDGFRβ following PDGF-BB stimulation would correlate with NG2 localisation.

Following stimulation with PDGF-BB we observed sequestration of pPDGFRβ into circular dorsal ruffles identified by F-Actin labelling (figure 3.9E). In parallel NG2 redistributed into CDRs strongly co-localising with PDGFRβ. This substantiated the suggested co-receptor function of NG2 towards the growth factor receptor.

What are the consequences of an increased PDGFRβ phosphorylation? Persson et al. (2004) showed that with an increased phosphorylation of PDGFRβdownstream signalling cascades are strengthened. We hypothesised that absence of Stn1 would lead to increased PDGFR signalling following PDGF-BB stimulation and therefore subsequently to an elevated formation of CDRs. Stimulation with PDGF-BB strongly induced formation of CDRs in WT MEFs within 3 min (figure 3.10A) and as expected Stn1 KO MEFs hyper-reacted to the same stimulus. A detailed analysis of CDR formation in WT MEFs over time clearly showed that formation of the F-Actin rings was strongly induced 1 min after stimulation and declined to baseline within 30 min (figure 3.10B). The same time-dependent behaviour was observed for Stn1 KO MEFs, however, the number of cells forming CDRs was remarkably increased at all time points observed. An independent second WT and Stn1 KO MEF pair reacted similarly to PDGF-BB stimulation confirming that the observed phenotype is caused by loss

of Stn1 and not a cell line artefact. (figure 3.10C). Moreover, when stimulated with different concentrations of PDGF-BB ranging from 5 - 50 ng/ml to induce formation of circular dorsal ruffles, Stn1 KO MEFs displayed an increased sensitivity towards PDGF-BB compared to WT cells (figure 3.10D).

Taken together, Stn1 absence stimulated PDGF-BB induced signalling via the PDGFRβ by increasing its sensitivity for the ligand. Based on the published role of NG2 we suggest that elevated NG2 protein levels due to Stn1 deletion increase PDGF-BB capturing, thereby facilitating PDGFRβ activation and downstream signalling.

Upon PDGF-BB stimulation NG2 has been shown to be phosphorylated thereby regulating its sub-cellular localisation (Makagiansar et al., 2007). Likewise, Stn1 was demonstrated to be post-translationally modified by phosphorylation (Feutlinske, 2014). In fact, it frequently appears with a characteristic double band in immunoblots at steady state (figure 3.11A, Feutlinske 2014). Strong starvation depleted the upper band, but following stimulation with 10% serum or PDGF-BB only the post-translationally modified band was detected. This behaviour provoked the question whether a mechanism similar to the one described for NG2 regulates Stn1 localisation. Indeed, the modified band of Stn1 localised to the cytosolic pool while the non-modified version was found in the membrane pellet in fractionation experiments (figure 3.11B) confirming observations from immunostainings (Feutlinske, 2014).

In summary, our data suggest that Stn1 in its non-modified state localises to the plasma membrane. Upon growth factor stimulation with e.g. PDGF-BB it interacts with its cargo protein NG2 and facilitates the internalisation of the proteoglycan. During tumour development, enhanced PDGF-BB secretion from the tumour recruits pericytes from the host tissue reinforcing neovascularisation and tumour growth. Stn1 absence increases the surface availability of NG2 which likely reinforces PDGF-BB induced signalling and tumour growth.

3.3. Absence of Stn1 regulates the migratory behaviour of cells

Besides cell signalling also the migratory behaviour of cells influences tumour progression dramatically. Stromal cells like pericytes and macrophages are recruited to the malignant tissue and stimulate tumour growth. On the other side metastasising cells move out of the primary tumour to settle at new areas within the organism. Mesenchymal cell migration proceeds in a coordinated series of steps called the migratory cycle (Petrie et al., 2009) in

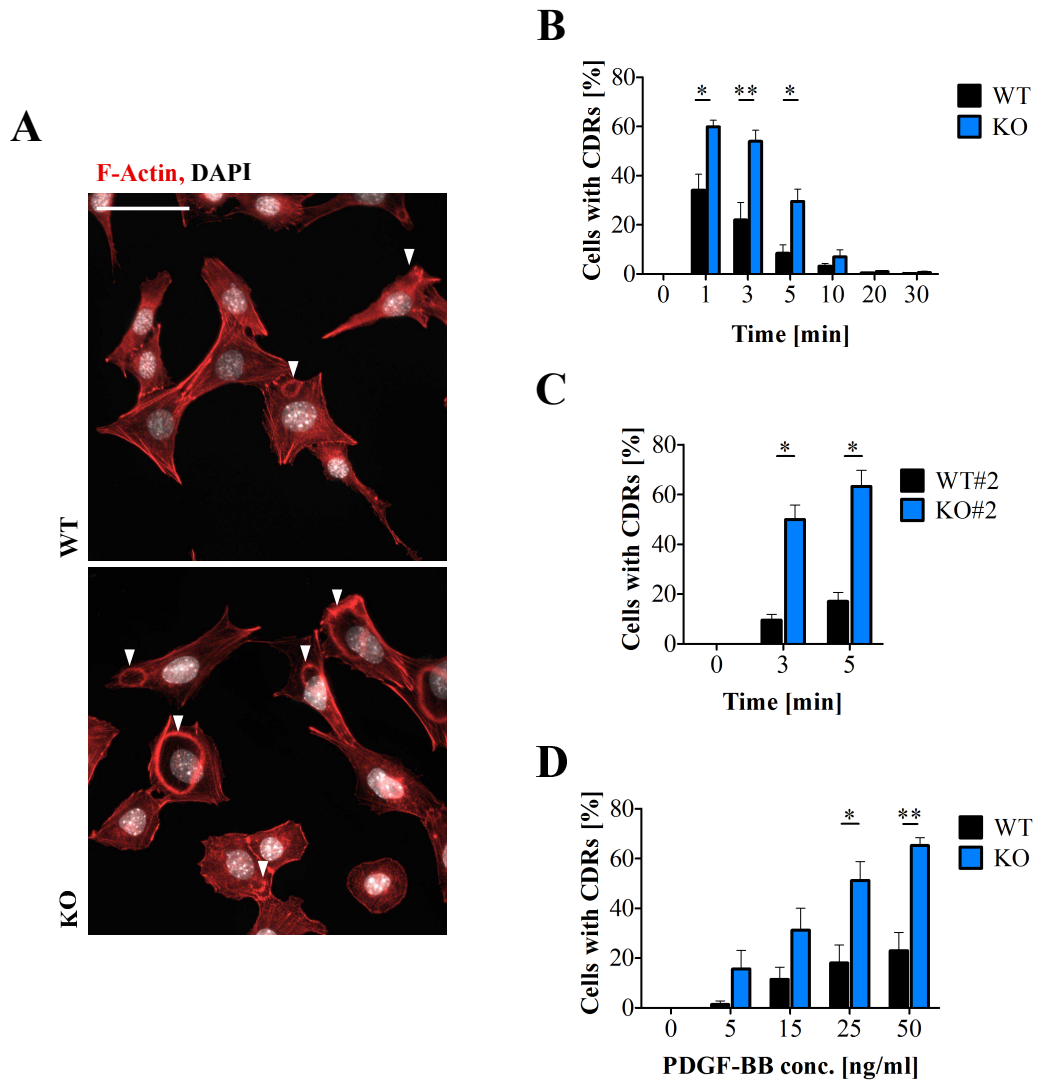

Figure 3.10.: Stn1 inhibits circular dorsal ruffle formation. MEFs were starved overnight in DMEM without additives and stimulated with PDGF-BB for the indicated time points. To visualise CDRs, MEFs were labelled with fluorescent phalloidin to stain for fibrillar actin. Relative number of cells with CDRs were determined in each condition using phalloidin staining. **A,B)** Stn1 KO MEFs formed significantly more CDRs following PDGF-BB stimulation. A) Exemplary epifluorescent images showing CDR formation in WT and Stn1 KO MEFs following stimulation with 50 ng/ml PDGF-BB for 3 min. Scale bar: 50 µm. B) Quantification of A showing the relative number of cells with CDRs at the indicated time points (n=5, paired, two-tailed t-test). **C)** Using another MEF pair confirmed the enhanced CDR formation after PDGF-BB stimulation (50 ng/ml) in Stn1 KO cells compared to WT counterparts (n=3, paired, two-tailed t-test). **D)** Stn1 KO MEFs were more sensitive towards PDGF-BB. WT and Stn1 KO MEFs were stimulated with different PDGF-BB concentrations for 3 min (n=4, paired, two-tailed t-test). (*CDR - circular dorsal ruffle, (p)PDGFRβ- (phospho) platelet-derived growth factor receptor β*)

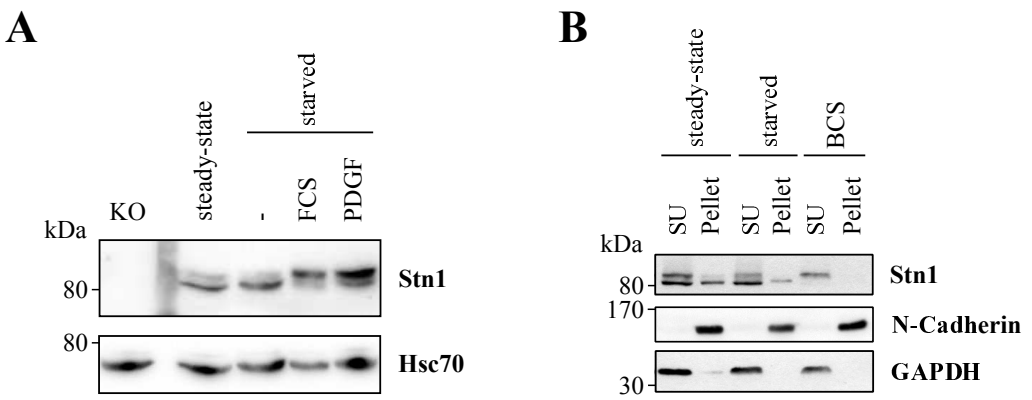

Figure 3.11.: Growth factor stimulation determines the sub-cellular localisation of Stn1. A) Post-translational modifications of Stn1 depend on growth factor signalling. Starvation for 4 h with HBSS shifted the characteristic double band of Stn1 in immunoblots towards the lower band. When starved MEFs were stimulated for 10 min with 10% FCS or 50 ng/ml PDGF-BB the modified band became prominent. **B)** Post-translational modification of Stn1 determined its membrane association. WT MEFs at steady-state, starved as in A, or stimulated with 10% BCS were processed for membrane fractionation. N-Cadherin and GAPDH demonstrated the purity of membrane (pellet) and cytosolic (SU) fraction, respectively. (*BCS - bovine calf serum, FCS - fetal calf serum, PDGF - platelet-derived growth factor, SU - supernatant*)
Experiment A was carried out by Betül Baz.

---

which cell protrusions, exploring the surrounding, are stabilised onto the substrate by nascent adhesions, that mature to focal adhesions generating the traction force. For displacement and the flexibility to react to changing cues, however, contact to the substrate needs to be reversible. Hence focal adhesion (FA) dynamics are intimately linked with cell motility.

3.3.1. NG2 might determine directional migration due to stabilisation of protrusions

During migration cells can follow a random or a persistent mode of migration (Petrie et al., 2009) depending on a) extracellular matrix (ECM) receptor availability, b) stability of protrusion and trailing end, c) substrate and d) focal adhesion stability. Alongside its function as a co-receptor for growth factors, NG2 regulates directional migration of astrocytoma cells (Makagiansar et al., 2004) and oligodendrocyte precursors (Binamé et al., 2013). Feutlinske (2014) showed that increased levels of NG2 also promote directional migration in Stn1 KO MEFs when compared to WT cells (figure 3.12A), however, the mechanism was not investigated so far. We wondered how exactly NG2 influences directionality of Stn1-depleted cells.

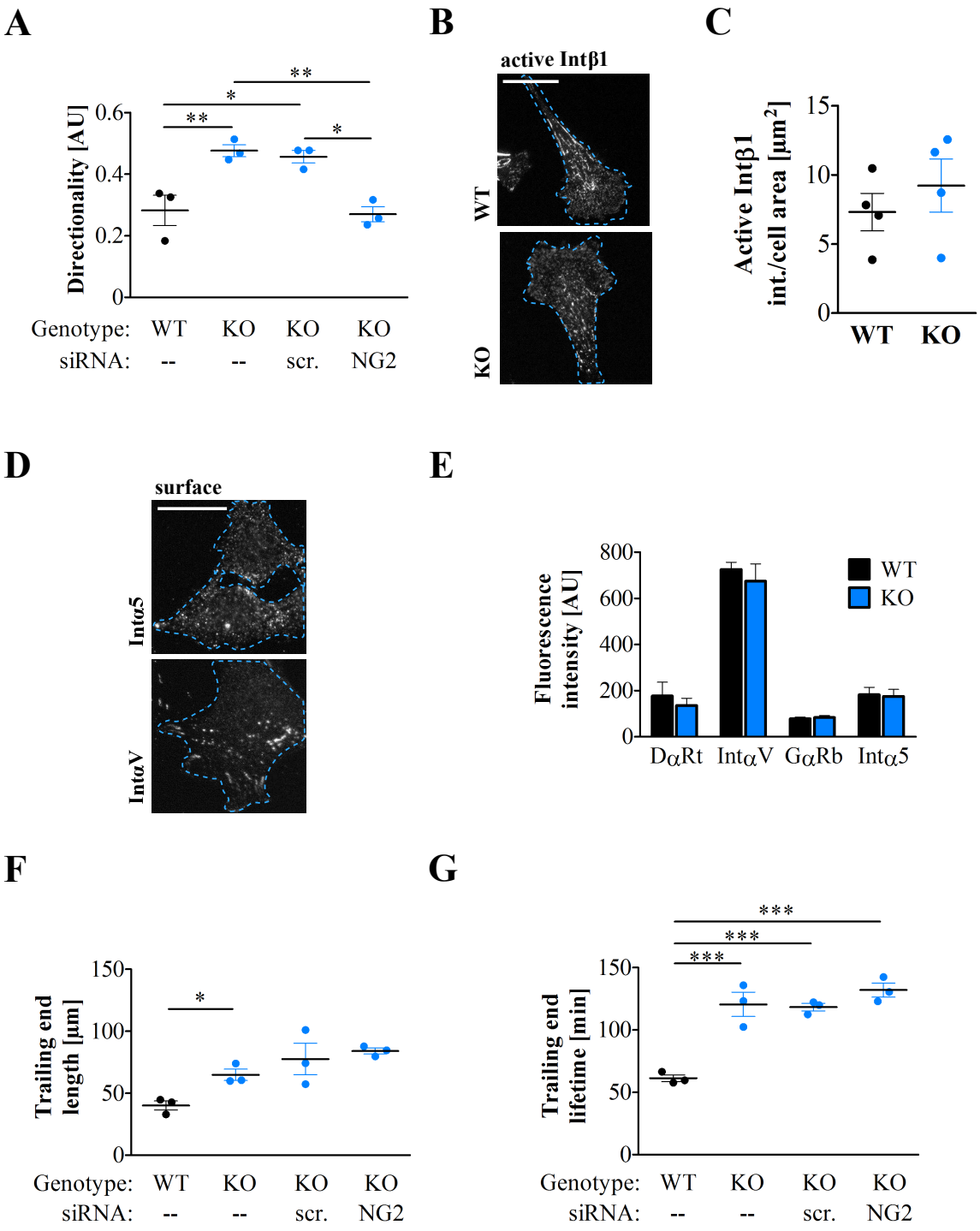
A
Directionality [AU]
0.6
0.4
0.2
0
**
*
**
*
Genotype: WT KO KO KO
siRNA: -- -- scr. NG2
B
active Intβ1
WT
KO
C
Active Intβ1 int./cell area [µm²]
15
10
5
0
WT
KO
D
surface
Intα5
IntαV
E
Fluorescence intensity [AU]
800
600
400
200
0
WT
KO
DαRt
IntαV
GαRb
Intα5
F
Trailing end length [µm]
150
100
50
0
*
Genotype: WT KO KO KO
siRNA: -- -- scr. NG2
G
Trailing end lifetime [min]
150
100
50
0
***
***
***
Genotype: WT KO KO KO
siRNA: -- -- scr. NG2

Figure 3.12.: Increased directionality in Stn1 KO MEFs is influenced by NG2. A) Increased directionality of Stn1 KO MEFs in random migration assays was rescued by NG2 knockdown (n=3, 1-Way Anova,Tukey post test). Time-laps movies of randomly migrating cells were recorded in 15 min intervals overnight with an epifluorescent microscope. Directionality was calculated as the ratio of displacement to total path length based on Petrie et al. (2009). **B)** Epifluorescence microscopy images demonstrating accumulation of activated β1 integrins at trailing ends of immunolabelled WT and Stn1 KO MEFs. Cell outlines are illustrated in blue. Scale bar: 25 μm. **C)** Quantification of activated β1 integrin levels depicted in B revealed no difference between the genotypes. **D)** WT MEFs displaying surface integrin αV and integrin α5 immunostaining in epifluorescent imaging. Cell outlines are illustrated in blue. Scale bar: 25 μm. **E)** FACS analysis using the same primary antibodies as in D did not show differences between the genotypes in surface integrin levels. Specificity of immunostaining was controlled with samples incubated only with secondary antibody (DαRt/IntαV: n=3; GαRb/Intα5: n=4). **F,G)** Increased trailing end length (n=3, paired, two-tailed t-test) as well as trailing end lifetime (n=3, 1-Way Anova, Dunnett post test) in Stn1 KO MEFs during random migration was not influenced by NG2 levels. Analysis of both parameters was performed on the same time-laps movies described in A. (*DaRt - rat secondary antibody raised in donkey, GaRb - rabbit secondary antibody raised in goat, Int - integrin, scr. - scrambled siRNA*)
Experiment A was performed and analysed by Fabian Feutlinske (Feutlinske, 2014). The same movies were used for quantification of F and G.

Endothelial cells stimulated with NG2 display enhanced integrin β1 activity (Fukushi et al., 2004). Increased integrin activity would suggest an intensified engagement to the substratum which would decrease the flexibility of directional changes and increase directional movements. To examine the integrin β1 activity in MEFs we used a conformation-specific antibody in immunostainings. But between WT and Stn1 KO MEFs no significant difference in cellular localisation of the cell surface receptor (figure 3.12B) or its total activity (figure 3.12C) was observed.

Directional movement of cells has been linked to alterations in the surface levels of different types of integrins (Morgan et al., 2013). A shift from α5β1 to αVβ3 has been shown to promote directional migration. Depending on the phosphorylation status of the cell surface proteoglycan syndecan 4, integrin αVβ3 recycling is reduced due to inhibition of adenosine diphosphate (ADP) -ribosylation factor 6 (Arf6). This stabilises focal adhesions and promotes directional migration. In absence of syndecan 4 phosphorylation, integrin α5β1 surface expression increases at the expense of integrin αVβ3, stimulating random migration. Interestingly, syntenin 1, which functions as an adaptor between syndecan 4 and Arf6 in this process, also interacts with NG2 (Chatterjee et al., 2008). Therefore, we speculated that

NG2 like syndecan 4 might influence the migration behaviour via a syntenin/Arf6-mediated shift in integrin surface levels. In fact, comparing the surface proteome of WT and Stn1 KO MEFs indicated elevated surface levels of integrin αV in Stn1 KO cells while integrin α5 levels seemed reduced (Feutlinske, 2014). Therefore, we analysed the surface-localised integrin α5 and integrin αV levels by flow cytometry (figure 3.12E). The integrin subtypes were immunolabelled using antibodies specific for the integrin subtype (figure 3.12D). We could not detect a difference in surface levels of integrin α5 and integrin αV between the genotypes (figure 3.12E). However, using the integrin α5 specific antibody in immunostainings did also not give the expected localisation of the integrin subtype (see Morgan et al. 2013). A repetition using another integrin α5 specific antibody might be necessary to substantiate the data gained by FACS analysis.

Trailing end stability (Petrie et al., 2009) generates the traction force that pulls the rear of the cell forward, limiting in parallel protrusion flexibility and changes in orientation (Theisen et al., 2012). Both, Stn1 and its cargo NG2, localise to the trailing end proximal to focal adhesions Feutlinske (2014). In addition, Stn1 KO MEFs display an increased trailing end length. We hypothesised that in absence of Stn1, NG2 accumulates in retraction fibres thereby stabilising the tail on the extracellular matrix to stir directionality. Disproving our hypothesis, depletion of NG2 in Stn1 KO MEFs did not weaken trailing end stability as indicated by measurements of length and lifetime (figure 3.12F,G). Elongated tails of migrating cells also appear upon block of endocytosis by reducing clathrin or Dab2/ARH protein levels in NIH3T3 cells due to slowed FA disassembly (Ezratty et al., 2009). It might therefore be that depletion of Stn1 affected FA disassembly which might lead to a greater stability of focal adhesions resulting in elongated tails.

In addition to trailing end stability also persistent protrusion formation increases directional persistence. Stn1 KO MEFs have been shown to pronouncedly form protrusions giving them a digitate look while WT cells appear more roundish (Feutlinske, 2014). Protrusion formation depends on the dynamic interplay between Actin assembly and subsequent stabilisation on the substratum by cell surface receptors (Choi et al., 2008). We speculated that increased formation of protrusions in Stn1 KO MEFs might correlate with an elevated cell attachment due to the increased levels of the proteoglycan NG2. Depletion of NG2 in Stn1 KO MEFs, however, did not restore the cell morphology pointing towards a NG2-independent role for

Stn1 (figure 3.13A,B).

With a pronounced formation of multiple protrusions at steady state one would expect migrating mesenchymal cells to change directions quickly and move more randomly. However, while Stn1 KO MEFs form more protrusions at steady state, the cells move with an increased directionality compared to WT cells (figure 3.12A). Increased protrusion stability stirs directional movements (Petrie et al., 2009). In fact, Feutlinske (2014) demonstrated that Stn1 KO cells consistently extend only one protrusion while WT cells explore their surrounding in several directions. This suggests that once the direction was established at steady state, stable protrusions guided Stn1 KO cells resulting in a persistent migration. Since increased directionality in Stn1 KO MEFs had been already demonstrated to be dependent on NG2, we speculated that elevated NG2 protein levels in absence of Stn1 affect protrusion dynamics. To test this, we compared protrusion dynamics of randomly migrating MEFs using kymographs which depict protrusions movements (distance x) over time (t). In contrast to protrusions of Stn1 KO cells, which continuously progressed into one direction, WT MEFs also retracted the protrusive front. Decreasing NG2 levels in Stn1-depleted cells seemed to recover the protrusion flexibility. Still, quantitative analysis will be needed to substantiate the finding.

In summary, the enhanced persistent motility of Stn1 KO cells, visually characterised with increased the stability of trailing end and protrusions, did not arise from altered β1 integrin localisation or activity or from misregulated α5 or αV integrin traffic. Preliminary data of protrusion dynamics point towards a pronounced engagement of NG2 to the substratum, evoking directional migration due to increased protrusion formation.

3.3.2. Stn1 stimulates focal adhesion dynamics

Protrusion formation and retraction is predominantly influenced by the dynamic interplay between Rac1-driven Actin assembly and subsequent stabilisation on the substratum by cell surface receptors (Choi et al., 2008). We speculated that the increasing protrusion stability in Stn1 KO MEFs might correlate with an elevated cell attachment due to the increased levels of the proteoglycan NG2. Burg et al. (1996) showed with *in vitro* binding assays that purified NG2 binds laminin as well as the collagens type 2, 5 and 6 but cannot interact with collagen 1, 3 and 4. Later Tillet et al. (1997) confirmed the interaction with the collagen types 5 and 6 and correlated an increased expression of NG2 with stronger cell attachment (Tillet et al., 2002); attachment to fibronectin, collagen 1 and 4 as well as laminin was unchanged. Due to

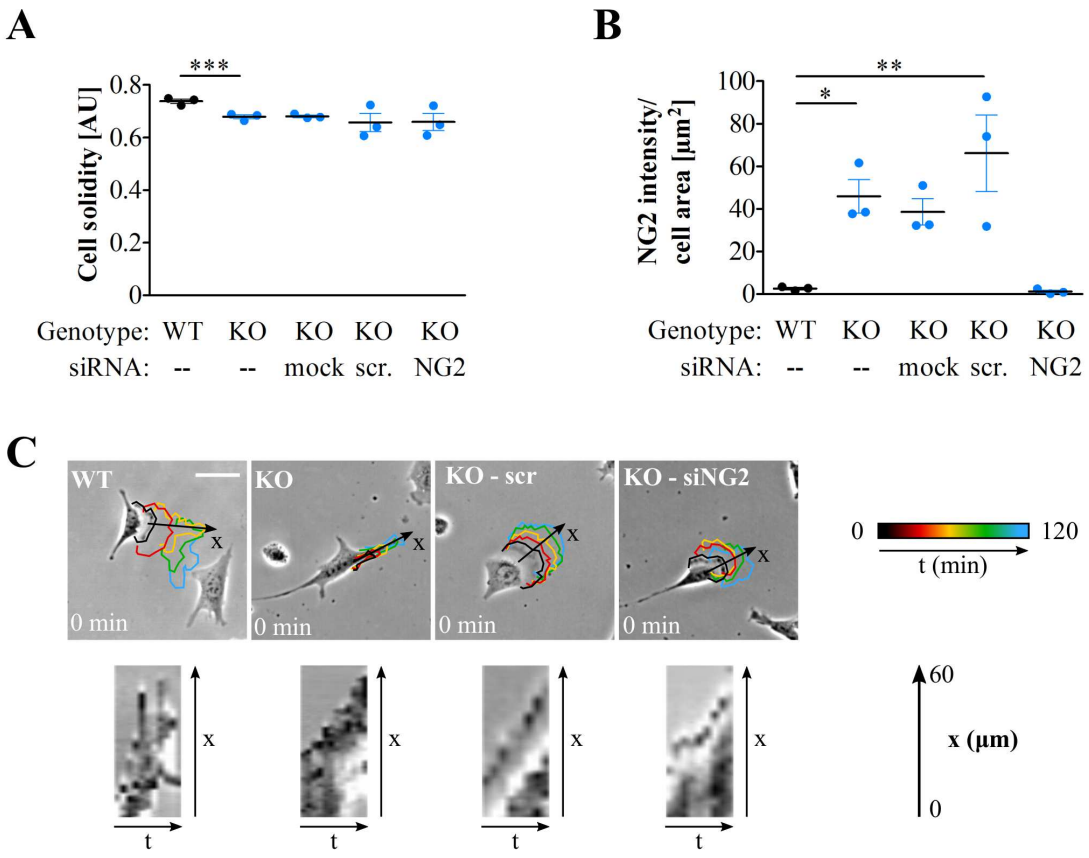

Figure 3.13.: Stn1 regulates protrusion formation. A,B) Reduced cell body solidity of Stn1 KO MEFs at steady-state, indicating a more digitate morphology in comparison to WT cells, was not NG2 dependent. Cell body solidity was defined by the convex hull divided by the cell perimeter. Shape parameters were determined based on confocal images from F-Actin stainings with fluorescent phalloidin (n=3, paired, two-tailed t-test). Knockdown efficiency - depicted in B - was determined based on parallel NG2 immunostainings (n=3, 1-Way Anova, Dunnett post test). **C)** Strengthened protrusion stability of Stn1-depleted MEFs during migration might originate from elevated NG2 levels. Exemplary images of randomly migrating cells depicting the developing protrusive front over time in colour-coded protrusion perimeters (30 min intervals). Kymographs (below) were generated along the moving protrusion (arrow). Scale bar: 50 µm. (*scr - scrambled, t - time, x - length of the protrusion*)
Experiment C was analysed from random migration time-lapse movies generated by Dr. Fabian Feutlinske (see also figure 3.12).

the increased NG2 levels in Stn1 KO MEFs we expected a stronger attachment to laminin 1 and collagen 6 while adhesion on collagen 1 should remain unaltered.

To test whether increased NG2 protein levels affected the cell attachment, WT and Stn1 KO cells were detached from cell culture plates and subsequently seeded on untreated or coated 96 wells for the indicated time points. Using Toluidin Blue to stain adherent cells, values proportional to the cell number were measured with a plate reader. Within 15 min, limited number of cells attached to untreated plastic surfaces (figure 3.14A). In contrast matrigel, which is a basement membrane mixture generated from a mouse sarcoma cell line, strongly stimulated cell attachment and was utilised here as a positive control for successful coating (figure 3.14B). Interestingly, Stn1 KO MEFs adhered significantly more to matrigel at early time points. Beside extracellular matrix proteins including laminin, collagen 4 or heparan sulfate proteoglycans, matrigel contains numerous growth factors including PDGF (BD Bioscience, 2011). Since Stn1 KO MEFs are more sensitive towards growth factor ligands one might speculate that these stimulated early adhesion of Stn1 KO MEFs. However, also other ECM components of the matrigel, e.g. collagen 4, might have facilitated cell attachment of Stn1 KO cells.

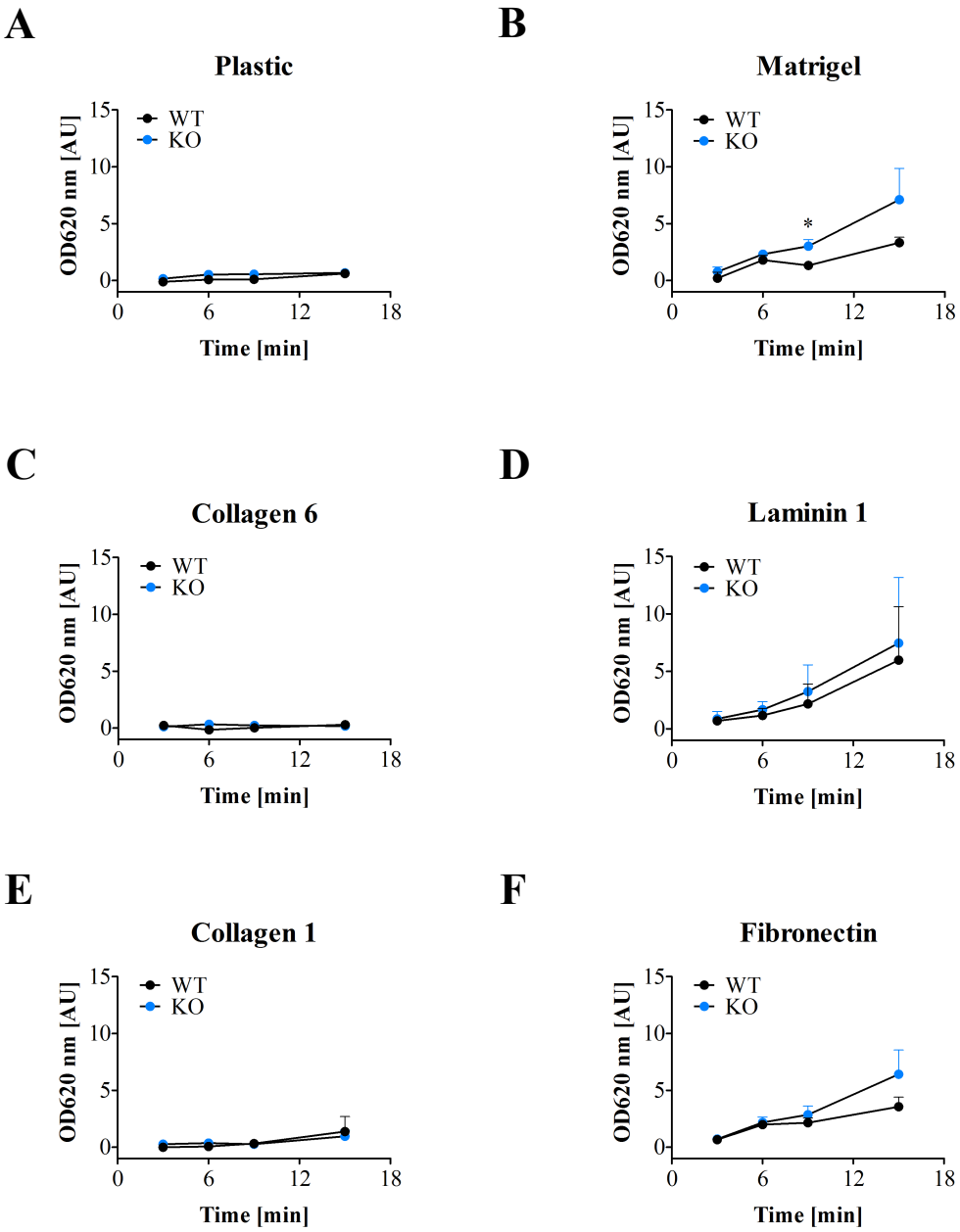

Figure 3.14.: Absence of Stn1 stimulates early adhesion to matrigel. A tendency for stronger adhesion on both, matrigel and Fibronectin, was observed when Stn1 was absent. Significance was reached only for matrigel, 9 min after seeding. WT and Stn1 KO MEFs were detached with EDTA from 90% confluent cell culture dishes and seeded for the indicated time points on **A)** plastic (n=5), **B)** matrigel (n=5, paired, two-tailed t-test),**C)** collagen 6 (n=3), **D)** laminin 1 (n=3), **E)** collagen 1 (n=3), **F)** fibronectin (n=5) in 96 well plates. The fixed cell bodies were dyed using a Toluidine Blue solution. The dye was dissolved in a SDS solution and read out with plate readers yielding values proportional to the number of attached cells.

As expected no differences between WT and Stn1 KO MEFs were observed when seeded on plastic or collagen 1 (figure 3.14E), however, also attachment to collagen 6 (figure 3.14C) and laminin 1 (figure 3.14D) was unchanged between the genotypes. This indicated that attachment to collagen 6 and laminin 1 occurred without any benefit of the increased surface expression of NG2 in Stn1 KO MEFs.

The best studied ligand for integrin engagement is fibronectin which interacts with the extracellular domain of RGD-binding integrins (Margadant et al., 2011). To our surprise, Stn1 KO MEFs had a tendency to adhere faster, albeit not significant, to fibronectin-coated surfaces 15 min after seeding (figure 3.14F).

To conclude, in most cases attachment onto the tested coatings was unaltered between WT and Stn1 KO MEFs and therefore did not correlate with the different surface levels of NG2. The only exception was adhesion to matrigel which was increased in the case of Stn1 KO cells. Apart from laminin, representing 60% of matrigel ingredients, collagen 4 (30%) and entactin (8%) constitute most of the matrix (BD Bioscience, 2011). Attachment to laminin as well as collagen 4 are not supported by NG2 (Tillet et al., 2002). Thus, additional surface-receptors misregulated in Stn1 absence might contribute to the faster cell attachment on matrigel. Alternatively, elevated NG2 levels in Stn1 KO MEFs might act as co-receptors for growth factor receptors stimulating early attachment.

Based on these findings we concluded that the increased protrusion stability in Stn1 KO MEFs did not originate from a reinforced cell attachment due to increased NG2 engagement with the substratum.

Protrusion stability is also modulated by FA dynamics (Petrie et al., 2009). Thus, we next investigated whether Stn1 influences FA dynamics by performing fluorescence recovery after photobleaching (FRAP) of Pax-GFP overexpressing WT and Stn1 KO MEFs. Using that approach allowed us to examine the protein exchange rates within focal adhesions. Distinct focal adhesions identified by fluorescently-labelled paxillin were bleached with a laser beam. Replacement of bleached Pax-GFP molecules with non-bleached was measured as fluorescence recovery over time (figure 3.15A,B). Hence, the maximum fraction of exchanged Pax-GFP molecules represented the maximum fluorescence recovery and is referred to as the mobile fraction. While kinetics of fluorescence recovery were not different between WT and Stn1 KO MEFs, the extent of recovery was markedly reduced in Stn1-depleted cells (figure 3.15C).

Differences due to unequal bleaching did not contribute (figure 3.15E). Quantitatively, the extent of Pax-GFP recovery was only ~70% of WT cells, indicating an increased immobile fraction due to an ineffective exchange in Stn1 KO cells (figure 3.15D). Introduction of Stn1-tdTomato into Stn1 KO MEFs restored the Pax-GFP exchange in FA demonstrating that depletion of Stn1 in KO cells slowed FA dynamics.

Exchange of focal adhesion proteins within focal adhesions represent the balance between assembly and disassembly of adhesion components. Thus, assembly as well as disassembly

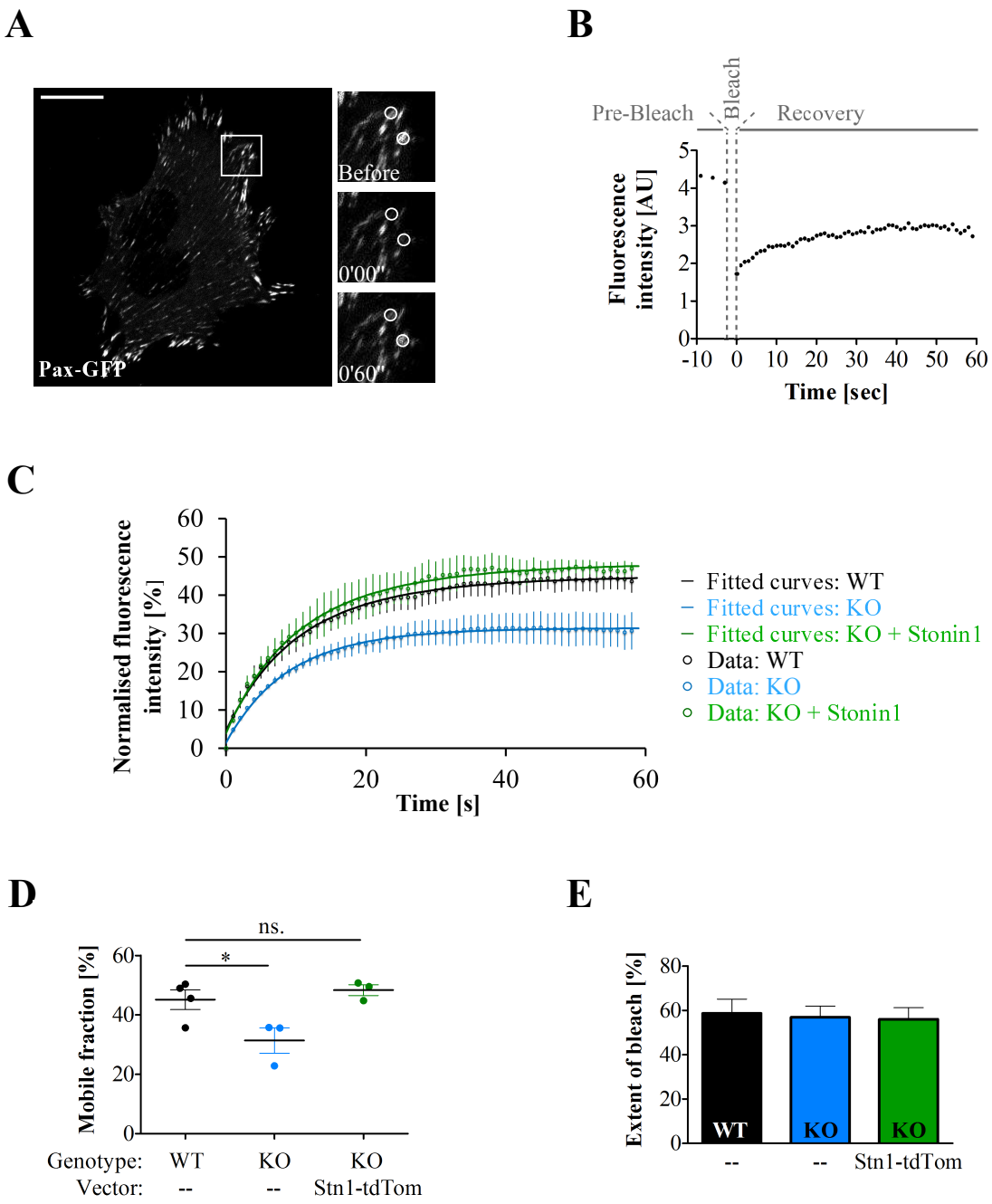

Figure 3.15.: Stn1 accelerates focal adhesion dynamics. Focal adhesion dynamics were examined by bleaching regions of focal adhesions, visualised with overexpressed Pax-GFP, and observing the recovery of fluorescence over time, which is a measure for the exchange of focal adhesion components. **A)** Exemplary confocal image of a MEF overexpressing Pax-GFP. Zoomed images depict focal adhesions before as well as directly after bleach and 60 s of recovery. Encircled regions were bleach areas. Scale bar: 20 µm, zoom: 5 µm. **B)** Exemplary FRAP curve of a cell visualising the changes of fluorescence intensity during the procedure. **C,D)** Stn1 depletion slowed exchange of Pax-GFP at focal adhesions. C) Curves representing the fluorescence recovery for WT, Stn1 KO and Stn1-tdTomato transfected Stn1 KO MEFs (WT: n=4, KO/ KO+Stn1: n=3). D) Recovered Pax-GFP representing the mobile fraction within focal adhesions was calculated from curve fittings in C (WT: n=4, KO/ KO+Stn1: n=3, 1-Way Anova, Dunnett post test). **E)** Bleach extent reached within the experiments (n=4). (*Pax-GFP - paxillin-GFP*)
The experiment was performed in collaboration with Fabian Feutlinske.

---

might contribute to altered dynamics in Stn1-depleted cells. Focal adhesion disassembly has been already reported to relay on clathrin-mediated endocytosis by several groups (Chao et al., 2010; Chao and Kunz, 2009; Ezratty et al., 2009). therefore, we speculated that Stn1, as an endocytic adaptor, facilitates focal adhesion disassembly. To analyse focal adhesion disassembly in cells, we performed the nocodazole washout assay which was developed by Ezratty et al. (2005). The technique is based on the fact, that microtubule regrowth after nocodazole washout induces synchronous FA disassembly.

Treatment with nocodazole and subsequent washout induced synchronous disassembly of focal adhesions within 10 min in WT MEFs (figure 3.16A). In contrast, focal adhesions of Stn1 KO cells remained for up to 30 min, when WT cells already had begun to form new contact sites. Quantification of focal adhesion number per cell revealed that Stn1 KO MEFs retained almost twice as much FA 10 min after washout when compared to WT cells at the same time (figure 3.16B). We concluded that Stn1 was needed to efficiently dissolve focal adhesions.

In summary, absence of Stn1 inhibited microtubule-induced focal adhesion disassembly resulting in slowed FA dynamics. As a consequence, FAs of Stn1 KO cells are more stable. This might contribute to trailing end as well as protrusion persistence which establish directional cell migration.

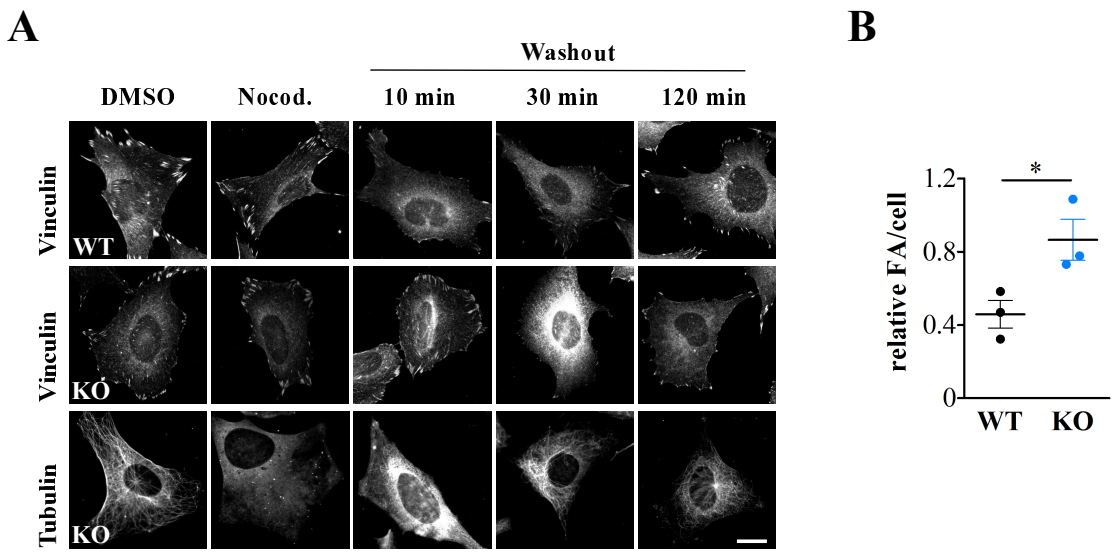

Figure 3.16.: Decreased focal adhesion disassembly in the absence of Stn1. WT MEFs disassembled FAs faster than Stn1 KO cells. **A)** Exemplary epifluorescence images of WT and Stn1 KO MEFs stained for vinculin and tubulin during nocodazole washout assays. MEFs were treated with nocodazole for 4 h. Subsequently, the compound was washed off to trigger microtubule re-polymerisation and FA disassembly. Treatment with the nocodazole diluent DMSO was used as control. Scale bar: 25 µm. **B)** Quantified FA number per cell 10 min after nocodazole washout. Data was normalised to DMSO controls (n=3, paired, two-tailed t-test).

3.4. Stn1 regulates focal adhesion maturation by controlling F-Actin re-arrangements

As a consequence of the inhibition of focal adhesion disassembly, number and size of focal contacts usually increases due to an accumulation of focal adhesion components (Schiefermeier et al., 2014). Blocking endocytosis by downregulation of essential contributors was also reported to increase focal adhesion area per cell (Chao and Kunz, 2009). But although focal adhesion number increased, their size was even smaller in Stn1 absence (Feutlinske et al., 2015). This led us speculate that besides the defect in focal adhesion disassembly also FA growth might be inhibited when Stn1 is depleted. Therefore we investigated FA maturation in WT and Stn1 KO MEFs.

3.4.1. FA assembly is inhibited in Stn1 absence

Following Rac1-dependent outgrowth of the lamellipodium, nascent adhesions evolve and mature into focal adhesions to stabilise the protrusion front and migratory direction (Scales and Parsons, 2011). Maturation of focal contact sites is dependent on the activation of focal adhesion kinase (FAK) which recruits additional components by direct interaction or phosphorylation (Mitra et al., 2005). Hence, measurements of FAK activity represent a strong indication for successful FA maturation. FAK itself contains multiple phosphorylations sites that regulate its kinase activity, serve as interaction sites for downstream factors (Mitra et al., 2005) and regulate residential time in focal adhesions (Hamadi et al., 2005). One of the best characterised phosphorylation sites is the tyrosine position 397 (Y397): FAK is recruited upon integrin engagement and dimerisation of the kinase allows autophosphorylation at Y397 fully activating the kinase (Sulzmaier et al., 2014). Alternatively, upon growth factor stimuli for example, recruitment of Src-family kinases mediate phosphorylation at Y397 thereby transmitting guidance cues towards focal adhesions (Mitra et al., 2005).

Consequently, we decided to compare FAK phosphorylation (Y397) between WT and Stn1 KO MEFs at the onset of focal adhesion formation - during attachment of cells. To stimulate focal adhesion assembly, a fibronectin coating, which promotes integrin activation, was used. Since total FAK protein levels could not be determined due to strong background labelling with the antibody, stainings for paxillin (Pax), a structural component of focal adhesions, were used to check total protein levels. 10 min after seeding of WT cells onto fibronectin, Pax-positive structures were detected across the entire cell (figure 3.17A). After 30 min, focal adhesions oriented towards the cell edge to establish the necessary resistance against membrane tension (Gauthier et al., 2012). Already 60 min after seeding cells had begun to polarise, forming stable focal adhesions to generate the traction force. Pax-positive focal adhesions of Stn1 KO MEFs behaved similar to WT cells, though smaller focal adhesions were observed (representative images of figure 3.17A). Nevertheless, quantification of paxillin intensity per cell was not different between WT and Stn1 KO cells for the time points analysed (figure 3.17B).

p(Y397)FAK intensity levels gradually rose within 1 hour after seeding indicating an increase of FAK activity and focal adhesion maturation (figure 3.17C). But in contrast to WT cells, p(Y397)FAK levels of Stn1 KO MEFs increased at a slower rate. Intensity quantification of p(Y397)FAK revealed a significant difference between WT and Stn1 KO MEFs 60 min after

seeding (figure 3.17D). This indicated a reduced focal adhesion maturation in Stn1 deficient cells.

However, FAK activation can occur downstream of activated integrins as well as growth factor receptor signalling (Seong et al., 2011). Therefore, the presence of serum in spreading experiments might likely contribute to p(Y397)FAK protein levels. We wanted to distinguish FAK phosphorylation stimulated by fibronectin from growth factor dependent FAK

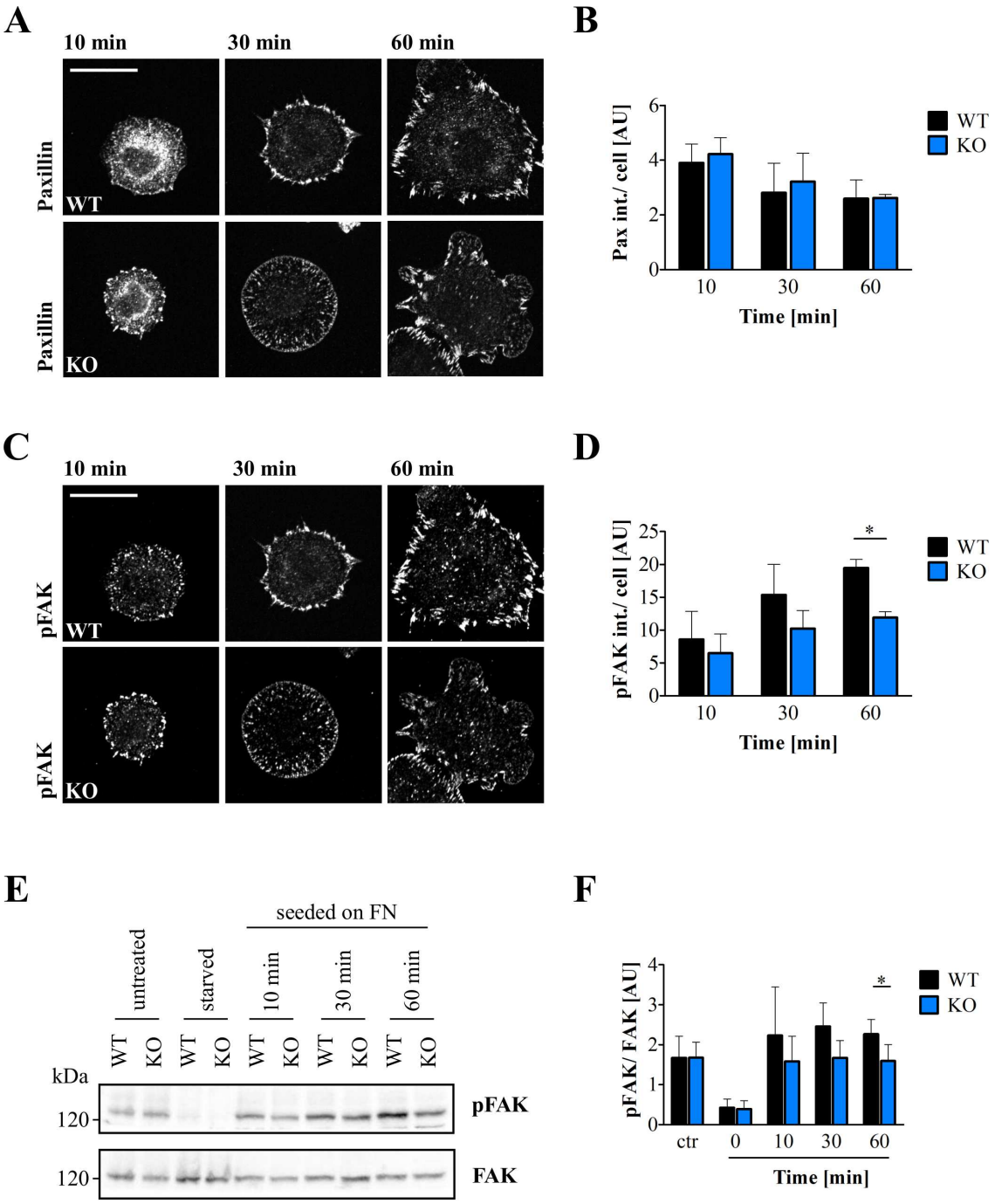

Figure 3.17.: Slowed FAK activation in Stn1 KO MEFs upon spreading on fibronectin. A,B) Paxillin incorporation into FAs was unchanged between both genotypes. A) Exemplary confocal images of WT and Stn1 KO MEFs stained for paxillin during spreading on fibronectin. Scale bar: 25 µm. B) Fluorescence intensity quantification of A (n=3). **C,D)** Phosphorylation of FAK (Y397) was significantly reduced in Stn1 KO compared to WT MEFs 60 min after spreading on fibronectin, indicating a diminished kinase activity. Scale bar: 25 µm. C) Exemplary confocal images of FAK phosphorylation (Y397) in WT and Stn1 KO MEFs during spreading. Scale bar: 25 µm. D) Fluorescence intensity quantification of A at the indicated time points (n=3, paired, two-tailed t-test). **E,F** In absence of serum, FAK phosphorylation (Y397) was significantly diminished in Stn1 KO MEFs 60 min after seeding on fibronectin, demonstrating inhibited FAK activation downstream of engaged integrins. E) Representative immunoblot depicting depletion of p(Y397)FAK upon starvation and increasing activation of the kinase after seeding. Total FAK protein levels were used as loading control. F) Band intensity quantifications of p(Y397)FAK relative to FAK protein levels from immunoblots represented in A (n=3, paired, two-tailed t-test). (*FN - fibronectin, Pax - paxillin, pFAK - phosphorylated focal adhesion kinase*)

---

activation in spreading experiments. Therefore, starved MEFs were seeded on fibronectin and p(Y397)FAK levels were monitored by immunoblotting (figure 3.17E,F). In accordance with previous experiments (figure 3.17C,D), FAK phosphorylation at position Y397 was delayed in Stn1 KO MEFs upon spreading on fibronectin (figure 3.17E,F). Thus, the slowed p(Y397)FAK levels mainly originated from activated integrins. Stimulating starved Stn1 KO MEFs with PDGF for the same time points leads to a similar phenotype (Feutlinske, 2014). Following stimulation of Stn1 KO MEFs, FAK is phosphorylated at Y397 to a similar extent as in WT cells, but the activation rate stalls over time. Hence, delayed FAK activation in Stn1-depleted MEFs occurred downstream of growth factor receptor activation as well as integrin engagement on fibronectin.

To sum up, in addition to inhibited focal adhesion disassembly Stn1-depleted cells exhibited also reduced focal contact maturation. Thus, both processes might contribute to slowed focal adhesion dynamics.

3.4.2. Stn1 regulates actin fibre organisation during spreading and at steady-state

NG2 also functions as co-receptor for β1 integrins thereby stimulating Integrin-mediated FAK phosphorylation (Yang et al., 2004) which promotes cell attachment (Tillet et al., 2002). But though Stn1 KO cells display elevated protein levels of the proteoglycan, slowed p(Y397)FAK

levels were observed. A previous study by Feutlinske (2014) suggested that the lack of its endocytic adaptor Stn1 might result in NG2 segregation in clusters leading to inefficient FAK activation. But reducing NG2 protein levels by siRNA treatment did not restore p(Y397)FAK levels following PDGF treatment. This indicates that the reduced FAK activation of Stn1 KO MEFs does not correlate with its function as endocytic adaptor for NG2. However, re-introduction of Stn1 recovered p(Y397)FAK levels indicating that diminished FA maturation was specifically caused by Stn1 absence (Feutlinske, 2014). Therefore we wanted to dissect how Stn1 regulates FA maturation.

Besides FAK activity also linkage with the F-actin cytoskeleton is required for FA maturation (Oakes et al., 2012). Nascent adhesions stabilised onto the ECM quickly connect with the bundled actin fibres to allow traction force transmission. The resulting tension recruits further focal adhesion components promoting maturation into higher-order focal adhesions. In addition, the F-Actin cytoskeleton provides the main mechanical strength of a cell to define its cell shape (Pollard and Cooper, 2009). Therefore, we first characterised the morphology of cells which spread on fibronectin. WT and Stn1 KO MEFs were allowed to spread on fibronectin and the formation of the F-Actin network during attachment was visualised using fluorescently labelled phalloidin (figure 3.18A). Measurements of cell area confirmed equal spreading rates between both genotypes (figure 3.18B). Yet, a close look at the cellular shape of both genotypes indicated a different spreading behaviour. WT cells begun to spread and unfold membrane reservoirs 10 min after seeding (figure 3.18A). Already 20 min later, cells formed small protrusions indicating polarisation which became even more pronounced at 60 min after seeding. On the contrary, Stn1 KO cells appeared to form less protrusions 30 min after seeding. 30 min later Stn1 KO cells started to form protrusions but to a reduced extent compared to WT MEFs. Quantification of round cells 30 min after seeding revealed that in fact two times more KO cells remained roundish (WT: 24.3 +/- 5.7%, KO: 53.0 +/- 7.5%, figure 3.18C). Since counting of 'round' versus 'not round' cells was a subjective measurement, we next decided to validate the shape of cells using quantitative parameters like cell body solidity (figure 3.18D), which describes cell convexity, and cell body circularity (figure 3.18E) measuring roundness of cells (see section 2.6). Due to the increase in cell polarisation of WT MEFs during spreading, the values for both parameters decrease over time. Although the initial spreading shape 10 min after seeding was unaltered between WT and Stn1 KO MEFs, Stn1 depleted cells spread with a significantly increased cell body solidity indicating

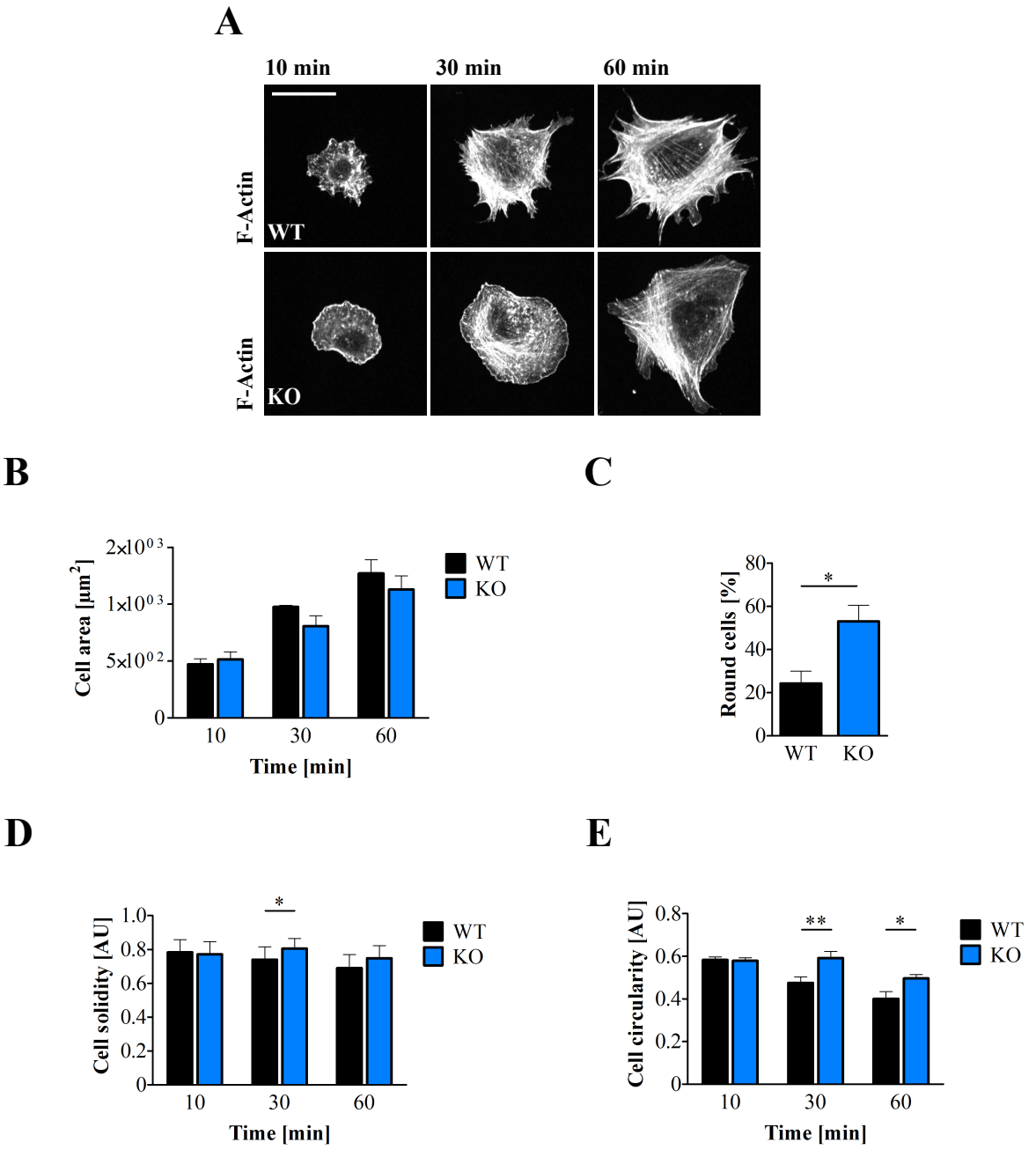

Figure 3.18.: Stn1 KO MEFs spread with a more roundish morphology than WT cells. To observe changes in spreading morphology WT and Stn1 KO MEFs were seeded on fibronectin-coated surfaces, fixed at the indicated time points and stained with phalloidin to outline the cell shape for quantifications by visualising F-Actin. **A)** Exemplary confocal images of WT and Stn1 KO MEFs during spreading. Scale bar: 25 µm. **B)** Cell area quantification for the indicated time points (n=3). **C)** Compared to WT, significantly more round cells were observed in Stn1 KO samples 30 min after seeding (n=5, paired, two-tailed t-test). **D,E)** Quantification of cell body solidity (D, n=5, paired, two-tailed t-test), indicating cell convexity, and cell circularity (E, n=5, paired, two-tailed t-test) to measure roundness based on section 2.6.

a reduced formation of membrane extensions proceeding from the cell body. This was even more apparent using cell body circularity as measurement (figure 3.18E). Since Stn1 KO cells formed fewer extensions they appeared significantly more circular 30 min after seeding. Though Stn1 KO cells started to form protrusions thereafter, they retained a more circular shape 60 min after seeding while the cell body solidity was unaltered.

Gauthier et al. (2012) described that cells pass through characteristic spreading shapes. Early adhesion on the substratum is mainly characterised by unfolding of membrane reservoirs until the maximum membrane tension is reached and the cells appear circular. Then, cells start to polarise by increasing myosin II contractility along actin fibres connected with focal complexes allowing polarisation of the cell by reinforcing FA maturation in one direction. We speculated that Stn1 KO MEFs inefficiently incorporate Actin fibres into FAs during spreading leading to slower FA maturation. This might result in a reduced traction force transmission towards focal adhesions and inhibited polarisation. Consequently, more Stn1 KO cells remain in a round state during spreading.

To check whether the observed maturation defect might really be caused by altered Actin, we decided to thoroughly check whether the F-Actin cytoskeleton was organised similarly between WT and Stn1 KO cells 30 min after seeding. First, to exclude differences originating from an overall altered actin assembly in Stn1 KO MEFs total F-Actin intensity per cell was determined in WT and Stn1 KO MEFs. For all time points investigated during spreading, no difference in total F-actin intensity was detected between both genotypes (figure 3.19A) indicating that rather local F-Actin arrangements than the overall fibre formation might be altered in Stn1 KO MEFs.

In migrating cells 3 main subtypes of F-Actin can be distinguished according to their subcellular localisation within the cell (Vallenius, 2013). Dorsal stress fibres (DSFs) connecting leading edge focal adhesions with transverse arcs (TAs). TAs are contractile actin fibres within the protrusive front generating the tension along the linked focal adhesions giving them a bent look. Ventral stress fibres (VSFs) shape the front-to-rear polarisation by establishing retraction at the trailing end (see also figure 1.3). 30 min after seeding we categorised fibres of spreading cells accordingly: bent fibres were classified as TAs, fibres connecting focal adhesions with transverse arcs were regarded as DSFs, and long fibres that seemed to establish the polarisation of cells were referred to VSFs (exemplary images given in figure 3.19B). Additionally cells with a pronounced dendritic actin network at the lamellipodium

were counted. 30 min after seeding significantly more Stn1 KO cells formed a pronounced lamellipodium at the expense of VSFs. The appearance of TAs and DSFs was unaltered between both genotypes.

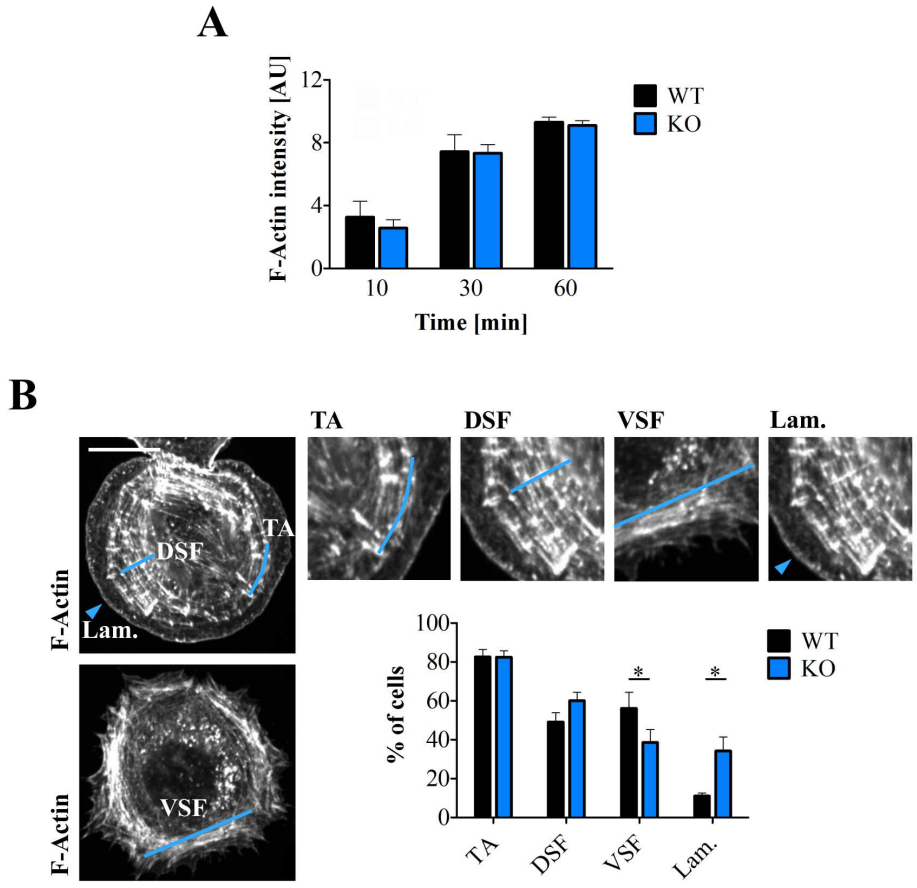

Figure 3.19.: Misregulated F-Actin reorganisation during spreading in Stn1 KO MEFs. MEFs were seeded on fibronectin-coated surfaces, fixed using PFA and stained with fluorescent phalloidin to visualise F-Actin. **A)** During spreading, F-Actin fluorescence intensity per cell was unchanged between both genotypes suggesting a similar extent of F-Actin formation. **B)** Exemplary images illustrating the evaluated Actin structures and quantification of the number of cells displaying transverse arcs (TAs), dorsal stress fibres (DSFs), ventral stress fibres (VSFs) and pronounced lamellipodium (Lam.) 30 min after seeding on fibronectin. Significantly more Stn1 KO cells exhibited a pronounced lamellipodium at the expense of VSFs when compared to WT cells (n=5, paired, two-tailed t-test). The relative number of cells was calculated from confocal images based on visual criteria depicted in exemplary images. Scale bar: 15 µm.

In summary, spreading WT and Stn1 KO MEFs formed F-Actin to a similar extent. However,

Stn1-depleted cells displayed a reduced number of VSFs while TAs and DSFs were unaltered. Interestingly, a study by Hotulainen and Lappalainen (2006) suggested a mechanism in which VSFs are built from TA and DSF fragments. This could suggest that cells depleted for Stn1 were defective in efficient F-actin cytoskeleton re-arrangements. As a consequence, Stn1 KO MEFs might remain for a longer period in a state with strong membrane tension caused by pronounced lamellipodia formation.

At steady-state, mis-regulation of DSF assembly was demonstrated to reduce focal adhesion size due to defective transmission of traction force to leading edge focal adhesions (Oakes et al., 2012). We wondered whether defective actin fibre re-arrangements in absence of Stn1 also occur at steady-state. In accordance with previous results during spreading, total F-Actin intensities were unchanged between WT and Stn1 KO MEFs at steady-state (figure 3.20A). Nevertheless, in comparison to WT cells, Stn1 KO cells seemed to elongate DSFs insufficiently, consequently relocating TAs close to the leading edge (figure 3.20B). In fact, mean DSF length per cell was significantly smaller in Stn1 KO cells indicating a defect in DSF formation (figure 3.20C). In addition, meticulous classification of VSFs and TAs of WT and Stn1 KO MEFs at steady-state revealed that significantly more Stn1-depleted cells were observed with TAs (figure 3.20D).

To sum up, in line with being defective in F-Actin re-arrangements during spreading, Stn1 KO MEFs appeared to misregulate actin fibre organisation at steady-state. A study by Hotulainen and Lappalainen (2006) suggested that TAs are assembled from actin bundles. These are generated at the leading edge and get stabilised by α-Actinin and Myo2 incorporation during TA formation. Therefore, enhanced formation of TAs in Stn1 absence might indicate an increased actin bundle pool originating from the cell edge or an increased availability of Myo2.

3.4.3. α-Actinin, a key crosslinking protein of the F-Actin cytoskeleton, mis-localises in Stn1 absence

From the data acquired we assumed that the reduced size of FAs in Stn1 KO MEFs originates from a defect in focal adhesion maturation due to mis-regulation in F-Actin arrangements. α-Actinin was reported to be essential for proper DSF formation and FA maturation (Kovac et al., 2013; Oakes et al., 2012). As a general F-Actin crosslinker, it is recruited to focal adhesions when traction forces are applied (Ye et al., 2014) to organise and strengthen the

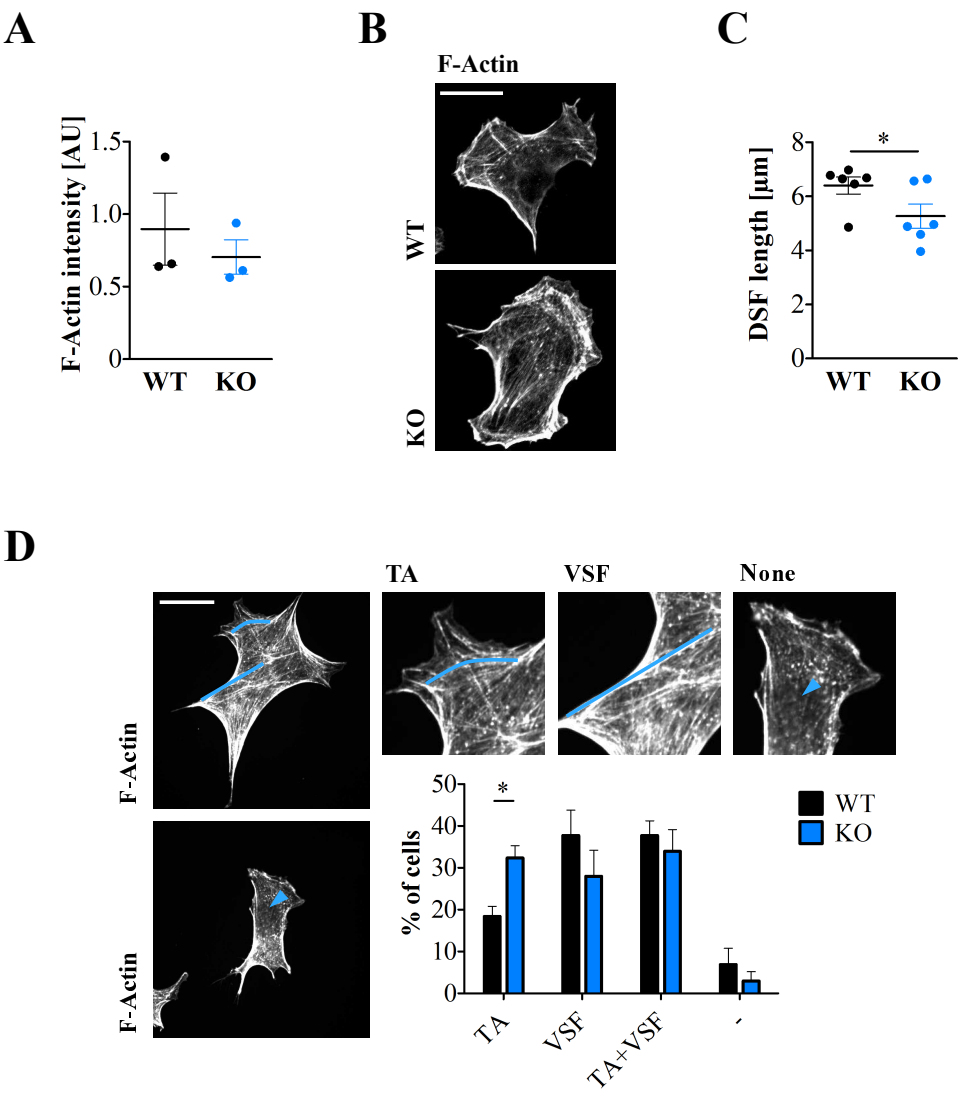

Figure 3.20.: Altered F-Actin network arrangement in Stn1 KO MEFs at steady-state. **A)** No change of F-Actin fluorescence intensity per cell between WT and Stn1 KO MEFs at steady state. Quantitative analysis was based on fluorescently labelled phalloidin staining acquired with a spinning disc confocal microscope. **B,C)** Dorsal stress fibre (DSF) length is significantly reduced in Stn1 KO MEFs. A) Exemplary confocal images of WT and Stn1 KO MEFs, stained for F-Actin using phalloidin. Scale bar: 25 µm. B) Quantitative analysis of DSF length per cell (n=6, paired, two-tailed t-test). **D)** Relative number of cells either displaying transverse arcs (TAs) and/or ventral stress fibres (VSFs), or without detectable F-Actin cytoskeleton (none). Significantly more Stn1 KO cells were observed with pronounced TAs (n=3, paired, two-tailed t-test). Quantification was carried out based on visual criteria demonstrated in exemplary images. Scale bar: 25 µm.

connectivity between FA and F-Actin. Thus, at the leading edge α-Actinin incorporation into DSFs coincides with FA growth. We hypothesised that α-Actinin incorporation was reduced

in Stn1 KO MEFs in line with the reduced FA size.

Stainings of α-Actinin in WT cells confirmed its localisation within and shortly behind focal adhesions indicating proper actin bundling along focal adhesions (figure 3.21A). Interestingly in Stn1 KO MEFs α-Actinin mainly localised proximal to the plasma membrane of the lamellipodia and only a minor portion could be observed along focal adhesions. Yet, the overall α-Actinin levels were unaltered between both genotypes (figure 3.21B). We examined changes in localisation of α-Actinin around focal adhesions using line scans (figure 3.21C). Averaged fluorescence intensities were measured along focal adhesions towards the cell nucleus. The distance between the leading edge, identified using F-Actin staining, and the nucleus, detected with the DNA dye DAPI, was used for normalisation between cells. Directly behind the leading edge, focal adhesions were identified by increasing vinculin (Vinc) fluorescence intensity (figure 3.21C) which drops at the end of the focal adhesions. In average Vinc intensity of WT MEFs was stronger compared to Stn1 KO. This indicated higher Vinc concentrations per focal adhesion in WT cells confirming previous analyses performed on Pax immunostainings (Feutlinske, 2014). In addition, Stn1 KO cells appeared to have smaller focal adhesions (∼3.5 µm) compared to WT cells (∼4.5 µm) which is consistent with previous analyses (Feutlinske, 2014). We could clearly identify 2 characteristic α-Actinin peaks within the lamellipodia of WT cells (figure 3.21C, upper graph, arrows) demonstrating that a) α-Actinin is recruited in close proximity to the plasma membrane (arrow 1) and b) is incorporated at the end of focal adhesions (arrow 2). Interestingly in Stn1 KO cells α-Actinin predominantly localised proximal to the cell edge, in front of focal adhesions, as indicated by the strong fluorescence intensity peak (lower graph, arrow 1). In fact the second peak, was undetectable in Stn1 depleted cells (arrow 2). The differences in colocalisation between α-Actinin and Vinc in Stn1 KO cells, however, were not detectable using Pearson's correlation which might be due to the strong cytosolic pools of both proteins (figure 3.21D).

Based on the literature we would suggest that the α-Actinin which localises proximal to the plasma membrane identifies an actin fibre pool necessary to generate transverse arcs (Hotulainen and Lappalainen, 2006) while its localisation near the end of focal adhesions indicate enhanced F-Actin crosslinking of growing FAs (Oakes et al., 2012). Thus, Stn1 KO MEFs might inefficiently incorporate α-Actinin into F-Actin fibres that are connected with focal complexes. Alternatively, FAs of Stn1 depleted cells might not reach the maturation status at which connection with the F-Actin cytoskeleton occurs, hence, α-Actinin would not be

present. In addition, Stn1 KO MEFs displayed a stronger pool of α-Actinin positive structures at the leading edge indicating a pronounced pool of F-Actin bundles.

Another study by Dolat et al. (2014) described that defective FA maturation correlated with a reduced DSF length upon septin 2/9 (Sept2/9) depletion. They suggested a model in which Sept2/9 act as connectors between focal adhesions and DSFs to efficiently transmit the traction force from TAs. Interestingly, mass-spectrometry from surface biotinylation-based analysis of WT and Stn1 KO MEFs showed a tendency for reduced Sept9 levels in Stn1 depleted cells (Feutlinske, 2014). Thus, we hypothesised that Stn1 depletion might diminish protein levels or plasma membrane association of septins resulting in a defective FA

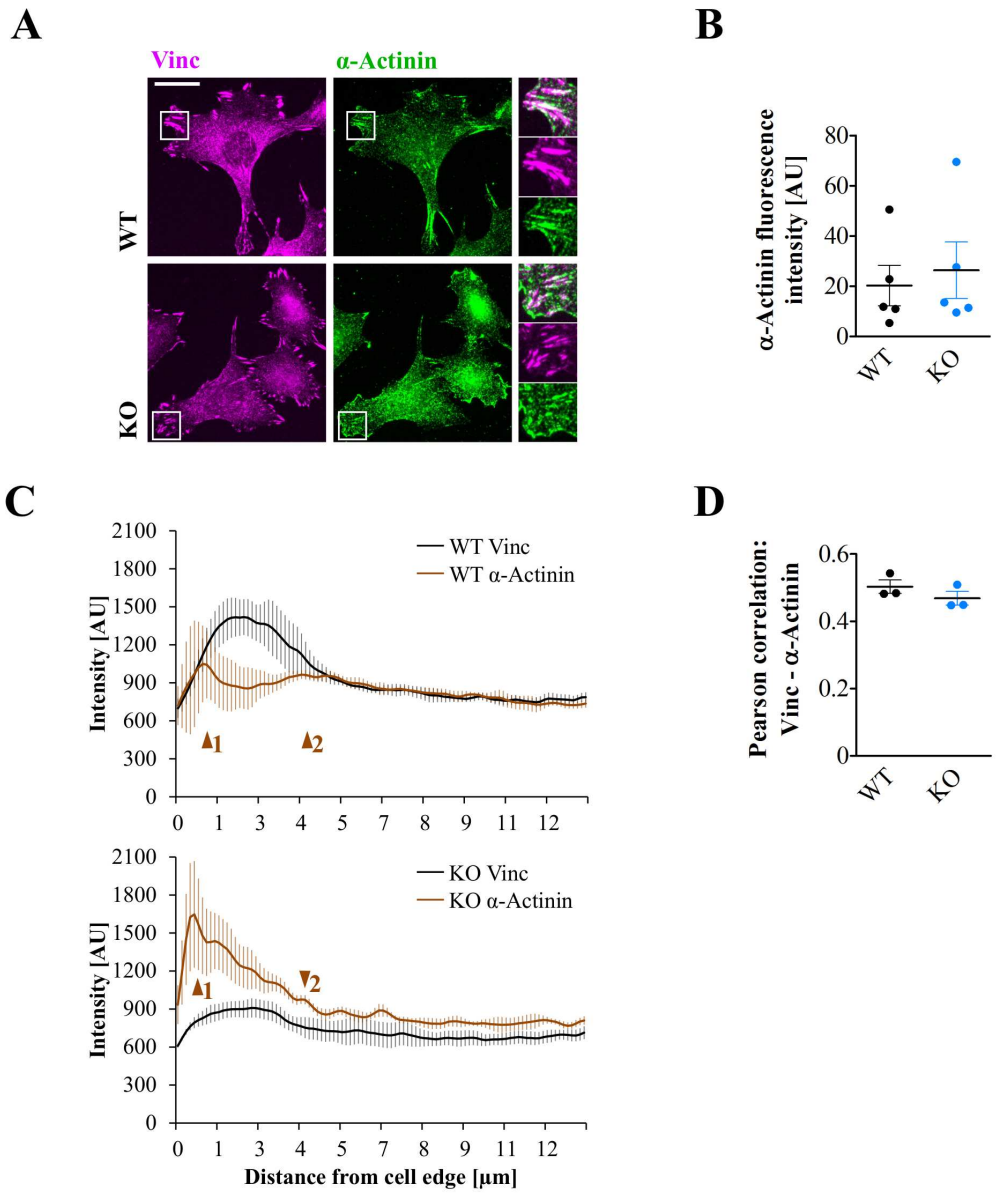

Figure 3.21.: α-Actinin is disorganised in Stn1 KO MEFs. MEFs at steady-state were fixed with PFA, stained with fluorescent phalloidin to visualise F-Actin and immunolabelled using a α-Actinin and Vinc antibody. **A)** Exemplary epifluorescent images of WT and Stn1 KO MEFs demonstrating α-Actinin localisation within the cell. α-Actinin was inefficiently incorporated in focal adhesions of Stn1 KO cells (zoom). Scale bar: 25 μm. **B)** α-Actinin fluorescence intensity per cell, quantified from epifluorescent images, was unchanged between WT and Stn1 KO cells. **C)** Line scans along Vinc-positive focal adhesions (black curves) illustrated the disturbed incorporation of α-Actinin (brown curves) into focal adhesions when Stn1 was depleted. Two characteristic α-Actinin intensity peaks were observed in WT cells (indicated by arrows) while only the first one was detected in Stn1 KO MEFs, though, with a stronger intensity (n=3). Line scans from confocal images were created as described in section 2.6. **D)** Pearson correlation determined to analyse the colocalisation between vinculin and α-Actinin remained unaltered between both genotypes. (*Vinc - vinculin*)

maturation.

Due to limited antibody availability, the analysis was performed based on Sept2 detection which has been shown to fulfil a similar role in FA maturation as Sept9 (Dolat et al., 2014). Sept2 was distributed throughout the cell, partially forming septin fibres without visual differences between WT and Stn1 KO MEFs (figure 3.22A). Accordingly, no difference in Sept2 intensity per cell was detected between both genotypes (figure 3.22B). However, Stn1 KO MEFs displayed a higher variability, hence more repetitions are needed. From immunofluorescent images we could not confirm a pronounced localisation of Sept2 directly behind focal adhesions. Therefore line scans to examine changes in the localisation of Sept2 were generated (figure 3.22C) as described before. Again, focal adhesions, identified using again vinculin (Vinc) as marker, were smaller and had a reduced fluorescence intensity in Stn1 KO MEFs when compared to WT cells (upper graph, figure 3.22C). We expected Sept2 localisation to be enriched directly behind focal adhesions to connect actin fibres with focal adhesions. Despite the formation of smaller focal adhesions of Stn1 KO cells no difference of Sept2 localisation behind focal adhesions was observed (lower graph, figure 3.22C). Instead, Sept2 intensity of both genotypes steadily increased towards the cell nucleus reflecting observations from immunostainings (figure 3.22A). It might be that due to differences in antibody specificity, the differences in Sept2 localisation reported by Dolat et al. (2014) were not detected. We concluded that reduced DSF length of Stn1 KO MEFs did not originate from diminished Sept2 protein levels or its absence from the FA-DSF interface.

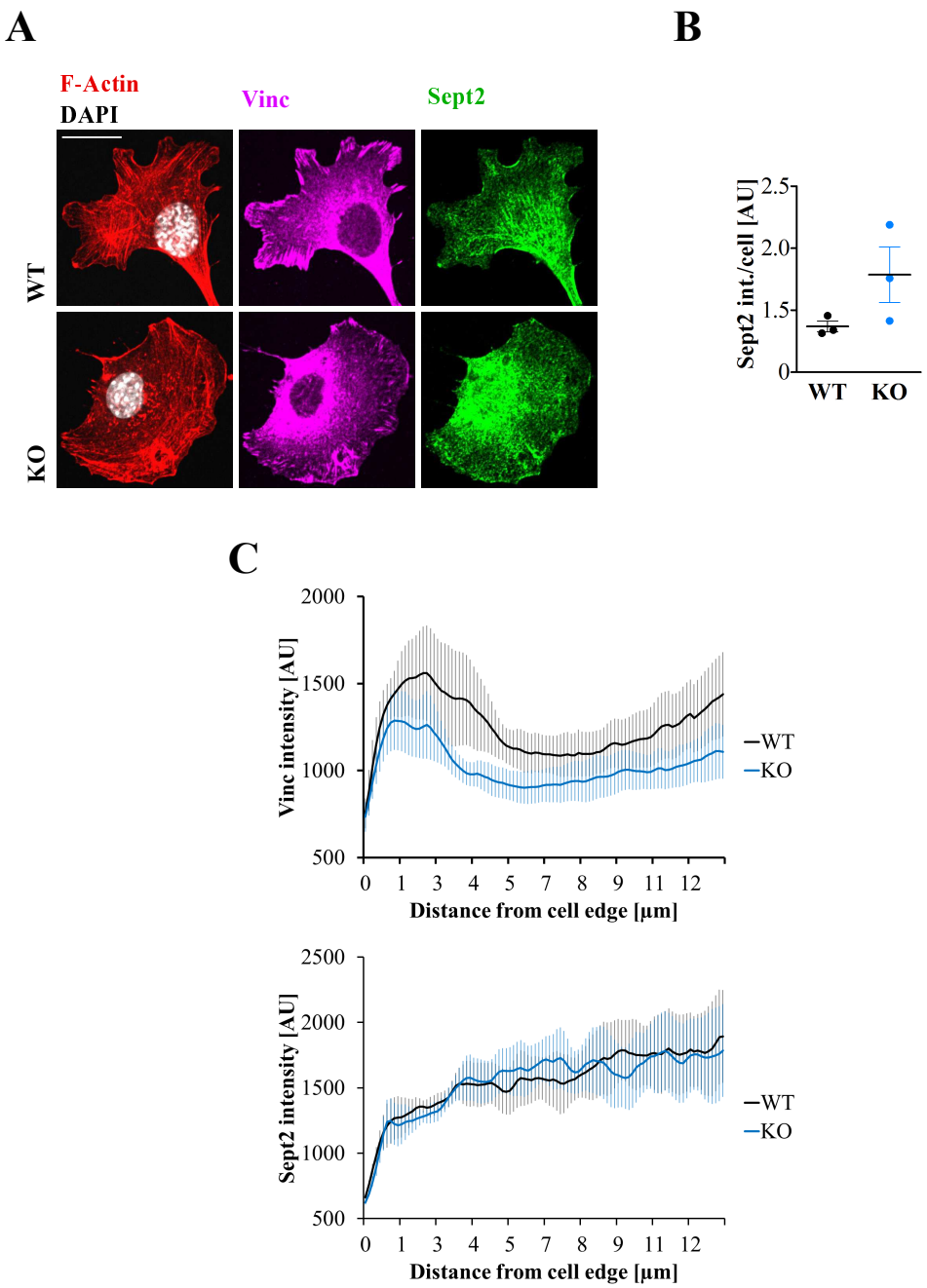

Figure 3.22.: Sept2 localisation is unperturbed in Stn1 KO MEFs. MEFs that were stimulated with 50 ng/ml PDGF-BB overnight were fixed with PFA, stained with fluorescent phalloidin to visualise F-Actin and immunolabelled using a Sept2 and Vinc antibody. **A)** Exemplary confocal images of WT and Stn1 KO MEFs showing the typical Sept2 distribution within the cell. Scale bar: 20 µm. **B)** Sept2 fluorescence intensity per cell, quantified from confocal images, was unaltered between both genotypes. **C)** Line plots along Vinc-positive focal adhesions (upper graph) to compare Sept2 (lower graph) localisation from cell edge to nucleus in WT and Stn1 KO MEFs. No changes in Sept2 localisation were observed. Line plots from confocal images were generated as described in section 2.6 (n=3). (*Sept2 - septin 2, Vinc - vinculin*)

3.4.4. Defects in F-Actin re-arrangements in Stn1 KO cells might originate from Destrin mislocalisation

α-Actinin which localises proximal to the plasma membrane identifies an actin fibre pool necessary to generate transverse arcs (Hotulainen and Lappalainen, 2006). Therefore, the increased α-Actinin pool close to the plasma membrane (figure 3.21) suggested an enhanced formation of α-Actinin stabilised F-Actin structures at this site. We speculated that the activity of an actin-regulatory protein was out of balance in Stn1 absence. It seemed likely that Stn1 might interact with a regulatory protein of the Actin cytoskeleton thereby controlling focal adhesions size. Mass-spectrometry data from a immunoprecipitation using a Stn1 antibody (conducted and analysed by Feutlinske (2014)) were carefully examined by Dr. Tanja Maritzen to identify potential candidates. In addition, the results were compared with another mass-spectrometry approach which characterised the changes in FA composition following myosin 2 inhibition using blebbistatin (Kuo et al., 2011). Due to myosin 2 inhibition, FAs loose their mechanosensitivity and FA disassembly of mature FAs is induced.

Since Stn1 has been demonstrated to become enriched at FAs following myosin 2 inhibition using the inhibitor blebbistatin (Feutlinske, 2014) we focussed on candidates showing the same behaviour. Amongst others, 2 proteins caught our special interest: the Actin depolymerisation factors Destrin as well as its close homologue Cofilin. Both proteins were found to be highly enriched in mass-spectrometry data from an immunoprecipitation using a Stn1 antibody (Feutlinske, 2014). In addition, both actin depolymerising factors were found to be recruited to focal adhesions upon block of myosin 2 activity using blebbistatin (Kuo et al., 2011).

First, we confirmed the interactions with Stn1 found by mass-spectrometry of the Stn1 immunoprecipitation with GST pull-down experiments. Endogenous Stn1 was concentrated from lung tissue using GST-Destrin (figure 3.23A). In fact, Stn1 interaction with Destrin was found to be significantly stronger than Stn1 binding to GST indicating strong binding over background levels (figure 3.23B). Consistent, no binding between Stn1 and Cofilin was detected. This demonstrated the high binding specificity of Stn1 and Destrin since both actin depolymerising factors share a 70% sequence similarity (Moriyama et al., 1990).

Next, we examined Destrin localisation in WT and Stn1 KO MEFs. Immunostainings revealed a cytosolic distribution of Destrin similar to Cofilin (Yonezawa et al., 1987) in both genotypes (figure 3.23C). Fluorescence intensity quantifications did not indicate altered ex-

pression levels between WT and Stn1 KO cells (figure 3.23D). However, in WT cells Destrin formed characteristic clusters at focal adhesion sites (figure 3.23C zoom). These were almost absent in Stn1 KO MEFs. In fact, Stn1 KO MEFs had almost three times less Destrin clusters at focal adhesions (figure 3.23E).

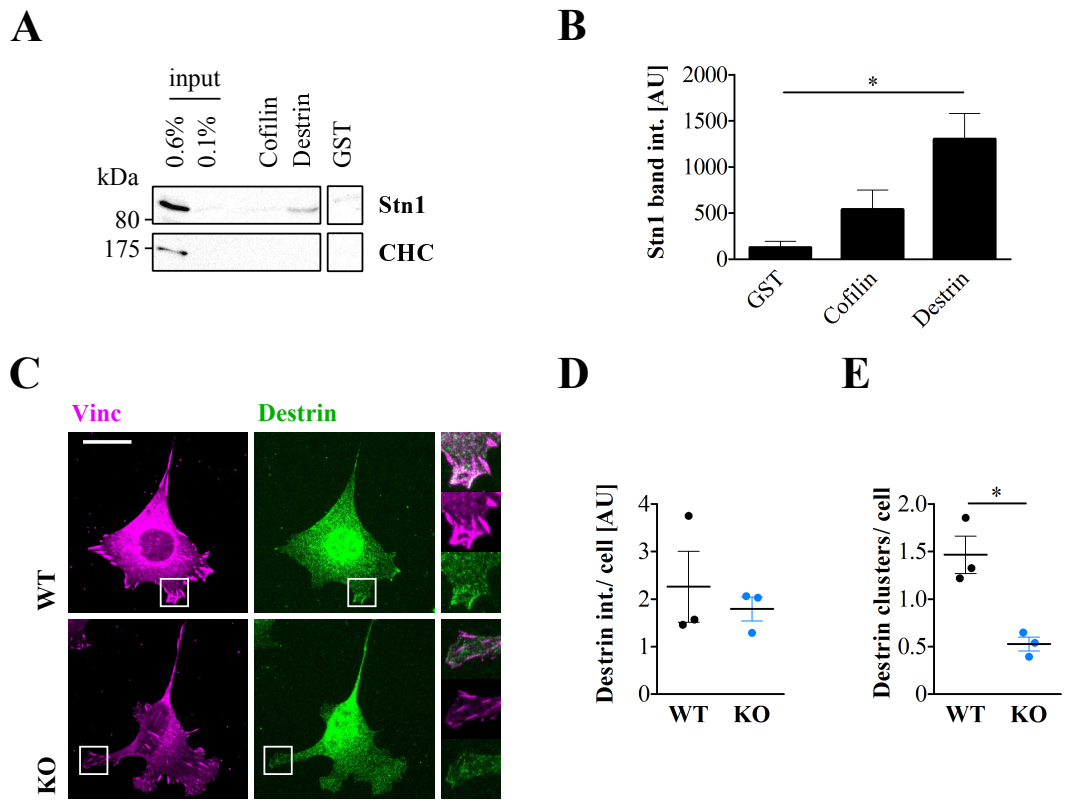

Figure 3.23.: Destrin interacts with Stn1. A,B) Endogenous Stn1 was concentrated from mouse lung by the interaction with Destrin in GST pull-down assays. Extracts of mouse lungs were incubated with GST-Destrin, GST-Cofilin or GST and precipitated binding partners were analysed by immunoblotting. A) Exemplary immunoblot demonstrating the interaction of Stn1 with Destrin while no significant binding with Cofilin or GST was detected. Endocytic proteins like Clathrin did not interact with Destrin. B) Quantification of Stn1 band intensity detected in A showed a significantly stronger interaction of Stn1 with Destrin compared to Cofilin and GST control (n=4, 1-Way Anova, Dunnett post test). **C)** Exemplary epifluorescent images showing the cellular distribution of Destrin in WT and Stn1 KO MEFs. Zooms highlight Destrin clusters near focal adhesions that were absent in Stn1 KO MEFs. Cells at steady-state were fixed with PFA and immunolabelled using antibodies against endogenous Destrin and vinculin. Scale bar: 25 µm. **D)** Destrin intensity quantifications from epifluorescent images did not reveal differences between both genotypes. **E)** Destrin clusters, highlighted in C, were significantly more in WT when compared to Stn1-depleted cells (n=3, paired, two-tailed t-test). (*Vinc - vinculin*)
Experiment A was performed and analysed by Dr. Tanja Maritzen.

In summary, while Destrin localised to focal adhesions in WT MEFs, Stn1 deletion prevented correct recruitment of Destrin. Whether Destrin recruitment into focal adhesions was achieved via a direct interaction with Stn1 will be part of further studies. Since Cofilin has already been demonstrated to regulate DSF formation (Tojkander et al., 2015) as well as FA growth (Marshall et al., 2009), we would suspect a similar role for Destrin. However, this hypothesis needs to be substantiated with further experiments.

4. Discussion

Dysregulated endocytosis results in altered surface levels of receptor proteins affecting cell signalling as well as migration which can potentiate cancer development. The specialised endocytic adaptor stonin 1 (Stn1) has only recently been demonstrated to be involved in cell migration by controlling the surface levels of the proteoglycan and oncogene neuron glial 2 (NG2). But the molecular details and the physiological context of Stn1's role as an endocytic adaptor of NG2 remained vague. In this study we identify Stn1 as a potential tumour suppressor in human and mice and describe two functions of the endocytic adaptor potentially contributing to tumour progression (figure 4.2). First, Stn1 limits cell signalling through the platelet-derived growth factor receptor β which might suppress neovascularisation of tumour tissues. Second, Stn1 regulates focal adhesion dynamics, thereby modifying cell adhesion and motility. These data provide evidence for a so far unknown function of Stn1 and might help to understand tumour development evoked through dysregulated endocytosis.

4.1. Stn1 is the endocytic adaptor for the oncogene NG2

4.1.1. Stn1 is recruited into endocytic pits through an interaction with AP2

Clathrin-mediated endocytosis controls a plethora of cellular processes including nutrient uptake and cellular signalling by regulating the surface availability of diverse cell receptors. While the majority of cargos is internalised via general endocytic adaptors, fine tuning of cellular processes is achieved by specialised endocytic adaptors (Traub and Bonifacino, 2013). These have been demonstrated to connect the endocytic machinery with cargo proteins to facilitate their uptake. The stonins (Stn's) are a family of specialised endocytic adaptors comprising two homologues - termed Stn1 and Stn2 (Maritzen et al., 2010). Stn2 has been reported to interact with the general endocytic adaptor AP2 via three WxxF motives located at the N-terminus. In addition, Stn2 recruitment into endocytic pits is facilitated through interactions with Eps15-homolgy (EH) domain proteins via two NPF motifs at the N-terminus

of Stn2 (Martina et al., 2001). How Stn1 is incorporated into clathrin-coated pits, however, has not been investigated in detail.

In this work, we show that Stn1 interacts with the endocytic adaptor AP2 (figure 3.1A,B) which is concordant with previous studies (Feutlinske, 2014; Martina et al., 2001). Similar to Stn2, Stn1 has been suggested to interact with AP2. However, Stn1 only comprises a single WxxF motif within the aminoterminus (Walther et al., 2004). Surprisingly, Stn1 interacts with AP2 even if the potential WxxF motif is mutated to prevent AP2 binding (figure 3.1B). This suggests to us that additional interaction motifs support AP2 binding. The WxxF motif is recognised by AP2 when it is flanked by non-charged amino acids at the amino terminus and amino acids with negative residues at the C-terminus (Ritter et al., 2004). Indeed within the primary sequence of mouse Stn1, we found an AP2 interaction motif close to the C-terminus fulfilling the criteria (ms-Stn1: AA711-714, figure 4.1). However, the newly identified WxxF motif does not have all the basic elements that were described to bind the AP2 α-ear. The basic elements include a tryptophan at the first position, either valine, alanine, isoleucine, glutamic acid or aspartic acid at second, phenylalanine or tryptophan at the fourth and negatively charged amino acids at positions 5, 6 and 7 (Ritter et al., 2004). The identified C-terminal WxxF motif of Stn1, however, has a valine at the fourth and does not contain the full stretch of negatively charged amino acids. In addition, sequence alignments with human Stn1 have revealed that C-terminal WxxF motif of Stn1 is not conserved in humans (figure 4.1). In fact, AP2 interaction studies with human Stn1 failed so far (Martina et al., 2001) implying that indeed the suggested motif might only strengthen the AP2-Stn1 interaction in mouse. Since the C-terminal WxxF motif also does not contain all basic elements, the function of the C-terminal mouse WxxF motif in Stn1 might only play a minor role for the AP2 interaction. In accordance, Stn1's μ-homology domain on its own does not promote NG2 uptake when re-introduced in Stn1 KO MEFs (Feutlinske, 2014) indicating that the classical WxxF motif is necessary for recognition of Stn1 by the endocytic machinery.

In addition to the aminoterminal WxxF motif, mouse Stn1 also comprises a NPF motif in the N-terminus (Martina et al., 2001). In case of Stn2 the NPF motifs bind EH-domain proteins which contribute in recruiting Stn2 to the endocytic machinery (Martina et al., 2001). Interestingly, mutating the NPF motif of Stn2, blocked the interaction with the EH-domain protein Eps15 as well as AP2 indicating that Stn2 is mainly recruited to the endocytic machinery via EH-domain proteins. Hence, the NPF motif might substantially contribute

to AP2 binding in mouse Stn1. However, Stn1 recruitment to the endocytic machinery via EH-domain proteins does not play a role in the human system since the NPF motif is not conserved in human Stn1 (Martina et al., 2001).

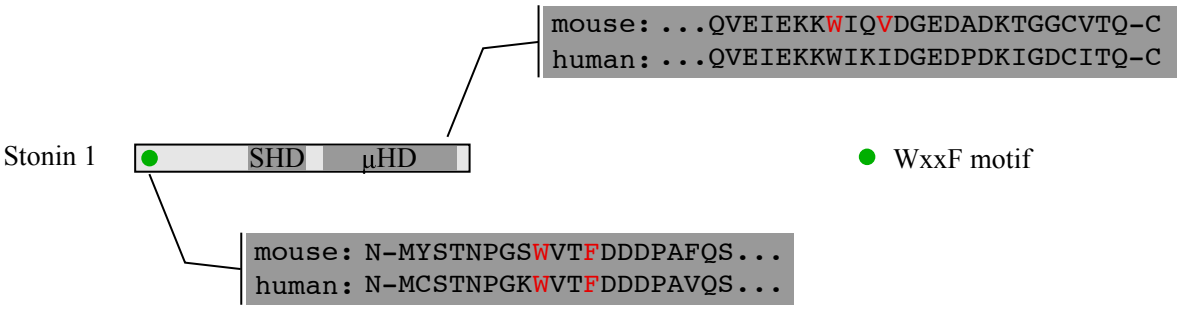

Figure 4.1.: Primary sequences around the conventional and the newly identified WxxF motif of mouse and human Stn1. The scheme of Stn1 that illustrates localisation of the characteristic stonin homology domain (SHD) and the µ-homology domain (µHD). The mouse and human primary sequence around the conventional WxxF motif at the N-terminus (green dot) and the suggested unconventional WxxF motif at the C-terminus are noted in the grey boxes. Motifs are marked in red.

Prohibiting the AP2 interaction by mutating the WxxF motif in the N-terminus of Stn1 also reduces total Stn1 expression levels (figure 3.1B). The same has been observed upon depletion of total AP2 levels from AP2 Lox/Lox×CAG cre/Esr1 astrocytes (figure 3.1D,E). These results indicate a) that the AP2 interaction protects Stn1 from degradation which has been shown to be mediated via the proteasome (Feutlinske, 2014). However, this hypothesis needs further investigation using AP2 Lox/Lox×CAG cre/Esr1 astrocytes blocked for proteasomal degradation. And b) that the classical WxxF motif at the N-terminus of mouse Stn1 mediates the majority of AP2 interaction while the C-terminal WxxF motif might only contribute to a minor degree in mice.

By comparing the Stn1 localisation in AP2 Lox/Lox×CAG cre/Esr1 astrocytes, we demonstrated that AP2 regulates Stn1 recruitment to endocytic pits near the centre of the cell (figure 3.1F). Yet, another fraction of Stn1-positive structures does not depend on AP2. One might speculate that additionally to AP2, Stn1 accumulates at distal cell regions due to the interaction with its cargos. In fact, the neuron glial 2 (NG2), one of Stn1's cargos already established, has been demonstrated to co-localise with Stn1 at protrusive fronts as well as trailing ends within migrating glial and mouse embryonic fibroblasts (MEFs, Feutlinske

2014).

4.1.2. NG2 is a cargo of the specialised endocytic adaptor Stn1

Efficient endocytic uptake of NG2 depends on the presence of Stn1 (Feutlinske, 2014). However, the underlying details have remained obscure. From our analysis we can conclude that Stn1 interacts with the cytosolic domain of NG2 via its cargo binding domain - the μ-homolgy domain (figure 3.3, 3.4). Still, NG2 binding with full-length Stn1 was only detected in GST pull-down approaches (figure 3.2) and not by performing co-immunoprecipitation (figure 3.3). Thus the NG2-Stn1 interaction seems to require further regulatory steps, e.g. to release an autoinhibitory conformation by Stn1. Stn1 has been demonstrated to be a multiphosphorylated protein (Feutlinske, 2014) pointing towards a similar regulation for numb 1. The endocytic adaptor numb 1 localises to clathrin-coated structures to facilitate integrin β1 internalisation (Nishimura and Kaibuchi, 2007). Following phosphorylation via the atypical protein kinase C, numb 1 exits clathrin-coated pits. Similarly, Stn1 phosphorylation regulates its subcellular localisation (figure 3.11). While nonphosphorylated Stn1 predominantely localises to the plasma membrane, phosphorylation of Stn1 causes its release into the cytosol. However, due to multiple combinations of phosphorylations sites the precise mechanism will need further investigations. Alternatively, Stn1 might undergo conformational changes needed for cargo recognition. Conformational changes could be either driven by posttranslational modifications like phosphorylations or transmitted via another binding partner. Partially Stn1-positive structures get stabilised by AP2 (section 4.1.1). Hence, AP2 interaction might be considered to trigger an intrinsic conformational change resulting in cargo recognition by Stn1.

Interestingly, Stn1 interacts with NG2 via the NG2 PDZ-domain interaction motif (figure 3.4) despite the absence of any PDZ-domain in Stn1. Hence, it might be conceivable that a PDZ-domain containing protein bridges the interaction to NG2 and potentially also regulates the discussed conformational changes in Stn1. The function of the three PDZ-domain proteins found to interact with NG2 - MUPP1, GRIP1 and syntenin (Barritt et al., 2000; Chatterjee et al., 2008; Stegmüller et al., 2003) - were mainly described in brain-derived cells and only syntenin has been shown so far to be also expressed in other organs like lung and placenta (Zimmermann et al., 2001) where Stn1 is predominantely found (Feutlinske, 2014). Additionally, none of these binding partners have been found in Stn1 immunoprecip-

Table 4.1.: PDZ-domain proteins found with mass-spectrometry in Stn1 immunoprecipitation.

PDZ-domain protein	Heavy/ Light	Description
PDZ and LIM domain protein 1 (Pdlim1)	1.23	Actin-binding proteins involved in cell adhesion and migration
PDZ and LIM domain protein 2 (Pdlim2)	0.23	
PDZ and LIM domain protein 5 (Pdlim5)	1.05	
Serine protease 1 (Htra1)	1.0	Serine protease mediating cleavage of ECM proteins to release growth factors
Serine protease (Htra2)	0.67	Serine protease involved in apoptosis
Tight-junctional protein 1 (Tjp1)	0.67	Tight-junction proteins
Tight-junctional protein 2 (Tjp2)	0.49	
Myosin-XVIIIa (Myo18a)	∼0.60	Involved in vesicle budding from the Golgi and the actomyosin retrograde flow
Signal-induced proliferation-associated protein 1 (Sipa1)	0.58	Cell cycle regulation
Syntrophin, acidic 1 (Snta1)	0.44	Actin-binding protein organising cell surface receptors

PDZ-domain proteins from *mus musculus* (SMART5, Letunic et al. 2006) were compared to interaction candidates detected with Stn1 immunoprecipitation (Feutlinske, 2014). Heavy/Light ratios ∼1 are considered to be unspecific. Mass-spectrometry was performed on enzymatically digested H_2O^{16} and H_2O^{18} labelled WT samples. Stn1 immunoprecipitation was executed in O^{18} and IgG control in O^{16} labelled cells. Heavy/Light (O^{18}/O^{16})- isotope ratios were calculated according to the Mascot Distiller software (version 2.2.07, Matrix Science).

itations pointing towards another PDZ-domain protein which might mediate the interaction with NG2. 10 of the 147 yet known PDZ-domain proteins in mouse (2017, SMART5, Letunic et al. 2006) are found by mass-spectrometry of Stn1 immunoprecipitations, however, all have low heavy/light ratios (H/L∼1) indicating background or unspecific binding (table 4.1). Hence, further investigations are needed to identify putative PDZ-domain binding partners that bridge Stn1 and its cargo NG2. Comparison of mass-spectrometry data of Stn1 and of NG2 immunoprecipitations might identify the potential linking protein.

The absence of an endocytic adaptor often leads to cargo accumulation at the plasma membrane due to the lack of internalisation. For example, Stn2 defective for recognition of the endocytic machinery results in elevated surface levels of its cargo synaptotagmin 1 (Diril

et al., 2006; Kaempf et al., 2015). In accordance, Feutlinske (2014) reported elevated NG2 levels in Stn1 KO MEFs, mouse lung fibroblasts (MLFs) and glial cultures. In vivo, Stn1 and NG2 are expressed within the same tissues (figure 3.5A), however, only in p14 brain NG2 protein levels increase in Stn1 absence. Feutlinske (2014) demonstrated that NG2 accumulation occurs over time. Thus, fast cell turnover rates might limit the experimental procedures here. In fact, lung alveoli are considered to turnover within 8 days (Milo and Phillips, 2016) while NG2-positive cells in brain accumulate over 15-20 days postnatally to promote myelination of the young brain (Niehaus et al., 1999). Thus, different turnover rates in lung of NG2/Stn1-positive cell lines might prevent detection of different expression levels.

4.2. Stn1 protects from tumour progression potentially by regulating NG2 availability

Stn1 KO animals grow into adulthood without any phenotypical abnormalities. Also a thorough examination by the German mouse clinic (Munich) did not reveal any significant changes due to Stn1 absence (unpublished data). In accordance, Stn1 does not influence brain or lung architecture in immunohistological stainings (figure 3.5, 3.7). What is the physiological context of Stn1's functions then?

4.2.1. Stn1 acts as tumour suppressor

With our work we have established that Stn1 is an endocytic adaptor for NG2. NG2 is a well known oncogene which is expressed by a myriad of tumours including melanoma (Burg et al., 1998), glioblastoma (Chekenya et al., 2002, 1999; Shoshan et al., 1999), chrondrosarcoma (Leger et al., 1994) and lymphoid leukemia (Smith et al., 1996). In fact, elevated NG2 expression in glioblastomas increases tumour angiogenesis and proliferation resulting in increased tumour growth (Wang et al., 2011). Thus, by regulating the surface levels of NG2, Stn1 might control NG2's oncogenic potential and function as tumour suppressor. In fact, high levels of Stn1 inversely correlate with a diminished expression of NG2 in biopsies obtained from brain tumours which have been analysed on microarrays (Feutlinske, 2014). In addition, we show for the first time that Stn1-depletion increases brain tumour growth (figure 3.8C-E) supporting data gained from public data bases which demonstrate that increased Stn1 expression levels increase glioma patient survival (figure 3.8A).

Elevated protein levels of NG2 in glioblastoma increase the proliferation rate thereby promoting tumour growth (Wang et al., 2011). Thus, by regulating NG2 surface availability, Stn1 might play a role within malignant tissues. In fact, absence of Stn1 in transformed NPCs seemed to stimulate brain tumour growth (figure 3.8C,D). However, using transformed NPCs to investigate brain tumour growth had only limited success in inducing brain tumours, hence these results need to be validated. Nevertheless, the preliminary data might indicate that by regulating NG2 surface availability, Stn1 might control NG2-dependent proliferation. However, it is unlikely that Stn1 affects the proliferation of NG2-positive cells directly since no such effect has been documented from isolated primary cells (from own observation). However, by facilitating endocytic uptake of NG2, Stn1 might promote lysosomal degradation and downregulation of NG2 protein levels in cells. The precise time-dependent downregulation of the protein levels of NG2 is of particular importance for the differentiation of self-renewing polydendrocytes into mature oligodendrocytes (Nishiyama et al., 2009). To achieve differentiation, polydendrocytes asymmetrically segregate NG2 during cell division which leads to polydendrocyte self-renewal and to differentiation of the NG2-negative daughter cell (Sugiarto et al., 2011). This mechanism is often affected in malignant tissues maintaining NG2 expression and sustained polydendrocyte proliferation. In fact, Stn1 absence prevents proper down regulation of NG2 within the OB, a brain region where NG2-positive cells are increasingly recruited between p8-p16 (figure 3.7A). In accordance, isolated primary MEFs from both, WT and Stn1 KO animals, show high levels of NG2, but only immortalised Stn1 KO cells maintain the elevated NG2 levels while WT cells downregulate NG2 expression (mentioned in Feutlinske 2014). Thus, the elevated NG2 levels in OBs of young animals suggest that Stn1 might be important for NG2 downregulation and subsequent polydendrocyte differentiation into oligodendrocytes. Already first indications might be revealed by comparing the amount of differentiated oligodendrocytes in p14 WT and Stn1 KO mice. In addition, the NG2 segregation during differentiation in WT and Stn1 KO cells, e.g. isolated NPCs, might support our understanding in the contributions of Stn1 in the process of differentiation.

Also, Stn1 absence from stromal tissues significantly affects tumour growth (figure 3.8E). Of note, NG2 plays an important role during tumour vascularisation by being expressed by pericytes and macrophages (Stallcup et al., 2016). As the endocytic adaptor for NG2, Stn1 might control the functions of NG2 in these stromal cells thereby promoting tumour angiogenesis. Pericytes and macrophages are recruited to the tumour tissue to support the

integrity of the newly formed vessel by stimulating formation of adherens junctions between endothelial cells (section 1.3.2). To efficiently support tumour angiogenesis, both cell types rely on NG2 expression (Stallcup et al., 2016). Pericytes-specific ablation of NG2 reduces the recruitment of pericytes into the tumour tissue in response to PDGF-BB, leading to a reduced tumour growth due to diminished vessel patency (You et al., 2013). Specific deletion of NG2 in macrophages inhibits the extravasation of macrophages potentially due to the lack of the co-receptor function of NG2 towards integrin β1 (Yotsumoto et al., 2015). As a consequence, the patency of the tumour vascularisation is reduced and tumour growth is inhibited. By regulating the surface levels of NG2, Stn1 might control the NG2-dependent functions in macrophages and pericytes. Thus, the increased tumour growth in Stn1 KO animals might reflect increased tumour angiogenesis as a consequence of elevated NG2 surface levels e.g. in macrophages or pericytes. In fact, Feutlinske (2014) showed that Stn1 is present in RAW264.7, a murine macrophage cell line, as well as HBVP (human brain vascular pericyte cell line). Therefore it will be important for future projects to identify Stn1 expressing cell types *in vivo*. So far, detecting Stn1-positive cells *in vivo* under physiological as well as under pathological conditions failed due to the lack of an antibody suitable for immunohistochemistry. However, expression of endogenous Stn1 might be unveiled by performing immunoblotting of isolated cell types from WT and Stn1 KO tissues. In addition, characterisation of the generated tumours for presence of pericytes, macrophages, and endothelial cells might reveal whether Stn1 protein levels indeed affect tumour vascularisation.

4.2.2. Stn1 influences cell signalling via PDGF-BB

The extent of tumour growth is confined by the way malignant cells interact with their surrounding. Cell signalling cascades and modes of cell migration are often altered in cancer tissues. Specifically, secretion of PDGF-BB by tumour tissue has been shown to attract stromal cells to support tumour vascularisation and metastasis (Hosaka et al., 2016). Therefore tight control of growth factor receptor activation limits tumour development. Stn1 controls PDGFRβ activation following PDGF-BB stimulation and subsequent intracellular signalling (figure 3.9, 3.10). This is not a consequence of elevated PDGFRβ levels (figure 3.9A) disproving initial tendencies from surface biotinylation experiments (Feutlinske, 2014). Instead we predict that Stn1 regulates PDGF signalling by being the endocytic adaptor for NG2 due to

the following reasons. Firstly, NG2 forms clusters following stimulation with PDGF-BB that represent signalling hubs (Feutlinske, 2014). Secondly, NG2 clusters need to be resolved by endocytosis (Feutlinske, 2014). Thirdly, NG2 co-localises with the phosphorylated PDGFRβ at CDRs after PDGF-BB stimulation. And finally, NG2 co-localises with Rab5-positive endosomes following PDGF-BB stimulation indicating growth factor stimulated internalisation (Feutlinske, 2014). Nevertheless, NG2 has not been shown to capture PDGF-BB (Grako et al., 1999). In fact, aortic smooth muscle cells (aSMC) isolated from NG2 KO animals respond normally to PDGF-BB while PDGF-AA induced signalling is diminished (Grako et al., 1999; Grako and Stallcup, 1995). This is intriguing since PDGF-BB has been shown to bind to all known PDGF receptor combinations (αα, αβ and ββ) though with different affinities, while PDGF-AA only binds to the homodimeric PDGFRα (Seifert et al., 1989). In addition, signalling from PDGFRα does not contribute to CDR formation (Eriksson et al., 1992; Hammacher et al., 1989) indicating that the observed phenotypes in Stn1 MEFs originate solely from PDGFRβ activation. Furthermore, a study by Makagiansar et al. (2007) demonstrate that NG2 overexpressing U251 cells show an increased chemotaxis towards PDGF-BB. Also pericytes expressing NG2 migrate faster towards PDGF-BB in transwell migration assays than pericytes with reduced NG2 protein levels (You et al., 2013).

Therefore, we predict the following model for Stn1's function in cell signalling affecting tumour growth based on the literature (for overview see figure 4.2). Stn1 regulates surface levels of NG2 (Feutlinske, 2014) thereby controlling its availability as co-receptor for growth factor receptors. By clustering the PDGFRβ, NG2 might stabilise the ligand-bound PDGFRβ leading to enhanced PDGFRβ activation and signalling. PDGF sensitivity fine-tunes stromal cell activation and recruitment into tumour tissues. Consequently, Stn1 counteracts tumour development by facilitating NG2 uptake.

4.2.3. Stn1 influences directional migration through NG2

Chemoattraction by growth factors leads to polarisation of cells and subsequent migration (Petrie et al., 2009). How efficient cells can react to the environmental cues depends on the mode of cell migration which is often dictated by a chemotactic gradient. In absence of a chemotactic gradient, cells migrating randomly change their intracellular polarisation continuously which can be observed through the formation of multiple protrusions probing the environment and short trailing ends allowing fast directional changes (Petrie et al., 2009).

In contrast, directionally migrating cells - often observed along a chemical gradient that attracts the cell - maintain their internal polarity over longer time periods resulting in rapid cell translocation in one direction and a short total path length. Focal adhesion dynamics influence the mode of migration: to allow flexibility for random migration focal adhesion dynamics need to be high (Morgan et al., 2013). Stn1-depletion remarkably reduces focal adhesion dynamics (figure 3.15) which is in accordance with increased directional migration (Feutlinske, 2014). Other endocytic proteins like numb have been shown to be recruited to disassembling focal adhesions (Chao et al., 2010; Ezratty et al., 2009; Nishimura and Kaibuchi, 2007). In fact, also Stn1 localises directly behind focal adhesions (Feutlinske, 2014), the place of focal adhesion disassembly (Ezratty et al., 2009; Nishimura and Kaibuchi, 2007). Using the nocodazole assay developed by Ezratty et al. (2005) we demonstrate that Stn1 inhibits focal adhesion disassembly (figure 3.16) confirming indications from life cell imaging experiments (Feutlinske, 2014). In conclusion, Stn1 affects focal adhesion dynamics by controlling their disassembly.

Additionally, NG2, the cargo of Stn1, regulates directional migration of astrocytoma cells (Makagiansar et al., 2004) and oligodendrocyte precursors (Binamé et al., 2013). In fact, the elevated NG2 levels in Stn1-depleted MEFs correlate with an increased directionality (Feutlinske 2014, figure 3.12A) confirming that NG2 is a regulator of persistent migration (Binamé et al., 2013; Makagiansar et al., 2004). Visually, directional persistence of Stn1 KO cells is reflected by a pronounced trailing end and increased protrusion stability (Feutlinske, 2014). However, trailing end stability in Stn1 KO MEFs does not depend on NG2 levels (figure 3.12F,G). But preliminary data suggests that the elevated protrusion steadiness of Stn1 KO cells might originate from Stn1's function as endocytic adaptor for NG2 (figure 3.13). Since NG2 is a transmembrane receptor that supports cell attachment, the increased protrusion stability might have originated from elevated NG2 levels in Stn1 KO MEFs. NG2 associates with the ECM molecules laminin (Burg et al., 1997) and the collagens 5 and 6 Tillet et al. (1997). However, only cell attachment to the collagens 5 and 6 is promoted by elevated levels of NG2 (Tillet et al., 2002). In accordance, Stn1 KO MEFs have no benefit from elevated NG2 levels upon seeding on collagen 1, which does not bind NG2, or laminin 1 (figure 3.14). However, enhanced NG2 availability in Stn1 KO MEFs also does not result in enhanced substrate engagement to collagen 6 (figure 3.14). Of note, NG2-dependent cell

attachment to collagen 6 is masked by the presence of β1 integrins in GD25 cells which overexpress NG2 together with β1 integrins (Tillet et al., 2002). Therefore, the NG2-dependent cell attachment of MEFs to collagen 6 might be masked by the basal protein levels of β1 integrins. By reducing β1 integrin levels in MEFs, the effects of NG2 on cell attachment might become unveiled. Interestingly, Stn1 KO MEFs adhered significantly faster to matrigel 9 min after seeding (figure 3.14). Matrigel is a commercially available basal membrane mixture which mainly contains the extracellular matrix proteins collagen 4 and laminin (∼90%, BD Bioscience 2011). However, adhesion to collagen 4 and laminin is not promoted by NG2 expression (Tillet et al., 2002). Instead, adhesion of Stn1 KO MEFs to matrigel might be stimulated due to their increased sensitivity towards growth factors like PDGF (section 4.2.2) since matrigel also contains numerous growth factors including PDGF (BD Bioscience, 2011). Besides promoting cell attachment, NG2 is supposed to assemble with β1 integrins to regulate their subcellular distribution and ECM engagement (Stallcup and Huang, 2008) to control cell motility. In case of Stn1 KO cells, however, we can exclude altered total β1 integrin levels (Feutlinske, 2014), integrin internalisation (Feutlinske, 2014) as well as altered integrin activity (figure 3.12B,C) from playing a role in directional migration. Also contributions from integrin α5 and αV (figure 3.12D,E) seem unlikely to contribute to NG2-evoked persistent migration. Nevertheless, indirect effects of NG2, e.g. by acting as co-receptor for a so far unknown surface receptor, cannot be excluded.

In addition to an increased protrusion persistence, the directionality of migrating Stn1 KO cells is also reflected by a pronounced trailing end (Feutlinske, 2014). A study by Ezratty et al. (2009) demonstrated that also diminished FA disassembly upon block of endocytosis increases trailing end persistence. Therefore, increased trailing end stability might be a consequence of slowed FA disassembly in absence of Stn1 (figure 3.16). This might also explain how elevated levels of NG2 in Stn1 KO MEFs increase protrusion persistence (for overview see figure 4.2). NG2 engages with the substratum and forms clusters mainly within focal adhesions. Its accumulation supports protrusion persistence, therefore stimulating directional migration. Upon depletion of Stn1, NG2 clusters cannot get resolved leading to reduced exchange of focal adhesion components and an imbalance of migration modes. However, the influence of elevated NG2 protein levels in focal adhesion dynamics and disassembly needs further investigation to substantiate the hypothesis.

Besides cell signalling also the migratory behaviour of cells influences tumour progression dramatically. For instance, stromal cells are recruited to the malignant tissue and stimulate tumour growth. Thus, together with the enhanced sensitivity for growth factors, the increased directionality might favour tumour growth in Stn1 absence.

4.3. Destrin and Stn1 might act in concert to regulate focal adhesion dynamics and migration

A block of disassembly has been correlated with increased number and bigger size of focal adhesions (Schiefermeier et al., 2014). In accordance, blocking integrin endocytosis by Dab2 or dynamin knockdown increases the number of focal adhesions (Chao and Kunz, 2009). However, absence of Stn1 results in smaller focal adhesions (Feutlinske, 2014) although Stn1 is crucial for focal adhesion disassembly (figure 3.16). In this study we demonstrate that Stn1 is similarly important for focal adhesion assembly as indicated by reduced focal adhesion kinase phosphorylation (figure 3.17). Oakes et al. (2012) demonstrated that the crosslinkage between focal adhesions and the actomyosin network is crucial for FAK activation and subsequent efficient focal adhesion growth and assembly. Stn1 has been reported to localise to actin fibres and co-immunoprecipitate β-Actin (Feutlinske, 2014) indicating that Stn1 might modulate actin cytoskeleton dynamics. Here, we identify a new Stn1 binding partner that might assist Stn1-dependent actin filament re-arrangements: the actin depolymerising factor (ADF) Destrin (figure 3.23A,B). Destrin has already been found in mass-spectrometry approaches to localise to a subset of focal adhesions (Horton et al., 2015; Kuo et al., 2011; Robertson et al., 2015; Schiller et al., 2011). Albeit the vastly cytosolic pool we can confirm Destrin accumulation at focal adhesions (figure 3.23C,E). These clusters form Stn1-dependently as Stn1 depletion decreases their number within cells indicating that Stn1 affects Destrin localisation.

Interestingly Stn1 does not consistently interact with Destrin's close homologue Cofilin (figure 3.23A,B) although both proteins share over 70% amino acid sequence homology (Vartiainen et al., 2002). Therefore, Destrin and Stn1 might interact at regions that are disparate with Cofilin. Sequence alignments indicate that these lay predominantly outside of the actin binding regions (Vartiainen et al., 2002) suggesting that Stn1 might not hinder actin binding. Structurally the ADF/Cofilin family has been demonstrated to bind to G-Actin (amino ter-

minus) as well as F-Actin (N- and C-terminus, Vartiainen et al. 2002). Hence, mapping of the Stn1 interaction site might reveal how Stn1 affects Destrin function.

Cofilin has been shown to sever F-Actin filaments within the dendritic actin network (Bravo-Cordero et al., 2013). Subsequently, separated F-Actin filaments can get either capped for filament stabilisation and re-usage or depolymerised to allow regrowth of the protrusion. Similar activities are assumed for Destrin (Vartiainen et al., 2002). Since a high Cofilin activity is associated with focal adhesion disassembly (Marshall et al., 2009) we here suggest a model in which Stn1 interacts with Destrin and inhibits Destrin activity. Consequently, Stn1 deletion would result in hyperactivity of the actin depolymerising factor. This implies that the organisation of actin fibres would be affected (Tojkander et al., 2015). Indeed, absence of Stn1 results in reduced dorsal stress fibre length (figure 3.20B,C) which is in accordance with previous studies reporting the opposite effect upon Cofilin depletion (Tojkander et al., 2015). Additionally, Stn1 balances transverse arc formation (figure 3.20D) which arose from dorsal stress fibres (Hotulainen and Lappalainen, 2006; Tojkander et al., 2015). Though ADF/Cofilin depletion have been correlated with excessive F-Actin formation and actomyosin contractility (Kanellos et al., 2015; Wiggan et al., 2012), total F-Actin formation is not affected by Stn1 absence (figure 3.20A). The stronger F-Actin network in ADF/Cofilin depleted cells has been correlated to an ADF/Cofilin competitive binding with myosin 2 for F-Actin (Wiggan et al., 2012). But in Stn1 absence Destrin availability is not affected (figure 3.23D), hence, lack of competitive binding can be excluded.

How Stn1 regulates Destrin activity remains to be addressed in future studies. Cofilin activity is regulated by three distinct processes (Bravo-Cordero et al., 2013). Firstly, Cofilin phosphorylation at Serine 3 by LIM kinase inhibits F-Actin binding and severing. For instance, the protein 14-3-3ζ has been demonstrated to stabilise p(S3)Cofilin thereby supporting LIM kinase functions (Gohla and Bokoch, 2002). Similar to Cofilin, Destrin comprises the serine 3 (Shishkin et al., 2016) that can be phosphorylated following stimulation (Schiller et al. 2013 supplementary table 3). This suggests a similar regulation via phosphorylation as for Cofilin. Yet, it is unlikely that Stn1 blocks the phosphorylation site by direct interaction, since the critical phosphorylation site Ser3 lies within the actin binding site and is highly homologous to Cofilin. Secondly, the interaction with phosphoinositide-4,5-bisphosphate ($PI(4,5)P_2$) sequesters Cofilin and Destrin at the plasma membrane and inhibits their Actin depolymerisation activity (Gorbatyuk et al., 2006; Yonezawa et al., 1990). Instead, Destrin resides pre-

dominantly within the cytoplasm but concentrates at distal protrusions in a Stn1 dependent manner (figure 3.23C-E). In accordance, the endocytic adaptor Stn1 itself does not control phosphoinositide phosphate (PIP) levels directly. It also seems unlikely that Stn1 regulates the localisation of a metabolising enzyme for PIPs particularly since no such enzyme has been identified as binding partner by immunoprecipitation of Stn1 (data obtained by Feutlinske 2014). Finally, complex formation between Cofilin and cortactin hinders Cofilin activation, however, this mechanism has been associated solely with invadopodia.

From our data we propose the following involvement of Destrin within the Stn1-dependent focal adhesion maturation process (for overview see figure 4.2). Stn1 interacts with the actin depolymerising factor Destrin and regulates its activity by a yet undefined mechanism. In absence of Stn1, Destrin gains an increased activity stimulating F-Actin severing.

The question remains how exactly an increased Destrin activity in Stn1 KO MEFs hinders focal adhesion maturation. On the one hand, an elevated Destrin activity might free tensile forces that are needed for focal adhesion reinforcement and maturation (Schiller et al., 2013). On the other hand, the increased activity of Destrin in Stn1 depleted MEFs, might reduce the amount of F-Actin bundles that are necessary for focal adhesion maturation (Oakes et al., 2012). As a general F-Actin crosslinker, α-Actinin is recruited to focal adhesions when traction forces are applied (Ye et al., 2014) to organise and strengthen the connectivity between FAs and F-Actin. In Stn1 depleted MEFs, α-Actinin localises behind focal adhesions, however to a minor extent (figure 3.21A). This might indicate that FAs of Stn1 KO MEFs do not reach the maturation status at which the F-Actin connection occurs. Still, the major fraction of α-Actinin in Stn1-depleted MEFs is predominantly found close to the plasma membrane (figure 3.21A,C). Since α-Actinin crosslinks F-Actin its predominant fraction close to the plasma membrane suggest a pronounced pool of F-Actin bundles which might have been generated from increased F-Actin severing e.g. by Destrin.

4.4. Outlook

Dysregulated endocytosis modifies dynamics and surface concentrations of receptors triggering defects in cell signalling cascades and potentially migratory behaviour (Maritzen et al., 2015). Thus it is not surprising that several endocytic proteins have been correlated with cancer progression (McMahon and Boucrot, 2011). Based on our data Stn1 might play a decisive role for tumour development (see figure 4.2) broadening our understanding of the

disease. Nevertheless we are only at the beginning of understanding Stn1's cellular functions and physiological implications. Further investigations will contribute to position Stn1 within the complex network of proteins that suppress tumour progression and to extend our comprehension of the physiological functions of Stn1.

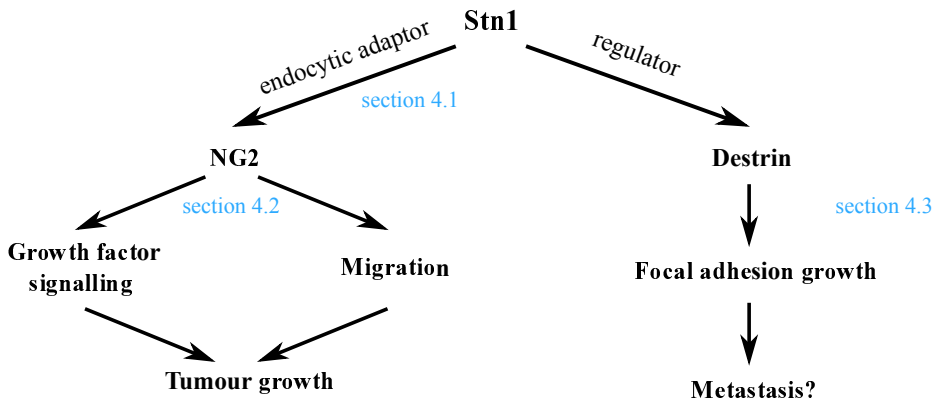

Figure 4.2.: Implications for Stn1. Stn1 performs two distinct roles. By acting as an endocytic adaptor for NG2, Stn1 controls growth factor signalling and cell migration to prevent tumour growth. Through balancing Destrin activity, Stn1 might determine focal adhesion size and mechanical strength transmitted to the substrate thereby affecting metastasis. According discussion sections are indicated in blue.

Stn1 as a member of the endocytic machinery. From surface biotinylation experiments NG2 has been identified as one of Stn1's cargos (Feutlinske, 2014). Further candidates might point to additional roles for Stn1 in other biological processes. Dachsous, a protein found to be important for embryonic development (Ishiuchi et al., 2009; Mao et al., 2011), was also strikingly enriched in the surface proteome of in Stn1 KO cells. However, the lack of any developmental defects in Stn1 KO mice does not link the two proteins together (unpublished data). In addition, several cell signalling surface receptors including the transforming growth factor β receptor 2 (TGFβ2) and the basic fibroblast growth factor receptor (bFGFR) are potentially upregulated in Stn1-depleted cells. In this study we show a remarkable influence of Stn1 on the signalling of PDGFRβ albeit without altered surface receptor levels. It will be interesting to see whether Stn1 influences other cell signalling pathways and their corresponding tissue functions.

Implications for Stn1 in tumour progression and tissue homeostasis. Here, we describe Stn1 as a tumour suppressor. But where does Stn1 mainly act - within the host

tissue or within the tumour itself? Is Stn1 inhibiting tumour growth by limiting tumour angiogenesis? Does Stn1 control tumour growth by reducing NG2 protein levels? Characterising Stn1-depleted tumours for abundance of critical cell types like macrophages and pericytes will support the identification of Stn1 functions during tumour progression. In cell culture experiments Stn1 has been shown to be expressed by macrophages, fibroblasts and pericytes (Feutlinske, 2014) and all of these might contribute to tumour growth. Fibroblasts act as cancer associated fibroblasts (CAFs) restructuring the ECM to generate 'highways' for cancerous cell expansion (Kalluri, 2016). Macrophages support tumour cell invasion by breaking down the ECM and supporting tumour and endothelial cell proliferation by secretion of growth factors (Noy and Pollard, 2014). And pericytes substantially contribute to neovascularisation (Trost et al., 2016). Though the latter two processes have been described to be influenced by NG2 expression (Stallcup et al., 2016), it is unlikely that NG2 remains the only cargo protein for Stn1 with implications in tumour progression. For instance, the above mentioned TGFβ and FGF receptors are upregulated in the surface proteome of Stn1 KO cells and both have been implicated in cancer progression thereby providing candidates as alternative Stn1 cargos beside NG2.

As mentioned earlier, asymmetric segregation of NG2 during cell division controls polydendrocyte differentiation to mature oligodendrocytes. Particularly pericytes and fibroblasts have the potential to differentiate into multiple cell types (Díaz-Flores et al., 2009) including fat tissue. In context of NG2, it has been shown that absence of NG2 leads to dysfunction of brown fat tissue and obesity in adulthood (Chang et al., 2012). Hence, Stn1 might also fulfil important functions for further tissues by controlling cell differentiation.

Stn1 as a regulator of the Actin cytoskeleton. Stn1 likely regulates focal adhesion growth through the actin cytoskeleton. First results indicate a cooperation between Stn1 and the actin depolymerising factor Destrin. It will be an issue for future studies how Stn1 and Destrin act together. Characterisation of Destrin phosphorylation and localisation of p(S3)Destrin in Stn1 absence might reveal first indications. Nevertheless only mapping of the interaction sites will allow detailed descriptions of their mutual influence on function and localisation.

Destrin and Cofilin compete with myosin 2 for F-Actin binding leading to increased actomyosin contractility upon ADF/Cofilin depletion (Wiggan et al., 2012). However, Stn1

depletion does not affect Destrin expression levels nor total F-Actin formation. Nevertheless, preliminary data indicate a reduced RhoA activity that might lower myosin 2 activity (Collaboration with Paul Markus Mueller, unpublished data). Focal adhesion maturation depends on the actomyosin contractility (Goetsch et al., 2014). Hence reduced RhoA activity correlates with smaller focal adhesions in Stn1 depleted MEFs. However whether reduced RhoA activity is a consequence of increased Destrin activity (feed backward loop) has never been investigated yet. Further studies are necessary to unveil their molecular relation.

Despite their close relation, Destrin and Cofilin have been shown to handle different aspects of directional cell migration (Tahtamouni et al., 2013). Both actin depolymerisation factors increase the rate of cell migration by promoting protrusion formation. But while Cofilin depletion increases protrusion stability, Destrin-depleted cells protrude more frequently. Also ablation of both genes in mice results in different consequences for the animals indicating specific functions for each member *in vivo* (Kanellos and Frame, 2016). Destrin ablation results in increased proliferation of and therefore thickening of the corneal epithelium (Ikeda et al., 2003). Cofilin deletion is embryonic lethal due to inefficient closure of the neuronal tube (Gurniak et al., 2005). Stn1 absence does not provoke any physiological saliences (report from the German mouse clinic (Munich), unpublished data). Nevertheless it will be interesting to see if the expected unbalance of Destrin activity in Stn1 depleted animals affects pathological situations like cancer development. Particularly during metastasis primary tumour cells need assistance from cancer-associated fibroblasts (CAFs) to invade the surrounding tissue. CAFs are contractile cells that bundle collagen fibrils within the extracellular matrix around the tumour tissue (Wei and Yang, 2016). Stiff collagen fibrils function like "highways" for the malignant cells and facilitate tumour escape. To form these fibrils CAFs need to bind to and pull on ECM fibrils generating tensile forces on the ECM as well as intracellularly (Butcher et al., 2009). Reduced FA size as well as altered actin fibre arrangements might affect mechanosensitivity and fibril formation of CAFs. Traction force measurements as well as gel contraction experiments might indicate whether Stn1 depleted cells are defective in sensing of rigidity and generation of actomyosin contractions.

5. Acknowledgements

I would like to thank my supervisors Prof. Dr. Volker Haucke and PD Dr. Tanja Maritzen for giving me the possibility to work in their labs. Their constant guidance and advice substantially prospered the project.

I would like to acknowledge Dr. Min Chi Ku and Prof. Dr. Rainer Glass for supporting our tumour studies with their expert knowledge.

I also express gratitude to all present and former Haucke lab members for creating such an enjoyable atmosphere in- and outside of the FMP building. The constructive discussions and advices from each of them broadened my scientific comprehension and gave raise to new perspectives. Particularly, I would like to thank Dr. Martin Lehmann who critically questioned my results to open up new experimental possibilities and for his comments on this thesis. Also I owe gratitude to our superb technicians Claudia Schmidt and Maria Mühlbauer who supported my work with their experimental expertise whenever it was possible. A special thanks to my closest friend Natalie Kaempf and Tania Lopez-Hernandez with whom I teamed up in bay two of the big laboratory C2.16. The endless evenings would have felt much longer without them.

I wish to extend special thanks to my 'new big family' for all their patience and encouragement throughout my studies. When everything seemed overwhelmingly complicated they gave me a harbour to rest and refresh my mindset.

Most deeply, I would like to thank the person who experienced the work, with all its ups and downs, most closest: my husband Mathias. He not just secured my physical survival with his fantastic cooking skills but also my mental strength by just being himself. Without him it would not have been possible! This work is as much his as mine.

Bibliography

Abramsson, A., Lindblom, P., and Betsholtz, C. (2003). Endothelial and nonendothelial sources of PDGF-B regulate pericyte recruitment and influence vascular pattern formation in tumors. *Journal of Clinical Investigation*, 112(8).

Andrew, N. and Insall, R. H. (2007). Chemotaxis in shallow gradients is mediated independently of PtdIns 3-kinase by biased choices between random protrusions. *Nature Cell Biology*, 9(2):193–200.

Andrews, J., Smith, M., Merakovsky, J., Coulson, M., Hannan, F., and Kelly, L. E. (1996). The stoned locus of Drosophila melanogaster produces a dicistronic transcript and encodes two distinct polypeptide. *Genetics Society of Amerika*, 143:1699–1711.

Antonny, B., Burd, C., Camilli, P. D., Chen, E., Daumke, O., Ford, M., Frolov, V. A., Frost, A., Hinshaw, J. E., Kirchhausen, T., Kozlov, M. M., Lenz, M., Low, H. H., McMahon, H., Merrifield, C., Pollard, T. D., Robinson, P. J., Roux, A., and Schmid, S. (2016). Membrane fission by dynamin: what we know and what we need to know. *EMBO Journal*, 35(21):1–15.

Appolloni, I., Calzolari, F., Tutucci, E., Caviglia, S., Terrile, M., Corte, G., and Malatesta, P. (2009). PDGF-B induces a homogeneous class of oligodendrogliomas from embryonic neural progenitors. *International Journal of Cancer*, 124:2251–2259.

Arber, S., Barbayannis, F. A., Hanser, H., Schneider, C., Stanyon, C. A., Bernard, O., and Caroni, P. (1998). Regulation of actin dynamics through phosphorylation of cofilin by LIM-kinase. *Nature*, 393:805–809.

Arlt, M. J., Born, W., and Fuchs, B. (2012). Improved visualization of lung metastases at single cell resolution in mice by combined in-situ perfusion of lung tissue and X-Gal staining of lacZ-tagged tumor cells. *Jove*, 66:1–4.

Armulik, A., Genové, G., and Betsholtz, C. (2011). Review pericytes: developmental, physiological and pathological perspectives, problems and promises. *Developmental Cell*, 21:193–215.

Arrieumerlou, C. and Meyer, T. (2005). A local coupling model and compass parameter for eukaryotic chemotaxis. *Developmental Cell*, 8:215–227.

Asher, R. A., Morgenstern, D. A., Properzi, F., Nishiyama, A., Levine, J. M., and Fawcett, J. W. (2005). Two separate metalloproteinase activities are responsible for the shedding

and processing of the NG2 proteoglycan in vitro. *Molecular and Cellular Neuroscience*, 29:82–96.

Bachir, A. I., Zareno, J., Moissoglu, K., Plow, E. F., Gratton, E., and Horwitz, A. R. (2014). Integrin-associated complexes form hierarchically with variable stoichiometry in nascent adhesions. *Current Biology*, 24:1845–1853.

Ballestrem, C., Hinz, B., Imhof, B. A., and Wehrle-Haller, B. (2001). Marching at the front and dragging behind: differential alphaVbeta3-integrin turnover regulates focal adhesion behavior. *Journal of Cell Biology*, 155(7):1319–1332.

Barritt, D. S., Pearn, M. T., Zisch, A. H., Lee, S. S., Javier, R. T., Pasquale, E. B., and Stallcup, W. B. (2000). The multi-PDZ domain protein MUPP1 is a cytoplasmic ligand for the membrane-spanning proteoglycan NG2. *Journal of Cellular Biochemistry*, 79:213–224.

Barron, L., Gharib, S. A., and Duffield, J. S. (2016). Lung pericytes and resident fibroblasts busy multitaskers. *The American Journal of Pathology*, 186(10).

BD Bioscience (2011). BD Matrigel matrix - Frequently asked questions.

Berg, J. M., Tymoczko, J. L., and Stryer, L. (2007). Biochemie. In *Spectrum Akademischer Verlag*, chapter 14. Signal, pages 439–446. Elsevier GmbH, München, 6 edition.

Bergers, G. and Song, S. (2005). The role of pericytes in blood-vessel formation and maintenance. *Neuro-Oncology*, 7:452–464.

Binamé, F. (2014). Transduction of extracellular cues into cell polarity: the role of the transmembrane proteoglycan NG2. *Molecular Neurobiology*, 50:482–493.

Binamé, F., Sakry, D., Dimou, L., Jolivel, V., and Trotter, J. (2013). NG2 regulates directional migration of oligodendrocyte precursor cells via Rho GTPases and polarity complex proteins. *The Journal of Neuroscience*, 33(26):10858–10874.

Bonfanti, L., Ponti, G., Luzzati, F., Crociara, P., Parolisi, R., and Armentano, M. (2013). Parenchymal neuro-glio-genesis versus germinal layer-derived neurogenesis: two faces of central nervous system structural plasticity. In Bonfanti, L., editor, *Neural Stem Cells - New Perspectives*, chapter 9, pages 241–268. InTech.

Bradford, M. M. (1976). A rapid and sensitive method for the quantitation of microgram quantities of protein utilizing the principle of protein-dye binding. *Analystische Biochemie*, 72(248-254).

Bravo-Cordero, J. J., Magalhaes, M. A. O., Eddy, R. J., Hodgson, L., and Condeelis, J. (2013). Functions of Cofilin in cell locomotion and invasion. *Nature Reviews Molecular Cell Biology*, 14:405–417.

Burg, A., Nishiyama, A., and Stallcup, W. B. (1997). A central segment of the NG2 proteoglycan is critical for the ability of glioma cell to bind and migrate towards type VI collagen. *Experimental Cell Research*, 235:254–264.

Burg, M. A., Grako, K. A., and Stallcup, W. B. (1998). Expression of the NG2 proteoglycan enhances the growth and metastatic properties of melanoma cells. *Journal of Cellular Physiology*, 177:299–312.

Burg, M. A., Tillet, E., Timpl, R., and Stallcup, W. B. (1996). Binding of the NG2 proteoglycan to type VI collagen and other extracellular matrix molecules. *Journal of Biological Chemistry*, 271(42):26110–26116.

Butcher, D. T., Alliston, T., and Weaver, V. M. (2009). A tense situation: forcing tumour progression. *Nature Reviews Cancer*, 9:108–122.

Calderwood, D. a., Fujioka, Y., de Pereda, J. M., García-Alvarez, B., Nakamoto, T., Margolis, B., McGlade, C. J., Liddington, R. C., and Ginsberg, M. H. (2003). Integrin beta cytoplasmic domain interactions with phosphotyrosine-binding domains: a structural prototype for diversity in integrin signaling. *PNAS*, 100(5):2272–2277.

Cao, Y. (2013). Multifarious functions of PDGFs and PDGFRs in tumor growth and metastasis. *Trends in Molecular Medicine*, 19(8):460–473.

Carlier, M.-F. and Shekhar, S. (2017). Global treadmilling coordinates actin turnover and controls the size of actin networks. *Nature Reviews Molecular Cell Biology*, pages 1–13.

Case, L. B. and Waterman, C. M. (2015). Integration of actin dynamics and cell adhesion by a three-dimensional, mechanosensitive molecular clutch. *Nature Cell Biology*, 17(8):955–963.

Cattaruzza, S., Ozerdem, U., Denzel, M., Ranscht, B., Bulian, P., Cavallaro, U., Zanocco, D., Colombatti, A., Stallcup, W. B., and Perris, R. (2013). Multivalent proteoglycan modulation of FGF mitogenic responses in perivascular cells. *Angiogenesis*, 16:309–327.

Cattaruzza, S. and Perris, R. (2005). Proteoglycan control of cell movement during wound healing and cancer spreading. *Matrix Biology*, 24:400–417.

Chamberlain, M. D., Oberg, J. C., Furber, L. A., Poland, S. F., Hawrysh, A. D., Knafelc, S. M., McBride, H. M., and Anderson, D. H. (2010). Deregulation of Rab5 and Rab4 proteins in p85R274A-expressing cells alters PDGFR trafficking. *Cellular Signalling*, 22:1562–1575.

Chang, Y., She, Z. G., Sakimura, K., Roberts, A., Kucharova, K., Rowitch, D. H., and Stallcup, W. B. (2012). Ablation of NG2 proteoglycan leads to deficits in brown fat function and to adult onset obesity. *PLoS one*, 7(1):1–11.

Chao, W.-T., Ashcroft, F., Daquinag, A. C., Vadakkan, T., Wei, Z., Zhang, P., Dickinson, M. E., and Kunz, J. (2010). Type I phosphatidylinositol phosphate kinase beta regulates focal adhesion disassembly by promoting 1 integrin endocytosis. *Molecular and Cellular Biology*, 30(18):4463–4479.

Chao, W. T. and Kunz, J. (2009). Focal adhesion disassembly requires clathrin-dependent endocytosis of integrins. *FEBS letters*, 583:1337–1343.

Chatterjee, N., Stegmüller, J., Schätzle, P., Karram, K., Koroll, M., Werner, H. B., Nave, K.-A., and Trotter, J. (2008). Interaction of syntenin-1 and the NG2 proteoglycan in migratory oligodendrocyte precursor cells. *The Journal of Biological Chemistry*, 283(13):8310–8317.

Chekenya, M., Enger, P. O., Thorsen, F., Tysnes, B. B., Al-Sarraj, S., Read, T. A., Furmanek, T., Mahesparan, R., Levine, J. M., Butt, A. M., Pilkington, G. J., and Bjerkvig, R. (2002). The glial precursor proteoglycan, NG2, is expressed on tumour neovasculature by vascular pericytes in human malignant brain tumours. *Neuropathology and Applied Neurobiology*, 28:367–380.

Chekenya, M., Rooprai, H. K., Davies, D., Levine, J. M., Butt, a. M., and Pilkington, G. J. (1999). The NG2 chondroitin sulfate proteoglycan: role in malignant progression of human brain tumours. *International Journal of Developmental Neuroscience*, 17(5-6):421–435.

Chen, H., Ko, G., Zatti, A., Di Giacomo, G., Liu, L., Raiteri, E., Perucco, E., Collesi, C., Min, W., Zeiss, C., De Camilli, P., and Cremona, O. (2009). Embryonic arrest at midgestation and disruption of Notch signaling produced by the absence of both epsin 1 and epsin 2 in mice. *PNAS*, 106(33):13838–13843.

Cheng, S. Y. S., Sun, G., Schlaepfer, D. D., and Pallen, C. J. (2014). Grb2 promotes integrin-induced focal adhesion kinase (FAK) autophosphorylation and directs the phosphorylation of protein tyrosine phosphatase α by the Src-FAK kinase complex. *Molecular and Cellular Biology*, 34(3):348–361.

Choi, C. K., Vicente-Manzanares, M., Zareno, J., Whitmore, L. A., Mogilner, A., and Horwitz, A. R. (2008). Actin and alpha-actinin orchestrate the assembly and maturation of nascent adhesions in a myosin II motor-independent manner. *Nature Cell Biology*, 10(9):1039–1050.

Clainche, C. L. and Carlier, M.-F. F. (2008). Regulation of actin assembly associated with protrusion and adhesion in cell migration. *Physiological Reviews*, 88:489–513.

Colaluca, I. N., Tosoni, D., Nuciforo, P., Senic-Matuglia, F., Galimberti, V., Viale, G., Pece, S., and Di Fiore, P. P. (2008). NUMB controls p53 tumour suppressor activity. *Nature*, 451:76–80.

Conner, S. D. and Schmid, S. L. (2003). Regulated portals of enrty into the cell. *Nature*, 422:37–43.

Danen, E. H. J., Sonneveld, P., Brakebusch, C., Fässler, R., and Sonnenberg, A. (2002). The fibronectin-binding integrins $\alpha5\beta1$ and $\alpha v\beta3$ differentially modulate RhoA-GTP loading, organization of cell matrix adhesions, and fibronectin fibrillogenesis. *Journal of Cell Biology*, 159(6):1071–1086.

Danen, E. H. J., Van Rheenen, J., Franken, W., Huveneers, S., Sonneveld, P., Jalink, K., and Sonnenberg, A. (2005). Integrins control motile strategy through a Rho-cofilin pathway. *Journal of Cell Biology*, 169(3):515–526.

Daumke, O., Roux, A., and Haucke, V. (2014). BAR domain scaffolds in dynamin-mediated membrane fission. *Cell*, 156(5):882–892.

Dawson, M. R. L., Polito, A., Levine, J. M., and Reynolds, R. (2003). NG2-expressing glial progenitor cells: an abundant and widespread population of cycling cells in the adult rat CNS. *Molecular and Cellular Neuroscience*, 24:476–488.

De Franceschi, N., Hamidi, H., Alanko, J., Sahgal, P., and Ivaska, J. (2015). Integrin traffic - the update. *Journal of cell science*, 128:1–14.

DelToro, R., Prahst, C., Mathivet, T., Siegfried, G., Kaminker, J. S., Larrivee, B., Breant, C., Duarte, A., Takakura, N., Fukamizu, A., Penninger, J., and Eichmann, A. (2010). Identification and functional analysis of endothelial tip cell enriched genes. *Blood*, 116(19):4025–4033.

Díaz-Flores, L., Gutiérrez, R., Madrid, J. F., Varela, H., Valladares, F., Acosta, E., Martín-Vasallo, P., and Díaz-Flores Jr, L. (2009). Pericytes. Morphofunction, interactions and pathology in a quiescent and activated mesenchymal cell niche. *Histology and Histopathology*, 24:909–969.

Diril, M. K. (2005). *Genetic analysis of stoned B/ stonin 2 function in vivo*. PhD thesis, Georg August University Goettingen.

Diril, M. K., Wienisch, M., Jung, N., Klingauf, J., and Haucke, V. (2006). Stonin 2 is an AP-2-dependent endocytic sorting adaptor for synaptotagmin internalization and recycling. *Developmental Cell*, 10:233–244.

Dolat, L., Hu, Q., and Spiliotis, E. T. (2014). Septin functions in organ system physiology and pathology. *Biological Chemistry*, 395(2):123–141.

Dowrick, P., Kenworthy, P., McCann, B., and Warn, R. (1993). Circular ruffle formation and closure lead to macropinocytosis in hepatocyte growth factor/ scatter factor-treated cells. *European Journal of Cell Biology*, 61(1):44–53.

DuBridge, R. B., Tang, P., Hsia, H. C., Leong, P.-M., Miller, J. H., and Calos, M. P. (1987). Analysis of mutation in human cells by using an Epstein-Barr virus shuttle system. *Molecular and Cellular Biology*, 7(1):379–387.

Eisenberg, E. and Greene, L. E. (2007). Multiple roles of auxilin and Hsc70 in clathrin-mediated endocytosis. *Traffic*, 8:640–646.

Eisenmann, K. M., McCarthy, J. B., Simpson, M. a., Keely, P. J., Guan, J. L., Tachibana, K., Lim, L., Manser, E., Furcht, L. T., and Iida, J. (1999). Melanoma chondroitin sulphate proteoglycan regulates cell spreading through Cdc42, Ack-1 and p130cas. *Nature Cell Biology*, 1:507–513.

Elosegui-Artola, A., Oria, R., Chen, Y., Kosmalska, A., Pérez-González, C., Castro, N., Zhu, C., Trepat, X., and Roca-Cusachs, P. (2016). Mechanical regulation of a molecular clutch defines force transmission and transduction in response to matrix rigidity. *Nature Cell Biology*, 18(5):540–548.

Eng, E. T., Smagghe, B. J., Walz, T., and Springer, T. A. (2011). Intact alpha2beta3 integrin is extended after activation as measured by solution x-ray scattering and electron microscopy. *Journal of Biological Chemistry*, 286(40):35218–35226.

Eriksson, A., Siegbahn, A., Westermark, B., Heldin, C.-H., and Claesson-Welsh, L. (1992). PDGF α- and β-receptors activate unique and common signal transduction pathways. *The EMBO Journal*, 11(2):543–550.

Estes, P. S., Jackson, T. C., Stimson, D. T., Sanyal, S., Kelly, L. E., and Ramaswami, M. (2003). Functional dissection of a eukaryotic dicistronic gene: Transgenic stonedB, but not stonedA, restores normal synaptic properties to Drosophila stoned mutants. *Genetics*, 165:185–196.

Etienne-Manneville, S. (2004). Cdc42 - the centre of polarity. *Journal of Cell Science*, 117(8):1291–1300.

Etienne-Manneville, S. and Hall, A. (2001). Integrin-mediated activation of Cdc42 controls cell polarity in migrating astrocytes through PKCζ. *Cell*, 106:489–498.

Ezratty, E. J., Bertaux, C., Marcantonio, E. E., and Gundersen, G. G. (2009). Clathrin mediates integrin endocytosis for focal adhesion disassembly in migrating cells. *Journal of Cell Biology*, 187(5):733–747.

Ezratty, E. J., Partridge, M. A., and Gundersen, G. G. (2005). Microtubule-induced focal adhesion disassembly is mediated by dynamin and focal adhesion kinase. *Nature Cell Biology*, 7(6):581–590.

Feutlinske, F. (2014). *Stonin1 facilitates endocytosis of NG2 and regulates signaling and cellular motility.* PhD thesis, Free university Berlin.

Feutlinske, F., Browarski, M., Ku, M.-C., Trnka, P., Waiczies, S., Niendorf, T., Stallcup, W. B., Glass, R., Krause, E., and Maritzen, T. (2015). Stonin1 mediates endocytosis of

the proteoglycan NG2 and regulates focal adhesion dynamics and cell motility. *Nature Communications*, 6(8535):1–13.

Forsberg, K., Valyi-Nagy, I., Heldin, C. H., Herlyn, M., and Westermark, B. (1993). Platelet-derived growth factor (PDGF) in oncogenesis: development of a vascular connective tissue stroma in xenotransplanted human melanoma producing PDGF-BB. *PNAS*, 90:393–397.

Franceschi, N. D., Arjonen, A., Elkhatib, N., Denessiouk, K., Wrobel, A. G., Wilson, T. A., Pouwels, J., Montagnac, G., Owen, D. J., and Ivaska, J. (2016). Selective integrin endocytosis is driven by interactions between the integrin alpha-chain and AP2. *Nature Publishing Group*, 23(2):172–179.

Franco, O. E., Shaw, A. K., Strand, D. W., and Hayward, S. W. (2010). Cancer associated fibroblasts in cancer pathogenesis. *Seminars in Cell and Developmental Biology*, 21:33–39.

Franco, S. J. and Huttenlocher, A. (2005). Regulating cell migration: calpains make the cut. *Journal of Cell Science*, 118:3829–3838.

Frantz, C., Stewart, K. M., and Weaver, V. M. (2010). The extracellular matrix at a glance. *Journal of Cell Science*, 123(24):4195–4200.

Fredriksson, L., Li, H., and Eriksson, U. (2004). The PDGF family: four gene products form five dimeric isoforms. *Cytokine and Growth Factor Reviews*, 15:197–204.

Fretto, L. J., Snape, A. J., Tomlinson, J. E., Seroogy, J. J., Wolf, D. L., LaRochelle, W. J., and Giese, N. A. (1993). Mechanism of platelet-derived growth factor (PDGF) AA, AB, and BB binding to alpha and beta PDGF receptor. *The Journal of Biological Chemistry*, 268(5):3625–3631.

Fritz, R. D. and Pertz, O. (2016). The dynamics of spatio-temporal Rho GTPase signaling: formation of signaling patterns. *F1000Research*, 5:1–12.

Fukushi, J.-i., Makagiansar, I. T., and Stallcup, W. B. (2004). NG2 proteoglycan promotes endothelial cell motility and angiogenesis via engagement of galectin-3 and alpha3beta1 integrin. *Molecular Biology of the Cell*, 15:3580–3590.

Gaggioli, C., Hooper, S., Hidalgo-Carcedo, C., Grosse, R., Marshall, J. F., Harrington, K., and Sahai, E. (2007). Fibroblast-led collective invasion of carcinoma cells with differing roles for RhoGTPases in leading and following cells. *Nature Cell Biology*, 9(12):1392–1400.

Gateva, G., Tojkander, S., Koho, S., Carpen, O., and Lappalainen, P. (2014). Palladin promotes assembly of non-contractile dorsal stress fibers through VASP recruitment. *Journal of cell science*, 127:1887–1898.

Gauthier, N. C., Masters, T. A., and Sheetz, M. P. (2012). Mechanical feedback between membrane tension and dynamics. *Trends in Cell Biology*, 22(10):527–535.

Gerhardt, H., Golding, M., Fruttiger, M., Ruhrberg, C., Lundkvist, A., Abramsson, A., Jeltsch, M., Mitchell, C., Alitalo, K., Shima, D., and Betsholtz, C. (2003). VEGF guides angiogenic sprouting utilizing endothelial tip cell filopodia. *Journal of Cell Biology*, 161(6):1163–1177.

Goetsch, K. P., Snyman, C., Myburgh, K. H., and Niesler, C. U. (2014). ROCK-2 is associated with focal adhesion maturation during myoblast migration. *Journal of Cellular Biochemistry*, 115:1299–1307.

Goh, L. K. and Sorkin, A. (2013). Endocytosis of receptor tyrosine kinases. *Cold Spring Harbor Perspectives in Biology*, 5:1–17.

Gohla, A. and Bokoch, G. M. (2002). 14-3-3 Regulates actin dynamics by stabilizing phosphorylated cofilin. *Current Biology*, 12(19):1704–1710.

Goicoechea, S. M., Awadia, S., and Garcia-Mata, R. (2014). I'm coming to GEF you: Regulation of RhoGEFs during cell migration. *Cell Adhesion and Migration*, 8(18):535–549.

Gorbatyuk, V. Y., Nosworthy, N. J., Robson, S. A., Bains, N. P. S., Maciejewski, M. W., dos Remedios, C. G., and King, G. F. (2006). Mapping the Phosphoinositide-Binding Site on Chick Cofilin Explains How PIP2 Regulates the Cofilin-Actin Interaction. *Molecular Cell*, 24:511–522.

Goretzki, L., Burg, M. a., Grako, K. a., and Stallcup, W. B. (1999). High-affinity binding of basic fibroblast growth factor and platelet-derived growth factor-AA to the core protein of the NG2 proteoglycan. *The Journal of Biological Chemistry*, 274(24):16831–16837.

Graham, F., Smiley, J., Russel, W. C., and Nairin, R. (1977). Characteristics of a human cell line transformed by DNA from human adenovirus type 5. *Journal of General Virology*, 36:59–72.

Graham, F. L. and van der Eb, A. J. (1973). A new technique for the assay of infectivity of human adenovirus 5 DNA. *Virology*, 52:456–467.

Grako, K. A., Ochiya, T., Barritt, D., Nishiyama, A., and Stallcup, W. B. (1999). PDGF alpha-receptor is unresponsive to PDGF-AA in aortic smooth muscle cells from the NG2 knockout mouse. *Journal of Cell Science*, 112:905–915.

Grako, K. A. and Stallcup, W. B. (1995). Participation of NG2 proteoglycan in rat aortic smooth muscle cell responses to platelet-derived growth factor. *Experimental Cell Research*, 221:231–240.

Grigliatti, T., Hall, L., Rosenbluth, R., and Suzuki, D. (1973). Temperature-sensitive mutations in Drosophila melanogaster. XIV. A selection of immobile adults. *Molecular Genetics and Genomics*, 120(2):107–114.

Gu, Z., Noss, E. H., Hsu, V. W., and Brenner, M. B. (2011). Integrins traffic rapidly via circular dorsal ruffles and macropinocytosis during stimulated cell migration. *Journal of Cell Biology*, 193(1):61–70.

Gundem, G., Van Loo, P., Kremeyer, B., Alexandrov, L. B., Tubio, J. M. C., Papaemmanuil, E., Brewer, D. S., Kallio, H. M. L., Högnäs, G., Annala, M., Kivinummi, K., Goody, V., Latimer, C., O'Meara, S., Dawson, K. J., Isaacs, W., Emmert-Buck, M. R., Nykter, M., Foster, C., Kote-Jarai, Z., Easton, D., Whitaker, H. C., Group, I. U., Neal, D. E., Cooper, C. S., Eeles, R. a., Visakorpi, T., Campbell, P. J., McDermott, U., Wedge, D. C., and Bova, G. S. (2015). The evolutionary history of lethal metastatic prostate cancer. *Nature*, 520:353–357.

Guo, P., Hu, B., Gu, W., Xu, L., Wang, D., Huang, H.-J. S., Cavenee, W. K., and Cheng, S.-Y. (2003). Platelet-derived growth factor-B enhances glioma angiogenesis by stimulating vascular endothelial growth factor expression in tumor endothelia and by promoting pericyte recruitment. *The American Journal of Pathology*, 162(4):1083–1093.

Gurniak, C. B., Perlas, E., and Witke, W. (2005). The actin depolymerizing factor n-cofilin is essential for neural tube morphogenesis and neural crest cell migration. *Developmental Biology*, 278:231–241.

Gustavsson, N. and Han, W. (2009). Calcium-sensing beyond neurotransmitters: functions of synaptotagmins in neuroendocrine and endocrine secretion. *Bioscience Reports*, 29:245–259.

Hamadi, A., Bouali, M., Dontenwill, M., Stoeckel, H., Takeda, K., and Rondé, P. (2005). Regulation of focal adhesion dynamics and disassembly by phosphorylation of FAK at tyrosine 397. *Journal of Cell Science*, 118:4415–4425.

Hammacher, A., Mellström, K., Heldin, C. H., and Westermark, B. (1989). Isoform-specific induction of actin reorganization by platelet-derived growth factor suggests that the functionally active receptor is a dimer. *The EMBO Journal*, 8(9):2489–2495.

Hanahan, D. and Weinberg, R. A. (2011). Hallmarks of cancer: The next generation. *Cell*, 144:646–674.

Heldin, C. H., Oestman, A., and Rönnstrand, L. (1998). Signal transduction via platelet-derived growth factor receptors. *Biochimica et Biophysica Acta*, 1378:F79–F113.

Hellberg, C., Schmees, C., Karlsson, S., Ahgren, A., and Heldin, C. H. (2009). Activation of protein kinase C alpha is necessary for sorting the PDGF beta receptor to Rab4a-dependent recycling. *Molecular Biology of the Cell*, 20:2856–2863.

Hellström, M., Gerhardt, H., Kalén, M., Li, X., Eriksson, U., Wolburg, H., and Betsholtz, C. (2001). Lack of pericytes leads to endothelial hyperplasia and abnormal vascular morphogenesis. *Journal of Cell Biology*, 152(3):543–553.

Hellström, M., Phng, L. K., Hofmann, J. J., E, W., Coultas, L., P, L., Alva, J., Nilsson, A. K., Karlsson, L., Gaiano, N., Yoon, K., Rossant, J., Iruela-Arispe, M. L., Kalen, M., Gerhardt, H., and Betsholtz, C. (2007). VEGF and Notch signaling: the yin and yang of angiogenic sprouting. *Nature*, 445:133–136.

Herbert, S. P. and Stainier, D. Y. R. (2011). Molecular control of endothelial cell behaviour during blood vessel morphogenesis. *Nature Reviews Molecular Cell Biology*, 12:551–564.

Hodge, R. G. and Ridley, A. J. (2016). Regulating Rho GTPases and their regulators. *Nature Reviews Molecular Cell Biology*, pages 1–15.

Hoon, J.-L., Wong, W.-K., and Koh, C.-G. (2012). Functions and regulation of circular dorsal ruffles. *Molecular and Cellular Biology*, 32(21):4246–4257.

Horton, E. R., Byron, A., Askari, J. A., Ng, D. H. J., Millon-Frémillon, A., Robertson, J., Koper, E. J., Paul, N. R., Warwood, S., Knight, D., Humphries, J. D., and Humphries, M. J. (2015). Definition of a consensus integrin adhesome and its dynamics during adhesion complex assembly and disassembly. *Nature Cell Biology*, 17(12):1577–1587.

Hosaka, K., Yang, Y., Seki, T., Fischer, C., Dubey, O., Fredlund, E., Hartman, J., Religa, P., Morikawa, H., Ishii, Y., Sasahara, M., Larsson, O., Cossu, G., Cao, R., Lim, S., and Cao, Y. (2016). Pericyte - fibroblast transition promotes tumor growth and metastasis. *PNAS*, pages E5618–E5627.

Hotulainen, P. and Lappalainen, P. (2006). Stress fibers are generated by two distinct actin assembly mechanisms in motile cells. *Journal of Cell Biology*, 173(3):383–394.

Huang, F.-J., You, W.-K., Bonaldo, P., Seyfried, T. N., Pasquale, E. B., and Stallcup, W. B. (2010). Pericyte deficiencies lead to aberrant tumor vascularizaton in the brain of the NG2 null mouse. *Developmental Biology*, 344:1035–1046.

Huang, M., Satchell, L., DuHadaway, J. B., Prendergast, G. C., and Laury-Kleintop, L. D. (2011). RhoB links PDGF signaling to cell migration by coordinating activation and localization of Cdc42 and Rac. *Journal of Cellular Biochemistry*, 112:1572–1584.

Huber, F., Boire, A., López, M. P., and Koenderink, G. H. (2015). Cytoskeletal crosstalk: When three different personalities team up. *Current Opinion in Cell Biology*, 32:39–47.

Hung, C., Linn, G., Chow, Y.-h., Kobayashi, A., Mittelsteadt, K., Altemeier, W. A., Gharib, S. A., Schnapp, L. M., and Duffield, J. S. (2013). Role of lung pericytes and resident fibroblasts in the pathogenesis of pulmonary fibrosis. *American Journal of Respiratory and Critical Care Medicine*, 188(7):820–830.

Iida, J., Meijne, A. M. L., Oegema, T. R., Yednock, T. A., Kovach, N. L., Furcht, L. T., and McCarthy, J. B. (1998). A role of chondroitin sulfate glycosaminoglycan binding site in

alpha4beta1 integrin-mediated melanoma cell adhesion. *Journal of Biological Chemistry*, 273:5955–5962.

Iida, J., Meijne, A. M. L., Spiro, R. C., Roos, E., Furcht, L. T., and McCarthy, J. B. (1995). Spreading and focal contact formation of human melanoma cells in response to the stimulation of both melanoma-associated proteoglycan (NG2) and a4b1 integrin. *Cancer Research*, 55:2177–2185.

Ikeda, S., Cunningham, L. A., Boggess, D., Hobson, C. D., Sundberg, J. P., Naggert, J. K., Smith, R. S., and Nishina, P. M. (2003). Aberrant actin cytoskeleton leads to accelerated proliferation of corneal epithelial cells in mice deficient for destrin (actin depolymerizing factor). *Human Molecular Genetics*, 12(9):1029–1036.

Ishiuchi, T., Misaki, K., Yonemura, S., Takeichi, M., and Tanoue, T. (2009). Mammalian Fat and Dachsous cadherins regulate apical membrane organization in the embryonic cerebral cortex. *Journal of Cell Biology*, 185(6):959–967.

Itoh, T. and Hasegawa, J. (2012). Mechanistic insights into the regulation of circular dorsal ruffle formation. *Journal of Biochemistry*, 153(1):21–29.

Jones, L. L., Yamaguchi, Y., Stallcup, W. B., and Tuszynski, M. H. (2002). NG2 is a major chondroitin sulfate proteoglycan produced after spinal cord injury and is expressed by macrophages and oligodendrocyte progenitors. *The Journal of Neuroscience*, 22(7):2792–2803.

Jung, N., Wienisch, M., Gu, M., Rand, J. B., Müller, S. L., Krause, G., Jorgensen, E. M., Klingauf, J., and Haucke, V. (2007). Molecular basis of synaptic vesicle cargo recognition by the endocytic sorting adaptor stonin 2. *Journal of Cell Biology*, 179(7):1497–1510.

Kaempf, N., Kochlamazashvili, G., Puchkov, D., Maritzen, T., Bajjalieh, S. M., Kononenko, N. L., and Haucke, V. (2015). Overlapping functions of stonin 2 and SV2 in sorting of the calcium sensor synaptotagmin 1 to synaptic vesicles. *PNAS*, 112(23):7297–7302.

Kalluri, R. (2016). The biology and function of fibroblasts in cancer. *Nature Reviews Cancer*, 16:582–598.

Kanellos, G. and Frame, M. C. (2016). Cellular functions of the ADF/Cofilin family at a glance. *Journal of Cell Science*, 129:3211–3218.

Kanellos, G., Zhou, J., Patel, H., Ridgway, R. A., Huels, D., Gurniak, C. B., Sandilands, E., Carragher, N. O., Sansom, O. J., Witke, W., Brunton, V. G., and Frame, M. C. (2015). ADF and Cofilin1 control actin stress fibers, nuclear integrity, and cell survival. *Cell Reports*, 13:1949–1964.

Karlsson, S., Kowanetz, K., Sandin, Å., Persson, C., Oestman, A., Heldin, C. H., and Hellberg, C. (2006). Loss of T cell protein tyrosine phosphatase induces recycling of the

platelet-derived grwoth factor (PDGF) beta receptor but not the PDGF alpha receptor. *Molecular Biology of the Cell*, 17:4846–4855.

Karram, K., Goebbels, S., Schwab, M., Jennissen, K., Seifert, G., Steinhäuser, C., Nave, K.-A., and Trotter, J. (2008). NG2-expressing cells in the nervous system revealed by the NG2-EYFP-knockin mouse molecular cloning of targeting vector. *Genesis*, 46:743–757.

Kelly, B. T., Graham, S. C., Liska, N., Dannhauser, P. N., Höning, S., Ungewickell, E. J., and Owen, D. J. (2014). AP2 controls clathrin polymerization with a membrane-activated switch. *Science Research Reports*, 345(6195):459–463.

Kirchhausen, T., Owen, D., and Harrison, S. C. (2014). Molecular structure, function and dynamics of clathrin-mediated membrane traffic. *Cold Spring Harbor Perspectives in Biology*, 6:1–26.

Komitova, M., Zhu, X., Serwanski, D. R., and Nishiyama, A. (2009). NG2 cells are distinct from neurogenic cells in the postnatal mouse subventricular zone. *The Journal of Comparative Neurology*, 512:702–716.

Kononenko, N. L., Diril, M. K., Puchkov, D., Kintscher, M., Koo, S. J., Pfuhl, G., Winter, Y., Wienisch, M., Klingauf, J., Breustedt, J., Schmitz, D., Maritzen, T., and Haucke, V. (2013). Compromised fidelity of endocytic synaptic vesicle protein sorting in the absence of stonin 2. *PNAS*, pages E526–E535.

Kovac, B., Teo, J., Mäkelä, T., and Vallenius, T. (2013). Assembly of non-contractile dorsal stress fibers requires α-actinin-1 and Rac1 in migrating and spreading cells. *Journal of Cell Science*, 126:263–273.

Krock, B. L., Skuli, N., and Simon, M. C. (2011). Hypoxia-Induced Angiogenesis: Good and Evil. *Genes & Cancer*, 2(12):1117–1133.

Krueger, E., Orth, J. D., Cao, H., and McNiven, M. A. (2003). A dynamin-cortactin-Arp2/3 complex mediates reorganisation in growth factor-stimulated cells. *Molecular Biology of the Cell*, 14:1058–1096.

Kucharova, K., Chang, Y., Boor, A., Yong, V. W., and Stallcup, W. B. (2011). Reduced inflammation accompanies diminished myelin damage and repair in the NG2 null mouse spinal cord. *Journal of Neuroinflammation*, 8(158):1–13.

Kucharova, K. and Stallcup, W. B. (2010). The NG2 proteoglycan promotes oligodendrocytes progenitor proliferation and developmental myelination. *Neuroscience*, 166:185–194.

Kumar, A., Coleman, I., Morrissey, C., Zhang, X., True, L. D., Gulati, R., Etzioni, R., Bolouri, H., Montgomery, B., White, T., Lucas, J. M., Brown, L. G., Dumpit, R. F., DeSarkar, N., Higano, C., Yu, E. Y., Coleman, R., Schultz, N., Fang, M., Lange, P. H., Shendure, J., Vessella, R. L., and Nelson, P. S. (2016). Substantial interindividual and

limited intraindividual genomic diversity among tumors from men with metastatic prostate cancer. *Nature Medicine*, 22(4):369–378.

Kuo, J.-C., Han, X., Hsiao, C.-T., Yates III, J. R., and Waterman, C. M. (2011). Analysis of the myosin-II-responsive focal adhesion proteome reveals a role for β-Pix in negative regulation of focal adhesion maturation. *Nature Cell Biology*, 13(4):383–393.

Laemmli, U. K. (1970). Cleavage of structural protein during the assembly of the head of bacteriophage T4. *Nature*, 228:680–685.

Leger, O., Johnson-Leger, C., Jackson, E., Coles, B., and Dean, C. (1994). The chondroitin sulfate proteoglycan NG2 is a tumour-specific antigen on the chemically induced rat chondrosarcoma HSN. *International Journal of Cancer*, 58:700–705.

Lemmon, M. A. and Schlessinger, J. (2010). Cell signaling by receptor tyrosine kinases. *Cell*, 141:1117–1134.

Letunic, I., Copley, R. R., Pils, B., Pinkert, S., Schultz, J., and Bork, P. (2006). SMART 5: domains in the context of genomes and networks. *Nucleic Acids Research*, 34:D257–D260.

Levine, J. M., Reynolds, R., and Fawcett, J. W. (2001). The oligodendrocyte precursor cell in health and disease. *Trends in Neurosciences*, 24(1):39–47.

Lindblom, P., Gerhardt, H., Liebner, S., Abramsson, A., Enge, M., Hellström, M., Bäckström, G., Fredriksson, S., Landegren, U., Nyström, H. C., Bergström, G., Dejana, E., Östman, A., Lindahl, P., and Betsholtz, C. (2003). Endothelial PDGF-B retention is required for proper investment of pericytes in the microvessel wall. *Genes and Development*, 17:1835–1840.

Lobov, I. B., Renard, R. a., Papadopoulos, N., Gale, N. W., Thurston, G., Yancopoulos, G. D., and Wiegand, S. J. (2007). Delta-like ligand 4 (Dll4) is induced by VEGF as a negative regulator of angiogenic sprouting. *PNAS*, 104(9):3219–3224.

Majumdar, M., Vuori, K., and Stallcup, W. B. (2003). Engagement of the NG2 proteoglycan triggers cell spreading via rac and p130cas. *Cellular Signalling*, 15:79–84.

Makagiansar, I. T., Williams, S., Dahlin-Huppe, K., Fukushi, J. I., Mustelin, T., and Stallcup, W. B. (2004). Phosphorylation of NG2 proteoglycan by protein kinase C-alpha regulates polarized membrane distribution and cell motility. *Journal of Biological Chemistry*, 279(53):55262–55270.

Makagiansar, I. T., Williams, S., Mustelin, T., and Stallcup, W. B. (2007). Differential phosphorylation of NG2 proteoglycan by ERK and PKCalpha helps balance cell proliferation and migration. *The Journal of Cell Biology*, 178(1):155–165.

Mao, Y., Mulvaney, J., Zakaria, S., Yu, T., Morgan, K. M., Allen, S., Basson, M. A., Francis-West, P., and Irvine, K. D. (2011). Characterization of a Dchs1 mutant mouse reveals requirements for Dchs1-Fat4 signaling during mammalian development. *Development*, 138:947–957.

Margadant, C., Monsuur, H. N., Norman, J. C., and Sonnenberg, A. (2011). Mechanisms of integrin activation and trafficking. *Current Opinion in Cell Biology*, 23:607–614.

Maritzen, T., Podufall, J., and Haucke, V. (2010). Stonins - specialized adaptors for synaptic vesicle recycling and beyond? *Traffic*, 11:8–15.

Maritzen, T., Schachtner, H., and Legler, D. F. (2015). On the move: endocytic trafficking in cell migration. *Cellular and Molecular Life Sciences*, pages 2119–2134.

Marshall, T. W., Aloor, H. L., and Bear, J. E. (2009). Coronin 2A regulates a subset of focal-adhesion-turnover events through the Cofilin pathway. *Journal of Cell Science*, 122:3061–3069.

Martina, J. a., Bonangelino, C. J., Aguilar, R. C., and Bonifacino, J. S. (2001). Stonin 2: an adaptor-like protein that interacts with components of the endocytic machinery. *The Journal of Cell Biology*, 153(5):1111–1120.

Mazzieri, R., Pucci, F., Moi, D., Zonari, E., Ranghetti, A., Berti, A., Politi, L. S., Gentner, B., Brown, J. L., Naldini, L., and De Palma, M. (2011). Targeting the ANG2/TIE2 Axis Inhibits Tumor Growth and Metastasis by Impairing Angiogenesis and Disabling Rebounds of Proangiogenic Myeloid Cells. *Cancer Cell*, 19:512–526.

McMahon, H. T. and Boucrot, E. (2011). Molecular mechanism and physiological functions of clathrin-mediated endocytosis. *Nature Reviews Molecular Cell Biology*, 12:517–533.

Midwood, K. S. and Salter, D. (1998). Expression of NG2/ human melanoma protepglycan in human adult articular chrondrocytes. *Osteoarthritis and Cartilage*, 6:297–305.

Milo, R. and Phillips, R. (2016). *Cell biology by the numbers.*

Mishra, S. K., Hawryluk, M. J., Brett, T. J., Keyel, P. A., Dupin, A. L., Jha, A., Heuser, J. E., Fremont, D. H., and Traub, L. M. (2004). Dual engagement regulation of protein interactions with the AP-2 adaptor alpha appendage. *Journal of Biological Chemistry*, 279(44):46191–46203.

Mitchison, T. and Kirschner, M. (1988). Cytoskeletal dynamics and nerve growth. *Neuron*, 1:761–772.

Mitra, S. K., Hanson, D. A., and Schlapfer, D. D. (2005). Focal adhesion kinase: in command and control of cell motility. *Nature Reviews Molecular Cell Biology*, 6:56–68.

Morgan, M. R., Hamidi, H., Bass, M. D., Warwood, S., Ballestrem, C., and Humphries, M. J. (2013). Syndecan-4 phosphorylation Is a control point for integrin recycling. *Developmental Cell*, 24:472–485.

Moriyama, K., Nishida, E., Yonezawa, N., Sakai, H., Matsumotos, S., Iida, K., and Yahara, I. (1990). Destrin, a Mammalian actin-depolyerizing protein is closely related to Cofilin. *Journal of Biological Chemistry*, 265(10):5768–5773.

Mosesson, Y., Mills, G. B., and Yarden, Y. (2008). Derailed endocytosis: an emerging feature of cancer. *Nature reviews. Cancer*, 8:835–850.

Mueller, M. M. and Fusenig, N. E. (2004). Friends or foes - bipolar effects of the tumour stroma in cancer. *Nature Reviews Cancer*, 4:839–849.

Murfee, W. L., Skalak, T. C., and Peirce, S. M. (2005). Differential arterial/ venous expression of NG2 proteoglycan in perivascular cells along microvessels: identifying a venule-specific phenotype. *Microcirculation*, 12:151–160.

Nagano, M., Hoshino, D., Koshikawa, N., Akizawa, T., and Seiki, M. (2011). Turnover of focal adhesions and cancer cell migration. *International Journal of Cell Biology*, 2012:1–10.

Niehaus, A., Stegmüller, J., Diers-Fenger, M., and Trotter, J. (1999). Cell-surface glycoprotein of oligodendrocyte progenitors involved in migration. *The Journal of Neuroscience*, 19(12):4948–4961.

Nishimura, T. and Kaibuchi, K. (2007). Numb controls integrin endocytosis for directional cell migration with aPKC and PAR-3. *Developmental Cell*, 13:15–28.

Nishishita, T. and Lin, P. C. (2004). Angiopoietin 1, PDGF-B, and TGF-beta gene regulation in endothelial cell and smooth muscle cell interaction. *Journal of Cellular Biochemistry*, 91:584–593.

Nishiyama, A., Dahlin, K. J., Prince, J. T., Johnstone, S. R., and Stallcup, W. B. (1991). The primary strcuture of NG2, a novel membrane-spanning proteoglycan. *The Journal of Cell Biology*, 114(2):359–371.

Nishiyama, A., Komitova, M., Suzuki, R., and Zhu, X. (2009). Polydendrocytes (NG2 cells): multifunctional cells with lineage plasticity. *Nature Reviews Neuroscience*, 10:9–22.

Nissen, L. J., Cao, R., Hedlund, E. M., Wang, Z., Zhao, X., Wetterskog, D., Funa, K., Bråkenhielm, E., and Cao, Y. (2007). Angiogenic factors FGF2 and PDGF-BB synergistically promote murine tumor neovascularization and metastasis. *Journal of Clinical Investigation*, 117(10):2766–2777.

Noskovicova, N., Petrek, M., Eickelberg, O., and Heinzelmann, K. (2014). Platelet-derived growth factor signaling in the lung: From lung development and disease to clinical studies. *American Journal of Respiratory Cell and Molecular Biology*, 52(3):263–284.

Noy, R. and Pollard, J. W. (2014). Review tumor-associated macrophages: from mechanisms to therapy. *Immunity*, 41:49–61.

Oakes, P. W., Beckham, Y., Stricker, J., and Gardel, M. L. (2012). Tension is required but not sufficient for focal adhesion maturation without a stress fiber template. *Journal of Cell Biology*, 196(3):363–374.

Orth, J. D., Krueger, E. W., Weller, S. G., and McNiven, M. a. (2006). A novel endocytic mechanism of epidermal growth factor receptor sequestration and internalization. *Cancer Research*, 66(7):3603–10.

Ozerdem, U., Monosov, E., and Stallcup, W. B. (2002). NG2 proteoglycan expression by pericytes in pathological microvasculature. *Microvascular research*, 63(1):129–34.

Ozerdem, U. and Stallcup, W. B. (2004). Pathological angiogenesis is reduced by targeting pericytes via the NG2 proteoglycan. *Angiogenesis*, 7(3):269–276.

Paez-Cortez, J., Krishnan, R., Arno, A., Aven, L., Ram-Mohan, S., Patel, K. R., Lu, J., King, O. D., Ai, X., and Fine, A. (2013). A new approach for the study of lung smooth muscle phenotypes and its application in a murine model of allergic airway inflammation. *PLoS one*, 8(9).

Pang, Z. P. and Südhof, T. C. (2010). Cell biology of Ca2+ -triggered exocytosis. *Current Opinion in Cell Biology*, 22:496–505.

Pankova, D., Jobe, N., Kratochvilova, M., Buccione, R., Brabek, J., and Rösel, D. (2012). NG2-mediated Rho activation promotes amoeboid invasiveness of cancer cells. *European Journal of Cell Biology*, 91:969–977.

Park, T. I.-h., Monzo, H., Mee, E. W., Bergin, P. S., Teoh, H. H., Montgomery, J. M., Faull, R. L. M., Curtis, M. A., and Dragunow, M. (2012). Adult human brain neural progenitor cells (NPCs) and fibroblast-like cells have similar properties in vitro but only NPCs differentiate into neurons. *PLoS one*, 7(6).

Pasula, S., Cai, X., Dong, Y., Messa, M., McManus, J., Chang, B., Liu, X., Zhu, H., Mansat, R. S., Yoon, S. J., Hahn, S., Keeling, J., Saunders, D., Ko, G., Knight, J., Newton, G., Luscinskas, F., Sun, X., Towner, R., Lupu, F., Xia, L., Cremona, O., De Camilli, P., Min, W., and Chen, H. (2012). Endothelial epsin deficiency decreases tumor growth by enhancing VEGF signaling. *Journal of Clinical Investigation*, 122(12):4424–4438.

Pear, W. S., Nolan, G. P., Scott, M. L., and Baltimore, D. (1993). Production of high-titer helper-free retroviruses by transient transfection. *PNAS*, 90:8392–8396.

Persson, C., Sävenhed, C., Bourdeau, A., Tremblay, M. L., Markova, B., Böhmer, F. D., Haj, F. G., Neel, B. G., Elson, A., Heldin, C.-H., Rönnstrand, L., Oestman, A., and Hellberg, C. (2004). Site-selective regulation of platelet-derived growth factor beta receptor tyrosine

phosphorylation by T-cell protein tyrosine phosphatase. *Molecular and Cellular Biology*, 24(5):2190–2201.

Petrie, R. J., Doyle, A. D., and Yamada, K. M. (2009). Random versus directionally persistent cell migration. *Nature Reviews Molecular cell biology*, 10:538–549.

Phillips, A. M., Smith, M., Ramaswami, M., and Kelly, L. E. (2000). The products of the Drosophila stoned locus interact with synaptic vesicles via synaptotagmin. *The Journal of Neuroscience*, 20(22):8254–8261.

Polacheck, W. J., Zervantonakis, I. K., and Kamm, R. D. (2012). Tumor cell migration in complex microenvironments. *Cellular and Molecular Life Sciences*, pages 1335–1356.

Pollard, T. D. and Cooper, J. A. (2009). Actin, a central player in cell shape and movement. *Science*, 326:1208–1212.

Quail, D. F. and Joyce, J. A. (2013). Microenvironmental regulation of tumor progression and metastasis. *Nature Medicine*, 19(11):1423–1437.

Reig, G., Pulgar, E., and Concha, M. L. (2014). Cell migration: from tissue culture to embryos. *The Company of Biologists Development*, 141:1999–2013.

Ritter, B., Denisov, A. Y., Philie, J., Deprez, C., Tung, E. C., Gehring, K., and McPherson, P. S. (2004). Two WXXF-based motifs in NECAPs define the specificity of accessory protein binding to AP1 and AP2. *The EMBO Journal*, 23:3701–3710.

Robert-Koch-Institut (2016). Epidemiologie von Krebserkrankungen. Technical report, Robert Koch Institut.

Roberts, M., Barry, S., Woods, A., van der Sluijs, P., and Norman, J. (2001). PDGF- regulated Rab4-dependent recycling of alphaV beta3 integrin from early endosomes is necessary for cell adhesion and spreading. *Current Biology*, 11(18):1392–1402.

Robertson, J., Jacquemet, G., Byron, A., Jones, M. C., Warwood, S., Selley, J. N., Knight, D., Humphries, J. D., and Humphries, M. J. (2015). Defining the phospho-adhesome through the phosphoproteomic analysis of integrin signalling. *Nature communications*, 6:1–13.

Rock, J. R., Barkauskas, C. E., Cronce, M. J., Xue, Y., Harris, J. R., Liang, J., Noble, P. W., and Hogan, B. L. M. (2011). Multiple stromal populations contribute to pulmonary fi brosis without evidence for epithelial to mesenchymal transition. *PNAS*, 108(52):E1475–E1483.

Sanger, F., Nicklen, S., and Coulson, A. R. (1977). DNA sequencing with chain-terminating inhibtors. *PNAS*, 74(12):5463–5467.

Scales, T. M. E. and Parsons, M. (2011). Spatial and temporal regulation of integrin signalling during cell migration. *Current Opinion in Cell Biology*, 23:562–568.

Schiefermeier, N., Scheffler, J. M., de Araujo, M. E. G., Stasyk, T., Yordanov, T., Ebner, H. L., Offterdinger, M., Munck, S., Hess, M. W., Wickström, S. A., Lange, A., Wunderlich, W., Fässler, R., Teis, D., and Huber, L. A. (2014). The late endosomal p14-MP1 (LAMTOR2/3) complex regulates focal adhesion dynamics during cell migration. *Journal of Cell Biology*, 205(4):525–540.

Schiller, H. B., Friedel, C. C., Boulegue, C., and Fässler, R. (2011). Quantitative proteomics of the integrin adhesome show a myosin II-dependent recruitment of LIM domain proteins. *EMBO reports*, 12(3):259–266.

Schiller, H. B., Hermann, M.-R., Polleux, J., Vignaud, T., Zanivan, S., Friedel, C. C., Sun, Z., Raducanu, A., Gottschalk, K.-E., Théry, M., Mann, M., and Fässler, R. (2013). Beta1- and alphaV-class integrins cooperate to regulate myosin II during rigidity sensing of fibronectin-based microenvironments. *Nature Cell Biology*, 15(6):625–636.

Schink, K. O., Tan, K.-W., and Stenmark, H. (2016). Phosphoinositides in control of membrane dynamics. *Annual Review of Cell and Developmental Biology*, 32(1):143–171.

Seifert, R. A., Hart, C. E., Phillips, P. E., Forstrom, J. W., Ross, R., Murray, M. J., and Bowen-Pope, D. F. (1989). Two different subunits associate to create isoform-specific platelet-derived growth factor receptors. *Journal of Biological Chemistry*, 264(15):8771–8778.

Seong, J., Ouyang, M., Kim, T., Sun, J., Wen, P. C., Lu, S., Zhuo, Y., Llewellyn, N. M., Schlaepfer, D. D., Guan, J. L., Chien, S., and Wang, Y. (2011). Detection of focal adhesion kinase activation at membrane microdomains by fluorescence resonance energy transfer. *Nature Communications*, 2(406):1–9.

Seppa, H., Grotendorst, G., Seppa, S., Schiffmann, E., and Martin, G. R. (1982). Platelet-derived growth factor is chemotactic for fibroblasts. *The Journal of Cell Biology*, 92:584–588.

Sero, J. E., Thodeti, C. K., Mammoto, A., Bakal, C., Thomas, S., and Ingber, D. E. (2011). Paxillin mediates sensing of physical cues and regulates directional cell motility by controlling lamellipodia positioning. *PLoS ONE*, 6(12):1–17.

Shafaq-Zadah, M., Gomes-Santos, C. S., Bardin, S., Maiuri, P., Maurin, M., Iranzo, J., Gautreau, A., Lamaze, C., Caswell, P., Goud, B., and Johannes, L. (2016). Persistent cell migration and adhesion rely on retrograde transport of β1 integrin. *Nature Cell Biology*, 18(1):54–64.

Shattil, S. J., Kim, C., and Ginsberg, M. H. (2010). The final steps of integrin activation: the end game. *Nature Reviews Molecular Cell Biology*, 11:288–300.

Shishkin, S., Eremina, L., Pashintseva, N., Kovalev, L., and Kovaleva, M. (2016). Cofilin-1 and other ADF/ Cofilin superfamily members in human malignant cells. *International Journal of Molecular Sciences*, 18(10):1–27.

Shoshan, Y., Nishiyama, A., Chang, A., Mörk, S., Barnett, G. H., Cowell, J. K., Trapp, B. D., and Staugaitis, S. M. (1999). Expression of oligodendrocyte progenitor cell antigens by gliomas: implications for the histogenesis of brain tumors. *PNAS*, 96:10361–10366.

Sieg, D. J., Hauck, C. R., Ilic, D., Klingbeil, C. K., Schaefer, E., Damsky, C. H., and Schlaepfer, D. D. (2000). FAK integrates growth-factor and integrin signals to promote cell migration. *Nature Cell Biology*, 2:249–256.

Sims, D. E. (1986). The Pericyte - A Review. *Tissue and Cell*, 18(2):153–174.

Skau, C. T., Plotnikov, S. V., Doyle, A. D., and Waterman, C. M. (2015). Inverted formin 2 in focal adhesions promotes dorsal stress fiber and fibrillar adhesion formation to drive extracellular matrix assembly. *PNAS*, pages E2447–E2456.

Smith, F. O., Rauch, C., Williams, D. E., March, C. J., Arthur, D., Hilden, J., Lampkin, B. C., Buckley, J. D., Buckley, C. V., Woods, W. G., Dinndorf, P. A., Sorensen, P., Kersey, J., Hammond, D., and Bernstein, I. D. (1996). The human homologue of rat NG2, a chondroitin sulfate proteoglycan, is not expressed on the cell surface of normal hematopoietic cells but is expressed by acute myeloid leukemia blasts from poor-prognosis patients with abnormalities of chromosome band 11q. *Blood*, 87(3):1123–1133.

Stallcup, W. B. and Beasley, L. (1987). Bipotential glial precursor cells of the optic nerve express the NG2 proteoglycan. *The Journal of Neuroscience*, 7(9):2737–2744.

Stallcup, W. B. and Huang, F.-j. (2008). Special focus: glioma therapy a role for the NG2 proteoglycan in glioma progression. *Cell Adhesion & Migration*, 2(3):192–201.

Stallcup, W. B., You, W.-k., Kucharova, K., Cejudo-Martin, P., and Yotsumoto, F. (2016). NG2 proteoglycan-dependent contributions of pericytes and macrophages to brain tumor vascularization and progression. *Microcirculation*, 23:122–133.

Stegmüller, J., Werner, H., Nave, K. A., and Trotter, J. (2003). The proteoglycan NG2 is complexed with alpha-amino-3-hydroxy-5-methyl-4-isoxazolepropionic acid (AMPA) receptors by the PDZ glutamate receptor interaction protein (GRIP) in glial progenitor cells. *Journal of Biological Chemistry*, 278(6):3590–3598.

Stehbens, S., Paszek, M., Pemble, H., Ettinger, A., Gierke, S., and Wittman, T. (2014). CLASPs link focal adhesion-associated microtubule capture to localized exocytosis and adhesion site turnover. *Nature Cell Biology*, 16(6):561–573.

Stehbens, S. and Wittmann, T. (2012). Targeting and transport: How microtubules control focal adhesion dynamics. *Journal of Cell Biology*, 198(4):481–489.

Stimson, D. T., Estes, P. S., Rao, S., Krishnan, K. S., Kelly, L. E., and Ramaswami, M. (2001). Drosophila stoned proteins regulate the rate and fidelity of synaptic vesicle internalization. *The Journal of Neuroscience*, 21(9):3034–3044.

Su, L. T., Agapito, M. A., Li, M., Simonson, W. T. N., Huttenlocher, A., Habas, R., Yue, L., and Runnels, L. W. (2006). TRPM7 regulates cell adhesion by controlling the calcium-dependent protease calpain. *Journal of Biological Chemistry*, 281(16):11260–11270.

Sugiarto, S., Persson, A. I., Munoz, E. G., Waldhuber, M., Lamagna, C., Andor, N., Hanecker, P., Ayers-Ringler, J., Phillips, J., Siu, J., Lim, D. A., Vandenberg, S., Stallcup, W., Berger, M. S., Bergers, G., Weiss, W. A., and Petritsch, C. (2011). Asymmetry-defective oligodendrocyte progenitors are glioma precursors. *Cancer Cell*, 20:328–340.

Sulzmaier, F. J., Jean, C., and Schlaepfer, D. D. (2014). FAK in cancer: mechanistic findings and clinical applications. *Nature Reviews Cancer*, 14:598–610.

Sun, Z., Lambacher, A., and Fässler, R. (2014). Nascent adhesions: from fluctuations to a hierarchical organization. *Current Biology*, 24(17):R801–R803.

Swaminathan, V., Fischer, R. S., and Waterman, C. M. (2016). The FAK-Arp2/3 interaction promotes leading edge advance and haptosensing by coupling nascent adhesions to lamellipodia actin. *Molecular Biology of the Cell*, 27:1085–1100.

Swaminathan, V. and Waterman, C. M. (2016). The molecular clutch model for mechanotransduction evolves. *Nature Cell Biology*, 18(5):459–461.

Tahtamouni, L. H., Shaw, A. E., Hasan, M. H., Yasin, S. R., and Bamburg, J. R. (2013). Non-overlapping activities of ADF and Cofilin-1 during the migration of metastatic breast tumor cells. *BMC Cell Biology*, 14(45):1–16.

Tao, W., Moore, R., Smith, E. R., and Xu, X.-X. (2016). Endocytosis and Physiology: Insights from Disabled-2 Deficient Mice. *Frontiers in Cell and Developmental Biology*, 4:1–11.

Teckchandani, A., Toida, N., Goodchild, J., Henderson, C., Watts, J., Wollscheid, B., and Cooper, J. A. (2009). Quantitative proteomics identifies a Dab2/integrin module regulating cell migration. *Journal of Cell Biology*, 186(1):99–111.

Tessneer, K. L., Cai, X., Pasula, S., Dong, Y., Liu, X., Chang, B., McManus, J., Hahn, S., Yu, L., and Chen, H. (2013). Epsin Family of Endocytic Adaptor Proteins as Oncogenic Regulators of Cancer Progression. *Journal of Cancer Research Updates*, 2:144–150.

Theisen, U., Straube, E., and Straube, A. (2012). Directional persistence of migrating cells requires Kif1C-mediated stabilization of trailing adhesions. *Developmental Cell*, 23:1153–1166.

Theocharis, A. D., Skandalis, S. S., Gialeli, C., and Karamanos, N. K. (2016). Extracellular matrix structure. *Advanced Drug Delivery Reviews*, 97:4–27.

Tian, X., Hansen, D., Schedl, T., and Skeath, J. B. (2004). Epsin potentiates Notch pathway activity in Drosophila and C. elegans. *Development*, 131:5807–5815.

Tillet, E., Gential, B., Garrone, R., and Stallcup, W. B. (2002). NG2 proteoglycan mediates alpha1 integrin-independent cell adhesion and spreading on collagen VI. *Journal of Cellular Biochemistry*, 86:726–736.

Tillet, E., Ruggiero, F., Nishiyama, A., and Stallcup, W. B. (1997). The membrane-spanning proteoglycan NG2 binds to collagens V and VI through the central nonglobular domain of its core protein. *Journal of Biological Chemistry*, 272(16):10769–10776.

Tojkander, S., Gateva, G., Husain, A., Krishnan, R., and Lappalainen, P. (2015). Generation of contractile actomyosin bundles depends on mechanosensitive actin filament assembly and disassembly. *eLife*, 4:1–28.

Traub, L. M. and Bonifacino, J. S. (2013). Cargo recognition in clathrin-mediated endocytosis. *Cold Spring Harbor Perspectives in Biology*, 5(11):1–23.

Trost, A., Lange, S., Schroedl, F., Bruckner, D., Motloch, K. A., Bogner, B., Kaser-Eichberger, A., Strohmaier, C., Runge, C., Aigner, L., Rivera, F. J., and Reitsamer, H. A. (2016). Brain and retinal pericytes: origin, function and role. *Frontiers in Cellular Neuroscience*, 10(20):1–13.

Tu, S., Wu, W. J., Wang, J., and Cerione, R. A. (2003). Epidermal growth factor-dependent regulation of Cdc42 is mediated by the Src tyrosine kinase. *The Journal of Biological Chemistry*, 278(49):49293–49300.

Vallenius, T. (2013). Actin stress fibre subtypes in mesenchymal-migrating cells. *Open Biology*, 3:1–10.

Vartiainen, M. K., Mustonen, T., Mattila, P. K., Ojala, P. J., Thesleff, I., Partanen, J., and Lappalainen, P. (2002). The three mouse actin-depolymerizing factor/Cofilins evolved to fulfill cell-type-specific requirements for actin dynamics. *Molecular biology of the Cell*, 13:183–194.

Vicente-Manzanares, M., Choi, C. K., and Horwitz, A. R. (2009). Integrins in cell migration - the actin connection. *Journal of Cell Science*, 122:199–206.

Walther, K., Diril, M. K., Jung, N., and Haucke, V. (2004). Functional dissection of the interactions of stonin 2 with the adaptor complex AP-2 and synaptotagmin. *PNAS*, 101(4):964–969.

Wang, J., Svendsen, A., Kmiecik, J., Immervoll, H., Skaftnesmo, K. O., Planagumà, J., Reed, R. K., Bjerkvig, R., Miletic, H., Enger, P. Ø., Rygh, C. B., and Chekenya, M. (2011). Targeting the NG2/CSPG4 proteoglycan retards tumour growth and angiogenesis in preclinical models of GBM and melanoma. *PloS one*, 6(7).

Wei, S. C. and Yang, J. (2016). Forcing through tumor metastasis: the interplay between tissue rigidity and epithelial-mesenchymal transition. *Trends in Cell Biology*, 26(2):111–120.

Wieffer, M., Maritzen, T., and Haucke, V. (2009). SnapShot: endocytic trafficking. *Cell*, 137:382–384.

Wiggan, O., Shaw, A. E., DeLuca, J. G., and Bamburg, J. R. (2012). ADF/Cofilin regulates actomyosin assembly through competitive inhibition of myosin II binding to F-Actin. *Developmental Cell*, 22:530–543.

Williams, C. K., Li, J. L., Murga, M., Harris, A. L., and Tosato, G. (2006). Up-regulation of the Notch ligand Delta-like 4 inhibits VEGF-induced endothelial cell function. *Blood*, 107(3):931–939.

Winkler, E. a., Bell, R. D., and Zlokovic, B. V. (2011). Central nervous system pericytes in health and disease. *Nature Neuroscience*, 14(11):1398–1405.

Xu, W., Baribault, H., and Adamson, E. D. (1998). Vinculin knockout results in heart and brain defects during embryonic development. *Development*, 125:327–337.

Xue, Y., Lim, S., Yang, Y., Wang, Z., Jensen, L. D. E., Hedlund, E.-M., Andersson, P., Sasahara, M., Larsson, O., Galter, D., Cao, R., Hosaka, K., and Cao, Y. (2012). PDGF-BB modulates hematopoiesis and tumor angiogenesis by inducing erythropoietin production in stromal cells. *Nature Medicine*, 18(1):100–110.

Yang, J., Price, M. A., Neudauer, C. L., Wilson, C., Ferrone, S., Xia, H., Iida, J., Simpson, M. A., and McCarthy, J. B. (2004). Melanoma chondroitin sulfate proteoglycan enhances FAK and ERK activation by distinct mechanisms. *Journal of Cell Biology*, 165(6):881–891.

Yang, N., Higuchi, O., Ohashi, K., Nagata, K., Wada, A., Kangawa, K., Nishida, E., and Mizuno, K. (1998). Cofilin phosphorylation by LIM-kinase 1 and its role in Rac-mediated actin reorganization. *Nature*, 393:809–812.

Ye, N., Verma, D., Meng, F., Davidson, M. W., Suffoletto, K., and Hua, S. Z. (2014). Direct observation of α-actinin tension and recruitment at focal adhesions during contact growth. *Experimental Cell Research*, 327:57–67.

Yonezawa, N., Nishida, E., Iida, K., Yahara, I., and Sakai, H. (1990). Inhibition of the interactions of cofilin, destrin, and deoxyribonuclease I with actin by phosphoinositides. *Journal of Biological Chemistry*, 265(15):8382–8386.

Yonezawa, N., Nishida, E., Koyasu, S., Maekawa, S., Ohta, Y., Yahara, I., and Sakai, H. (1987). Distribution among tissues and intracellular localization of Cofilin, a 21kDa actin-binding protein. *Cell structure and function*, 12:443–452.

Yotsumoto, F., You, W.-k., Cejudo-Martin, P., Kucharova, K., Sakimura, K., and Stallcup, W. B. (2015). sNG2 proteoglycan-dependent recruitment of tumor macrophages promotes pericyte-endothelial cell interactions required for brain tumor vascularization. *OncoImmunology*, 4(4).

You, W.-K., Yotsumoto, F., Sakimura, K., Adams, R. H., and Stallcup, W. B. (2013). NG2 proteoglycan promotes tumor vascularization via integrin-dependent effects on pericyte function. *Angiogenesis*.

Zimmermann, P., Tomatis, D., Rosas, M., Grootjans, J., Leenaerts, I., Degeest, G., Reekmans, G., Coomans, C., and David, G. (2001). Characterization of syntenin, a syndecan-binding PDZ protein, as a component of cell adhesion sites and microfilaments. *Molecular biology of the cell*, 13:339–350.

Appendix

A. Abbreviations

3D	Three-dimensional
AA	Amino acids
ADP	Adenosine diphosphate
AP1/2	Adaptor protein 1/2
APS	Ammonium persulfate
Arf6	ADP-ribosylation factor 6
ARH	Autosomal recessive hypercholesteremia
ATP	Adenosine triphosphate
AU	Arbitrary units
BAR	Bin-amphiphysin-rvs
bFGF	Basic fibroblast growth factor
br	Bronchiole
BSA	Bovine serum albumin
bv	Blood vessel
CAF	Cancer-associated fibroblast
CD	Cytosolic domain
CDR	Cricular dorsal ruffle
CHC	Clathrin heavy chain
CIP	Calf intestinal alkaline phosphatase
CNPase	2',3'-Cyclic-nucleotide 3'-phosphodiesterase
CME	Clathrin-mediated endocytosis
CS	Coverslip
CSF-1	Colony-stimulating factor 1
CSPG4	Chrondroitin sulfate proteoglycan 4
Dab2	Disabled 2
DAPI	4',6-Diamidine-2'-phenylindole
Dlg1	Drosophila disc large tumor suppressor
DNA	Deoxyribonucleic acid
DMEM	Dulbecco's modified eagles medium
DSF	Dorsal stress fibres
DTT	Dithiothreitol
EB	Electroporation buffer
ECM	Extracellular matrix
E. coli	Escherichia coli
EDTA	Ethylenediamine tetra-acetic acid
e.g.	exempli gratia, meaning: for example

EGF	Epidermal growth factor
eGFP	Enhanced green fluorescent protein
EH	Eps15 homology
Eps15	epidermal growth factor receptor pathway substrate 15
Erk	Extracellular signal-regulated kinase
FA	Focal adhesion
FACS	Fluorescence- activated cell sorting
F-Actin	Filamentous actin
FAK	Focal adhesion kinase
FCHo	Fes/CIP4 homolgy only
FCS	Fetal calf serum
FL	Full length
FN	Fibronectin
FRAP	Fluorescent recovery after photobleaching
G-Actin	Globular Actin
GAG	Glucosaminoglycan
GAP	GTPase activating protein
GAPDH	Glyceraldehyde-3-phosphate dehydrogenase
GDI	Guanine nucleotide dissociation inhibitor
GEF	Guanine nucleotide exchange factor
GFAP	Glial fibrillary acidic protein
gp	Guinea pig
GRIP1	Glutamate receptor-interacting protein 1
GSDB	Goat serum dilution buffer
GST	Glutathion-S-transferase
GTP	Guanosine triphosphate
HA	Hemagglutinin
HBS	HEPES-buffered saline
HBSS	Hank's balanced salt solution
μHD	μ-homology domain
HEK293T	Human embryonic kidney cells from 293rd experiment stably expressing SV40 large T antigen
HEPES	4-(2-hydroxyethyl)-1-piperazineethanesulfonic acid
HF	High-fidelity
Hsc70	Heat shock cognate 70
IHC	Immunohistochemistry
IP	Immunoprecipitation
iPBS	Ice-cold PBS
IPTG	Isopropyl-β-D-thiogalactopyranosid
KO	Knock out
MAPK	Mitogen-activated protein kinase
MEF	Mouse embryonic fibroblast
miRNA	Micro RNA
MRI	Magnetic resonance imaging
ms	Mouse
MUPP1	Multi-PDZ domain protein 1

NG2	Neuron glial antigen 2
nt	Nucleotides
OB	Olfactory bulb
OCT	Optimum cutting temperature
OD	Optical density
Opti-MEM	Modified Eagle's minimum essential media for optimal cationic lipid transfections
PAGE	Polyacrylamide gel electrophoresis
Pax	Paxillin
PB	Phosphate buffer
PBS	Phosphate buffered saline
PCR	Polymerase chain reaction
PDGFRβ	Platelet-derived growth factor receptor β
PDZ	PSD95, Dlg1, ZO1
PECAM	Platelet endothelial cell adhesion molecule
PFA	Paraformaldehyde
Phall	Phalloidin
PI(P)	Phosphoinositide (phosphate)
PI3K	Phosphatidylinositol 3 kinase
PKC	Protein kinase C
PMSF	Phenylmethane sulfonyl fluoride
PNK	T4 Polynucleotide kinase
PSD95	Post-synaptic density protein 95
rb	Rabbit
RISC	RNA-induced silencing complex
RNA	Ribonucleic acid
rpm	Rotation per minute
ROCK	Rho kinase
ROI	Region of interest
rt	Rat
RS	Restriction site(s)
RT	Room temperature
SB	Sample buffer
scr	Scrambled
SH2/3	Src homology 2/3
SHD	Stonin homology domain
SDS	Sodium dodecyl sulfate
siRNA	Small interfering RNA
αSMA	α Smooth muscle actin
SNX	Sorting nexin
Stn	Stonin
SV40	Simian virus 40
TA	Transverse arcs
TBS	Tris-buffered saline
td	Tandem
TEMED	N,N,N',N'-Tetramethylethylenediamine
TGFβ	transforming growth factor β

Tris	Tris(hydroxymethyl) aminomethane
VEGF	Vascular endothelial growth factor
VSF	Ventral stress fibres
Vinc	Vinculin
v/v	Volume per volume
WT	Wild type
w/v	Weight per volume
ZO1	Zonula occludens 1

B. Material

Material	Company, specifications
Cell culture	
Accutase	Gibco, #A11105-01
Antibiotics	Gibco
B-27 Supplement (50x)	Gibco, #17504-044
bFGF (human)	PeproTech, #100-18B
Cell culture dishes/ plates	Corning, tissue culture treated
Cell culture flasks	Nunc, T25/ T75 flasks for suspension cells
DMEM, high glucose	Biozym/ Lonza, #880029
DMEM/ F12	Gibco, #11320-074
EGF (human)	R&D, #236-EG
Electroporation cuvettes	Peqlab, cuvettes LE (2 mm electrode gab)
Electroporation pipettes	Peqlab, disposable pipettes
Serum (FCS/ BCS)	Hyclone, BCS: #SH300-72.03, Lot: 29803
	Thermo Fisher Scientific, FCS: #10270106, Lot: 41F0143K
	Thermo Fisher Scientific, FCS: #10270106, Lot: 42F3556K
Collagen 1 (rat)	BD Bioscience, # 354236
Collagen 6 (human)	-
Fibronectin (human)	Roche, # 11051407001
HBSS (+Ca/ +Mg)	Thermo Fisher Scientific/ Gibco, #14025-100
jetPRIME	Polyplus
Laminin 1 (mouse)	-
Lipofectamine 3000	Thermo Fisher Scientific
Matrigel	BD Bioscience, #356231
Opti-MEM	Thermo Fisher Scientific/ Gibco, #51985-042
PBS (- Ca/ - Mg)	Thermo Fisher Scientific, #14190250
PDGF-BB (human)	Peprotech, #100-14B
Poly-D-Lysin	Sigma, #P6407
RNAiMax	Thermo Fisher Scientific
Tamoxifen	-
Trypsin/EDTA	Biozym/ Lonza, #882040-12
Chemicals and disposables	
Antibiotics (for bacteria)	Roth
β-Mercaptoethanol	Fluka
Benzonase	Sigma
Coomassie Brilliant Blue G250	Roth
DTT	Fluka
Ethidium bromide	Roth
GST-bind resin	Merck, Novagen
Heparin	Sigma, #H4784
Igepal (nonident-P40)	Sigma
Immumount	Thermo Fisher Scientific
Lysozym	Roth
Phosphatase inhibitor 2 and 3	Sigma, #P5726/ #P0044

Protease inhibitor cocktail	Sigma, #P8340
Protein A/G Plus Agarose	Santa Cruz, #sc-2003
Toluidine Blue O	Sigma, #198161
Trypsin inhibitor (soybean)	Sigma, #T6522
Disposables	
Coverslips	Roth, Menzel Gläser, 12/ 18/ 24 mm
Cryotubes/ Plugs	Sarstedt, cryotubes with colour coded insets
Falcons (15/ 50 ml)	Sarstedt
Gloves	ecoShield, Econitrile PF250
Microscopy Slides	Roth
Pipettes (sterile)	Corning
RNAse-free tips	Sarstedt, safe seal filter tips
RNAse-free tubes	Sarstedt, biosphere safe seal micro tubes
Tips	Biozym Surphob, Tips: low binding, graduated
Tubes (1.5 ml)	Sarstedt, safe seal micro tubes
Tubes (2.0 ml)	Roth, multi- safe seal tubes
Material for IHC	
Coverslips (rectangular)	Roth, 24x50 mm
Cryomold	Tissue- Tek, Cryomold standard, biopsy, intermediate
Entellan	Merck, #1.07961.0100
Ketamin	WDT, Ketamin 10%
Microscopy Slides	Thermo Fisher Scientific, Menzel Gläser, SuperfrostPlus, #867.1
OCT	Tissue-Tek
PAP pen	Vector laboratories, #H-40000
Rompun	Ceva, Xylazin 2%

C. Curriculum Vitae and Publications

For reasons of data protection, the curriculum vitae is not included in the online version.